Experimental Evaluation and Characterization of a Mobility Assist Device Physical Interface

Laurent De B Levesque

Thesis Submitted in Partial Fulfilment of the Requirements for the Masters of Applied Science in Biomedical Engineering

Ottawa-Carleton Institute for Biomedical Engineering
Department of Mechanical Engineering
Faculty of Engineering
University of Ottawa

Abstract

Ageing is linked to a decrease in mobility, which affects the quality of life of many elderly individuals. This is a growing challenge in industrialised societies since the proportion of elderly individuals is becoming larger. One potential solution that would keep these individuals active and independent is the use of mobility assist devices. These devices are designed to reduce the energy demand of the user with the use of electric motors providing torques at joints of the lower limb. Although promising, these devices have a problem: they become uncomfortable after prolonged usage. This is especially true for devices designed to produce substantial assistance.

The research goal consisted of quantifying the performance of the physical interfaces, or points of attachments, of an experimental device with multiple interface adjustments. The device was fabricated with design criteria similar to active assist devices to simulate the mechanical behaviour of these particular devices. This analysis provided design recommendations that could ultimately enhance the performance of assist devices available on the market and thus the quality of life of many individuals. This research used force mapping and motion capture to quantify the kinetic and the kinematic compatibility of the device.

Experimental results have shown that the position, shape and other parameters of the interfaces had an effect on the relative movement of the brace, or the brace performance. The device interface migration was greater when the interfaces were positioned furthest away form the joint. An increasing level of assistance showed more relative movement between the brace and the user. Interface geometry had a noticeable effect on force distribution over the interface.

The results and methodology of this research offers an in depth understanding of the mechanical behavior of the physical interfaces of the developed assist device. Nevertheless, further research and development in the field of human machine interactions are needed in order to develop a physical human-machine interface that will ensure the success of powered assist devices in the future.

Acknowledgements

Thanks to Dr. Doumit for supervising and reviewing the work that was done during this project.

Thanks to Scott Pardoel as well as my other lab mates for sharing their knowledge and helping to address unexpected problems as they arose.

Thanks to Alexander Helal for reviewing the manuscript.

Thanks to Danielle, Justine and Jason for their help.

Thanks to the University of Ottawa MakerSpace for the use of their 3D printers.

Thanks to the University of Ottawa machine shop personnel.

Contents

List of Figures vii

List of Tables xv

1 Introduction 1

1.1 Objectives 2
1.2 Methodology 3
1.3 Contributions 3
1.4 Thesis outline 4

2 Literature Review 5

2.1 Current human mobility assist devices 5
2.1.1 Powered exoskeletons 6
2.1.2 Experimental knee braces 12
2.2 Physical human-machine interface 16
2.2.1 Kinematics: alignment and migration 17
2.2.2 Kinetics: force and pressure transmission 20
2.3 Interface performance evaluation techniques 25

3 Methods: Brace design, fabrication and testing 29

3.1 Passive assist knee brace design criteria 29
3.2 Knee brace conceptual design 30
3.3 Knee brace fabrication 31
3.3.1 Knee upright 32
3.3.2 Extension moment mechanism 33
3.3.3 Interface support 35
3.3.4 Shank sliding mechanism 41
3.3.5 Suspension system and supplemental strap 42
3.4 Mechanical testing and validation 43

4 Experimental methodology and instrumentation **47**
4.1 Knee brace instrumentation 47
4.1.1 Flexiforce force sensors 47
4.1.2 Data acquisition and processing 52
4.2 Motion capture 53
4.2.1 Motion capture calibration 53
4.2.2 Marker set 54
4.2.3 Hardware 56
4.3 Human testing 57
4.3.1 Ethics approval and recruitment 57
4.3.2 Participant and consent form 57
4.3.3 Exercise protocol 57
4.4 Experimental variables and parameters 58
4.4.1 Experimental variables 58
4.4.2 Experimental parameters and measurements 61
4.4.3 Data processing and presentation of results 63

5 Results and discussion **65**
5.1 Kinematics 65
5.1.1 Interface anterior-posterior positioning (APP) 65
5.1.2 Exercise analysis 71
5.1.3 Padding analysis 77
5.1.4 Longitudinal position (LP) analysis 81
5.1.5 Stiffness analysis 94
5.2 Kinetics 99
5.2.1 Interface geometry comparison 104
5.3 Slider mechanism 106
5.4 Discussion 112
5.4.1 Kinematics 112
5.4.2 Kinetics 113
5.4.3 Design recommendations 116
5.5 Limitations and sources of error 116
5.5.1 Brace testing 116
5.5.2 Force sensors 117
5.5.3 Human testing 118

6 Conclusion and future work **120**
6.1 Conclusion 120

6.2 Future work 121

Appendix A Human anatomy and physiology **132**

A.1 Terminology 132
A.2 The knee joint 134
A.3 Muscles 135
A.3.1 Consequences of muscle fatigue 136
A.4 Blood vessels 137
A.4.1 External pressure 139
A.5 Nerves 139
A.6 Skin properties and injury mechanism 140
A.6.1 Anatomy of the skin 140
A.6.2 Proprieties of the skin 140
A.6.3 Skin injury 143
A.6.4 Deep tissue pressure 144
A.7 Design parameter impacting comfort 146

Appendix B Brace fabrication and instrumentation **147**

B.1 Conceptual design 147
B.2 3D scanning 149
B.3 3D printer specifications 152
B.4 Sensor circuitry 153
B.5 Force sensor calibration curves 154
B.6 Brace mechanical characterization 159
B.7 Motion capture 161
B.7.1 Software 161
B.7.2 Marker set 163
B.7.3 Visual3D pipeline 164
B.7.4 Camera specifications 165

Appendix C Motion capture and force mapping results **166**

C.1 Kinematics 166
C.1.1 Combination analysis 166
C.1.2 Exercise analysis 169
C.1.3 Padding analysis 172
C.1.4 Position analysis 174
C.1.5 Stiffness analysis 181
C.1.6 3D scanner-Iterated interface comparison 184

C.1.7 Sliding mechanism 204

Appendix D Ethics certificate **209**

Appendix E Coding **212**

E.1 Matlab and Arduino code 212

E.1.1 Matlab 212

E.1.2 Arduino 224

List of Figures

2.1 The BLEEX exoskeleton [12] 6
2.2 The eLEGS exoskeleton [14] 7
2.3 The B-Temia exoskeleton, the K-SRD [15] 8
2.4 The MIT knee exoskeleton [16] 9
2.5 The Honda SMA exoskeleton [17] 10
2.6 The Active pelvic orthotic exoskeleton, a) the physical device b) CAD model [3] 11
2.7 The orthosis by Shamaei et al. [22] 13
2.8 The orthosis by Ramsey et al. [23] 14
2.9 The orthosis by Dos Santos et al. [24] 15
2.10 The orthosis by Sawicki et al. [25] 16
2.11 Effects of misalignment [27]. x and y: distance between the two joints, F_x: internal joint force in x direction, F_y: internal joint force in y direction, F_{res}: resulting force, T_{act}: exoskeleton torque, L: longitudinal migration, α: exoskeleton joint angle, γ: interface tilt angle. 18
2.12 Areas where force transmission should be avoided (adapted from [42]) 22
2.13 a)Areas to be avoided on the lower limb b)Pressure measurements [42] 23
2.14 Force transmission guidelines [43] a) axial sliding allowed on right image b) increased surface area in upper picture, proper position and use of couplesin lower picture 24
2.15 Instrumentation of Tamez et al. [46] 27
2.16 Instrumentation of Rathore et al. [48] 27

3.1 Experimental knee brace. Interfaces are in the anterior-posterior combination without padding. 1: upper orthotic upright, 2: anterior thigh interface backing, 3: upper elastic element clamp, 4: rotary potentiometer, 5: posterior shank interface backing, 6: carbon fiber strip, 7: interface strap 8: lower elastic element clamp, 9: motion capture marker on lower upright. 32

3.2 Stainless steel orthotic uprights 33
3.3 Clamping bracket with top portion 33
3.4 Bracket clamp top and bottom 34
3.5 Elastic element composed of clamping brackets and the carbon fiber strip 34
3.6 Elastic element mounted on uprights 34
3.7 3D model of the outlines. a) anterior thigh b) anterior shank 35
3.8 Different views of the anterior thigh interface 36
3.9 Different views of the posterior thigh interface 37
3.10 Different views of the anterior shank interface 37
3.11 Different views of the posterior shank interface 38
3.12 Different views of the anterior thigh interface 38
3.13 Different views of the posterior thigh interface 39
3.14 Different views of the anterior shank interface 39
3.15 Different views of the posterior shank interface 40
3.16 Sliding element 41
3.17 Sliding element mounted on brace frame 42
3.18 Hip suspension system 42
3.19 Additional strap 43
3.20 Knee brace in linear testing machine 44
3.21 Brace moment as a function of brace angle for the medium stiffness. The brace angle is limited to this range due to limitations of the testing apparatus. 45

4.1 a) Actual sensor dimensions, b) Sensor circuitry (both taken from [52]) 48
4.2 Top view of the printed circuit board connected to the top of the microcontroller 49
4.3 Sensor pad resting on an interface contact area 50
4.4 Calibration interface made of multiple layers of rubber sheets. These layers are held down on the platform with white tape. 51
4.5 The 12 Flexiforce sensors under calibration test. 52
4.6 Digital and actual marker set used for the kinematic study 55
4.7 Layout of the cameras in the capture volume after calibration. The cameras are represented by the orange pyramidal shapes. 56
4.8 Example of APP of the interfaces. Left: TP_SP, right: TA_SP. 59
4.9 Graphical representation of the vectors used for the calculation of interface migration. The position of the brace is exaggerated to show the vectors properly. HH: Helen Hayes, BV: Brace Vector. 62

4.10 Location of the force sensors on the sensor pad 64

5.1 RJA (Iterated APP analysis). Mean and SD of squat exercise. 67
5.2 Thigh interface migration (3D scanner based APP analysis). Mean and SD of squat exercise. a) parallel b) perpendicular. 68
5.3 Shank perpendicular migration (APP analysis). Mean and SD of squat exercise. a) iterated geometry b) 3D geometry. 69
5.4 Joint SI misalignment (APP analysis). Mean and SD of squat exercise. a) iterated geometry b) 3D geometry. 70
5.5 Thigh interface migration (3D scanner based exercise analysis). Mean and SD of the different exercises. Left and right columns represent the parallel and perpendicular migrations respectively. a) lunge, b) sit-to-stand, c) squat, and d) stair descent. 73
5.6 Shank interface migration (3D scanner based exercise analysis). Mean and SD. Left and right columns represent the parallel and perpendicular migrations respectively. a) lunge, b) sit-to-stand, c) squat, and d) stair descent. 75
5.7 Thigh interface parallel migration (iterated based interfaces padding analysis). Mean and SD of squat exercise. 78
5.8 Shank interface perpendicular migration (padding analysis). Mean and SD of squat exercise. a) iterated geometry b) 3D geometry. 80
5.9 RJA (iterated LP analysis). Mean and SD of squat exercise. Thigh interface is in the a) high, b) low or c) mid position 83
5.10 Thigh interface parallel migration (3D LP analysis). Mean and SD of squat exercise. Thigh interface is in the a) high, b) low or c) mid position 85
5.11 Thigh interface perpendicular migration (LP analysis). Mean and SD of squat exercise. a) TH_SL condition b) TH_SM condition. 86
5.12 Shank interface parallel migration (iterated LP analysis). Mean and SD of squat exercise. Thigh interface is in the a) high, b) low or c) mid position 87
5.13 Shank interface perpendicular migration (iterated LP analysis). Mean and SD of squat exercise. Thigh interface is in the a) high, b) low or c) mid position 89
5.14 Joint anterior-posterior misalignment (iterated LP analysis). Mean and SD of squat exercise. Thigh interface is in the a) high, b) low or c) mid position 90

5.15 Joint anterior-posterior misalignment (3D LP analysis). Mean and SD of squat exercise. Thigh interface is in the a) high, b) low or c) mid position. 91
5.16 Joint superior-inferior misalignment (iterated LP analysis). Mean and SD of squat exercise. Thigh interface is in the a) high, b) low or c) mid position. 92
5.17 ”Climbing” of the shank interface during a squat trial 93
5.18 RJA (iterated stiffness analysis). Mean and SD of squat exercise. 95
5.19 Thigh interface parallel migration (iterated stiffness analysis). Mean and SD of squat exercise. 96
5.20 Shank interface migration (iterated-3D position analysis). Mean and SD of squat exercise. Left and right columns represent the parallel and perpendicular migrations respectively. a) Stiffness 1, b) Stiffness 2 and c) Stiffness 3. 97
5.21 Joint misalignment (iterated stiffness analysis). Mean and SD of squat exercise. a) anterior-posterior b) superior-inferior. 98
5.22 Effects of padding and stiffness on the force response of the iterated based interfaces 100
5.23 Effects of padding and stiffness on the force response of the 3D scanner based interfaces 102
5.24 Force response of the two interface geometries. Mean of maximal recordings of squat exercise. a) iterated based interface b) 3D scanner based interface. 105
5.25 RJA (sliding interface, Stiffness 2). Mean and SD of squat exercise. . . . 107
5.26 Thigh interface migration (sliding interface, Stiffness 2). Mean and SD of squat exercise. a) parallel b) perpendicular 108
5.27 Shank interface migration (sliding interface, Stiffness 2). Mean and SD of squat exercise. a) parallel b) perpendicular 109
5.28 Joint misalignment (sliding interface, Stiffness 2). Mean and SD of squat exercise. a) anterior posterior b) superior inferior 110
5.29 Contact loss of the anterior interface 115
5.30 Loss of interface contact could visually be seen 115

6.1 Spring and cam mechanism of the Leviation knee brace by Spring Loaded Technology LLC [53]. 122

A.1 The different anatomical planes [54] 132
A.2 Flexion and extension of the knee joint [ThingLink.com] 133

A.3 The different sides of the leg. Modified from [55]. 134
A.4 Anatomy of the lower leg [42] 135
A.5 Main arteries of the lower leg shown in anterior and posterior views [59] 138
A.6 Main veins of the lower leg shown in anterior and posterior views [59] 138
A.7 The skin layers [62] 140
A.8 Haptic interface [68] 142
A.9 Haptic compliance map [68] 143
A.10 FE model of the lower leg [70] 145

B.1 Conceptual design 1. Side view. Knee brace where the assistance is provided by a mechanism located behind the brace. 1: superior upright, 2: inferior upright, 3: interfaces, 4: rotary spring mechanism and 5: force transmitting links. 147
B.2 Conceptual design 2. Isometric view. Knee brace where the assistance is provided by linear spring and cam mechanism located to the side the brace. Figure B.2b shows a different version of the assist mechanism. . 148
B.3 Conceptual design 3. Isometric view. Knee brace where the assistance is provided by leaf springs attached to the sides of the brace. 1: superior upright, 2: inferior upright, 3: interfaces and 4: leaf spring. 149
B.4 Mesh of the lower leg 151
B.5 Conditioning circuit of the Flexiforce A301 sensors. Note that the boxes containing capital A simply indicate the analog input port of the micro controller. 153
B.6 Calibration curve of Sensor 1 154
B.7 Calibration curve of Sensor 2 154
B.8 Calibration curve of Sensor 3 155
B.9 Calibration curve of Sensor 4 155
B.10 Calibration curve of Sensor 5 156
B.11 Calibration curve of Sensor 6 156
B.12 Calibration curve of Sensor 7 157
B.13 Calibration curve of Sensor 8 157
B.14 Calibration curve of Sensor 9 158
B.15 Calibration curve of Sensor 10 158
B.16 Calibration curve of Sensor 11 159
B.17 Calibration curve of Sensor 12 159
B.18 Brace moment in function of brace angle for stiffness 1 160

B.19 Brace moment in function of brace angle for stiffness 3 160
B.20 Frontal and side view of the modified Helen Hayes marker set 161
B.21 Frontal and side view of the model used for data processing 162
B.22 Example of pipeline commands 164

C.1 Relative joint angle 166
C.2 Thigh interface migration 167
C.3 Shank interface migration 167
C.4 Joint misalignment 167
C.5 Relative joint angle 168
C.6 Thigh interface migration 168
C.7 Shank interface migration 168
C.8 Joint misalignment 169
C.9 Relative joint angle 169
C.10 Thigh interface migration 169
C.11 Shank interface migration 170
C.12 Joint misalignment 170
C.13 Relative joint angle 170
C.14 Thigh interface migration 171
C.15 Shank interface migration 171
C.16 Joint misalignment 171
C.17 Relative joint angle 172
C.18 Thigh interface migration 172
C.19 Shank interface migration 172
C.20 Joint misalignment 173
C.21 Relative joint angle 173
C.22 Thigh interface migration 173
C.23 Shank interface migration 174
C.24 Joint misalignment 174
C.25 Relative joint angle 174
C.26 Thigh interface migration (parallel) 175
C.27 Thigh interface migration (perpendicular 175
C.28 Shank interface migration (parallel) 176
C.29 Shank interface migration (perpendicular) 176
C.30 Joint misalignment (anterior-posterior) 177
C.31 Joint misalignment (superior-inferior) 177
C.32 Relative joint angle 178

C.33 Thigh interface migration (parallel) 178
C.34 Thigh interface migration (perpendicular 179
C.35 Shank interface migration (parallel) 179
C.36 Shank interface migration (perpendicular) 180
C.37 Joint misalignment (anterior-posterior) 180
C.38 Joint misalignment (superior-inferior) 181
C.39 Relative joint angle 181
C.40 Thigh interface migration 182
C.41 Shank interface migration 182
C.42 Joint misalignment 182
C.43 Relative joint angle 183
C.44 Thigh interface migration 183
C.45 Shank interface migration 183
C.46 Joint misalignment 184
C.47 Relative joint angle 184
C.48 Thigh interface migration 185
C.49 Shank interface migration 186
C.50 Joint misalignment 187
C.51 Relative joint angle 188
C.52 Thigh interface migration 189
C.53 Shank interface migration 190
C.54 Joint misalignment 191
C.55 Relative joint angle 192
C.56 Thigh interface migration 193
C.57 Shank interface migration 194
C.58 Joint misalignment 195
C.59 Relative joint angle 196
C.60 Thigh interface migration (parallel) 196
C.61 Thigh interface migration (perpendicular) 197
C.62 Shank interface migration (parallel) 197
C.63 Shank interface migration (perpendicular) 198
C.64 Joint misalignment (anterior-posterior) 199
C.65 Joint misalignment (superior-inferior) 200
C.66 Relative joint angle 201
C.67 Thigh interface migration 202
C.68 Shank interface migration 203
C.69 Joint misalignment 204

C.70 Relative joint angle 204
C.71 Thigh interface migration 205
C.72 Joint misalignment 205
C.73 Relative joint angle 205
C.74 Thigh interface migration 206
C.75 Shank interface migration 206
C.76 Joint misalignment 206
C.77 Relative joint angle 207
C.78 Thigh interface migration 207
C.79 Shank interface migration 207
C.80 Joint misalignment 208

List of Tables

3.1 Natural gum foam hardness specifications, from manufacturer (McMaster-Carr, LLC) . . . 40

4.1 Typical performance of the Flexiforce sensors [52] . . . 48
4.2 APP reference table . . . 59
4.3 LP reference table . . . 60

5.1 Combination analysis (iterated interfaces). Average value at maximal flexion with SD in parenthesis for the different testing conditions. . . . 66
5.2 Combination analysis (3D interfaces). Average value at maximal flexion with SD in parenthesis for the different testing conditions. . . . 66
5.3 Combination analysis (interface comparison). Ratio of mean value between the two types of interface geometry. . . . 66
5.4 Exercise analysis (iterated interfaces). Average value at maximal flexion with SD in parenthesis for the different testing conditions. . . . 71
5.5 Exercise analysis (3D interfaces). Average value at maximal flexion with SD in parenthesis for the different testing conditions. . . . 71
5.6 Exercise analysis (interface comparison). Ratio of mean value between the two types of interface geometry. . . . 72
5.7 Padding analysis (iterated interfaces). Average value at maximal flexion with SD in parenthesis for the different testing conditions. . . . 77
5.8 Padding analysis (3D interfaces). Average value at maximal flexion with SD in parenthesis for the different testing conditions. . . . 77
5.9 Padding analysis (interface comparison). Ratio of mean value between the two types of interface geometry. . . . 78
5.10 LP analysis (iterated interfaces). Average value at maximal flexion with SD in parenthesis for the different testing conditions. . . . 81
5.11 LP analysis (3D interfaces). Average value at maximal flexion with SD in parenthesis for the different testing conditions. . . . 82

5.12 LP analysis (interface comparison). Ratio of mean value between the two types of interface geometry. 82
5.13 Stiffness analysis (iterated interfaces). Average value at maximal flexion with SD in parenthesis for the different testing conditions. 94
5.14 Stiffness analysis (3D interfaces). Average value at maximal flexion with SD in parenthesis for the different testing conditions. 94
5.15 Stiffness analysis (interface comparison). Ratio of mean value between the two types of interface geometry. 95
5.16 Iterated based interface padding analysis. Average value at instant of maximal force recording with SD in parenthesis for the different testing conditions. 101
5.17 Iterated based interface stiffness analysis. Average value at instant of maximal force recording with SD in parenthesis for the different testing conditions. 101
5.18 3D scanner based interface padding analysis. Average value at instant of maximal force recording with SD in parenthesis for the different testing conditions. 103
5.19 3D scanner based interface stiffness analysis. Average value at instant of maximal force recording with SD in parenthesis for the different testing conditions. 103
5.20 Ratio of of mean value of the sensor maximum force response (interface comparison) 106
5.21 No-slider condition stiffness analysis (sliding interface). Mean and SD of squat exercise. 110
5.22 Slider condition stiffness analysis (sliding interface). Mean and SD of squat exercise. 111
5.23 Slider and no slider comparison stiffness analysis (sliding interface). Ratio of mean value. 111

B.1 Microsoft Kinect motion sensor specifications. These specifications were taken from the manufacturer's website [74] 150
B.2 Marker identification for motion capture trials, knee brace and Helen Hayes model. ASIS: anterior superior iliac spine. UpperBrace rigid body marker positions are relative to hip joint. LowerBrace rigid body marker positions are relative to knee joint. 163
B.3 Specifications of the V100:R2 Motion Capture Camera. These specifications were taken from the manufacturer's website (http://optitrack.com/)165

List of Acronyms

	Acronym	Definition
Analysis	APP	Anterior-posterior position
	LP	Longitudinal position
Direction	AP	Anterior-posterior
	SI	Superior-inferior
Interface Combination	TA_SA	Thigh and shank interfaces are in the anterior position
	TA_SP	Anterior thigh and posterior shank interface position
	TP_SA	Posterior thigh and anterior shank interface position
	TP_SP	Thigh and shank interfaces are in the posterior position
Interface Position	TH_SH	Thigh and shank interfaces are in the high position
	TH_SM	Thigh in high and shank interface in mid position
	TH_SL	Thigh in high and shank interface in low position
	TM_SH	Thigh in mid and shank interface in high position
	TM_SM	Thigh and shank interfaces are in the mid position
	TM_SL	Thigh in mid and shank interface in low position
	TL_SH	Thigh in low and shank interface in high position
	TL_SM	Thigh in low and shank interface in mid position
	TL_SL	Thigh and shank interfaces are in the low position
Experimental Parameters	RJA	Relative Joint Angle
	TM_Pa	Thigh interface Migration (Parallel direction)
	TM_Pe	Thigh interface Migration (Perpendicular direction)
	SM_Pa	Shank interface Migration (Parallel direction)
	SM_Pe	Shank interface Migration (Perpendicular direction)
	M_AP	Misalignment (Anterior-Posterior direction)
	M_SI	Misalignment (Superior-Inferior direction)

Chapter 1: Introduction

The rising mobility challenges for the aging population is a critical issue worldwide. Many studies have shown the overall negative impact on quality of life for elderly individuals that suffer from limited mobility [1, 2]. This dire situation requires novel solutions that would permit elderly individuals to remain active, creative, productive, and independent [3]. One such solution is a category of devices designed to provide assistance to locomotion. These devices include powered exoskeletons and active orthotics. Despite their history and development, it is only recently that a generation of devices geared towards empowering individual's mobility with the help of active assistance became available and viable. Powered devices are capable of augmenting and replacing one's mobility. Although, these devices are lacking in certain areas. The present study focuses on the active devices that provide assistance to the knee joint.

Presently, one of the main challenges in the development of powered assist devices is the physical interaction of the machine with the underlying biological system [4, 5, 6]. Assist device fixation to humans is a critical issue that presently limits the performance of these devices. The attachment system, which is responsible for transferring forces and managing the relative movements between the device and the user, should minimise undesirable forces and motions [7]. Unfortunately, most assist device systems are built primarily as machines and do not tailor the physical interfaces to the user or improve the human-machine physical interaction. Most acticles encountered in literature about assist devices do not emphasise the physical interface system. This is not surprising considering the general lack of information in literature regarding the physical interface mechanisms and the properties of the skin and biological tissues when in contact with external systems [8]. In other words, it seems that the main objective of these systems is to achieve the required kinetics and kinematics with little or no emphasis related to the human-machine interface solution. It appears that the majority of exoskeletons nowadays are designed primarily as a machine with little considerations for the underlying biological limitations that come from the human user.

All developed powered assist devices do not perfectly replicate and follow human natural motion in harmony, thus creating undesired relative motion and friction forces between the device and the skin of the user. The magnitude of these forces is directly related to the comfort of the user and ultimately affecting the device performance. It has been reported that the constant and repetitive distortion of the skin and underlying tissues causes user discomfort and injuries, particularly for individuals with neuromuscular pathologies that lack sensitivity in the lower limbs [9, 10]. Specific locations such as bony prominences, superficial nerves and blood vessels are sensitive to direct pressure and are thus more susceptible to discomfort and injuries when used as physical contact between the user and machine [8, 10, 11]. Thus, there is a critical need to comprehensively analyse and understand the physical relationship between powered assist devices and the user.

Bridging the gap between functionality and user comfort would improve the overall performance of powered assist devices. Enhanced device performance would extend the device usage period, which leads to a better quality of life for the user. This gap poses a design challenge and is a major obstacle for the long-term success of powered assist devices. With the impressive state of current robotics, the physical interface is one of the few remaining issues preventing the widespread adoption of assist devices. In order for these devices to reach their full potential and restore human mobility, an in depth understanding of the interface mechanisms and biological limitations associated with the user is required.

1.1 Objectives

The ultimate goal of this research is to achieve a comprehensive understanding of human-machine physical interface interactions such to enhance the overall performance of powered assist devices. This led the research to identify four main objectives, namely (1) to design, fabricate and instrument a low cost modular knee brace that replicates the mechanical behaviour of powered assist devices, (2) to conduct human testing while introducing variable design and operating parameters, (3) to achieve a comprehensive experimental analysis in order to understand the parameters that have an effect on the performance of powered assist devices, and (4) developing a method to evaluate and quantify performance.

1.2 Methodology

In order to achieve the aforementioned objectives, a three-part methodology was applied. First, a literature review was performed to study current assist devices and knee orthoses physical interface solutions, the means of force transmission and the kinematic mismatches that exists with the use of an external device. Moreover, throughout the literature, parameters and criteria were identified to quantify comfort and guide the design of the knee brace prototype. Second, based on existing powered assist devices, a modular knee brace design with an extension moment assist and two physical interfaces was developed for experimental testing. The brace design includes modified single degree of freedom orthotic uprights, machined aluminium parts, 3D printed interface components and fastening straps. The knee brace was instrumented to acquire kinematic and kinetic data, then was mechanically tested and calibrated using an universal linear testing machine. Lastly, a human experimental study was designed and implemented to analyse the effects of different brace design and operating parameters. A motion capture study was conducted to evaluate the kinematic behaviour of the brace and a kinetic instrumentation permitted the measurement of the relative force distribution and concentration over the interface contact area.

1.3 Contributions

This research firstly achieved a comprehensive literature review to examine current assist device designs of physical interface designs. This showed the lack of research and development concerning the physical interfaces mechanisms of all examined powered assist devices found in the literature. In addition, the review helped identify force mechanical parameters and biological restrictions when using assist devices to associate comfort to certain metrics.

Secondly, a novel low cost modular knee brace with extension moment assist was designed and fabricated. The developed device allows multiple physical interface adjustments that vary the position of the interfaces, the interface compliance, interface geometry and the level of assistance. This permitted knee brace testing under various conditions to evaluate the physical interface mechanism performance.

Lastly, a strong evidence of comfort was identified by conducting a comprehensive experimental testing and analysis with a human participant using motion capture and force mapping. The overall results provide a comprehensive understanding of the physical interface mechanisms and permitted an evaluation and the identification of the optimum knee brace testing parameters for each testing condition. These findings could be used to improve the design of active devices and therefore improve the quality of life of many individuals.

1.4 Thesis outline

This document is divided in six Chapters, namely: introduction, literature review, prototype development and testing, instrumentation and motion capture, results and discussion and a conclusion.

Chapter 1 introduces the general information regarding the problem that will be addressed as well as the approaches utilized. The objectives of this research and the achieved contributions are also included.

The literature review, Chapter 2, presents current challenges and relevant theory needed to understand the interactions between device interfaces and the user. The methods for the evaluation of the device performance are also presented.

Chapter 3 elaborates on the design and fabrication of a knee brace prototype. This chapter details on the techniques used to fabricate the different components of the brace and also includes the mechanical testing and calibration of the knee brace.

Chapter 4 presents the implemented knee brace instrumentation to capture kinetic data, to evaluate the interface force distribution, and kinematic data, to evaluate the relative movements between the brace and the user. The former is performed with a force capture system developed in-house and the latter is performed using a commercial motion capture system. The chapter focuses on hardware, software and testing protocol.

The results and discussion, Chapter 5, contains all the results of the human testing. Experimental results of different design and operating parameters with regards to kinematics and kinetics impacts are presented and compared. An in-depth discussion of the results is also included, including the limitations of the work.

Chapter 6 presents a conclusion, which summarises the work undertaken in this research project, and a future work section, which identifies areas of further development that would supplement the research.

Chapter 2: Literature Review

This literature review collected and summarized information from published studies on human-machine physical interfaces and advances in related technologies. The review mainly considered relevant material in research journals and conference papers as well as in books and graduate theses. Overall, the review aimed to identify knowledge and technology gaps that may merit further research.

The literature review chapter begins with a presentation of current human mobility assist devices. More specifically, the interfaces components and attachment systems of various exoskeletons and knee orthotic devices are examined. The second part of this chapter identifies key mechanical and biological parameter that are vital when examining the applied loads to the human body through mobility assist technologies. This will later form an understanding on how and where the human machine transfer loads should be applied.

More fundamental information regarding human anatomy and tissue mechanics can be found in Appendix A.

2.1 Current human mobility assist devices

Despite the numerous human mobility assist devices on the market and in research laboratories, this review focused on several powered devices that generate substantial mechanical assist and reflect common challenges related to human-machine physical interface mechanisms.

Experimental knee braces were also included in this review to evaluate the interfaces of such devices and for design inspiration.

2.1.1 Powered exoskeletons

In 2006, the BLEEX™, a fully active load carrying exoskeleton proposed by Zoss et al. [12] was released for military applications. The BLEEX was one of the first load carrying and energetically autonomous exoskeletons, with actuators capable of producing a torque up to 200 Nm [13]. This assist torque is mainly used to balance the weight of the payload that is carried by the user and transfer its weight to the ground. The only force applied to the user's limb is from pushing the limbs with the device structure. The cuffs used to attach the exoskeleton to the body of the user are located at the waist, below the knee and at the foot via a foot plate. They are made of a rigid material covered by breathable fabric and use Velcro to make the fit adjustable. The rigid sections of the interface are located posteriorly to the proximal shank. In addition to torque assist provided to the hip, knee and ankle, the system is also designed to reduce the energy cost of carrying a payload by transmitting load trough the machine and thus subjecting the human machine interface to further constraints. The BLEEX interfaces can be seen in Figure 2.1:

Figure 2.1: The BLEEX exoskeleton [12]

Following the release of the BLEEX, an exoskeleton intended for rehabilitation purposes was designed by Strausser and Kazerooni [14]. The eLEGS™ was unveiled in 2010 and has a similar interface to the BLEEX exoskeleton. The interfaces are located at the waist, upper portion of the thigh, just below the knee (upper shank) and the device has a foot plate. The interfaces of the upper thigh region are only made of a flexible strap. The interfaces located under the knee have their rigid portion located anteriorly. The eLEGS can be seen in Figure 2.2:

Figure 2.2: The eLEGS exoskeleton [14]

A similar device to the eLEGS is B-Temia's proprietary product, the K-SRD™. The assistance is provided by a compact electric motor at the knee joint. The main structure is a low profile metal frame and this active exoskeleton attaches to the user with straps around the waist, thigh and shank. This device predicts and augments the movements of the user with data from multiple sensors on the device [15]. The different interfaces may be seen in Figure 2.3.

Figure 2.3: The B-Temia exoskeleton, the K-SRD [15]

The thigh interface's rigid portion is located posteriorly and includes a Velcro strap anchored to the device's frame with a singular bolt, allowing it to pivot. This strap runs from the groin region up to the upper lateral thigh. The knee and shank interface systems feature a rigid shell positioned anteriorly and Velcro straps that tighten the interface from the posterior aspect of the limb. The shank interface covers most of the anterior portion of the shank segment.

The devices enumerated above are designed to be worn over the entire legs. Some other devices have been designed to provide assistance at a particular joint. Figure 2.4 shows an exoskeleton worn only at the knee joint intended to assist running [16]. The device is secured on the lower limb by posterior orthotic shells. The fit is adjusted with Velcro straps, that apply a pressure on the leg anteriorly. These straps have one rotational point of attachment, allowing for different strap orientation. The exoskeleton and its interface can be seen in Figure 2.4:

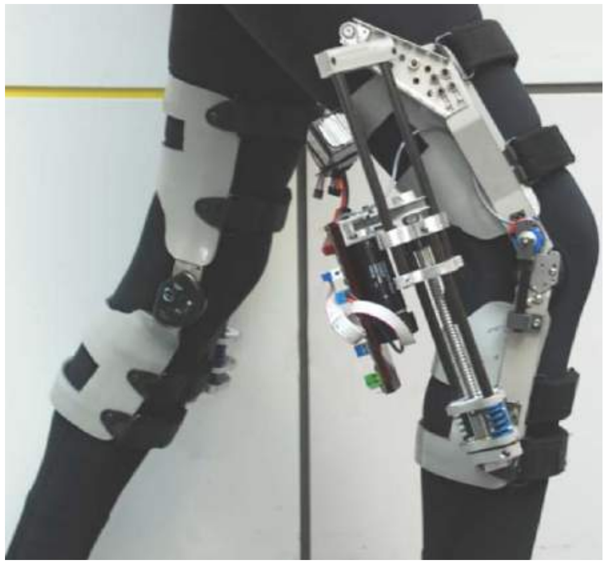

Figure 2.4: The MIT knee exoskeleton [16]

The Honda Stride Management Assist (SMA™) is a single joint exoskeleton designed for walking assistance [17]. With the use of sensors, the SMA delivers a torque at the hip joint to lift the upper leg forward during the swing phase and applies a torque in the opposite direction at heel contact to stabilise the leg on impact. Including the hip belt and structure, the device interfaces are based on straps that loop around the lower portion of the thigh. Curved beams transmit the hip moment. The interfaces have an orthotic shell on the anterior side of the leg with a Velcro strap that wraps around the leg, posteriorly. The rigid curved beam applies a force anteriorly. The interfaces are located at the waist and just over the knee. The SMA interfaces can be seen in Figure 2.5:

Figure 2.5: The Honda SMA exoskeleton [17]

Another interesting prototype similar to the SMA, is a light-weight Active Pelvis Orthosis (APO), by Giovacchini et al. [3]. The APO has an optimized design based on light-weight carbon fiber linkages and generates a hip torque to provide assistance. The APO also includes a manual adjustment mechanism for fitting the orthosis to a wide range of user sizes, and passive degrees of freedom that allow pelvis tilting and thigh abduction. The device can be seen in Figure 2.6:

Figure 2.6: The Active pelvic orthotic exoskeleton, a) the physical device b) CAD model [3]

The APO is in contact with the user's body in multiple zones. Three thermo-shaped orthotic trunk shells stabilize the frame over the user's waist, two orthotic shells (posterior and anterior) are tightened around the thighs with elastic belts and fastening straps. These come from the posterior waist structure and pass under the groin area and come back the waist structure anteriorly. The rigid curved beams responsible for the force transmission are pushing against the limb posteriorly.

Based on the reviewed powered human mobility assist devices and many others, current exoskeletons seem to have similar interfaces, mainly constructed of a rigid component and some form of strapping, to make the fit adjustable. Although their structure is similar, some parameters are varied, in particular the position of the interface's rigid portion and strapping system.

Active device moment requirement

Exoskeleton actuator design is dependant on multiple factors such as execution speed, weight of the user and whether the user is carrying a load. For example, Crowell et al. [18] reported biological knee sagittal extensor moment required for normal walking with a backpack payload could range from 0.72 to 1.37 Nm/kg (normalised to body mass) for loads between 6 and 47 kg. Kim et al. [19] designed a load carrying exoskeleton with 67 Nm of assistance at the knee joint for sit-to-stand exercise. In another case, Kanjanapas et al. [20] designed their prototype exoskeleton to have a moment of about 1 Nm/kg for walking. Farris et al. [21] reported that the largest extensor knee joint moment required during stair ascent for paraplegic patients was 0.87 Nm/kg for the device examined during their study. This shows the variability in exoskeleton actuator design and provides insight on the amount of assistance needed to accomplish specific goals.

2.1.2 Experimental knee braces

The following section describes different interface solutions that are currently available for knee orthoses, and will be serving as inspiration for the design of the prototype knee device used in this work. More specifically, for brace structure and physical interface variables such as shape and position.

In 2013, Shamaei et al. [22] presented a friction-based latching mechanism and a control algorithm that engages a spring in parallel with the knee during stance phase and disengages the spring during swing phase. This stance-control orthosis has a structural frame where the thigh and shank interfaces rigid portions are positioned posteriorly. the device also has a foot plate linked to the shank interface and subsequently to the rest of the structure. The strapping system is located on the anterior portion of the leg. The orthosis can be seen in Figure 2.7.

Figure 2.7: The orthosis by Shamaei et al. [22]

Another orthosis, developed by Ramsey et al. [23] consisted of a compliant mechanism with parallel coupled flexible plates and pennate elastic bands. The mechanism comprised of a base plate and a sliding plate attached to each other with fixed and sliding pins. This allows for a guided, relative motion between the plates and thus flexion of their knee brace prototype. This mechanism and prototype can be seen in Figure 2.8.

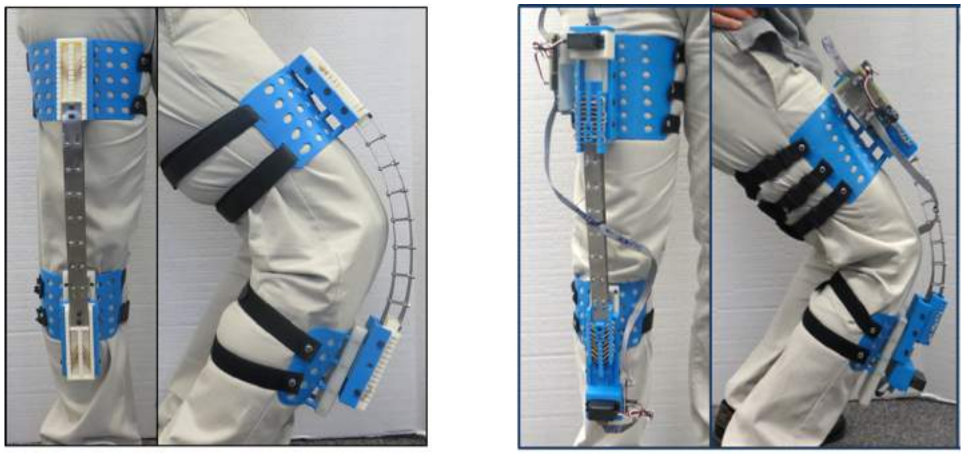

(a) (b)

Figure 2.8: The orthosis by Ramsey et al. [23]

The interfaces of this experimental knee brace were 3D printed and use multiple narrow straps at mid length of the thigh and shank segments. The rigid portion is placed anteriorly while the strapping system exerts a pressure on the posterior side of the leg.

An additional assist knee brace was developed by Santos et al. [24]. The device is driven by a customized rotary series elastic actuator, which is composed of a direct-current motor, a worm gear and a customized torsional spring. The interface system has a contact point at the waist, the upper portion of the thigh and over the entire surface of the shank. The rigid interfaces are positioned posteriorly and the flexible elements are located anteriorly. This device can be seen in Figure 2.9.

Figure 2.9: The orthosis by Dos Santos et al. [24]

Another knee and ankle orthosis was developed by Sawicki et al. [25] using pneumatic artificial muscles (PAM) actuators as can be seen in Figure 2.10. The interfaces of the device are rigid and cover the anterior and posterior portions of the lower leg. Due to the fixed volume of these interfaces, these contact points do not have a high degree of adjustability.

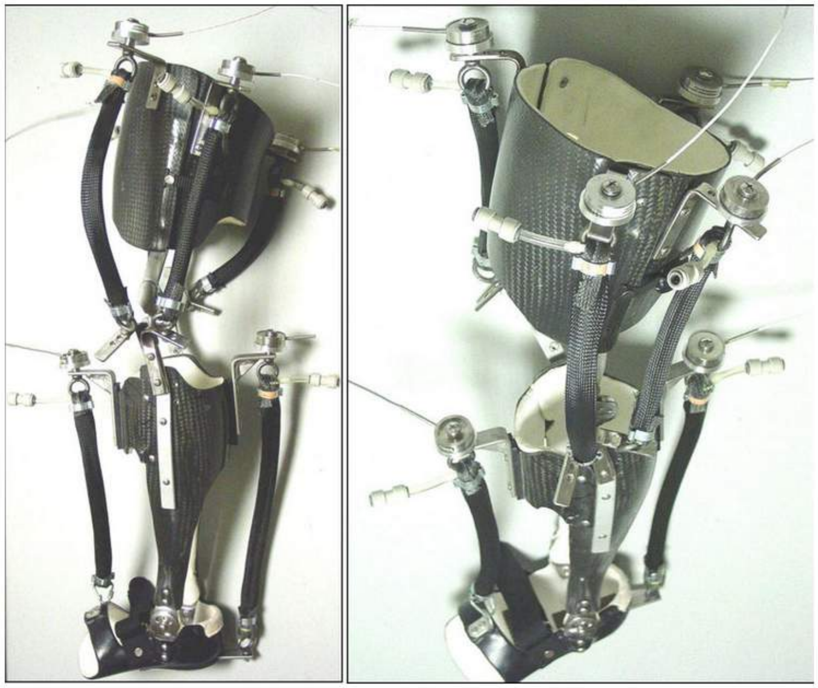

Figure 2.10: The orthosis by Sawicki et al. [25]

Similar to exoskeleton design, experimental knee brace interfaces differ greatly. The different interface solutions presented here show a lack of design standardisation or recommendations concerning the location, structure and other parameters of assist orthoses. In other words, there are no guidelines that are available to guide the design of interfaces that transmit loads to the human body.

2.2 Physical human-machine interface

Biomechanical studies are typically employed to track the motion of the human body while wearing assist devices to measure changes in gait patterns. The interactions between human and machines are not studied as much. This translates to interfaces solutions that could be improved and underlines the fact that more emphasis should be placed on the coupling side of the human system [26].

This section will review studies that have examined the human machine interface mechanism and have identified critical parameters that impact the performance of transferring an external load to a human limb.

2.2.1 Kinematics: alignment and migration

Assist device biomechanics are greatly affected by kinematic incompatibility between the device and human limbs. This is mainly attributed to the real-life variability of biomechanics parameters between users and a lack of adjustments of the device structure. The uniqueness that exist between individuals leads to different joint axis locations and body segment sizes. Kinematic incompatibilities between humans and exoskeletons are mainly associated with misalignments between the human joint axes and assist device joint axes [6]. As an example, a mismatch between the assist device and the natural knee joints will cause unwanted displacements that result in abnormal forces acting on the native joint. This will impose range of motion restrictions and will introduce relative movement of the device with respect to the user.

Schiele [27] further elaborated on this challenge using a diagram shown in Figure 2.11. In the case where the device joint is perfectly aligned with the biological joint, as in Figure 2.11a, it can be seen that the x and y values, which identify the exoskeleton joint center, have a null value; the two joint centers are concentric. When comparing with Figure 2.11b, in the case that the device and user's joint are not perfectly aligned (which is most likely the case during the fitting process), the x and y values are greater than zero and a small misalignment occurs. Small misalignments between the native and device joints will inevitably hinder the motion of the user. Furthermore, if the device is rigidly attached to the human limb, shear forces F_{res} would be generated within the knee joint by the applied exoskeleton torque T_{act} during relative movement. In this scenario, flexion or extension of the knee is hindered considerably. In a more realistic case as in Figure 2.11c, where the device is not rigidly attached and may move, the application of a torque through the mechanical joint will cause a longitudinal migration between the device attachments and the limb (denoted by L), and will cause tilting of the interface (denoted by γ). This will apply pressure and a frictional force on the skin while translating along the limb. This pressure will also induce a perpendicular migration from compressing the soft tissues.

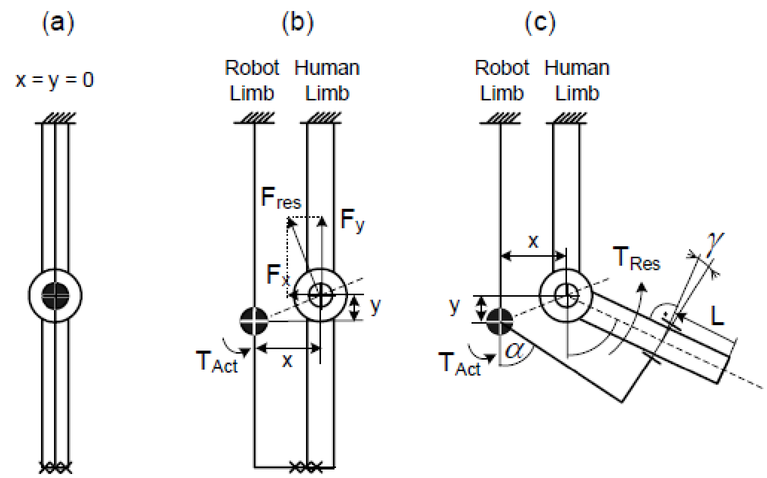

Figure 2.11: Effects of misalignment [27]. x and y: distance between the two joints, F_x: internal joint force in x direction, F_y: internal joint force in y direction, F_{res}: resulting force, T_{act}: exoskeleton torque, L: longitudinal migration, α: exoskeleton joint angle, γ: interface tilt angle.

The repetitive movement of the device relative to the human limb could lead to significant user discomfort. In addition to skin injuries, long-term damage to the human joint could occur if the device actuators are strong, subjecting soft tissue structures and joints to forces that are generally not experienced.

Alignment

Attempts to maintain proper alignment is complicated because the knee joint does not have a fixed centre of rotation. This, along with most mechanical joint design's inability to mimic knee kinematics even during simple flexion and extension create a challenge for the design of these devices. The effects of misalignment have thus been studied by multiple researchers.

Stienen et al. [28] stated that when rotating axes are misaligned, any rotation forces will cause relative translations on the human joint. The user's limbs may not be able to move in the desired direction and will result in large depressions of the soft tissue between the exoskeleton and the human limb. Depending on the amount of misalignment, tissue depression can vary significantly and cause pain or discomfort. To prevent this from occurring, joint axes should be perfectly aligned. This notion has also ben expressed by Regalbuto et al. [29].

Zanotto et al. [30] purposely induced misalignments in an exoskeleton developed by their group (ALEX II) and quantified the alterations in gait kinetics and kinematics during level walking. They experimentally tested the exoskeleton with varying thigh segment lengths at a short, ideal and long length. The short and long values of the thigh were defined by subtracting or adding 20 millimetres from the ideal value. After testing, they determined that the misalignments at the knee joint mostly affected the interface interaction force at the thigh and only slightly at the shank. The interaction forces were higher in the case of the short length compared to the long length.

Regalbuto et al. [29] found that, irrespective of the type of hinge used, greater than 12 mm of offset between the knee and brace axes of rotation increased the forces and moments at the hinge of the brace. These authors believed that this may lead to shearing of the soft tissues, altered joint mechanics, reduced ability of the brace to control anterior tibial translation and, consequently, abnormal ligament length patterns.

Migration

Another factor that should be taken into account is the minimization of interface migration. Migration is defined as the relative movement of the points of attachments with respect to the limb. Migration is caused by the weight of the device, joint misalignments and the inability of the brace to assure contact over the whole movement cycle. This movement is inevitably one of the most prominent problem in the design of knee orthoses. Migration results in an imbalance between brace and knee joint mechanics. A brace that is not in the correct position may place the user at risk for injury. If a brace migrates during activity and is not readjusted, abnormal forces may develop in the joint. If repetitive readjustments are required, the user becomes less inclined to use the brace.

Pierra et al. [31] stated that the majority of brace manufacturers assure that migration is minimised by design features such as silicon pads and a proper fit of the brace. Although, clinical experience would suggest that migration remains a major issue. This migration also causes misalignment of the hinge system of the brace. Singer et al. [32] and Mohseni et al. [33] suggest that accurate sizing and fitting as well as attention to correct hinge placement relative to the femoral condyles can limit brace migration and improve its effectiveness and performance at mid and deep knee flexion.

Lamontagne [34], Singer and Lamontagne [32] and Ramsey et al. [35] reported that if the brace moved during dynamic movement, misalignment of the knee and brace center of rotation might induce more resistance to the motion. With this displacement, external compression by the strapping of the brace might cause higher intramuscular pressure beneath the area of the brace straps. This pressure under the strapping decreased local muscle blood flow and muscular oxygenation, which induced premature muscle fatigue. In some cases, where the brace is not fitted and worn properly, functional knee braces do not improve performance and may even alter or decrease normal function of the knee. These authors also underline the fact that, among the published literature, one common problem regarding functional knee braces is their tendency to slip distally during physical activity. This may occur simply because the brace fails to adhere to the soft tissues of the leg during the repetitive muscular contractions.

Brownstein [36] measured experimentally the migration tendency of 14 commonly used functional knee braces. Brownstein suggests that the type and magnitude of forces were related to the placement of the brace axis rather than the type of hinge being used.

The effects of orthotic devices, such as knee braces, can provide insights on the kinematic compatibility of active assist devices. Since limited literature exist on the subject of exoskeleton kinematic compatibility and the scope of this research examines the effects of interface parameters of an experimental knee brace, information regarding knee orthoses is a good foundation. The design of an exoskeleton physical interface should ensure proper alignment and should offer multiple interface adjustments to fully adapt to the variable instantaneous center of rotation of the native joint and varying limb geometries. Interfaces should also be designed in order to have minimal relative displacements and reduce the negative effects on the native knee joint are as little as possible.

2.2.2 Kinetics: force and pressure transmission

Biological factors must be taken into account when designing wearable device support systems that will transfer forces. Among others, anatomical areas or structures able to effectively support loads, as well as maximum levels of pressure, without raising issues related to safety and comfort, should be considered.

Tissue biomechanics: superficial tissue pressure

Human locomotion augmentation involves applying force on soft tissue, which will inevitably have an effect on these biological structures. It is imperative to quantify pressure thresholds that can safely be applied onto the lower limbs for wearable mobility assist devices. Multiple studies have shown that local blood flow might be impaired with the application of an external device. Styf et al. [37] measured the muscle pressure (developed by muscle contraction) and blood flow in both legs simultaneously with the microcapillary infusion method and by inserting a Teflon catheter (Myopress, Atos Medical Inc., Hbrby, Sweden) into the anterior tibial muscle bilaterally. Muscle pressure, during exercise, exceeding 30 to 40 mm Hg (by external compression) significantly impeded muscle blood flow during exercise in normotensive athletes. In another study, Styf et al. [38] experimentally measured the effect of three different functional knee braces on intramuscular pressures of healthy subjects, using the same technique. The braces increased intramuscular pressure at rest and during exercise. The authors concluded that a resting muscle pressure between 30 and 50 mmHg impedes local blood flow. They did not specify the tension of the brace's straps during the experiment but mentioned that the recorded increase in muscle pressure (and resulting lower vascularisation) was responsible for early onset muscle fatigue that decreased stability and control of the knee and ankle joints potentially leading to other injuries.

Styf et al. [39] and Lundin and Styf [40] researched early muscle fatigue while wearing a knee brace. The braces were fitted and strapped with a known tensile force, within the lower range of the tension recommended by the brace manufacturer. Early fatigue was attributed to increased intramuscular pressure since muscle blood flow was impeded during muscle contraction and muscle contraction pressures exceeded systolic blood pressure. Therefore, the muscles could only be perfused during muscle relaxation between contractions.

Asthon [41] demonstrated that applying an inflatable splint around a limb could completely restrict blood flow with 40 mmHg of pressure in the limb, often resulting in a negligible or even zero blood flow measurements. Skin circulation is more easily compromised by external compression than muscle circulation since the muscles are located further away from the skin surface. Furthermore, if the pressure applied by assist device interfaces is greater than 30 to 50 mmHg, the application time should either be minimal or periods of no force application are required.

Tolerance areas

Particular structures of the lower limb require protection, or are less suitable to bear external pressures from assist devices [42]. More specifically, these areas can be seen in Figure 2.12. These tolerance areas have been determined by applying a static load on the limb.

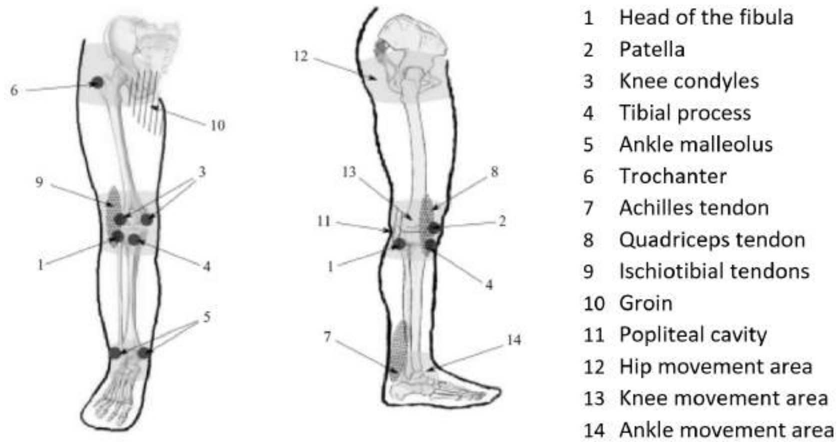

Figure 2.12: Areas where force transmission should be avoided (adapted from [42])

Pressure Pain Threshold values (PPT), defined as the limit of pressure above which a person feels pain, may be defined for particular regions of the human body with experimental tests [42]. This helps determine the maximum allowed forces on the lower limbs, which varies according to their point of application and the dimension of the contact area. The PPT is largely determined by the shape and size of the indenter or probe head of the measuring device. These indicators can therefore only be used for intrasubject comparison and for stabilizing pressure maps of the body. Nevertheless, the various areas and their associated PPT can be seen in Figure 2.13a and Figure 2.13b. These figures are plots of the pressure associated with the different points of measurements.

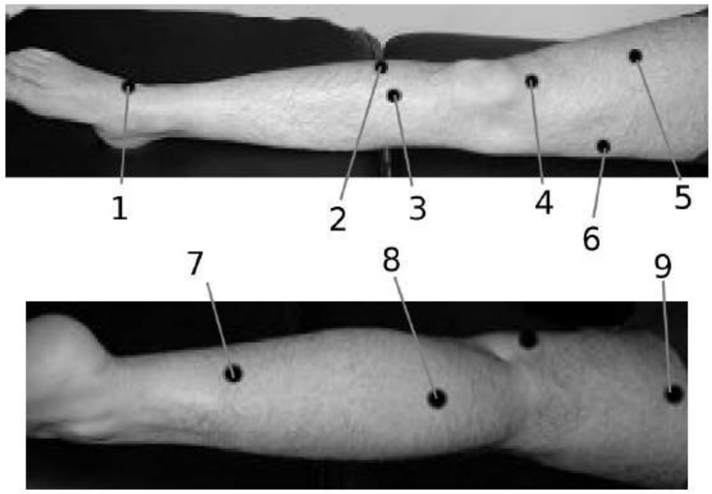

(a)

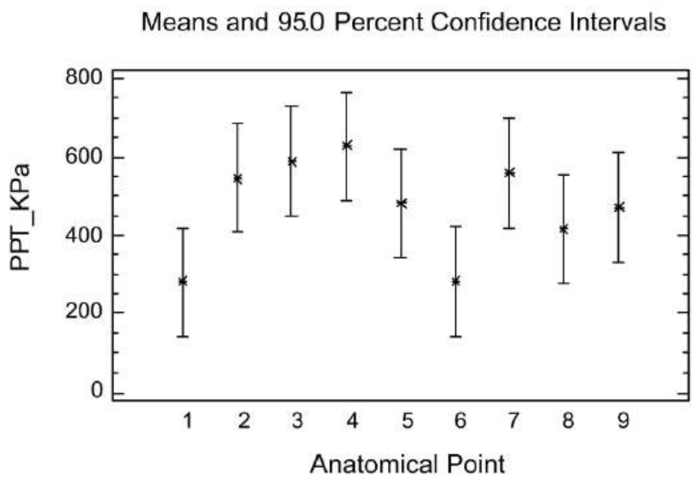

(b)

Figure 2.13: a)Areas to be avoided on the lower limb b)Pressure measurements [42]

It was found during the study that points 1 and 6 were significantly more delicate than other points. In other words, the front of the ankle and the medial distal portion of the thigh should be avoided in the design of assist devices.

Application of loads to human skin

The methods of force application are to be investigated. Jarrassé and Morel [43] suggest how forces should be transmitted to the human limb. Figure 2.14a shows an external device attached to the lower limb with no possibility (theoretically) of longitudinal translation (indicated by the red dash-dotted lines).

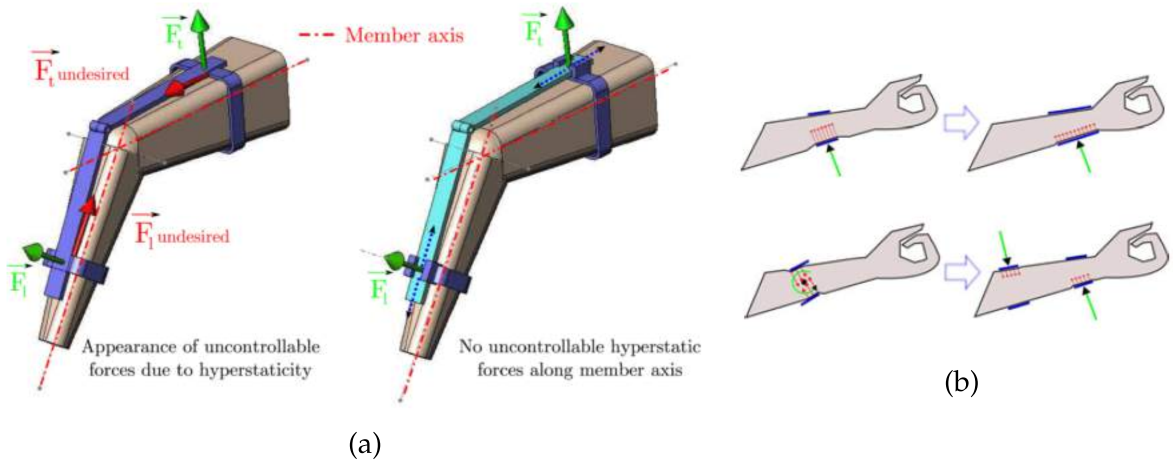

Figure 2.14: Force transmission guidelines [43] a) axial sliding allowed on right image b) increased surface area in upper picture, proper position and use of couplesin lower picture

Figure 2.14a would suggest greater benefit in permitting the translation of an external exoskeleton structure so that unwanted misalignment forces do not take place. An extra degree of freedom may be added to the device structure and interfaces. The addition thus could be beneficial particularly if the device consists of a hinge joint, and the native knee is a polycentric joint since this would inevitably cause some shearing forces $F_{undesired}$ (as shown in Figure 2.14a). An adequate interface contact area, large enough to diminish pressure to acceptable levels, and to transmit moments with the help of couples, which would diminish the depression of the interfaces into the limb, is also recommended as can be seen in Figure 2.14b.

Important kinetic factors

In order for the exoskeleton to transmit forces and help the user, it must do so by exerting pressure on the skin. Excessive pressure is one of the main concerns related to the application of loads to the body. The application of loads by the device to the human produces contact pressures that can be harmful. In this regard, two factors relating to the applied pressure have been defined: pressure distribution and pressure magnitude, both relating to comfort and tissue health. Regarding safety, the general guideline is to avoid pressure above the ischemic level which would compromise the tissue. The relationship between applied pressure and comfort is complex. Comfort is defined as a state of physical ease and freedom from pain or constraint, but there is no objective way to quantify comfort since it depends on every individual.

There are two strategies for managing an external loads: concentrate loads over a small area with high tolerance for pressure or distribute the load over a large area to reduce pressure. Ususally, a combination of both strategies is adopted to minimise discomfort. Nevertheless, this does not guarantee comfort. Some authors have shown that there may be a threshold beyond which it is better to concentrate than to distribute forces [42]. This is explained by the spatial summation theory, which establishes that as the area of contact increases, the number of excited skin receptors also increases and consequently comfort perception worsens.

Regardless of the magnitude of applied load, there are considerable differences between possible location of application. As a result, not all body parts are suitable for transmitting loads to the skeleton. Recommendations include [42]:

- allow a free area around joints so that they have their full range of movement,
- avoid bony prominences and tendons since bones in these areas can act as stressors and increase the likelihood of suffering injury,
- and avoid areas with surface vessels or nerves to limit the likelihood of injuries.

2.3 Interface performance evaluation techniques

Discomfort can arise from skin being repeatedly distorted under a force [8][42]. Thus, for the quantification of performance, interface migration or relative displacement is an appropriate performance parameter for this study since the moving interfaces will have a tendency to drag (pull along direction of movement) the skin. Another parameter of interest is the misalignment between the device and user joints. This parameter will quantify the kinematic mismatch between the two types of joints, which affects the performance of the brace. Interface contact force may also be measured to detect possible points of pressure concentration, which induces earlier discomfort.

Experimental studies can assess parameters that are difficult to measure with subjective questionnaires. Subjective data, recorded from the participants of the study, could easily be biased. Questionnaires with scales are usually used to gather subjective data. For example, they may ask questions about the ease of use, feeling of performance, feeling of stability or perceived comfort. The results from these questionnaires may well vary from subject to subject because of personal perception, pain thresholds and prior experience using braces. Thus, this research will propose to evaluate the experimental knee brace performance using two metrics: force and displacement.

Force sensing technology

Force at the interfaces of the device (i.e. thigh ans shank contact points) may be experimentally calculated with existing sensor technologies. Force can be experimentally acquired with force transducers, which calculate the force in function of another variable. For example, the most common type of force transducer relies on strain to calculate the force. They may also use piezoelectric materials, which relates the change in voltage to a force. Other types of transducers rely on hydraulic and pneumatic fluid movement to calculate force [44].

Force-Sensing Resistors (FSR) change resistance when the sensor material is deformed, which then influences the output voltage. FSRs are widely used to calculate forces in seating positions such as wheelchairs or automotive seats. For example, Yuen and Garrett [45] tested three different wheelchair cushions to determinate the one that had the greatest comfort and ability to decrease pressure using FSRs. The pressure data obtained from such experiments can be used to further improve the design of interfaces, by detecting the presence of pressure points and force distribution.

Tamez-Duque et al. [46] used 6 relatively large FSR (Flexiforce A401, Tekscan inc.) to acquire the forces exerted on an exoskeleton interface. These sensors were placed on a soft foam pad and then inserted between the interface and the user. They used this sensor pad to evaluate the force distribution of an able-bodied and paraplegic patient. In some instances of the walking cycle with a powered assist device, the pressure at the interface was higher than the ischemic level. From these results, the authors recommend that the use of such pressure sensing system should be used to alert paraplegic users of unsafe pressure levels. They also underlined that high pressure levels could be due to a poor fit of the device. Vidal-Verdu et al. [47] also constructed a similar apparatus but with a greater number of smaller sensors (FSR 408, Interlink Electronics Inc.). The sensor pad was used to control the movements of an industrial robot. Rathore et al. [48] measured the forces at the interfaces of an active exoskeleton by placing one FSR (FSR 400, Interlink Electronics Inc.) in every anatomical directions (anterior, posterior, medial and lateral) for all interfaces. An example of instrumentation may be seen in Figure 2.15 and Figure 2.16.

Figure 2.15: Instrumentation of Tamez et al. [46]

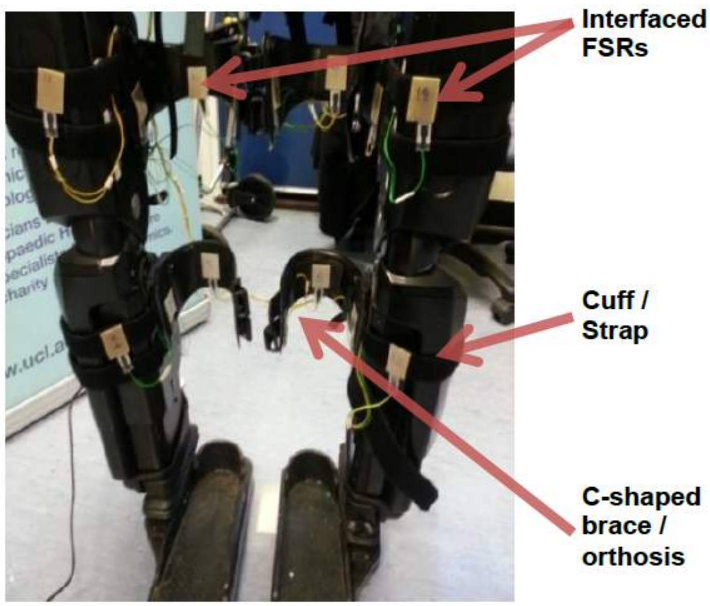

Figure 2.16: Instrumentation of Rathore et al. [48]

Motion Capture

Marker tracking in space may be done by using two or more cameras are needed in order to generate the data used for triangulation and provide the 3D position of a marker in space. Markers can be coated with a retroreflective material to reflect light that is generated near the cameras lens [49]. The 3D movement analysis that is acquired with this method can detect differences in gait pattern to improve the gait of an individual with a particular disease or in rehabilitation process. This technique will be used to track the relative movement between the brace and the user, or what will be referred as brace migration, and to tracking of the relative position between the bace and user joint centers, or what will be referred as misalignment.

Chapter 3: Methods: Brace design, fabrication and testing

This chapter introduces the design and fabrication of a novel knee brace prototype conceived for the experimental characterization of the performance of a human-machine interface. The metrics adopted to quantify performance for this study are the normal forces and relative motions occurring at the interface between the human and machine. Force mapping is used to examine the force distribution as well as quantify the magnitude of the force. Both of these are important factors for the identification of pressure points and force flow. Motion capture measurements will enable the quantification of the ability of the brace to follow the knee joint movements (kinematic compatibility) by measuring migration of the interfaces and misalignment between the device and user's joint. A modular knee brace with an extension assistance was conceptualized and fabricated such that various brace configurations and operating scenarios could be achieved and tested. The prototype was instrumented with force sensors, and motion capture technologies in order to quantify the kinetic and kinematic properties of the human machine interface.

This chapter also presents the methodology and experimental set-ups that were developed to mechanically analyse the performance of the proposed knee brace prototype and ultimately the human-machine interface performance. Various interface solutions in different configurations were designed and tested to provide insights on the biomechanics of assist device interfaces.

3.1 Passive assist knee brace design criteria

The interface mechanism for a human mobility assistive device is a critical parameter that may undermine the performance of the entire system. In this work, an experimental passive assist knee brace is designed and fabricated in house to test and analyse the performance of various interface variables which are linked to challenges faced in modern human mobility assist devices.

To achieve the objectives and to simulate real world conditions, the knee brace design must replicate the mechanical behaviour of current devices. Thus, the brace joint was chosen to be a single degree of freedom or a hinge based design, and produce a moment that is similar in magnitude to current devices. The knee brace transmits forces to the physical interfaces with an extension assist mechanism. These forces will be over the ischemic level but should not produce any pain for the participant.

To evaluate the interface mechanism performance with respect to various parameters, the prototype design must allow change of multiple physical interface variables, including: knee extension moment, interface shape, interface compliance, interface position and degree of freedom. It is essential that the brace is comfortable to wear and articulates naturally with the body but prevents abnormal movements such as hyperextension or hyperflexion. The knee brace pivot point and the human biological joint should be aligned for proper operation. The interface system should maintain the external structure in place to mitigate misalignments between the machine and user. The device should be light weight and durable, to withstand mechanical and human testing. A lighter brace translates to less downwards migration and fewer misalignments issues.

Orthopaedic manufacturing guidelines from the International Committee of the Red Cross (ICRC) [50] were followed to produce a brace which would resemble current orthotic devices. These guidelines provided information regarding important landmarks and the proper position of the brace mechanical axis during the design process.

3.2 Knee brace conceptual design

Given the design requirements, multiple conceptual designs were achieved and can be found in Appendix B.

The structure of the experimental device consists of 8 major components: thigh and shank interface support, interface padding, orthotic uprights that include the hinge joint, carbon fiber leaf springs, the clamps, interface straps and sliding rails. These components are held together with bolts, nuts and washers.

The brace performance is measured during daily physical activities while providing an extension moment and kinematic restraints similar to current human mobility assist devices. Furthermore, the design can achieve different testing conditions by varying 5 different key design variables, which are: interface position, interface padding density, interface shape, knee extension moment, and the shank interface degree of freedom.

3.3 Knee brace fabrication

The proposed knee brace prototype was fabricated in house using 3D printed components, off the shelf orthotic knee joints and uprights, padding material, fastening straps, rectangular carbon fibre strips, machined parts and fasteners. An assembled fabricated knee brace prototype can be seen in Figure 3.1.

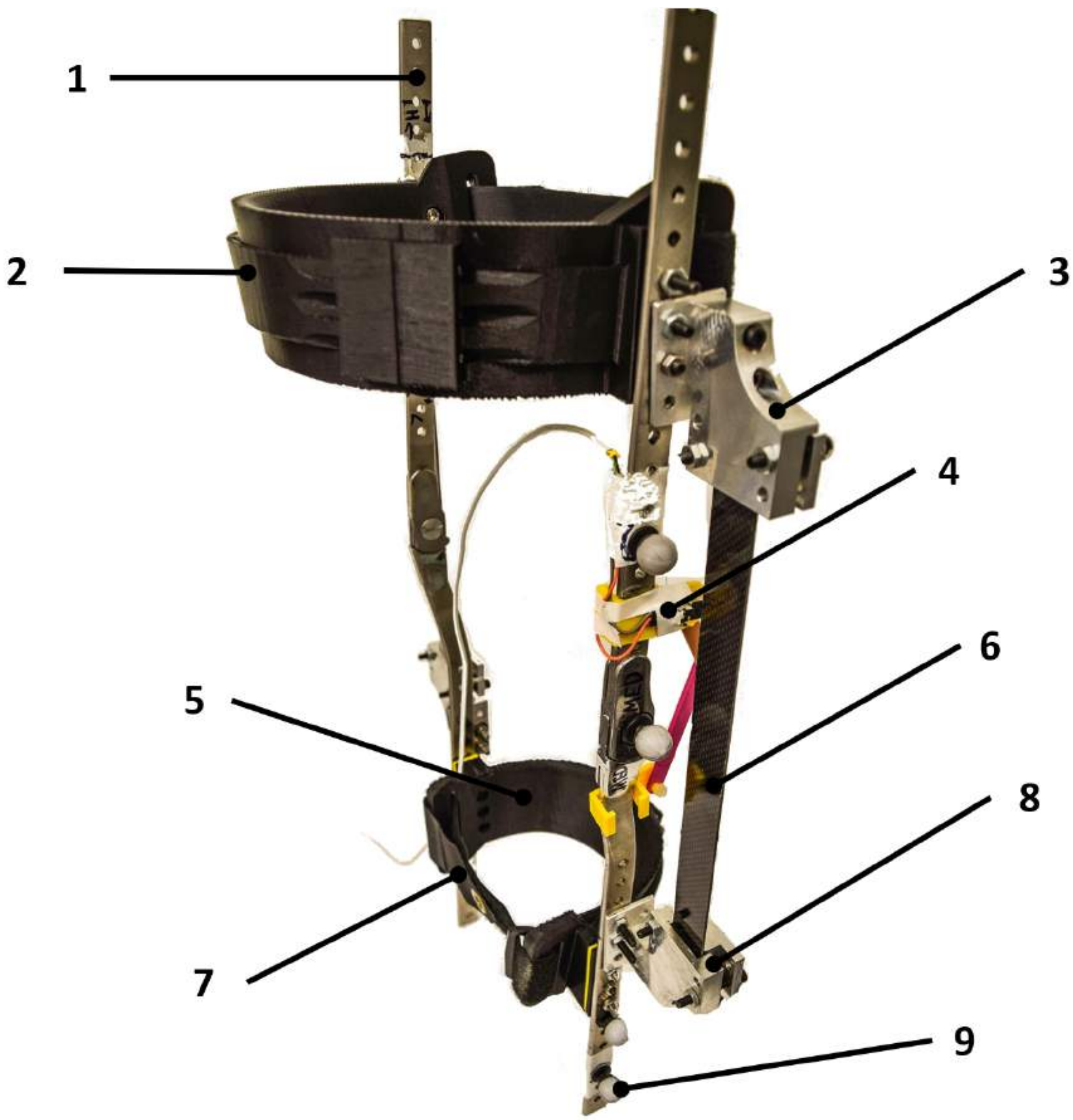

Figure 3.1: Experimental knee brace. Interfaces are in the anterior-posterior combination without padding. 1: upper orthotic upright, 2: anterior thigh interface backing, 3: upper elastic element clamp, 4: rotary potentiometer, 5: posterior shank interface backing, 6: carbon fiber strip, 7: interface strap 8: lower elastic element clamp, 9: motion capture marker on lower upright.

3.3.1 Knee upright

Stainless steel orthotic knee uprights (Becker Model 1002) with hinge joints were used. The uprights were bent so that the distal and proximal uprights became parallel. These bends were performed manually with the help of orthotic bending irons (Proline Tools, Cascade Orthopaedic Supply Inc.) and a bench top vise, to ensure proper bend curvature. Fastener holes were drilled at multiple locations to allow interface location adjustments. This was achieved with a milling machine given the precise position requirement and material strength of the steel. The uprights were cut to length based on the leg length of the participant. These modified uprights are referred to as the frame of the brace. Figure 3.2 below shows the uprights after alterations.

Figure 3.2: Stainless steel orthotic uprights

3.3.2 Extension moment mechanism

The spring element responsible for the extension moment assist was assembled using brackets designed to hold two rectangular carbon fiber sheet strips, positioned on both sides of the device.

The carbon fiber strips leaf springs (McMaster-Carr, LLC, part number 8194K12, 8194K14, 8194K16) is simple weaved and its dimensions were used to design the brackets used to hold the strip. The strips are 30 cm long and 2.5 cm wide and 0.8 and 1.6 mm thick.

The brackets were designed to hold the strips while the brace flexes, were machined out of aluminium and were designed to clamp the carbon fiber strip with a bottom and top component. Their structure can be seen in Figure 3.3 and Figure 3.4.

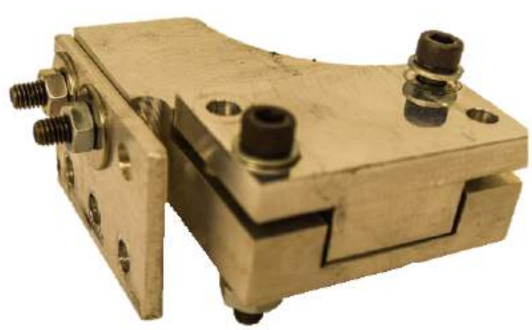

Figure 3.3: Clamping bracket with top portion

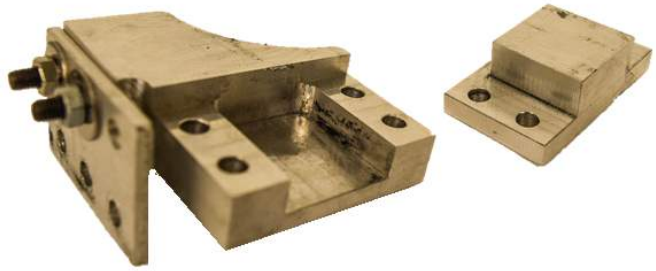

Figure 3.4: Bracket clamp top and bottom

The bracket-leaf spring assembly (spring elements) were placed in parallel with the brace, medially and laterally, to create the extension moment. Motion of the brace uprights resulted in the shortening of the distance between the attachment points of the strips, thus bending the carbon fibre strips and producing a moment that extended the brace. The stiffness of the elastic element was varied by changing the strip thickness and number of strips. The carbon fibre strips and the attachment system can be seen in Figure 3.5 and Figure 3.6.

Figure 3.5: Elastic element composed of clamping brackets and the carbon fiber strip

Figure 3.6: Elastic element mounted on uprights

3.3.3 Interface support

The medial and lateral orthotic uprights are connected together with a set of rigid thigh and shank interfaces. Fabricated using 3D printers and PLA filament, these interfaces transmit the forces between the user and the device. The interface supports are attached to the main frame of the brace with three bolts on the medial and lateral sides. Fastening strap slots were added to their structure to allow fit adjustments.

Two interface geometries were designed and fabricated, using the iterated and 3D scanner-based methods. These two different interfaces geometries were introduced in the research to see if the more complex geometry of the 3D scanner-based method is justifiable, compared to the iterated-based interfaces.

Iterated-based interfaces

The iteration method does not distinctively require many tools and is able to produce relatively good results in a short timespan. The first design geometry is based on physical measurements of the thigh and shank of the participant. To speed up the process of producing interfaces that would match the outline of the biological limb, 3D printing was used as the fabrication method. Simple curved rectangular cross section strips were printed instead of printing full pieces, which would have required greater resources and been time consuming. The outlines of the strips were compared to the biological limb at their respective location on the participant. The dimensions of the outlines where then modified until the interface outline followed the topography of the leg with satisfaction. This method required at least two iterations per interface but was time efficient since printing the outline only required a relatively short timespan (i.e. 30 min). An example of the 3D printed outlines can be seen in Figure 3.7.

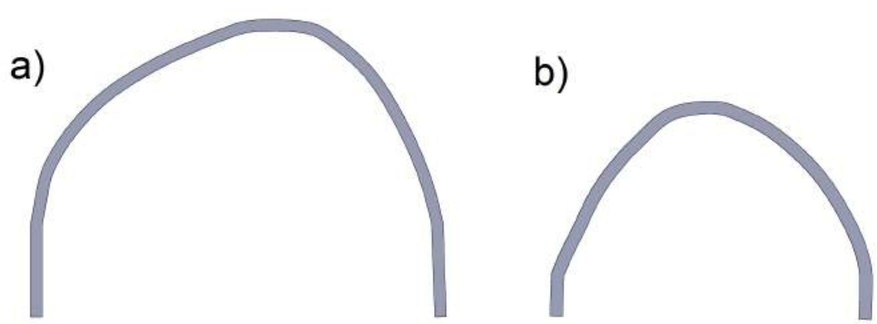

Figure 3.7: 3D model of the outlines. a) anterior thigh b) anterior shank

These interface contours were drafted with a three-dimensional modelling software (Solidworks, Dassault Systemes Inc.) spline function. After the iterations, the final interfaces were modelled and printed. The interfaces have thick sections and the addition of a ridge along the midline help stiffen the structure. This ensured that the interfaces would sustain the loading conditions throughout experimental tests. The interfaces were printed in two or three sections and then joined with fasteners to form the complete interface due to printing size limitation. More specifically, the anterior thigh interface was printed in three sections. The shape of this interface was fabricated so it would follow the topography of the quadriceps muscle group. Various views of the thigh interface can be seen in Figure 3.8.

(a) Front view

(b) Side view

(c) Top view

Figure 3.8: Different views of the anterior thigh interface

The posterior thigh interface component was created so it would push on the hamstring muscle group. This interface is less symmetric since the hamstring group sits slightly medially to the longitudinal axis of the upper leg. This interface can be seen in Figure 3.9.

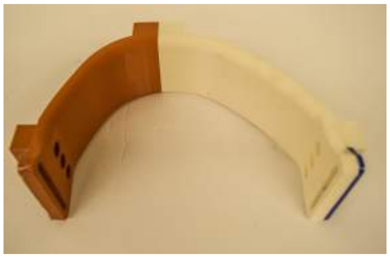

(a) Front view

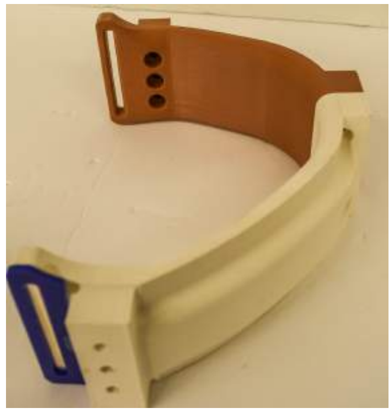

(b) Side view

(c) Top view

Figure 3.9: Different views of the posterior thigh interface

The anterior shank interface has a particular outline. Laterally, the shank surface is curved and medially it is relatively straight to match the geometry of the tibia bone and the tibialis anterior muscle. The tibia bone has a broad flat edge and is close to the skin anteriorly. The anterior tibialis has a rounded shape and is located beside the tibia, hence the transition from a straight to curved geometry. This interface can be seen in Figure 3.10.

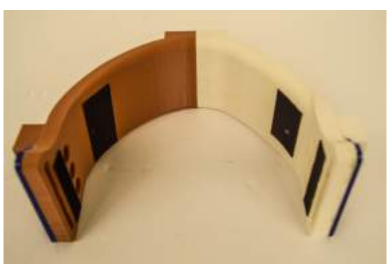

(a) Front view

(b) Side view

(c) Top view

Figure 3.10: Different views of the anterior shank interface

The posterior shank interface contacts with the calf muscle group. The shape of the calves changes considerably between the flexed and relaxed states. The geometry selected for the calves region is more suited for a relaxed state but the addition of the padding material compensates for the change in shape. This interface may be seen in Figure 3.11.

(a) Front view

(b) Side view

(c) Top view

Figure 3.11: Different views of the posterior shank interface

3D scanner based interfaces

For the 3D scanned method, a scanner and a computer were used to get the actual anatomy of the participant's leg. The resulting scan was imported into a CAD software (Solidworks, Dassault Systemes Inc.) to produce interfaces that match the natural shape of the limb surfaces. Supplemental information regarding the three-dimensional scan procedure may be found in Appendix B. The main geometrical aspect of the interfaces produced with this method is their tapered geometry.

The anterior thigh interface was printed in three sections since it was too large for a single printing session. This interface can be seen in Figure 3.12.

(a) Front view

(b) Side view

(c) Top view

Figure 3.12: Different views of the anterior thigh interface

It may be noted that the posterior thigh interface, similarly to the iterated posterior thigh interface, is asymmetric and can be seen in Figure 3.13.

(a) Front view

(b) Side view

(c) Top view

Figure 3.13: Different views of the posterior thigh interface

The anterior shank interface may be seen in Figure 3.14.

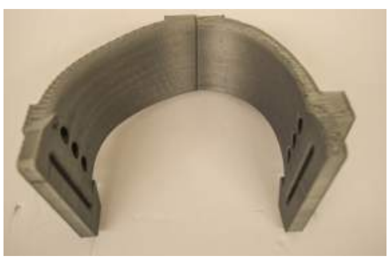

(a) Front view

(b) Side view

(c) Top view

Figure 3.14: Different views of the anterior shank interface

The posterior shank interface may be seen in Figure 3.15.

(a) Front view

(b) Side view

(c) Top view

Figure 3.15: Different views of the posterior shank interface

Details concerning the 3D printer specifications used for the printing of the different interface support sections may be found in Appendix B.

Padding materials

As part of the brace interface, the padding between the interface plate and the user was also examined. Different paddings material densities were examined to measure the effects of different padding properties on the load transfer and relative movement of the device. The interfaces were designed with an offset gap of 10 mm from the true leg geometry, allowing for padding material between the interface and user. Natural gum foam (McMaster-Carr, LLC) was chosen as the padding material, which resembles neoprene. This material is similar to the ones found in sport equipment padding or wet suit apparel, thus why it was chosen for this study. The natural gum foam was ordered in three different densities, which the supplier describes as ”ultra soft”, ”soft” and ”medium”. These three densities are characterised in Table 3.1 below. The foam strips were secured to the interfaces during testing using adhesive tape.

Table 3.1: Natural gum foam hardness specifications, from manufacturer (McMaster-Carr, LLC)

Hardness	Pressure to compress 25% (kPa)
Ultra soft	0-34.5
Extra soft	34.5-62.1
Medium	89.6-137.9

3.3.4 Shank sliding mechanism

Preliminarily experimental assessment of the brace demonstrated extensive relative motion between the user and the shank interface. Thus, for this study, a sliding shank mechanism was designed and incorporated as an additional parameter to study and analyse and to compare with the non sliding conditions. The proposed design of the sliding element consists of cylindrical metal rails and linear sleeve ball bearings. This was selected over a profiled rail guide, enclosed flat caged linear needle roller bearings or guide rollers due greater misalignment coping capabilities between the bearing and rail as well as size restrictions. Two sleeve bearings and two linear rails were used. These were attached to the brace with the use of custom-machined brackets. The shank interface was attached to the linear bearing using a 3D printed clamp. The sliding elements and its different components can be seen in Figure 3.16.

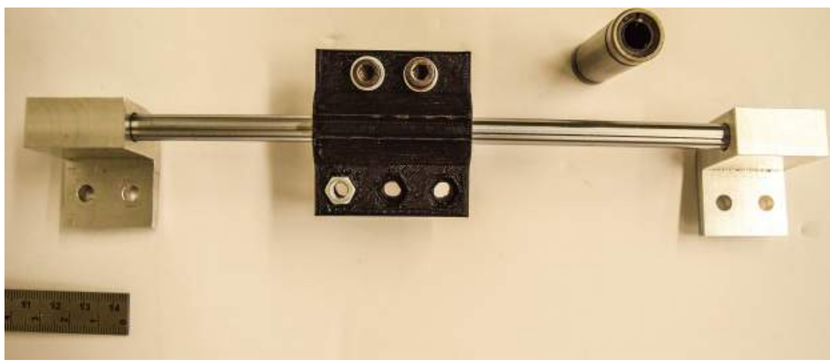

Figure 3.16: Sliding element

The rails and bearings are similar to the ones used in conventional 3D printers, making these parts readily available and inexpensive. The total travel of the interface sliding element is of 135 millimeters. The sliding mechanism mounted on the lower portion of the brace frame can be seen in Figure 3.17.

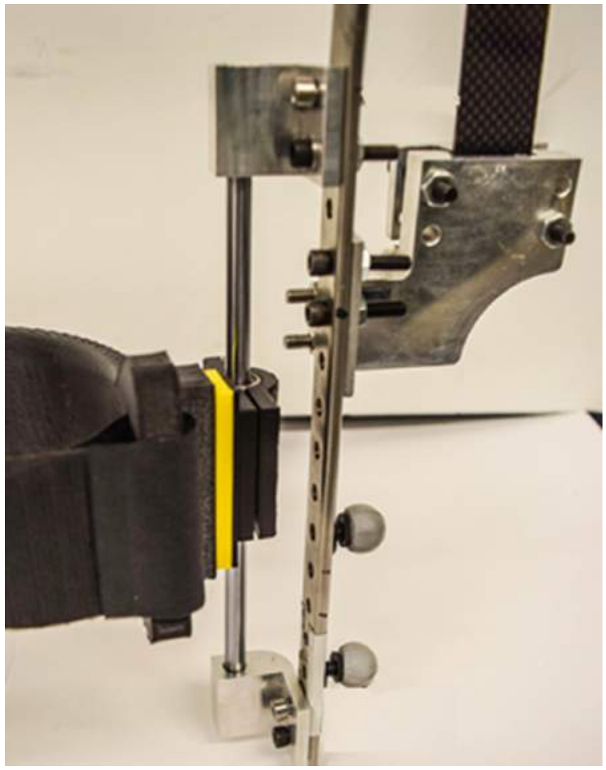

Figure 3.17: Sliding element mounted on brace frame

3.3.5 Suspension system and supplemental strap

A suspension system composed of a climbing harness and plastic covered wire cables were used in order to limit the downwards brace migration of the brace due to gravity. This was added after preliminary testing of the brace. The suspension system can be seen in Figure 3.18.

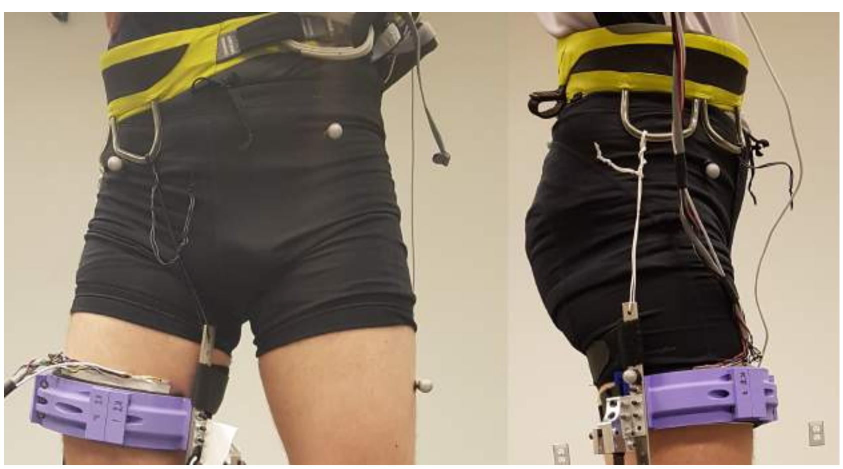

Figure 3.18: Hip suspension system

The implemented suspension system did not obstruct the view of the motion capture marker and offered an extra constraint at the hip. This solution did not affect the behaviour of the brace, other than maintaining it at the desired position when standing. Moreover, the addition of a suspension system can be justified by the fact that the weight of the device, mostly attributed to the metal frame, would be similar to assist devices since these devices also use metal as the main material for the structure of the device.

The addition of a Velcro strap on the knee brace frame located proximally and posteriorly to the thigh segment was also necessary. As shown in Figure 3.19, the interface support is in the posterior position.

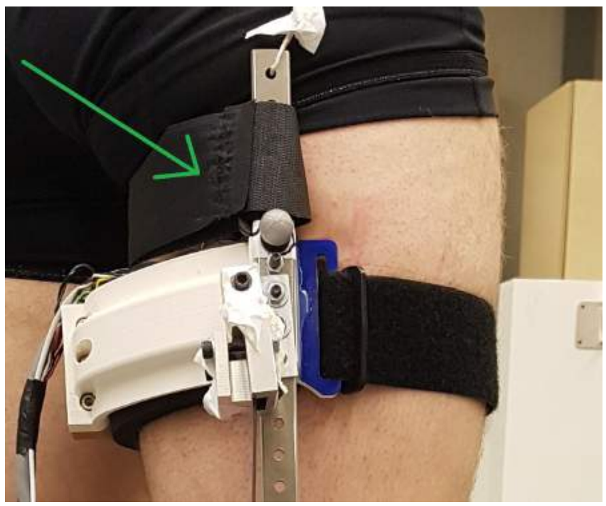

Figure 3.19: Additional strap

The additional strap created a more secure point of attachment, further stabilising the thigh interface from tilting in the sagittal plane. The high stiffness of the elastic elements produced a lot of interface tilt and downwards migration due to the resistance to flexion associated with passive assistance. was quite high and increased the angle between the leg and the brace with respect to their long axis, resulting in the tilt of the interfaces and making the edges the only point of contact with the user. The addition of the strap lowered the interface tilt and improve the interface contact.

3.4 Mechanical testing and validation

The mechanically validation consisted of an extension test using an universal linear testing machine (Instron 4482, Illinois Tool Works Inc.) to measure the brace moment produced by the elastic elements.

An aluminium block and plates secured the brace to the testing machine platform. The brace was attached to the plates, the plates were bolted to the block, and the block was bolted to the platform. The tests were conducted starting in extension rather than in flexion since starting from a straight structure risked the buckling of the prototype. Instrumentation limitations limited the range of motion between 90 to 40 degrees of flexion. The extension of the brace changed the position of the contact force on the load cell attachment as the cross-head moved upwards. The attachment was too short to allow full range of motion, or sliding of the brace for the range of extension. The prototype brace and the testing apparatus can be seen in Figure 3.20.

Figure 3.20: Knee brace in linear testing machine

With the known displacement of the machine's cross-head, the initial flexion angle and geometry of the brace, the brace angle is determined throughout the testing, using trigonometric relationships. The forces recorded by the load cell and the length of moment arm are then used to calculate the brace moment.

These tests were conducted for the variety of stiffness of the elastic element. The brace moment for the medium stiffness can be seen in Figure 3.21. The moment curves for the other degrees of stiffness can be found in Appendix C. The lowest stiffness configuration produced 2 Nm and the highest stiffness produced 23.1 Nm at 90 degrees of flexion. The lowest stiffness moment is considerably low and its resulting force could not be reliably measured with the used load cell (Instron 100 kN). The highest stiffness showed similar performance to the medium stiffness condition.

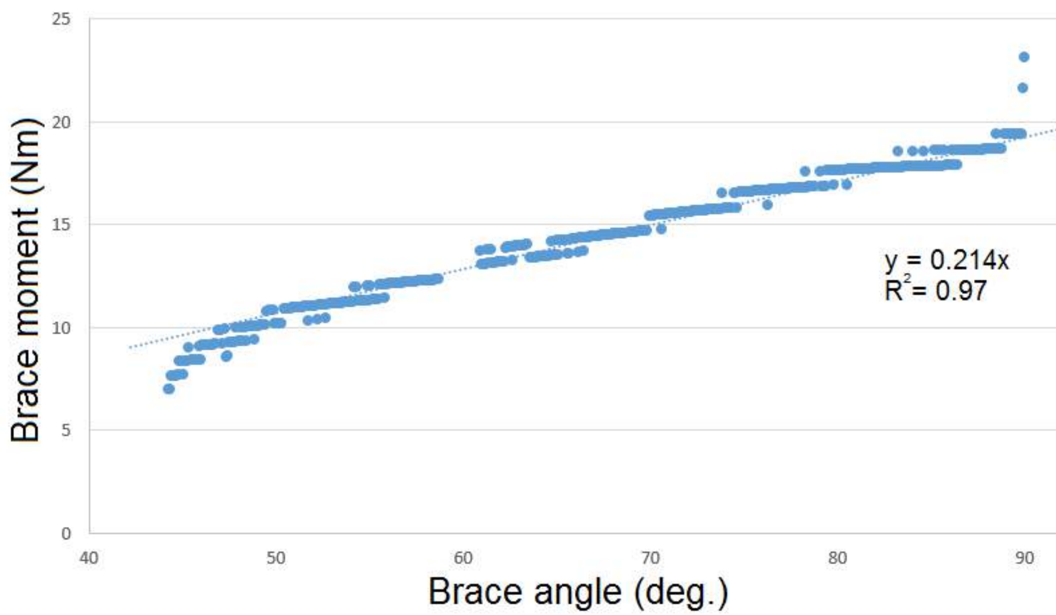

Figure 3.21: Brace moment as a function of brace angle for the medium stiffness. The brace angle is limited to this range due to limitations of the testing apparatus.

Figure 3.21 shows the linear response of the elastic element. Carbon fibers typically show a linear response when loaded in tension [51] which explains the linear relationship of the brace moment. The beginning and end of the curve show a sharp change in brace moment. This is attributed to the loss of contact of the brace with the load cell and the acceleration of the cross-head, respectively.

In the configuration where the medium stiffness was used, the device was able to produce a moment of 20 Nm at 90 degrees of flexion. At this flexion angle, a force of more than 80 N was recorded by the testing machine. As an estimate, this force distributed over the interface area is enough to surpass the blood ischemic pressure level, assuming a uniform distribution.

The brace joint moment achieved during testing is much lower than existing exoskeleton devices (e.g. BLEEX, B-Temia). However, since the device is passive, the user has to introduce an extra knee torque in order to flex the device. Active devices rely on electrical motors that do not require an input from the user. For example, designing a passive brace with a substantial assistance (e.g. 60 Nm) would offer substantial resistance in flexion and would not allow for the proper functioning of the device. The current assistance design still provides the user with a feasible assistance (e.g. 20 Nm) while permitting the proper functioning of the brace.

Chapter 4: Experimental methodology and instrumentation

This chapter introduces the methodology and instrumentation used for the evaluation of the brace during human testing. This instrumentation will measure different parameters which will be used to evaluate the brace. This Chapter first present the force sensing apparatus and brace angle detection sensor. Subsequently, the motion capture apparatus is discussed.

4.1 Knee brace instrumentation

In order to acquire and analyse the interface force magnitude and distribution, Force Sensing Resistors (FSR) were used to instrument the interface, for both iterated and 3D scanner based interfaces.

4.1.1 Flexiforce force sensors

To acquire interface force data, force sensors must be placed between the interface and the user. Thus, the sensors should be very thin and have minimal effect on the physical human-machine interaction. For this application, FSR are ideal for force mapping given they are small, thin and lightweight. There are multiple force mapping systems commercially available on the market (e.g. thin sensing sheets from Tekscan Inc.) which can easily be inserted between the physical interface and the user's limb however, they are very costly. Thus, an in-house force mapping apparatus was developed to measure the force at the interface contact surface using the same technology.

The chosen sensors (Flexiforce A301, Tekscan Inc.) are constructed of two layers of polyester film substrate. On each layer, a conductive material is applied followed by a layer of pressure-sensitive ink. Adhesive is used to laminate the two layers of substrate together to form the sensor. The sensor's electrical resistance changes in function of the applied force, thus influencing the output voltage. The sensor itself can be seen in Figure 4.1a and the basic circuitry recommended by the manufacturer can be seen in Figure 4.1b.

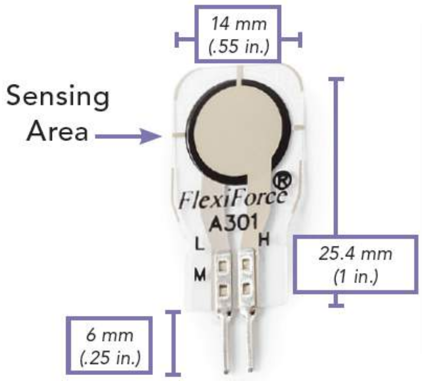

(a)

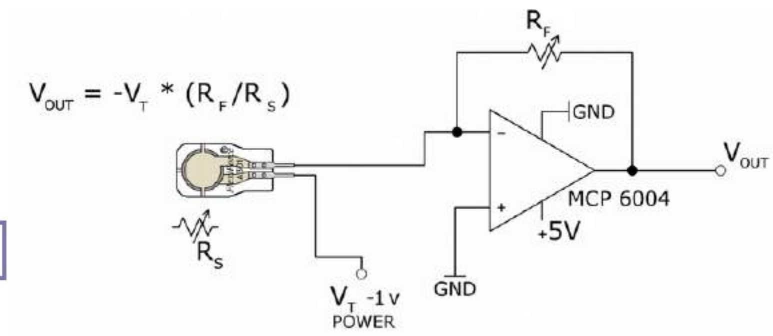

(b)

Figure 4.1: a) Actual sensor dimensions, b) Sensor circuitry (both taken from [52])

The silver circle on top of the pressure-sensitive ink defines the active sensing area. This silver material extends from this sensing area to the connectors at the other end of the sensor, forming the conductive leads [52]. The specifications of the sensors are given in Table 4.1.

Table 4.1: Typical performance of the Flexiforce sensors [52]

Linearity (Error)	<±3%	Line drawn from 0 to 50% load
Repeatability	<±2.5% of full scale	Conditioned, 80% of full force
Hysteresis	<4.5 % of full scale	Conditioned, 80% of full force
Drift	<5% (log time scale)	Constant load of 111 N (25 lb)
Response Time	<5 μsec	Impact load, recorded on oscilloscope
Operating Temp	-40°C - 60°C	Force change 0.36%/ deg C

12 Flexiforce force sensors were connected to a microcontroller (Arduino MEGA2560) following recommended electronic circuitry. Multiple integrated circuits were used for the data acquisition. More specifically, the MCP6004 was used as the operational amplifier to condition the sensor signals. This model is recommended

for the current electronic circuitry. The microcontroller supplied the positive voltage and an inverter circuit was needed to power the sensors with a negative supply voltage. To achieve this, a switch capacitor voltage converter (LTC1044) was selected and implemented to act as a negative voltage converter. The circuitry diagram of the Flexiforce sensors can be found in Appendix B.

This circuit was originally built on a breadboard then transferred over to a printed circuit board as shown in Figure 4.2. The new set-up is robust and compact which is desirable for the testing conditions.

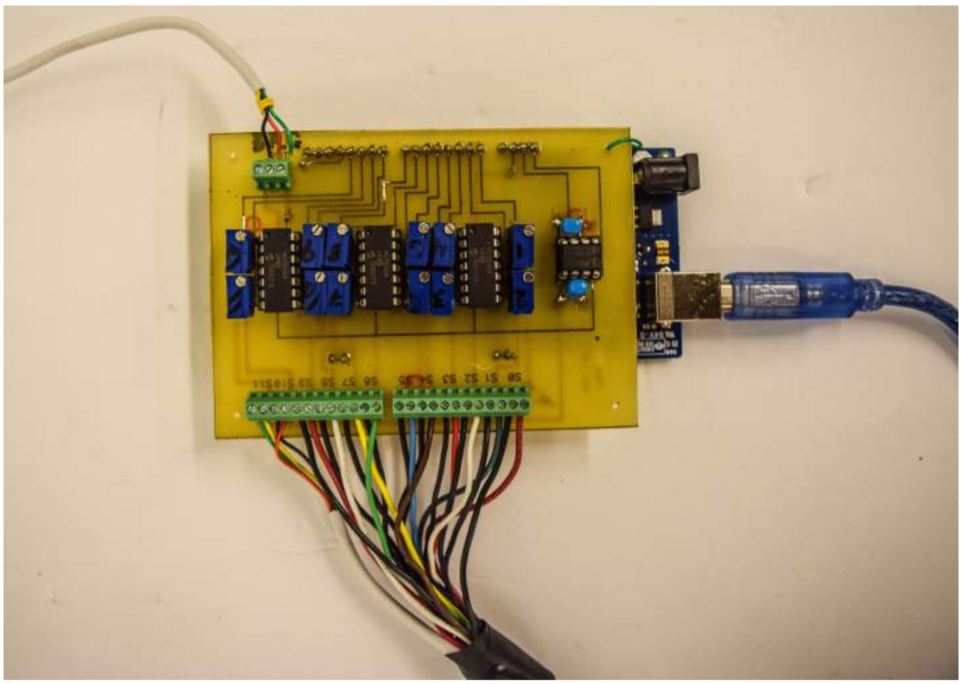

Figure 4.2: Top view of the printed circuit board connected to the top of the microcontroller

The components mounted on the board allowed for a secure connection of the sensor wires and flexibility in the circuitry for resistance adjustments. The screw terminal blocks ensure a proper connection and can easily accommodate different wire lengths. The small blue components seen in Figure 4.2 are rotational potentiometers. They have a range from zero to 200 kΩ, which allows for the fine tuning of every sensor response during calibration.

With the use of an operational amplifier, the sensor output voltage is a function of the input voltage and of the ratio of the reference resistance (R_f) and of the sensor resistance (R_s). The output voltage of the sensors must be adjusted so that it is between 0 and 5 volts to have full scale. To avoid saturation of the sensors during their usage, the circuitry was designed so that the maximal application force would produce a voltage slightly lower than the supply voltage. The sensor resistance corresponding to the estimated maximal force was recorded and used in the design of the circuitry. In order to capture forces in the lower end of the sensor's operational range (which is currently the case), higher supply voltages and reference resistances were used, as suggested by the manufacturer. Since every sensor had a slightly different behaviour, the resistances were fine tuned accordingly for each individual sensor.

As suggested by the manufacturer, the sensors were conditioned prior to calibration. Conditioning is the application of a force that would be greater than the maximal application force. This has the effect of "breaking-in" the sensors. For optimum conditioning, this force was applied multiple times. The manufacturer also suggests using thin cylindrical extrusions or pucks to help distribute the applied force over the sensing area of the sensors. The pucks used were thin discs measuring 7.6 mm in diameter, which covered 80% of the sensing area, and 1 mm in thickness. They were made by 3D printing and are a solid piece of PLA plastic.

The finished force sensing pad with the array of sensors can be seen in Figure 4.3.

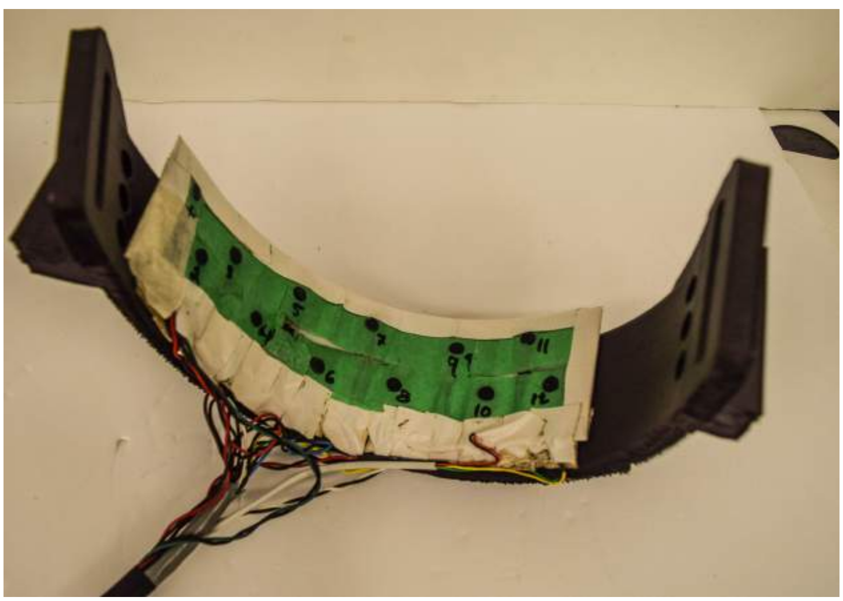

Figure 4.3: Sensor pad resting on an interface contact area

Force sensor calibration

The twelve force sensors were calibrated using a universal testing machine (Instron 4482), and a 1 kN load cell. A compression test was performed in order to acquire the voltage that was associated with a certain force. The compression test was designed so that it would stop when a certain force value was reached. The limits were set to 5, 10, 15 and 20 N (4-point calibration). This is deemed sufficient since the sensors are characterised as having a linear response. These calibration tests were carried out for all sensors. In order to avoid the sudden ramp up of force that is associated with a compression test, multiple layers of rubber were used as a base for the sensor to rest on. This ensured a smooth force transfer and minimal overshoot of the compressive force. This calibration interface can be seen in Figure 4.4.

Figure 4.4: Calibration interface made of multiple layers of rubber sheets. These layers are held down on the platform with white tape.

At the end of the test, the force was held constant for a short period of time in order to acquire the associated voltage from the sensors. This voltage was recorded with a custom Arduino script by the microcontroller and the average was performed over more than 1000 voltage data points. The sensors under the calibration test may be seen in Figure 4.5.

Figure 4.5: The 12 Flexiforce sensors under calibration test.

The linear calibration curves and equations were computed for each sensor. Pearson correlation coefficients were all above 0.9, which indicates that the curves represent the experimental data very well. The coefficients of the curves were transferred into the data acquisition script so that the data gathered from the sensors were expressed in N. The calibration curves of the 12 different sensors can be seen in Appendix E.

Sensor revisions

The selected sensors are ideally to be used on flat and hard surfaces. Their application to measure forces on a soft compliant human limb would likely introduce a certain amount of random error and inaccuracy of actual force transfer between the limb and machine. To improve the performance of these sensors, a thin polymeric sheet (flexible plastic cutting board material) was added behind the array of sensors. This was done in an attempt to influence the force flow trajectory. This means that the force would more likely be directed through the sensors themselves as opposed to simply compressing the surrounding structures. This slightly stiffer surface will concentrate more force on the sensors yielding a better response.

4.1.2 Data acquisition and processing

A custom Arduino code was written to acquire the force data. The voltage was recorded using the Arduino microcontroller and a simple serial port terminal application was used to save the data to a text file (Coolterm, Roger Meier's Freeware).

A custom MATLAB script was written to process the data from the force sensing apparatus, for both force and angle sensor. This script manipulated data from multiple experimental trials, which were stored in a 3D matrix. The data was trimmed with an experimental event, which was chosen to be 4 degrees of knee flexion from the standing position. In other words, the event starts after 4 degrees of flexion, and ends when the the knee comes back to this particular position after a whole cycle, or squat is performed. This permits the data to be normalised and then averaged. The instances of 4 degrees are used to indicate the beginning and ending of a squat cycle. These events are then fitted using a spline. The event is then reconstructed on a known base of 0-100% of a single event. Then, the average can be taken at 1% intervals. A low-pass second order Butterworth filter with a cut-off frequency of 10 Hz was used. Both scripts can be found in Appendix E.

4.2 Motion capture

Motion capture was used to track and quantify the relative motion between the user and the knee brace during the various activities of interest. The motion capture system used in this study relies on multiple infra-red cameras to track the position of light reflective markers placed on the participant lower limbs and the knee brace to determine their position in space. Using the acquired position data, the migration of the device (i.e. the displacement along the longitudinal and perpendicular axis of the leg relative to a fixed point on the brace) and the misalignment (i.e. the difference in position between the knee joint and device joint) were determined.

During experimental testing, two applications were used: Motive (NaturalPoint Inc.), to acquire raw data, and Visual3D (C-Motion Inc.) a data processing software. More information regarding the software can be found Appendix B.

4.2.1 Motion capture calibration

The protocol of the motion capture experiment started with system calibration. The calibration was performed with the calibration wand and the L-shape frame. The wand has three markers that are spaced at a distance known to the software, which it relies on to calibrate the cameras in space. The calibration is achieved after all the cameras have recorded more than 5000 frames. This yielded a highly successful calibration with sub-millimeter accuracy (mean 3D error of 0.7 mm). The L-frame was used to set the orientation of the ground plane and the coordinate axis.

4.2.2 Marker set

19 markers were used during motion capture for the creation of the Helen Hayes lower limb model. Several other markers were added to include the knee brace. The markers on the brace were positioned medially and laterally. Their positions were fixed throughout the tests.

The marker positioning and labelling was obtained from modifying the default Helen Hayes marker set. The lateral markers located at about mid-length of the thigh and shank segments of the right leg were moved anteriorly, closer to the knee joint, on their respective segments. This was necessary since the brace would cover these two markers for certain exercises. This modified shank marker location became the reference point for the shank migration computation. This was assumed as a position that would not move respective to the interface point. The knee migration was computed with the lateral femoral condyle marker. Two separate points were needed since the polycentric action of the knee joint could introduce migration of the interfaces due to the shortening of the leg.

Since the brace markers could not be associated with the skeleton segments. The brace was modelled with two rigid bodies called UpperBrace and LowerBrace. The modified marker set and the rigid bodies can be seen in Figure 4.6.

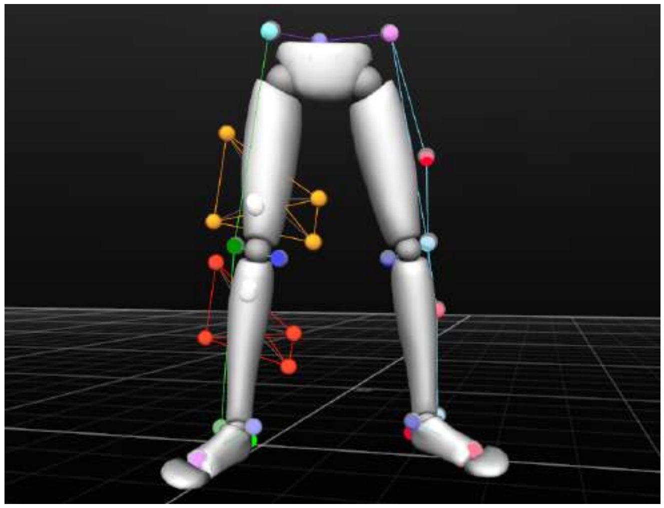

(a) Model skeleton with the rigid body markers (yellow and red)

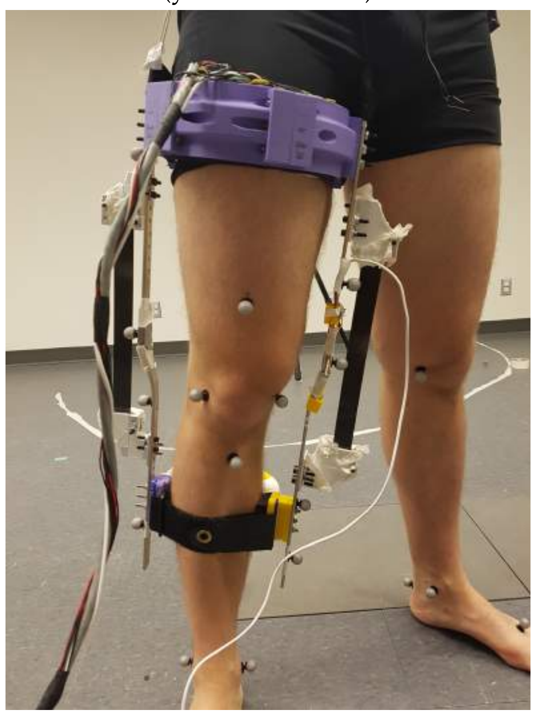

(b) Actual marker set

Figure 4.6: Digital and actual marker set used for the kinematic study

The lower and upper portions of the brace were defined with four markers each: two medial and two lateral. The upper brace rigid body had markers laterally and medially on the rotation axis, enabling the tracking of the brace angle. The maximal deformation of the rigid bodies was set to 12 mm. Smaller deformations would not allow for proper tracking of the rigid bodies since the brace, or interfaces, did flex slightly under loads from the various exercises. A table which offers details of the different markers used during the experimental testing may be found in Appendix E.

The reflective markers used were the 14-mm skin marker by Optitrack. Skin markers were used since they are directly fixed to the skin and no do not introduce artificial movement of the markers due to fabric stretching.

4.2.3 Hardware

Cameras

The gait laboratory is equipped with 16 infra-red motion capture cameras (Optitrack V100:R2, NaturalPoint Inc.). The specifications of the cameras may be seen in Appendix E.

All the cameras were spaced equally in the room walls along the same height (approximately 2 meters form the ground), except for two cameras, placed on tripods at about one meter from the ground. One of the cameras was placed in front and the other camera behind the participant. This improved the tracking of the markers when the participant performed motions that would lower the visibility of some markers. For example, hip markers were susceptible to become non-visible when performing a squat. The layout of the cameras can be seen in Figure 4.7.

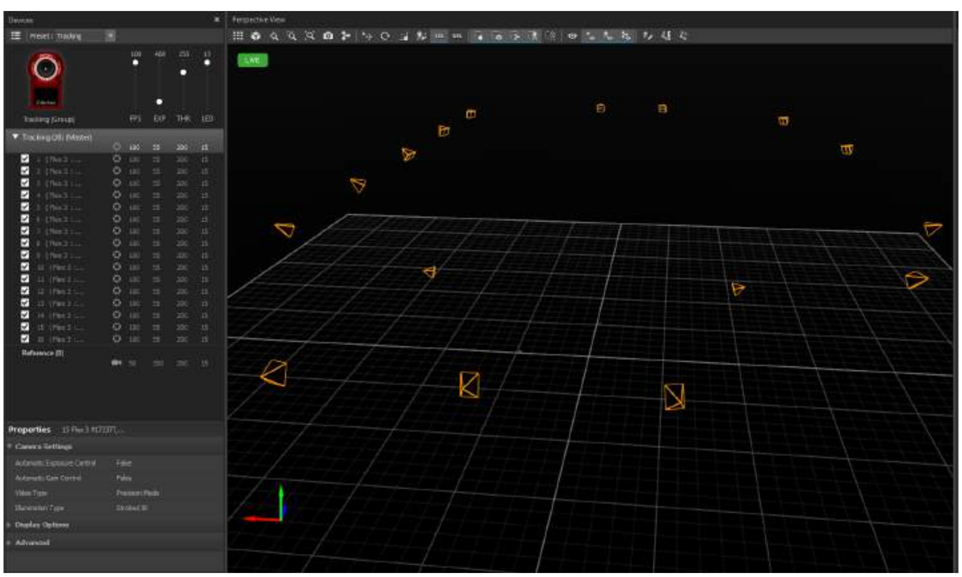

Figure 4.7: Layout of the cameras in the capture volume after calibration. The cameras are represented by the orange pyramidal shapes.

4.3 Human testing

4.3.1 Ethics approval and recruitment

The University of Ottawa Office of Research Ethics and Integrity has approved the human testing described in this section. The ethics certificate issued from the ethics board, file number H02-17-03, may be seen in Appendix E.

4.3.2 Participant and consent form

A 25-year-old male with a 168 cm height and 78 kg weight was selected from the University of Ottawa Graduate student population. The participant was required to be at least 18 years, be in good physical health, no history of lower limb injury, that would affect his ability to perform the various experimental exercises. The participant provided informed consent.

4.3.3 Exercise protocol

The subject was fitted with the prototype brace in the same manner for the various testing conditions which involved stationary exercises. The height of the brace was adjusted with the help of a belt worn over the hips and wires. When the brace was in position, the wires were tensioned to retain the position of the brace. The interface strap tension was adjusted with a dynamometer. The tension was adjusted every time the interface was taken off. The tension in every Velcro straps was set to 22 N since it was comfortable for the subject and still provided stability of the brace. Since the initial tension can affect the migration and force mapping, this standardisation lowers the variability in the results. The participant was placed at the same position in the lab environment for every test. This was achieved with the help of ground markers. The participant's foot was in-line with the X axis of the laboratory. This ensured that the limb of the participant was oriented in X-Y plane, which is the plane of interest. A visual aid (dot) was added on the wall in front of the participant in order to help align his shoulders and hip perpendicularly to this point, standardising the tests further. The experimental exercises were two-legged squat, lunge, stair descent and sit-to-stand, performed in that order. The participant was instructed to raise his arms while performing the squat, lunges and sit-to-stand so that the view of the reflective markers would not be obstructed. Moreover, the participant was instructed to perform the exercises at a comfortable speed and to be consistent as much as possible. Pauses were established between each set of exercises or whenever required so that the subject would not become tired. The squat and lunge exercises were retained if the knee flexion was over 90 degrees, the stair descent exercise always started with the same foot (right) and the sit-to-stand exercise was performed with a chair of standard height of 0.44 m. The leading leg of the lunge exercise was the right one, as the brace was placed on the right leg. The participant was asked to perform 3 sets of 5 repetitions for a specific exercise.

4.4 Experimental variables and parameters

This section presents and describes the various physical interface experimental variables for human testing and the parameters that were used to evaluate the performance of the brace, for this research.

4.4.1 Experimental variables

Presently, there are many challenges when developing or evaluating assistive devices for human mobility. To fully analyse and characterise the mechanical behaviour of the physical interface between the user and the knee brace, multiple design and operating characteristics were varied during human testing. Overall, six variables were selected for this analysis and represent the different possibilities of interface designs that are available in research or on the market. These can be grouped as Interface Variables (i.e. pertaining to the interfaces themselves), Brace Variables (i.e. pertaining to the mechanical contribution of the brace), and Testing Variables (i.e. pertaining to the physical testing of the brace). The variables are defined and described as follow:

Interface variables:

> **Interface geometry:** Two interface geometries were evaluated and compared, namely the iterated based and 3D scanner based interfaces, as earlier described in Chapter 3.
>
> **Interface Anterior-Posterior Position (APP):** Similar to presently available assist devices, the interfaces of the proposed knee brace only accommodate one solid side (either posteriorly or anteriorly). Generally, the other side of interface

is wrapped with Velcro to firmly hold the interface to the body segment. To analyse this variable, a posterior and anterior solid interface for the thigh and shank segments were fabricated. During testing, all combinations of these alternatives were tested. Positions with their respective acronyms can be seen in Figure 4.8. For the remainder of this report, the combination of pairs of interfaces will be referred by the acronyms listed in Table 4.2.

Table 4.2: APP reference table

	Thigh Anterior (TA)	**Thigh Posterior (TP)**
Shank Anterior (SA)	TA_SA	TP_SA
Shank Posterior (SP)	TA_SP	TP_SP

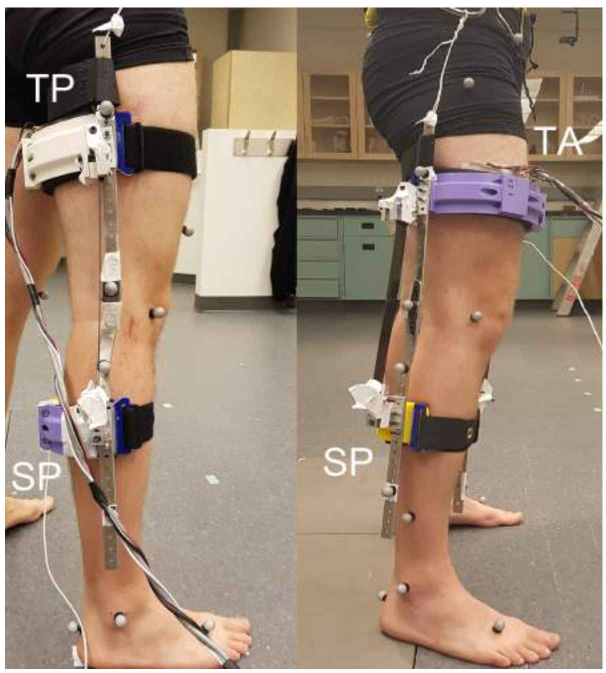

Figure 4.8: Example of APP of the interfaces. Left: TP_SP, right: TA_SP.

Interface padding: As discussed in Chapter 3, padding density has an effect on device comfort and performance. The three different padding densities will be referred as softest (Padding1), medium (Padding2) and hardest (Padding3). Unless otherwise stated, the medium padding density (i.e. Padding2) is the default variable for experimentation.

Interface Longitudinal Position (LP): The interfaces may be placed at various positions relative to the longitudinal axis of the brace structure. It is deemed critical that an interface must not be placed over a bony prominence or blood vessels, because it could lead to an uncomfortable experience. For this research, three positions where examined, namely low, mid, and high. The low and high positions of the thigh interface correspond to the distal and proximal positions to the hip joint. The same logic applied to the shank interface, with a reference to the knee joint. The mid position corresponds to the mid position of the limb (Thigh: half distance of gluteal furrow to lateral knee femoral condyle, Shank: half the distance between lateral knee tibial condyle and lateral ankle malleolus) and corresponds to the geometry of the interfaces. The distal and proximal positions are at a distance of 45 millimeters from the mid position, below or above respectively. Since three combinations were possible for each interface, nine positions were studied. For the remainder of this report, the combination of interface positions will be referred by the acronyms listed in Table 4.3. Unless otherwise stated, the mid level position is the default variable for both thigh and shank during experimentation.

Table 4.3: LP reference table

	Thigh High (TH)	**Thigh Mid (TM)**	**Thigh Low (TL)**
Shank High (SH)	TH_SH	TM_SH	TL_SH
Shank Mid (SM)	TH_SM	TM_SM	TL_SM
Shank Low (SL)	TH_SL	TM_SL	TL_SL

Brace variables:

Elastic element stiffness: The magnitude of mechanical contribution achieved by assistive devices is critical to their performance. To study this parameter, three different degrees of stiffness could be varied to achieve a range of extension moment produced about the knee. The different stiffness elements were qualitatively called Stiffness 1, Stiffness 2 and Stiffness 3, for the stiffness with the lowest, medium and highest values respectively. Unless otherwise stated, medium stiffness (i.e. Stiffness 2) for the elastic element is the default variable for experimentation.

Testing variables:

Testing exercise: Four extensive activities were selected. These activities all require a large knee flexion angle to activate the assistance from the device. These activities are the two-legged squat, lunge, sit-to-stand and stair descent. Unless otherwise stated, squatting is the default testing exercise during experimentation.

4.4.2 Experimental parameters and measurements

To comparatively evaluate the effect on results caused by modifying the aforementioned variables, kinematic and kinetic parameters were identified and measured during experimentation. Three key kinematic parameters were selected in order to evaluate the brace position with respect to the subject and two different kinetic parameters were measured while using the force mapping apparatus. The measured parameters are defined and described as follow:

Kinematic parameters:

Relative joint angle (RJA): This parameter is the difference in angle between the brace and knee joints. Relative joint angle was calculated using the three markers on the lateral side of the brace, and the measured knee angle of the subject using Visual3D default settings. Relative angle was not zeroed so that the initial difference could be observed and is with respect to the joint's own reference coordinates, in the flexion-extension plane.

Migration: The interface relative displacements with respect to the user's limbs was decomposed into parallel and perpendicular components for both the thigh and shank interfaces. The parallel direction can be associated with the rubbing of the interface against the user's limb and the perpendicular migration can be associated with the compression and loss of contact of the interface. Since both are defined as a function of the limb orientation, a vector composed of a fixed marker on the leg and a point on the interface (brace vector) was compared to a vector formed by connecting a joint and the same fixed marker (limb vector). The difference in magnitude of the brace vector represents the migration in the saggital plane of the lab. This difference was then split into the parallel and perpendicular components with respect to the limb coordinate axis to represent the migration, or the change in the brace vector length. The limb vector serves as a reference. An illustration of this can be seen in Figure 4.9. Interface migration was obtained by subtracting the initial brace vector length from the brace vector length for each subsequent frame of motion. Since the third repetition of the exercise period was chosen for the representation of the results, the curves of the graphs may not start at zero since the brace did not fully return to its initial position. The results were not zeroed, since this non-zero initial value is an indicator of the brace movement over time.

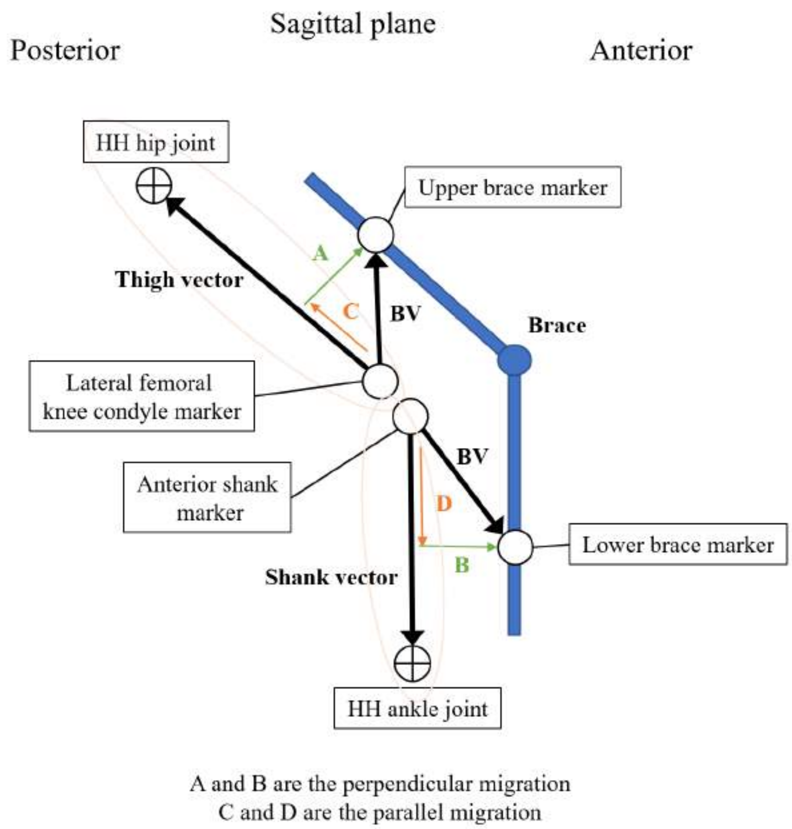

Figure 4.9: Graphical representation of the vectors used for the calculation of interface migration. The position of the brace is exaggerated to show the vectors properly. HH: Helen Hayes, BV: Brace Vector.

Misalignment: Misalignment was calculated with the difference between the position of the knee center of rotation (lower limb Helen Hayes model definition) and the position of the brace center of rotation. The magnitudes of the results represent the distance between the brace joint and the knee joint. The misalignment was decomposed in two directions: superior-inferior (SI) and anterior-posterior (AP). The data was zeroed by subtracting the initial value, which means that the results showed the relative difference in misalignment from the initial position of the two joints.

Kinetic parameters

Force magnitude: This parameter is the maximal force recorded during a test by a single sensor. This value is relatively compared to the other sensors in order to observe the relative force intensity.

Force distribution: The interface areas where the force was measured was divided into two zones: the upper and lower edge of the interface. Since a relative joint angle exist between the brace and the user, the interface tilt will concentrate the force on a particular edge of the interface.

4.4.3 Data processing and presentation of results

Following the experimental testing, the data were processed and presented to best represent each parameter. This section provides information to better understand the graphical results. The numerical signs associated with the migration and misalignment values are informative of the direction of their displacement. In the case of the thigh interface, parallel displacement is positive when the interface moves towards the hip, and negative when moving towards the knee. Perpendicular migration is positive when the interface moves posteriorly and negative when it moves anteriorly, relative to the long axis of the segment. Furthermore, a graph line slope changing from positive to negative, or vice-verse, is indicative of a change in direction.

In the case of the shank interface, parallel migration is positive when the interface moves towards the ankle and negative when moving towards the knee. Perpendicular migration is positive when the interface moves posteriorly and negative when the interface moves anteriorly, relative to the long axis of the segment. Similarly, a graph line slope changing from positive to negative, or vice-verse, is indicative of a change in direction.

The anterior-posterior and superior-inferior misalignments are relative to the natural knee joint. An increase in misalignment indicates that the device joint is moving away from the knee joint and a decrease in misalignment indicates a lesser distance between the two joints.

The third event of the experimental exercise was chosen to demonstrate and compare the results. This event was chosen since it represents the half way point, which is probably the most representative event; the subject is neither starting or ending the trial. The whole event cycle was still examined to see trends over time. The total amplitude of movement may be seen in the different figures and the results at maximum flexion is contained in the different tables. The maximum flexion frame data was chosen since it is the point where the assistance is the greatest and since it usually presented higher relative displacements. The figures show the average values and standard deviations of three trials, which was computed in Visual3D software. All motion capture trials were filtered with a second order bidirectional Butterworth filter which a cut-off frequency of 6 Hz.

The force mapping results are presented in the form of bar plots and tables. It should be noted that the values provided in the following chapter are the maximal force recorded by the sensors, irrespective of time. All results were filtered with a second order low-pass Butterworth filter with a normalised cut-off frequency of 10 Hz, then averaged over three trials. Maximal forces are presented since they reflect zones of force concentration. The force sensing pad sensor locations can be seen in Figure 5.1.

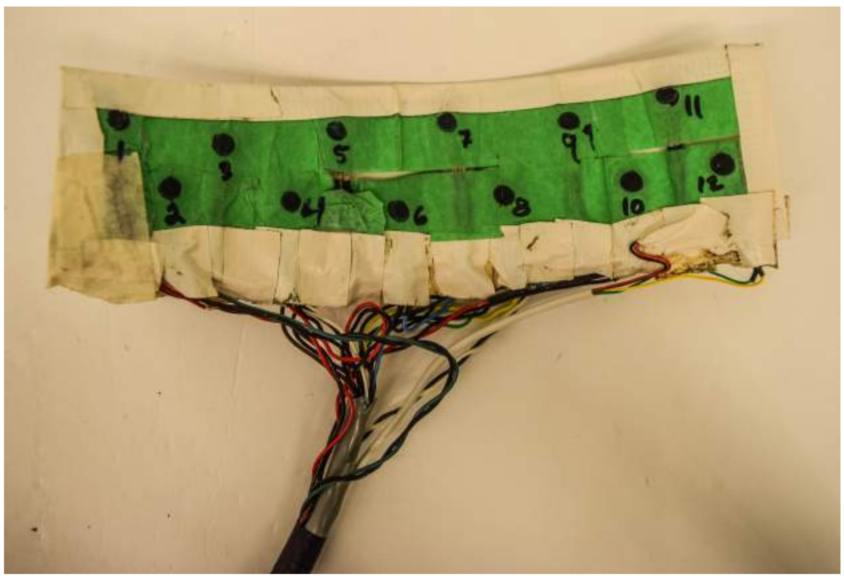

Figure 4.10: Location of the force sensors on the sensor pad

The sensor pad was inserted between the subject and the interface so the upper edge of the sensor pad corresponded to the lower edge of the interface. In other words, the lower edge of the interface is represented by sensor number 1, 3, 5, 7, 9 and 11. The lower numbered sensors represent the medial side and the higher numbered sensor represents the lateral side of the limb.

Chapter 5: Results and discussion

This chapter presents the results obtained from the experimental tests and includes a discussion of the results and other concepts in general. Throughout the tests, motion capture and force mapping data was acquired while changing one brace testing parameter and keeping all the others constant. The first sections of this paper present the kinematic results for the two types of fabricated interface, namely, iterated based and 3D scanner based interfaces. Subsequently, the kinetic results from each type of interface are presented. Lastly, the effect of adding a sliding degree of freedom at the shank interface is presented.

5.1 Kinematics

The kinematic results presented in this section correspond to the tests achieved with both types of fabricated interfaces (iterated and 3D scanner based). For each physical interface testing variables, kinematic results are presented as a function of RJA, parallel and perpendicular migration and superior-inferior misalignment.

5.1.1 Interface anterior-posterior positioning (APP)

The results for both types of interfaces at maximum flexion and their standard deviation (in parenthesis) can be found in Table 5.1 and Table 5.2.

Table 5.1: Combination analysis (iterated interfaces). Average value at maximal flexion with SD in parenthesis for the different testing conditions.

Combination Avg. (SD)	RJA (Deg.)	TM_Pa (m)	TM_Pe (m)	SM_Pa (m)	SM_Pe (m)	M_AP (m)	M_SI (m)
TA_SA	25.3 (1.2)	0.042 (0.004)	-0.055 (0.005)	0.060 (0.006)	0.021 (0.003)	0.034 (0.013)	-0.008 (0.012)
TA_SP	19.6 (0.5)	0.031 (0.005)	-0.055 (0.005)	0.050 (0.005)	0.013 (0.005)	0.003 (0.008)	0.002 (0.006)
TP_SA	17.3 (0.1)	0.037 (0.004)	-0.051 (0.002)	0.072 (0.002)	0.037 (0.009)	0.006 (0.009)	-0.039 (0.007)
TP_SP	10.3 (0.9)	0.040 (0.005)	-0.060 (0.011)	0.068 (0.001)	0.024 (0.005)	0.004 (0.004)	-0.020 (0.008)

Table 5.2: Combination analysis (3D interfaces). Average value at maximal flexion with SD in parenthesis for the different testing conditions.

Combination Avg. (SD)	RJA (Deg.)	TM_Pa (m)	TM_Pe (m)	SM_Pa (m)	SM_Pe (m)	M_AP (m)	M_SI (m)
TA_SA	16.7 (0.2)	0.017 (0.002)	-0.047 (0.001)	0.081 (0.001)	0.019 (0.003)	0.000 (0.006)	-0.055 (0.002)
TA_SP	19.5 (0.8)	0.015 (0.000)	-0.055 (0.002)	0.079 (0.004)	0.026 (0.003)	-0.007 (0.007)	-0.055 (0.006)
TP_SA	20.8 (0.6)	0.004 (0.005)	-0.029 (0.006)	0.063 (0.004)	0.014 (0.006)	-0.001 (0.009)	-0.057 (0.003)
TP_SP	18.2 (1.0)	0.027 (0.002)	-0.046 (0.002)	0.071 (0.012)	0.025 (0.004)	-0.002 (0.002)	-0.044 (0.010)

The ratio of the average of the 3D scan based interface results over the iterated based interface results at maximal flexion can be seen in Table 5.3. Numbers above 1 indicate that the 3D scanner based interfaces showed more relative movement than the iterated interfaces, and numbers below 1 are an indicator of a better performance at maximum flexion. Positive numbers translate to a movement in the same direction while negative number indicate a movement in the opposite direction.

Table 5.3: Combination analysis (interface comparison). Ratio of mean value between the two types of interface geometry.

Combination	RJA	TM_Pa	TM_Pe	SM_Pa	SM_Pe	M_AP	M_SI
TA_SA	0.65	0.40	0.84	1.35	0.89	0.10	6.64
TA_SP	0.97	0.48	0.96	1.59	2.08	-2.10	-26.00
TP_SA	1.19	0.11	0.57	0.89	0.39	-0.24	1.47
TP_SP	1.77	0.68	0.72	1.04	1.06	-0.50	2.20

The RJA for the iterated based interfaces achieved its optimum state (minimal value) when both interfaces were placed posteriorly. For this case, the average RJA at maximal flexion was of 10.3 degrees compared to the maximal RJA of 25.3 degrees achieved when both interfaces were placed anteriorly.

RJA of the 3D scanner based interfaces was lowest when both interfaces were placed anteriorly, with a value of 16.7 degrees. The results for all conditions are contained in a range of about four degrees across all the testing conditions, which can be seen in Table 5.2. This suggests that the different interface combinations had little effect on the RJA for this particular interface geometry compared to the iterated interface version which had a greater range of RJA. This range can be seen in Figure 5.1.

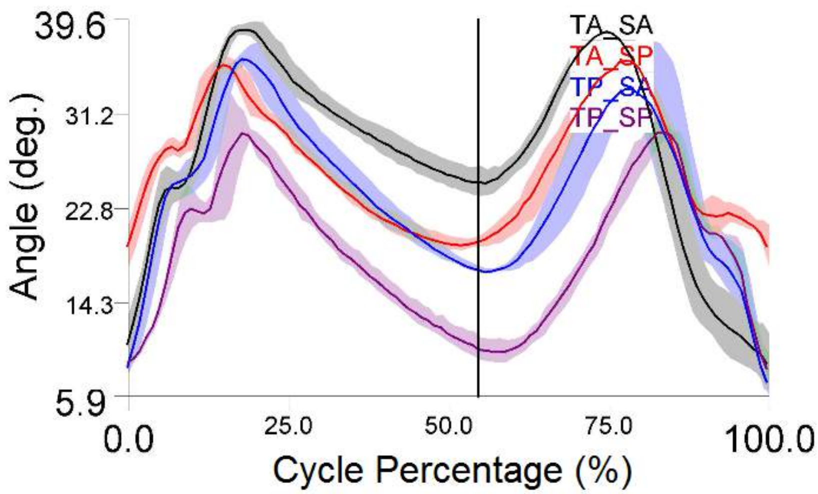

Figure 5.1: RJA (Iterated APP analysis). Mean and SD of squat exercise.

Thigh migration of the iterated based interfaces had similar results across the different combinations. As shown in Table 5.1, the results for all conditions are contained in a range of about 15 mm across all testing conditions.

The thigh parallel migration of the 3D scanner based interfaces had the greatest amplitude when both the thigh and shank interfaces were in the posterior position, with a value of 27 mm. The best result was obtained in the TP_SA configuration, with a value of 4 mm, on average, at maximum flexion. The TP_SA condition has the lowest amount of thigh perpendicular migration. This particular condition had an improvement of 36% over the second-best performance, when both interfaces were placed posteriorly. The migration of this condition can be seen in Figure 5.2.

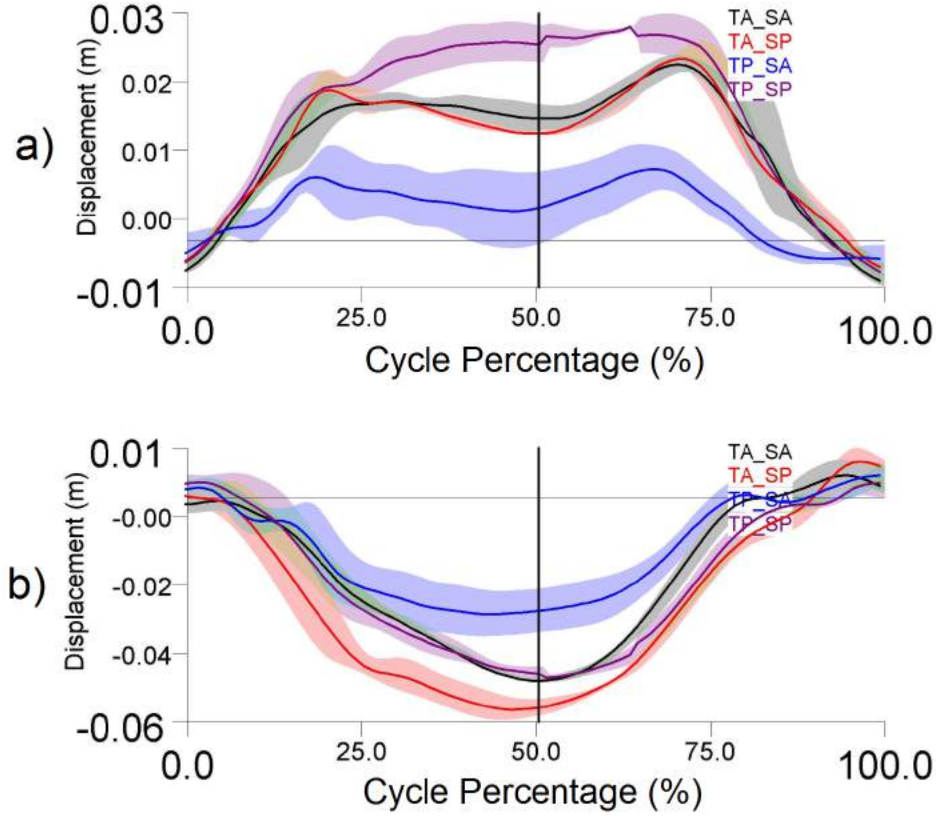

Figure 5.2: Thigh interface migration (3D scanner based APP analysis). Mean and SD of squat exercise. a) parallel b) perpendicular.

Shank migration of the iterated interfaces was the least pronounced when the interfaces were in the TA_SP configuration, in both the parallel and perpendicular directions. Displacements in the parallel direction varied between 50 and 68 mm and between 13 and 37 mm in the perpendicular direction. On average, the parallel and perpendicular migrations were 17 % and 38% less than the second-best performing testing condition, respectively.

Both the performance of the thigh and shank iterated based interfaces was improved when the other interface was in the anterior position. The anterior position implies that the assistance force is transmitted through the strapping portion of the interface and is less stable. Relative movement occurred more easily because of this aspect and thus less relative movement occurred for the posterior interface position.

The shank migration of the 3D scanner based interfaces had a similar behaviour for all conditions in both the parallel and perpendicular migration. The TP_SA condition had the lowest amount of relative movement. This particular position had an improvement of about 11% and 44% over the second-best performance for parallel and perpendicular migration respectively, averaged at maximum flexion. Figure 5.3 shows the results of the shank interface migration in the perpendicular directions for both interface geometries.

Both the thigh and shank 3D scanner based interfaces had better performance in the TP_SA condition. This is most likely due to the fact that this particular interface geometry had a greater limb adherence and was not as affected by the instability of the anterior interface position compared to the iterated interface geometry.

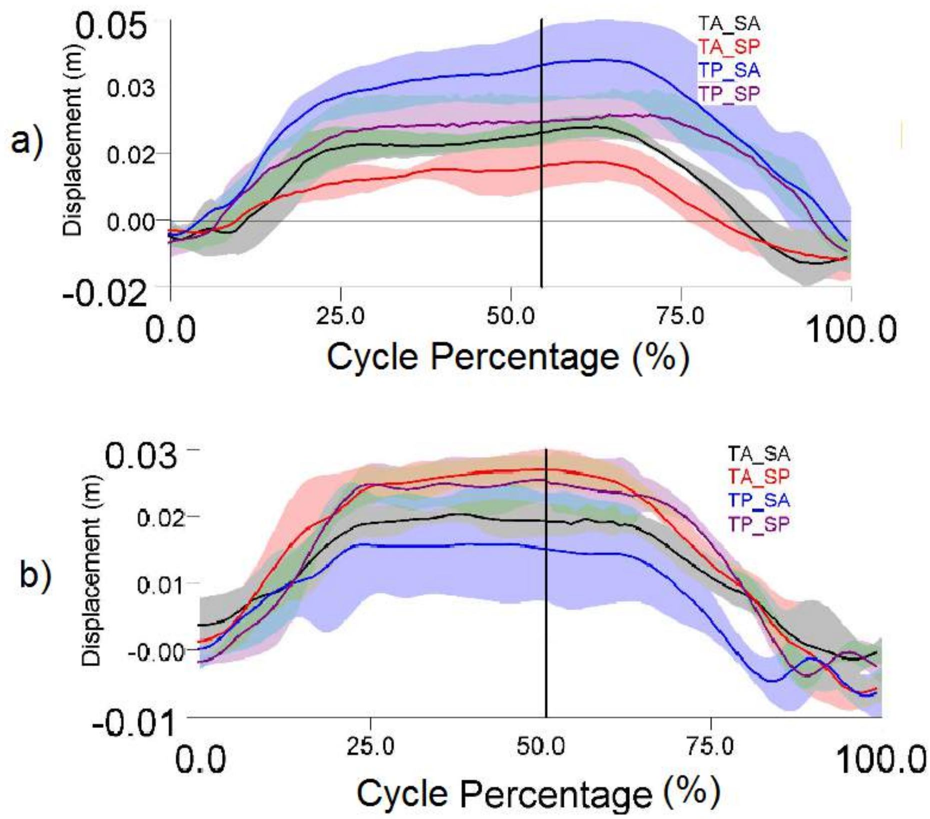

Figure 5.3: Shank perpendicular migration (APP analysis). Mean and SD of squat exercise. a) iterated geometry b) 3D geometry.

Joint misalignment for the iterated based interfaces in the anterior-posterior direction was similar for most conditions; however, the highest amplitude was recorded when both interfaces were positioned anteriorly with a value of 34 mm on average. Misalignment in the superior-inferior direction was the greatest in the TP_SA configuration with a value of 39 mm. The misalignment in the superior-inferior direction at maximum flexion were contained within a range between 2 and -39 mm. The condition where the interfaces are both positioned anteriorly presents the greatest standard deviation, which would indicate that this condition is the least reproducible or the least stable. The forces transmitted to the limb is through the interface straps, which are less stable than the rigid interfaces bodies for the brace design used in this thesis.

The anterior-posterior misalignment for the 3D scanner based interfaces was contained between 0 and -7 mm and the superior-inferior misalignments was all contained in a range of 13 mm on average at maximum flexion. The misalignments were similar, with the greatest amount for the TA_SP condition in the anterior-posterior direction. Figure 5.4 demonstrates the superior-inferior misalignment of both interface geometries.

For most testing conditions, the least amount of relative movement was observed when at least one or both interfaces were positioned posteriorly. This would suggest that the rigid portion of the interfaces should be placed posteriorly when a extension assistance is present. In other scenarios (i.e. flexion assistance) the rigid portion would perhaps not have the best performance in the posterior position. The anterior-posterior positioning of the interfaces is dependant on the assistance strategy.

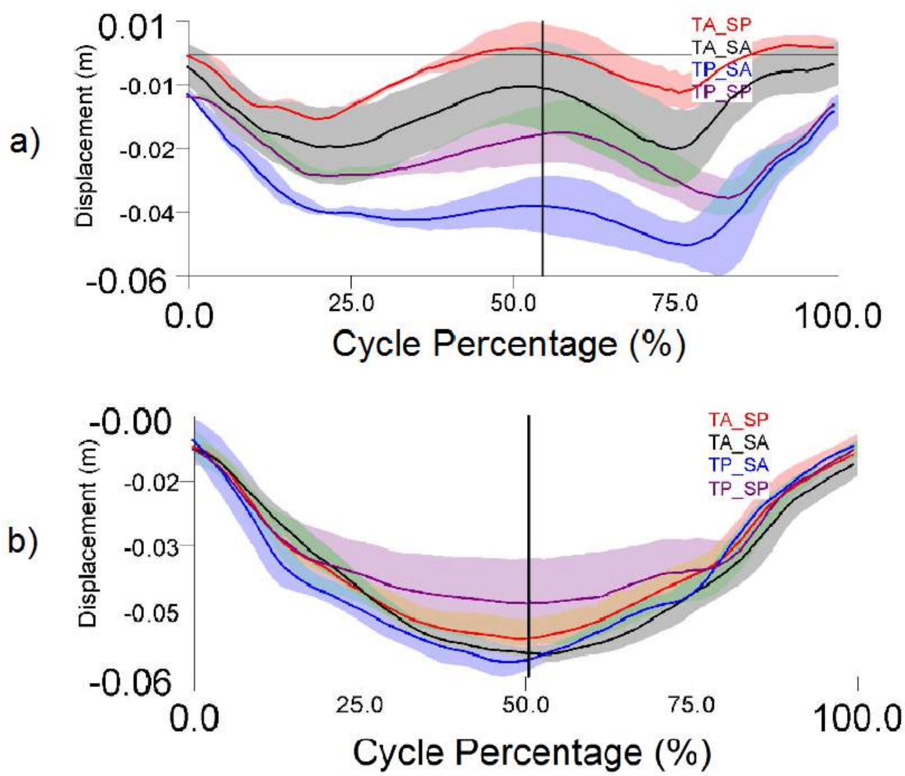

Figure 5.4: Joint SI misalignment (APP analysis). Mean and SD of squat exercise. a) iterated geometry b) 3D geometry.

Table 5.3 demonstrates that the RJA was generally higher with the 3D scanner based interface geometry. This table also shows the improvement of the 3D scan based interface for the thigh interface migration while having lesser performances for the shank interface migration. The misalignment was generally higher with the 3D scanner based interface geometry for the different combinations. All other graphs for the interface APP variable can be found in Appendix C.

5.1.2 Exercise analysis

The movement of a lunge, squat, sit-to-stand and stair at maximum flexion and their standard deviation (in parenthesis) can be found in Table 5.4 and Table 5.5.

Table 5.4: Exercise analysis (iterated interfaces). Average value at maximal flexion with SD in parenthesis for the different testing conditions.

Movement Avg. (SD)	**RJA (Deg.)**	**TM_Pa (m)**	**TM_Pe (m)**	**SM_Pa (m)**	**SM_Pe (m)**	**M_AP (m)**	**M_SI (m)**
Squat	19.1 (0.2)	0.025 (0.006)	-0.062 (0.007)	0.005 (0.004)	0.074 (0.002)	-0.006 (0.008)	-0.017 (0.005)
S Descent	24.9 (1.0)	0.033 (0.002)	-0.048 (0.007)	-0.013 (0.002)	0.084 (0.001)	-0.007 (0.008)	0.014 (0.001)
STS	23.2 (0.7)	-0.041 (0.003)	0.055 (0.001)	0.007 (0.002)	-0.092 (0.004)	-0.010 (0.003)	0.077 (0.001)
Lunge	17.6 (0.2)	0.016 (0.002)	-0.034 (0.009)	0.060 (0.003)	0.037 (0.014)	0.013 (0.009)	-0.035 (0.007)

Table 5.5: Exercise analysis (3D interfaces). Average value at maximal flexion with SD in parenthesis for the different testing conditions.

Movement Avg. (SD)	**RJA (Deg.)**	**TM_Pa (m)**	**TM_Pe (m)**	**SM_Pa (m)**	**SM_Pe (m)**	**M_AP (m)**	**M_SI (m)**
Squat	17.4 (0.4)	0.011 (0.005)	-0.044 (0.004)	0.077 (0.003)	0.015 (0.004)	-0.002 (0.003)	-0.050 (0.007)
S Descent	23.8 (3.0)	0.037 (0.002)	-0.039 (0.009)	0.088 (0.011)	0.030 (0.013)	0.016 (0.018)	0.011 (0.006)
STS	14.9 (3.1)	-0.028 (0.009)	0.047 (0.006)	-0.092 (0.021)	-0.062 (0.006)	0.030 (0.009)	0.101 (0.018)
Lunge	16.7 (0.5)	0.005 (0.006)	-0.024 (0.004)	0.072 (0.006)	0.053 (0.003)	-0.037 (0.004)	-0.074 (0.003)

The ratio of the average results at maximal flexion of both interface geometries can be seen in Table 5.6.

Table 5.6: Exercise analysis (interface comparison). Ratio of mean value between the two types of interface geometry.

Movement	RJA	TM_Pa	TM_Pe	SM_Pa	SM_Pe	M_AP	M_SI
Squat	0.88	0.44	0.74	14.44	0.20	0.33	2.92
S Descent	0.93	1.22	0.81	-7.49	0.35	-2.32	0.71
STS	0.58	0.71	0.85	-13.80	0.67	-2.72	1.32
Lunge	0.93	0.33	0.77	1.22	1.43	-3.08	2.12

The RJA of the iterated interface geometry was on average higher as a function of the following exercises at maximum flexion: lunge, squat, sit-to-stand and stair descent. The associated RJA values are 17.6, 19.1, 23.2 and 24.9 degrees, respectively. The RJA of the 3D scanner based interfaces was of 14.9, 16.7, 17.4 and 23.8 degrees for the sit-to-stand, lunge, squat and stair descent exercises, respectively. These values show the small improvements of the tapered geometry.

The iterated based thigh interface parallel migration at maximum flexion was the highest for the sit-to-stand exercise, with 41 mm of displacement, and was the lowest for the lunge exercise, with 16 mm of displacement on average. Perpendicular migration of this interface was between 55 and -62 mm, for the sit-to-stand and the squat exercise respectively.

The 3D scanner based thigh interface parallel migration was 9 mm greater for the stair descent compared to the sit-to-stand exercise, which had the second-best performance. The lowest amount of thigh interface parallel migration was of 5 mm for the lunge exercise. The thigh interface perpendicular migration also had the lowest amount of displacement with a value of 24 mm for the lunge exercise, which corresponds to 55, 61 and 51 percent of the migration of the squat, stair descent and sit-to-stand exercise respectively (for the averaged migration value at maximum flexion).

The thigh interface parallel and perpendicular migration was generally lower for the 3D scanner based interfaces, with exception to the stair descent exercise. The migration of the 3D scanner based interfaces represented 33 to 85% of the migration of the iterated based interfaces. The migration of the different exercises can be seen in Figure 5.5.

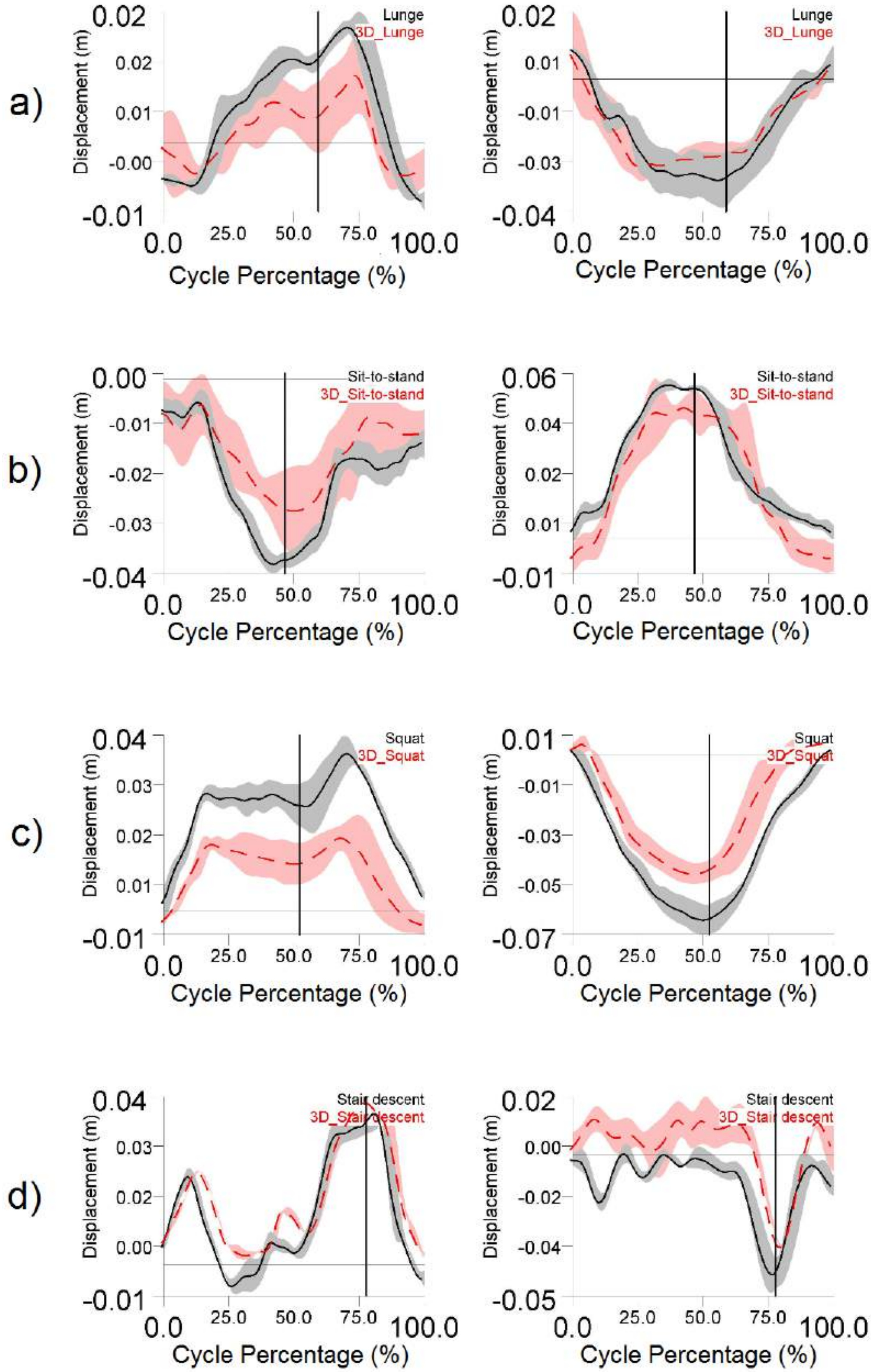

Figure 5.5: Thigh interface migration (3D scanner based exercise analysis). Mean and SD of the different exercises. Left and right columns represent the parallel and perpendicular migrations respectively. a) lunge, b) sit-to-stand, c) squat, and d) stair descent.

The parallel migration of the iterated based shank interface caused by the lunge was higher than the other exercises. On average, the lunge exercise produced about 4.5 times more parallel migration than the stair descent exercise, which has the second-best performance. The perpendicular migration was noticeably lower for the lunge exercise, with 37 mm of displacement compared to 74 mm for the squat exercise, which had the second-best performance.

The 3D scanner based shank interface parallel migration had a similar curve profile for the sit-to-stand, lunge and squat exercises. The lunge and squat exercises showed the lowest amount of movement, with 72 and 77 mm, which equates to 6.5% difference between both amplitudes at maximum flexion. The highest migration was achieved by the sit-to-stand exercise, with a value of 92 mm. Shank perpendicular migration had the lowest result for the squat exercise with 15 mm on average at maximum flexion. This was the best performance compared to values of 30 mm for the stair descent and 62 mm for the sit-to-stand (which showed the lowest performance). Figure 5.6 shows the shank interface migration for the two different interface geometries.

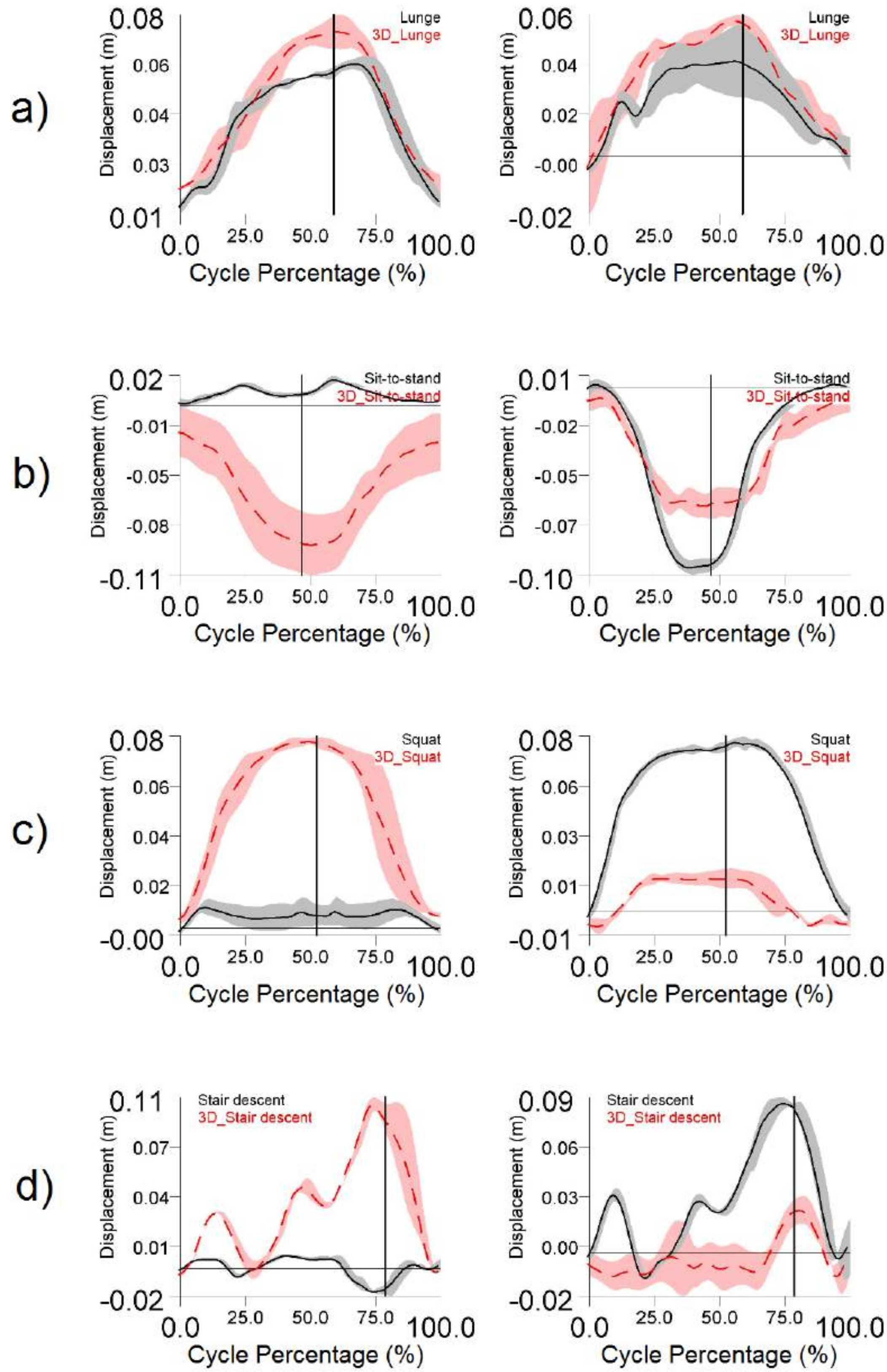

Figure 5.6: Shank interface migration (3D scanner based exercise analysis). Mean and SD. Left and right columns represent the parallel and perpendicular migrations respectively. a) lunge, b) sit-to-stand, c) squat, and d) stair descent.

The anterior-posterior misalignment associated with the iterated based interface geometry was similar for the squat, stair descent and sit-to-stand exercise, with values of -6, -7 and -10 mm. The lunge exercise had a misalignment in the opposite direction, with a value of 13 mm. The iterated based interface superior-inferior joint misalignment was noticeably higher for the sit-to-stand exercise, with a value of 77 mm of misalignment.

The anterior-posterior misalignment for the 3D scanner based interfaces had the lowest value for the lunge exercise, with -37 mm, indicating that the joint moved anteriorly for this particular direction. The greatest increase in anterior-posterior misalignment was seen during the sit-to-stand exercise, with 30 mm of movement posteriorly. The superior-inferior misalignment was noticeably higher for the sit-to-stand exercise. The increase in superior-inferior was of 101 mm for this particular position. The stair descent exercise showed the lo amount of movement in this particular direction with 11 mm at maximal flexion, on average. Similar to the iterated based interface, the sit-to-stand exercise shows a noticeable difference in results for the superior-inferior misalignment.

Table 5.6 showed lower relative movement when using 3D scanner based interfaces, for the RJA, thigh interface migration and for the shank interface perpendicular migration, for most or all exercises. Shank interface parallel migration and most misalignments showed more relative movement with the 3D scanner based interfaces.

All exercises with exception to the stair descent had a similar profile of migration and misalignment since they had relatively the same amount of knee flexion and the same flexion speed. The inertial effect and the different kinematics of the stair descent exercise could have contributed to the greatest values associated with some of the trials, even with a lower knee flexion.

The higher result amplitude during sit-to-stand could have been due to the brace moment at the initial exercise instant. This would have had the effect of pushing the brace interfaces and joint away from the leg of the participant. When relaxed and sitting, the thigh may deform by a relatively large amount. This could have influenced the initial position of the interface relative to the thigh segment, allowing for further relative movement of the brace and therefore affecting the misalignment values. Furthermore, the suspension system, described in Chapter 3 might not have been as efficient since the sitting position did not engage the system and could have affected the starting position of the brace.

The greater values associated with the lunge parallel migration may be attributed to the fact that more weight was applied to the reference leg, influencing the muscle contraction, and perhaps also by the fact that the tibia segment is kept more upright during the exercise. This upright angle offered less friction resistance to parallel migration since the weight of the device was not as well-supported. All other graphs for the exercise analysis can be found in Appendix C.

This analysis suggest that the interface system should also be designed in function of the operating exercise. The interfaces could be tailored to specific exercises. for example, an assist device mainly design to assist the user while performing a lunge, should place more emphasis on the shank interface. This analysis also suggest that the 3D scanner based interface geometry provided a thigh interface that was more stable than the thigh interface iterated geometry. Although, the performance of the shank interface was decreased when using the 3D scanner based interface geometry. The different interface geometries present advantages and disadvantages for the different performance parameters.

5.1.3 Padding analysis

The results for both types of interfaces at maximum flexion and their standard deviation (in parenthesis) for the squat exercise can be found in the Table 5.7 and Table 5.8.

Table 5.7: Padding analysis (iterated interfaces). Average value at maximal flexion with SD in parenthesis for the different testing conditions.

Padding Avg. (SD)	**RJA (Deg.)**	**TM_Pa (m)**	**TM_Pe (m)**	**SM_Pa (m)**	**SM_Pe (m)**	**M_AP (m)**	**M_SI (m)**
P1	19.2 (2.2)	0.039 (0.001)	-0.069 (0.006)	0.025 (0.007)	0.074 (0.004)	0.016 (0.010)	-0.002 (0.008)
P2	21.5 (0.5)	0.040 (0.003)	-0.069 (0.003)	0.027 (0.004)	0.075 (0.004)	0.017 (0.005)	-0.006 (0.004)
P3	19.1 (0.6)	0.029 (0.003)	-0.065 (0.003)	0.017 (0.001)	0.058 (0.002)	0.003 (0.005)	0.000 (0.003)

Table 5.8: Padding analysis (3D interfaces). Average value at maximal flexion with SD in parenthesis for the different testing conditions.

Padding Avg. (SD)	**RJA (Deg.)**	**TM_Pa (m)**	**TM_Pe (m)**	**SM_Pa (m)**	**SM_Pe (m)**	**M_AP (m)**	**M_SI (m)**
P1	19.9 (0.7)	0.017 (0.002)	-0.052 (0.002)	0.075 (0.005)	0.021 (0.001)	-0.016 (0.003)	-0.051 (0.002)
P2	17.6 (0.7)	0.017 (0.003)	-0.040 (0.004)	0.070 (0.004)	0.003 (0.003)	0.001 (0.005)	-0.046 (0.002)
P3	17.3 (1.6)	0.011 (0.004)	-0.050 (0.001)	0.062 (0.004)	0.024 (0.005)	-0.027 (0.003)	-0.045 (0.004)

The ratio of the average results at maximal flexion of both interface geometries can be seen in Table 5.9.

Table 5.9: Padding analysis (interface comparison). Ratio of mean value between the two types of interface geometry.

Padding	RJA	TM_Pa	TM_Pe	SM_Pa	SM_Pe	M_AP	M_SI
P1	1.01	0.47	0.76	2.95	0.29	-1.04	25.33
P2	0.80	0.43	0.60	2.63	0.04	0.06	8.18
P3	0.88	0.39	0.79	3.70	0.42	-11.57	-45.00

The RJA at maximum flexion of the iterated based interfaces had similar results across the different padding conditions. The results associated with this parameter may be seen in Table 5.7.

The RJA associated with the 3D scanner based interfaces had similar curve profiles and values at maximum flexion for the different padding densities. When referring to Table 5.8, the padding with highest density shows a marginal improvement of 13% and 2% over the low and medium density padding respectively, on average. Table 5.9 show that the tapered aspect of the 3D scanner based interfaces had similar or improved RJA over the iterated based interfaces.

The thigh interface parallel migration can be seen in Figure 5.7.

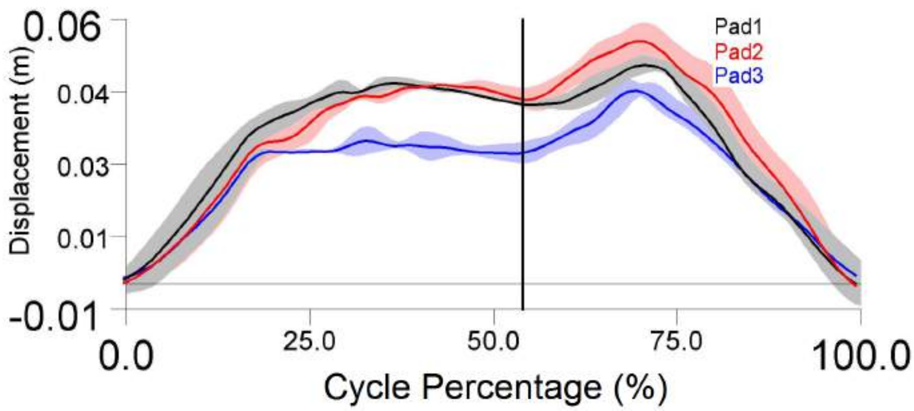

Figure 5.7: Thigh interface parallel migration (iterated based interfaces padding analysis). Mean and SD of squat exercise.

Referring to Figure 5.7, Padding 3 has the lowest amount of parallel migration, with 29 mm of relative movement. This represents about a 25% decrease in movement over the other two paddings. Besides this particular result, thigh migration at maximal flexion was similar for the other two padding densities and their respective values can be seen in Table 5.7.

The thigh interface parallel migration for the 3D scanner based geometry was the same, on average, between Padding 1 and Padding 2. Padding 3 showed less migration by 6 mm over the other two, with a difference of 35 %. The perpendicular thigh interface migration had similar results for Padding 1 and Padding 3, with values of 53 and 50 mm respectively. The best performance was observed when Padding 2 was used, with a value of 40 mm.

The padding with high density (Padding 3) showed less parallel migration for the iterated shank interface geometry, with a value of 17 mm, compared to 25 and 27 mm, when using Padding 1 and Padding 2, respectively. The maximal and minimal values of the perpendicular migration were of 75 and 58 mm, respectively. The lowest value was achieved when using Padding 3.

The parallel migration of the shank interface for the 3D scanner based geometry had the best performance when Padding 3 was used. On average, this condition showed and improvement of 17% and 11% over Padding 1 and Padding 2 respectively. Shank perpendicular migration was the lowest when Padding 2 was used. This particular padding showed 3 mm of perpendicular migration, compared to 21 and 24 mm of migration for Padding 1 and Padding 3 respectively, on average. The perpendicular shank interface migration for both interface geometries can be seen in Figure 5.8.

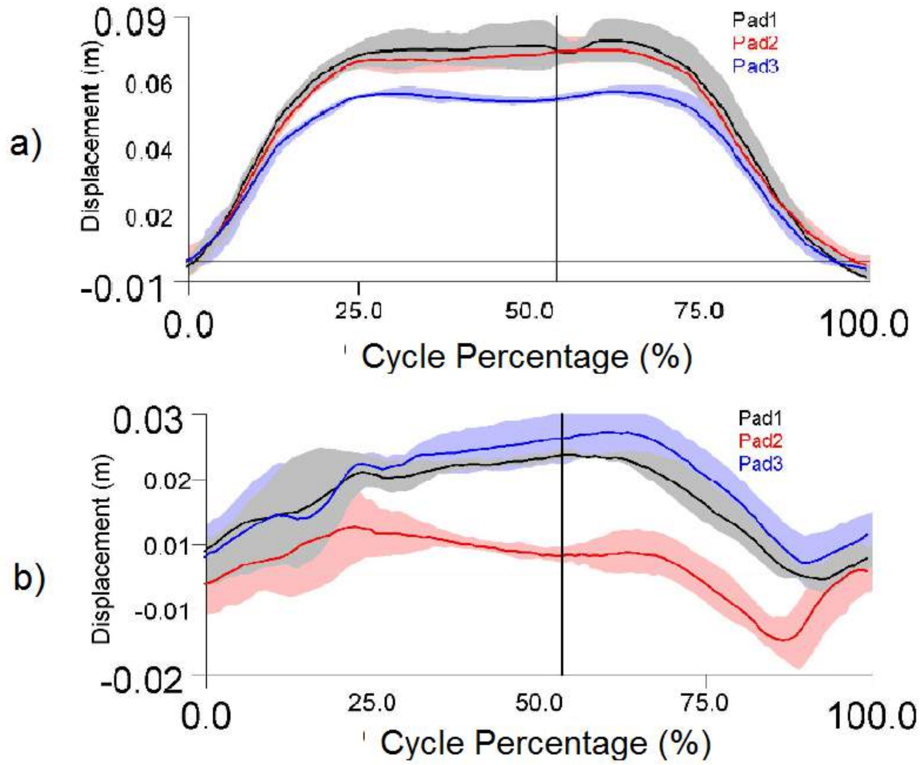

Figure 5.8: Shank interface perpendicular migration (padding analysis). Mean and SD of squat exercise. a) iterated geometry b) 3D geometry.

The padding with the highest density offered some improvements with respect to joint misalignment of the iterated based geometry in both directions on average, as shown in Table 5.7. The misalignments of the 3D scanner based geometry was not improved with the padding density, referring to Table 5.8.

The standard deviation of the results associated with the softest padding material was the greatest for most experiments, reflecting the fact that reproducibility is proportional to the permitted relative movement between the interface and padding system. Table 5.7 suggests that the padding with the highest density had the best performance at maximum flexion for the iterated based interfaces. This advantage was also noted for the 3D scanner based interfaces, but only for the RJA and the thigh and shank interface parallel migration. The range of padding density tested during this research may not be sufficient to detect the padding density with the best performance that should be used the the design of assist device interfaces. Nevertheless, this analysis suggests that firmer padding should be used during interface design.

Table 5.9 indicates that the thigh interface parallel and perpendicular migration was lower when using the 3D scanner based interfaces compared to the interfaces obtained with the iterative method. All other graphs for the padding analysis can be found in Appendix C.

5.1.4 Longitudinal position (LP) analysis

The results for both types of interfaces at maximum flexion and their standard deviation (in parenthesis) for the squat exercise, can be found in Table 5.10 and Table 5.11.

Table 5.10: LP analysis (iterated interfaces). Average value at maximal flexion with SD in parenthesis for the different testing conditions.

LP Avg. (SD)	RJA (Deg.)	TM_Pa (m)	TM_Pe (m)	SM_Pa (m)	SM_Pe (m)	M_AP (m)	M_SI (m)
TH_SH	31.1 (2.2)	31.3 (5.8)	-63.3 (3.2)	31.7 (3.5)	4.0 (4.0)	24.7 (6.5)	-7.0 (3.6)
TH_SL	40.3 (0.6)	42.3 (3.1)	-31.0 (5.3)	192.7 (6.8)	19.7 (3.1)	93.7 (3.1)	-114.3 (6.1)
TH_SM	13.5 (0.6)	42.0 (1.0)	13.0 (1.7)	48.0 (5.3)	8.3 (1.2)	33.7 (4.2)	4.0 (3.6)
TL_SH	29.2 (0.8)	33.0 (3.6)	-62.7 (6.5)	33.7 (4.0)	51.0 (3.5)	35.0 (5.2)	-24.3 (5.0)
TL_SL	17.2 (1.0)	9.7 (3.2)	-48.7 (4.0)	73.7 (0.6)	12.3 (3.2)	7.0 (4.6)	-49.3 (5.1)
TL_SM	16.6 (0.2)	25.3 (3.1)	-31.7 (5.7)	41.7 (6.1)	0.7 (0.6)	39.0 (5.0)	-13.7 (5.1)
TM_SH	25.5 (0.9)	23.7 (3.1)	-42.7 (3.2)	29.3 (0.6)	-16.3 (3.5)	27.0 (2.0)	-8.7 (2.1)
TM_SL	26.2 (1.9)	21.3 (4.2)	-30.3 (4.2)	106.3 (4.7)	5.7 (4.2)	34.7 (10.4)	-68.0 (1.7)
TM_SM	21.6 (0.3)	34.7 (6.7)	-58.3 (5.5)	34.7 (6.7)	1.7 (6.8)	37.7 (2.3)	5.3 (6.7)

Table 5.11: LP analysis (3D interfaces). Average value at maximal flexion with SD in parenthesis for the different testing conditions.

LP Avg. (SD)	RJA (Deg.)	TM_Pa (m)	TM_Pe (m)	SM_Pa (m)	SM_Pe (m)	M_AP (m)	M_SI (m)
TH_SH	31.3 (0.3)	41.7 (4.9)	-59.0 (1.0)	37.3 (5.7)	26.0 (4.4)	7.3 (8.5)	-0.7 (11.0)
TH_SL	32.2 (0.9)	16.0 (6.1)	-54.7 (13.7)	153.7 (2.9)	51.3 (11.6)	31.3 (16.3)	-108.0 (6.1)
TH_SM	32.8 (0.9)	29.0 (3.0)	-64.7 (8.7)	116.7 (3.2)	56.3 (9.9)	8.0 (6.6)	-81.7 (5.8)
TL_SH	29.7 (1.7)	42.0 (7.0)	-70.0 (12.2)	29.3 (6.7)	18.0 (6.1)	-3.3 (5.5)	8.0 (12.5)
TL_SL	19.8 (0.4)	9.3 (3.5)	-60.7 (4.5)	68.3 (4.2)	17.7 (1.5)	-15.7 (3.1)	-40.0 (7.8)
TL_SM	23.1 (1.0)	32.0 (1.7)	-68.0 (2.6)	43.7 (4.0)	19.0 (4.6)	-5.7 (3.2)	-3.0 (4.0)
TM_SH	26.6 (1.9)	26.7 (6.0)	-60.7 (3.2)	58.0 (1.0)	10.3 (9.0)	12.0 (15.4)	-1.7 (6.7)
TM_SL	22.5 (0.4)	15.0 (4.6)	-44.0 (1.0)	107.3 (1.2)	22.0 (5.0)	27.7 (9.0)	-66.0 (5.6)
TM_SM	21.1 (0.4)	38.7 (7.0)	-61.7 (5.0)	47.0 (7.8)	14.7 (5.7)	34.7 (7.2)	1.7 (4.2)

The ratio of the average results at maximal flexion of both types of interfaces can be seen in Table 5.12.

Table 5.12: LP analysis (interface comparison). Ratio of mean value between the two types of interface geometry.

LP	RJA	TM_Pa	TM_Pe	SM_Pa	SM_Pe	M_AP	M_SI
TH_SH	1.01	1.33	0.93	1.18	6.50	0.30	0.10
TH_SL	0.80	0.38	1.76	0.80	2.61	0.33	0.94
TH_SM	2.43	0.69	-4.97	2.43	6.76	0.24	-20.42
TL_SH	1.02	1.27	1.12	0.87	0.35	-0.10	-0.33
TL_SL	1.15	0.97	1.25	0.93	1.43	-2.24	0.81
TL_SM	1.39	1.26	2.15	1.05	28.50	-0.15	0.22
TM_SH	1.05	1.13	1.42	1.98	-0.63	0.44	0.19
TM_SL	0.86	0.70	1.45	1.01	3.88	0.80	0.97
TM_SM	0.98	1.12	1.06	1.36	8.80	0.92	0.31

The RJA associated with the different interface positions (iterated geometry) can be seen in Figure 5.9.

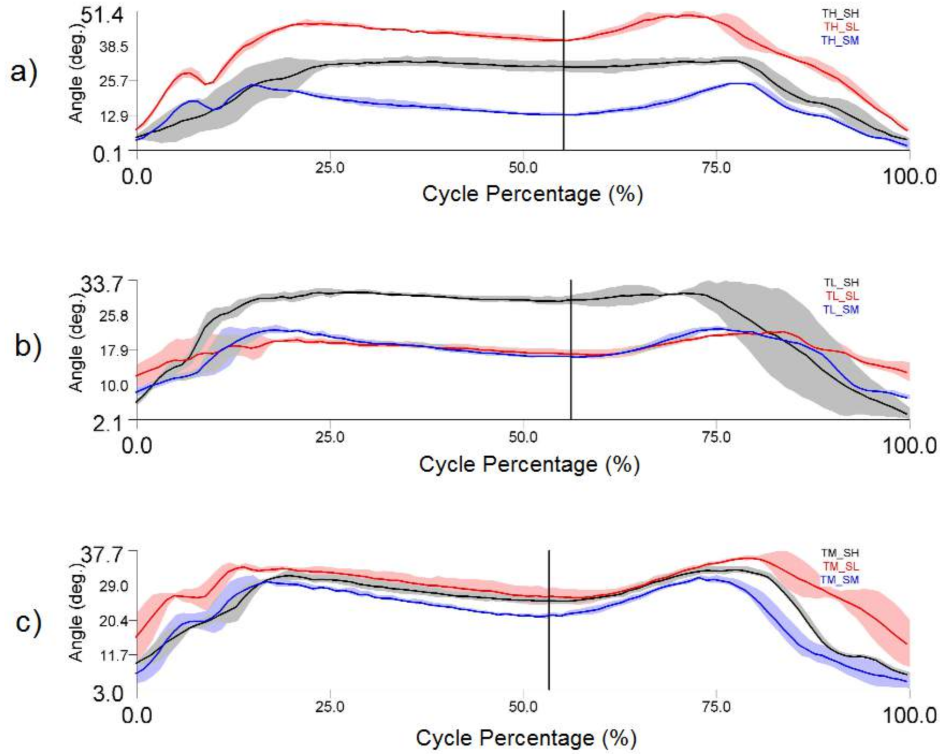

Figure 5.9: RJA (iterated LP analysis). Mean and SD of squat exercise. Thigh interface is in the a) high, b) low or c) mid position

As can be seen in Figure 5.9a, a difference with all the positions is noticeable. The testing condition where the two interfaces are the furthest away form the knee joint (TH_SL) showed the highest average of RJA at maximal flexion, with a value of 40.3 degrees. The lowest value of the RJA is of 13.5 degrees for the TH_SM condition. Furthermore, the RJA is similar in all cases of thigh interface in mid-position, regardless of shank interface position, as can be seen in Figure 5.9c.

The interface geometry obtained with the 3D scanner showed a RJA that is similar when the thigh interface is positioned in the high position. This testing condition only shows a difference of 1.5 degrees for the different shank interface positions. When the thigh interface was in the low position, the best performance was seen when the shank interface was in the low position as well, with a value of 19.8 degrees on average, which corresponds to a difference of 33 and 15% over the conditions where the shank interface was in the high and mid position respectively. The RJA, when the thigh interface was in the mid position, was within a range of 5.5 degrees. The lowest value of this parameter occurred when the shank interface was in the mid position (21.1 degrees) and the lowest performance was when the shank interface was in the high position (26.6 degrees).

During experimentation, the participant noted that the RJA is affected with the TH_SL position. The participant reported that this particular position added awkwardness to the squat motion. This interface LP position did not permit the proper functioning of the brace and promoted downwards parallel migration of the shank interface.

The iterated based thigh interface parallel migration was similar when this interface was in the high position as can be seen in Table 5.10. Despite this fact, differences exist when the thigh interface was in the low and mid positions. The best performance of the thigh interface was recorded when the shank interface was in the low position, with values of 9.7 and 21.3 mm (TL_SL and TM_SL). The shank interface was the least stable in the low position since the smaller diameter of the shank segment creates a considerable contact loss. Furthermore, since the shank is further away from the knee joint, the moment produced by the elastic element exerts less force on this interface. This has the effect of reducing friction, which allows for greater displacements. Since this position is less stable, the thigh interface migration shows less amplitude in this particular position since movements occur more easily at the shank interface.

The results of the 3D scanner based interfaces demonstrated the same behaviour. The condition where the shank interface was in the low position stands at 55, 29 and 56% relative to the movement produced by the second-best performances for the conditions where the thigh interface is positioned in the high, low and mid positions respectively.

The thigh interface parallel migration (3D interfaces) can be seen in Figure 5.10.

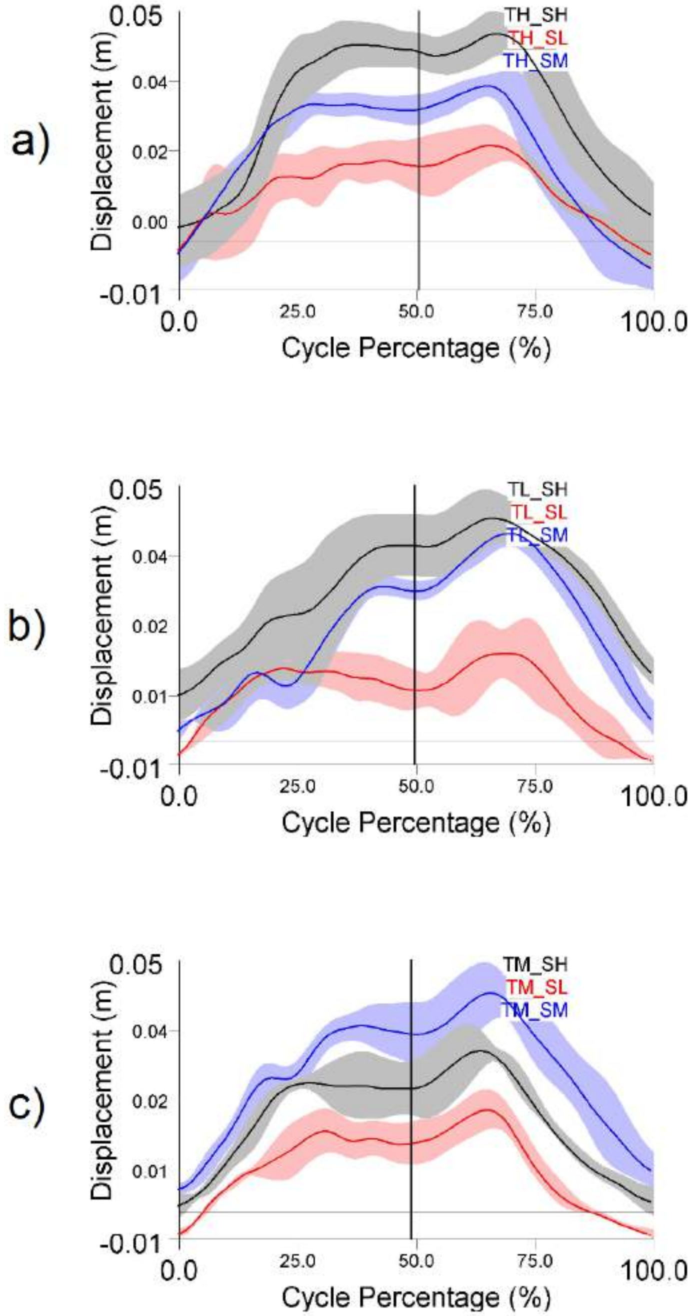

Figure 5.10: Thigh interface parallel migration (3D LP analysis). Mean and SD of squat exercise. Thigh interface is in the a) high, b) low or c) mid position

Iterated based thigh interface perpendicular migration showed lower results for the TH_SM, TL_SM and TM_SL conditions, with values of 13, 32 and 30 mm, which represent 42, 65 and 71 % of the movement of the second-best conditions respectively for the different thigh interface positions.

3D scanner based thigh interface perpendicular migration was similar. Although, the condition where the shank interface was in the low position showed small improvements. This shank interface position had perpendicular migrations of 55, 61 and 44 mm compared to 65, 70 and 62 mm, for the condition where the thigh interface was in the high, low or mid position respectively, when evaluating the worst performances.

An example of thigh interface perpendicular migration for both interface geometries can be seen in Figure 5.11 for the TH_SL and TH_SM conditions.

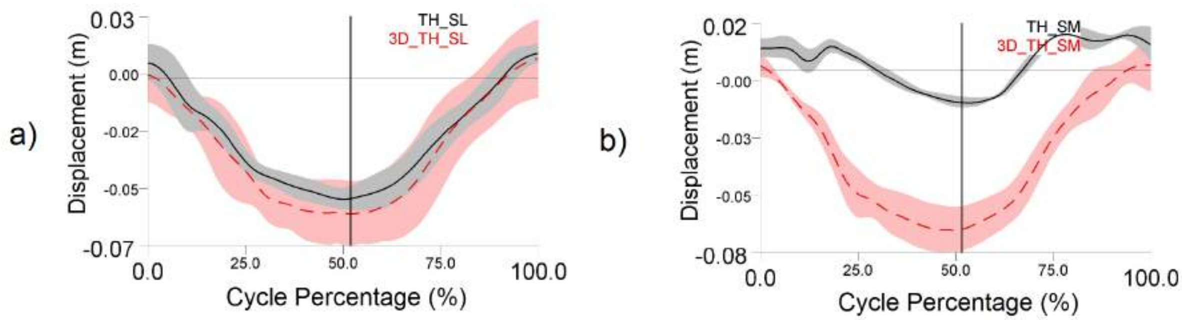

Figure 5.11: Thigh interface perpendicular migration (LP analysis). Mean and SD of squat exercise. a) TH_SL condition b) TH_SM condition.

In all cases where the shank interface was in the lowest position, the iterated shank interface parallel migration is noticeably higher, with values as high as 3.9 times the relative movement of the second-best performance. The smaller diameter of the shank in this particular position did not offer as much stability since the geometry of the limb became smaller than the one of the interface, offering less contact area. These high parallel migrations also increased the amplitude of the superior-inferior joint misalignments. These results show that perhaps an interface with a sliding element would permit a more natural motion and reduce friction at the interface. The brace frame could freely move while not affecting the interface position.

Iterated based Shank interface parallel migration can be seen in Figure 5.12.

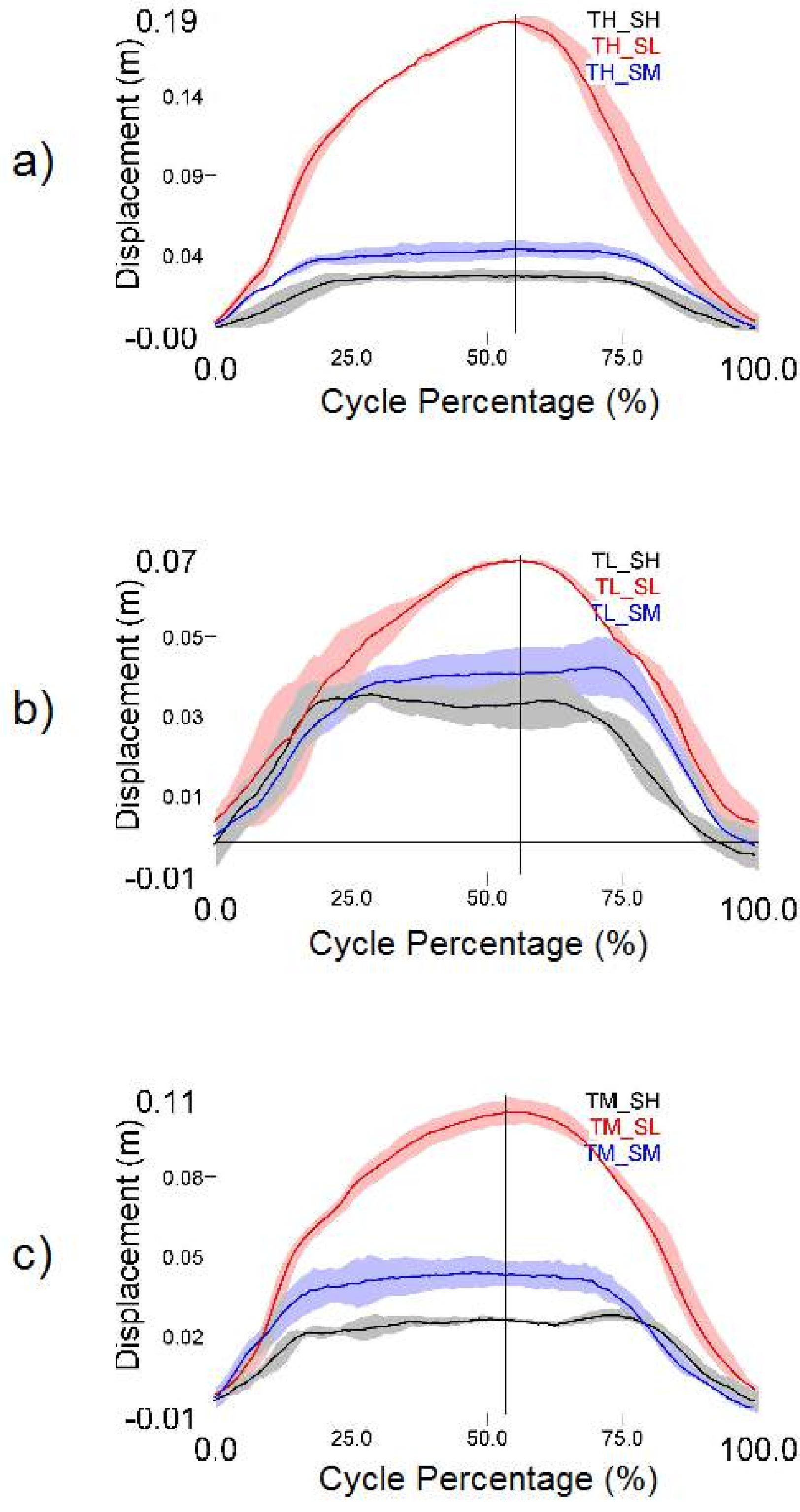

Figure 5.12: Shank interface parallel migration (iterated LP analysis). Mean and SD of squat exercise. Thigh interface is in the a) high, b) low or c) mid position

As can be seen in Figure 5.12, higher shank interface migration was also applicable to the 3D scanner based geometry when this interface was in the low position. In fact, this was applicable to all the positions of the thigh. The SL position showed 1.31, 1.55 and 1.85 times as much displacement at maximal flexion over the second-best performance of the conditions where the thigh interface was in the high, low and mid positions respectively, on average.

The lowest shank interface parallel migration was observed when this interface was positioned in its highest position. The smaller shank diameter of this position increases along the two longitudinal directions of the limb, and encouraged the interface to stay in this particular position. The location under the knee and over the calf muscle tapers down from the knee and tapers up towards the calf muscles, which offers a geometric constraint.

Iterated based shank interface perpendicular migration was noticeably higher when the shank interface was in the low or high positions. The greatest amplitude of perpendicular migration was seen for the TL_SH condition with 51 mm, representing 2.6 times more movement than the second-worst testing condition, irrespective of interface position.

The 3D scanner based TH position had the lowest amount of shank perpendicular migration when the shank interface was in the high position with a value of 26 mm, compared to 51 and 56 mm for the shank interface in the low and mid position respectively, on average. Perpendicular migration was similar on average for all the different shank interface positions when the thigh interface was in the low position. The values associated with this result may be seen in Table 5.11. Less relative movement for the testing conditions where the thigh interface was in the mid position was recorded when the shank interface was in the high position. These conditions represent 47 and 70% of the migration of the condition where the shank interface was in the low and mid position respectively, for the same thigh interface position. Shank perpendicular migration (iterated geometry) can be seen in Figure 5.13.

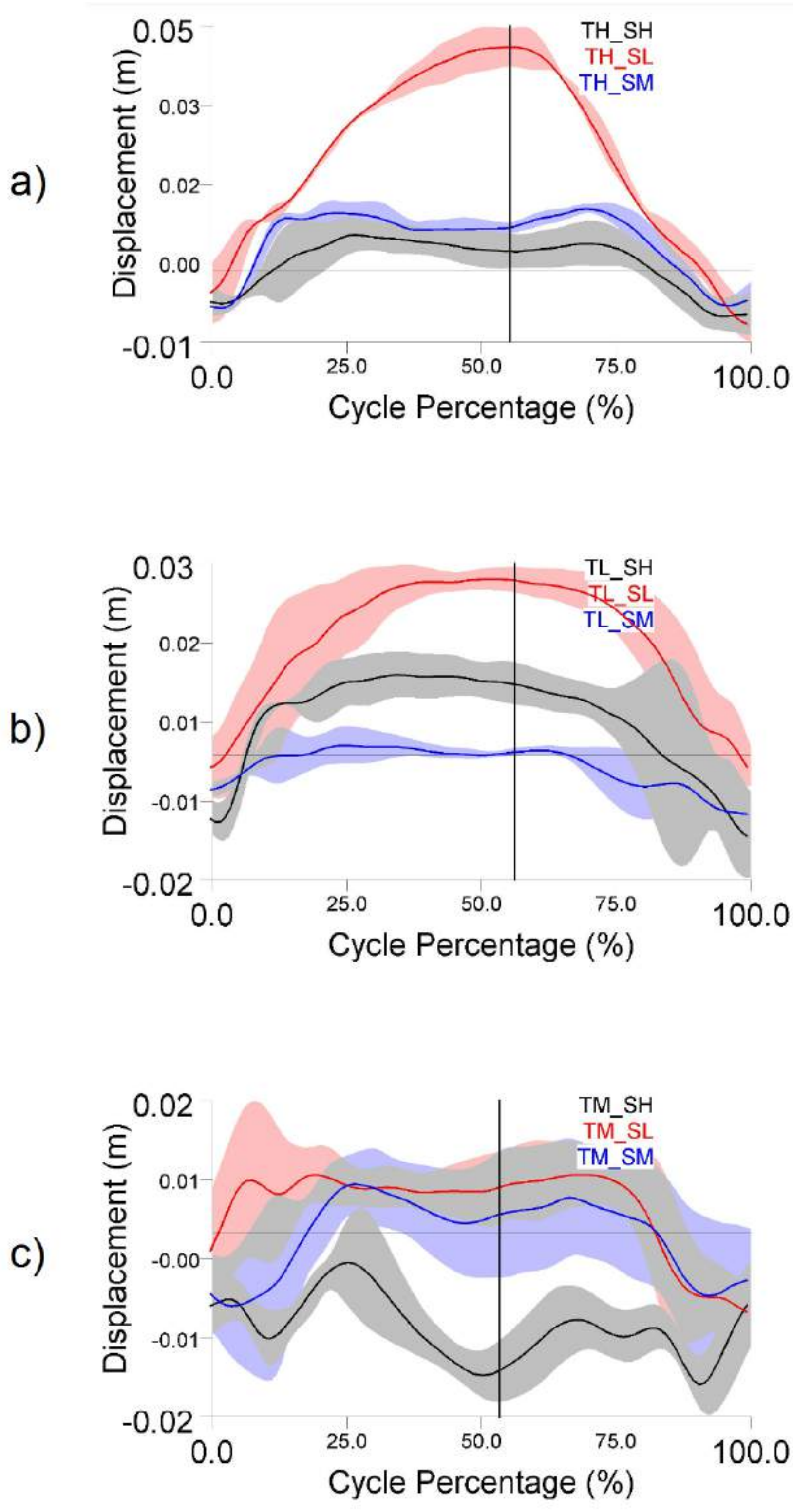

Figure 5.13: Shank interface perpendicular migration (iterated LP analysis). Mean and SD of squat exercise. Thigh interface is in the a) high, b) low or c) mid position

The most noticeable result of the anterior-posterior misalignment analysis for the iterated geometry is from the TH_SL testing condition with about 2.4 times more misalignment than the second-best performance by the TL_SM condition. This was attributed to the associated RJA of this condition, and did not allow for the proper bending of the brace and permit the brace joint to progress towards the knee joint. This misalignment can be seen in Figure 5.14.

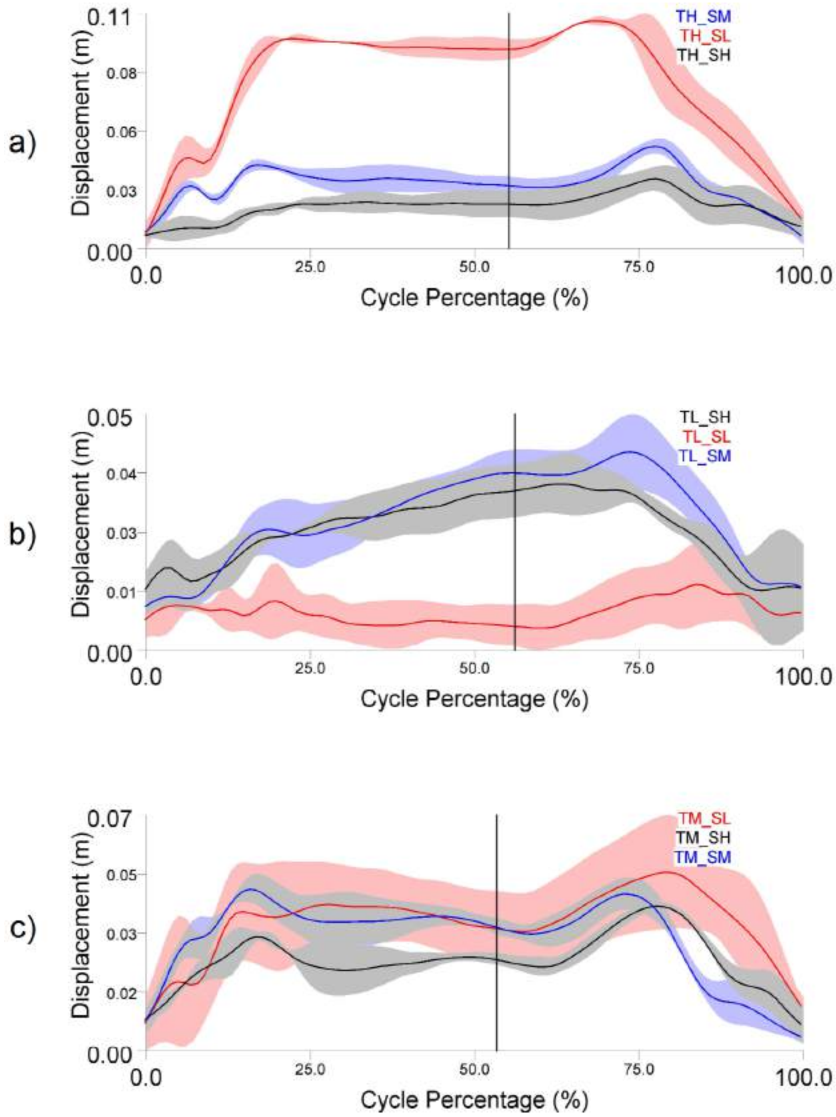

Figure 5.14: Joint anterior-posterior misalignment (iterated LP analysis). Mean and SD of squat exercise. Thigh interface is in the a) high, b) low or c) mid position

The anterior-posterior misalignment of the 3D scanner based interface geometry of the testing conditions where the thigh interface was in the high position demonstrated a noticeable difference when the shank interface was in the low position, similar to the iterated interfaces, with a value of 31.3 mm. This value was 3.8 times greater than the other two conditions for this particular thigh interface position. Anterior-posterior misalignment when the thigh interface was in the low position was the greatest when the shank interface was in the low position, with a value of 16 mm compared to 3 and 6 mm. The TM_SM condition showed the most misalignment with a value of 35 mm, which was 1.25 and 2.9 times higher than the other two positions, low and high respectively, for this particular thigh interface position. This can be seen in Figure 5.15.

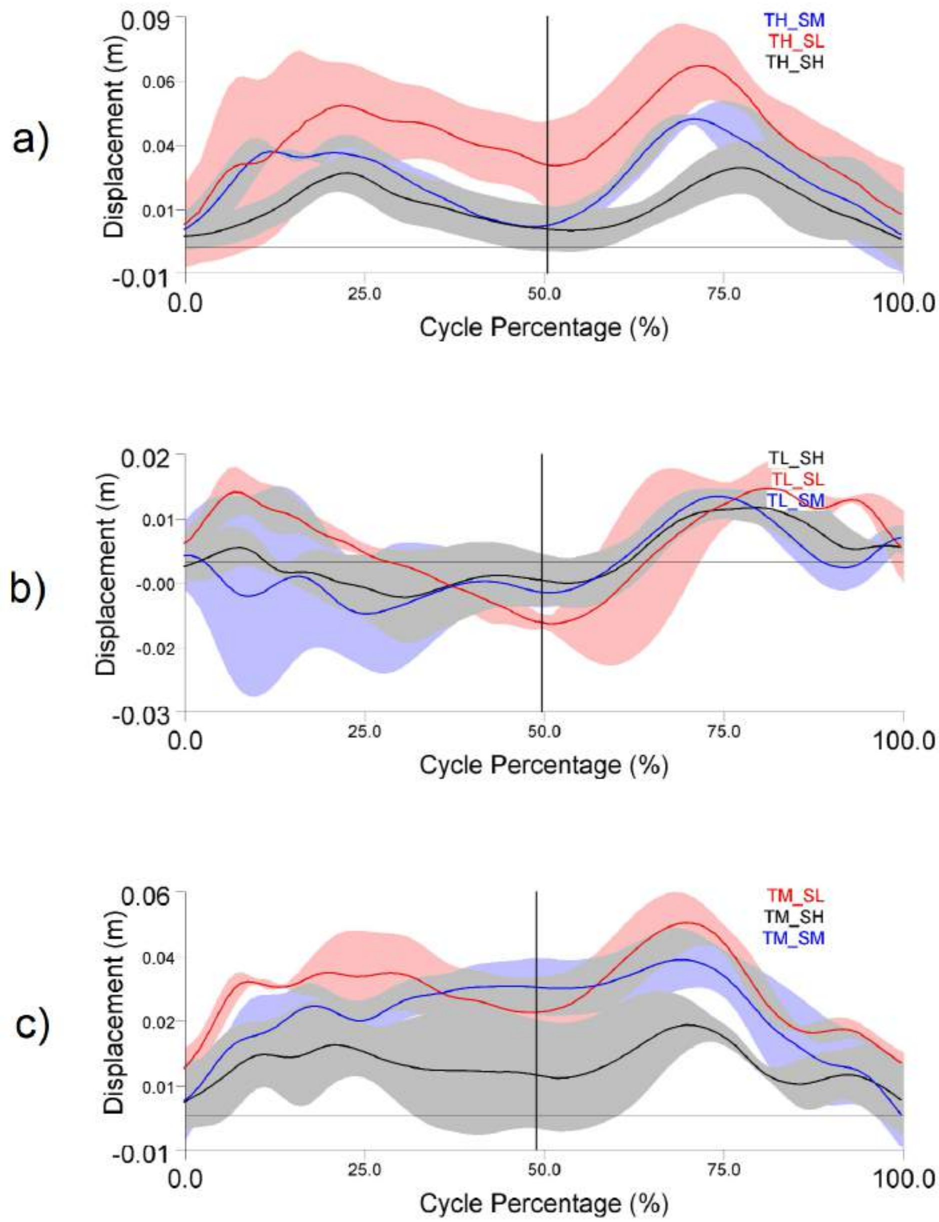

Figure 5.15: Joint anterior-posterior misalignment (3D LP analysis). Mean and SD of squat exercise. Thigh interface is in the a) high, b) low or c) mid position.

For both geometries, the important shank interface parallel migration had a direct effect on the superior-inferior joint misalignment, which was greatest for the testing conditions where the shank interface was in the low position. This allowed a non-restricted movement of the brace joint towards the ground as the knee flexed. The values at maximal flexion of Table 5.11 and Table 5.10 clearly show this trend. The TH_SM condition also showed an important misalignment, with 82 mm, compared to the greatest superior-inferior misalignment, which was 108 mm, for the 3D scanner based geometry. The iterated shank interface low position had 16.3, 2 and 7.7 times more movement compared to the high position, for each positions of the thigh interface.

The superior-inferior joint misalignments (iterated geometry) may be seen in Figure 5.16.

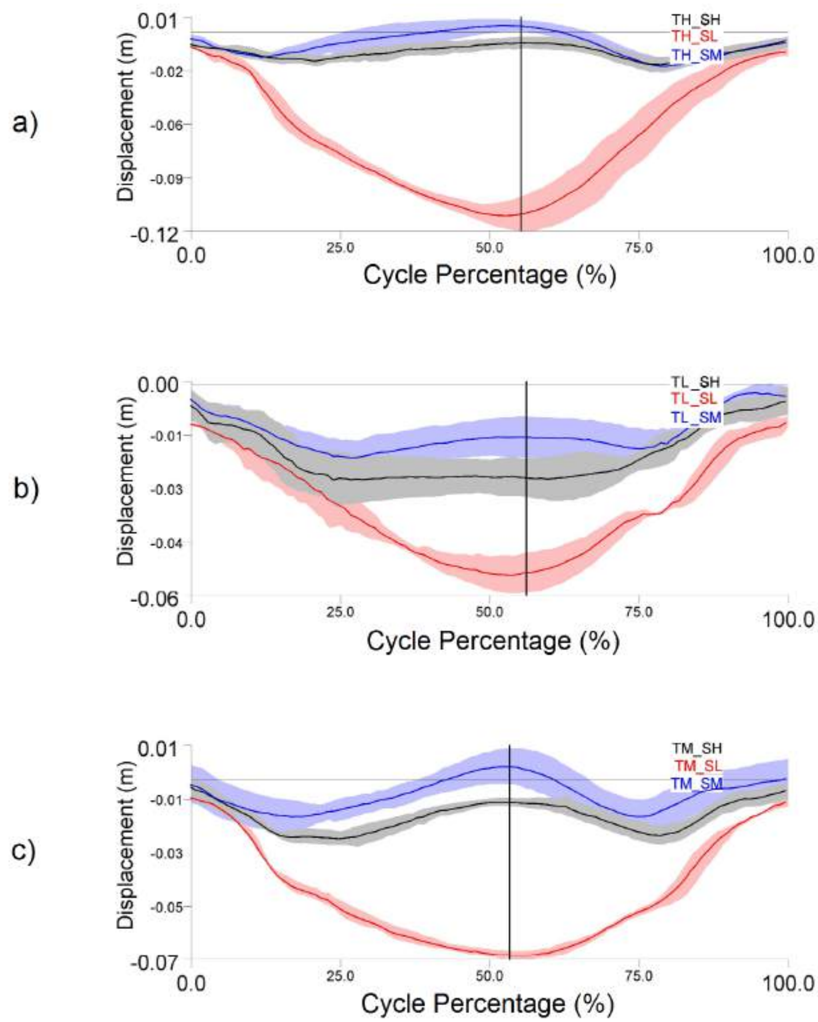

Figure 5.16: Joint superior-inferior misalignment (iterated LP analysis). Mean and SD of squat exercise. Thigh interface is in the a) high, b) low or c) mid position.

Overall, extreme positions, or positions where one of the interfaces was in the high or in the low position, inclined to show greater amplitude for RJA, migration and joint misalignment. Extreme positions affect the brace moment distribution. The interface with the largest moment portion would exert more force on the limb. The normal force contributes to the friction of the interfaces on the limb, which increases interface stability. This suggests that the longitudinal position of the interfaces have an effect on the brace performance.

Interface climbing

Since the 3D scanner based interfaces have a tapered geometry, positioning the interfaces outside of the limb segment surface that they were designed for had the effect of wedging (squeezing) or loosening the fit, if moved superiorly or inferiorly respectively. In some instances, the interfaces had the tendency to ”climb” the limb, the parallel migration was towards the hip. Further instances of the exercises would further displace the interface towards the hip, encouraging a migration in this particular direction. Climbing, or a gradual increase of the parallel migration, may be observed over the five instances of some of the experimental exercises. For example, this behaviour may be see in Figure 5.17, for the shank interface during a squat trial.

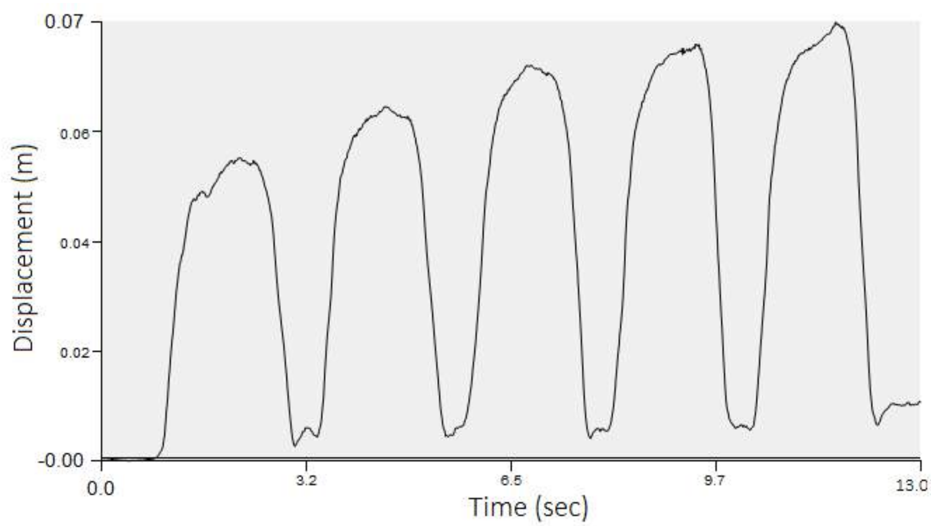

Figure 5.17: ”Climbing” of the shank interface during a squat trial

The performance of the 3D scanner based interfaces was improved when they were in their indented position. When this position differed, performance dropped considerably. This sensitivity to position alignment was less noticeable with the iterated interfaces. More specifically, the thigh interface was more stable when the shank interface had the greatest relative displacement, especially when the shank interface was in the low position. The positioning of the interfaces relative to the limb is crucial for stability. An interface that is positioned on a limb segment that is too small cannot assure contact. All other graphs for the longitudinal position analysis can be found in Appendix C.

5.1.5 Stiffness analysis

The results for both types of interfaces at maximum flexion and their standard deviation (in parenthesis) of the squat exercise, can be found in Table 5.13 and Table 5.14 for the different degrees of stiffness (S1, S2, S3).

Table 5.13: Stiffness analysis (iterated interfaces). Average value at maximal flexion with SD in parenthesis for the different testing conditions.

Stiffness Avg. (SD)	**RJA (Deg.)**	**TM_Pa (m)**	**TM_Pe (m)**	**SM_Pa (m)**	**SM_Pe (m)**	**M_AP (m)**	**M_SI (m)**
S1	10.2 (0.7)	-0.001 (0.002)	-0.067 (0.003)	0.046 (0.003)	0.015 (0.003)	-0.017 (0.004)	-0.002 (0.003)
S2	24.9 (0.3)	0.038 (0.005)	-0.067 (0.004)	0.040 (0.008)	0.007 (0.005)	0.029 (0.003)	0.013 (0.007)
S3	27.4 (1.0)	0.044 (0.007)	-0.064 (0.007)	0.041 (0.004)	0.012 (0.006)	0.030 (0.006)	0.010 (0.004)

Table 5.14: Stiffness analysis (3D interfaces). Average value at maximal flexion with SD in parenthesis for the different testing conditions.

Stiffness Avg. (SD)	**RJA (Deg.)**	**TM_Pa (m)**	**TM_Pe (m)**	**SM_Pa (m)**	**SM_Pe (m)**	**M_AP (m)**	**M_SI (m)**
S1	10.1 (0.4)	0.006 (0.004)	-0.045 (0.004)	0.057 (0.001)	0.009 (0.009)	-0.022 (0.009)	-0.045 (0.005)
S2	18.5 (0.5)	0.018 (0.006)	-0.056 (0.002)	0.078 (0.004)	0.022 (0.005)	-0.009 (0.006)	-0.048 (0.005)
S3	18.0 (0.3)	0.016 (0.001)	-0.051 (0.003)	0.070 (0.003)	0.023 (0.003)	-0.013 (0.008)	-0.046 (0.004)

The ratio of the average results at maximal flexion of both interface geometries can be seen in Table 5.9.

Table 5.15: Stiffness analysis (interface comparison). Ratio of mean value between the two types of interface geometry.

Stiffness	RJA	TM_Pa	TM_Pe	SM_Pa	SM_Pe	M_AP	M_SI
S1	0.99	-8.50	0.67	1.26	0.61	1.34	22.33
S2	0.74	0.47	0.83	1.94	2.95	-0.30	-3.82
S3	0.66	0.36	0.79	1.72	1.92	-0.44	-4.60

The RJA as a function of the different degrees of stiffness for the iterated based interface geometry can be seen in Figure 5.18.

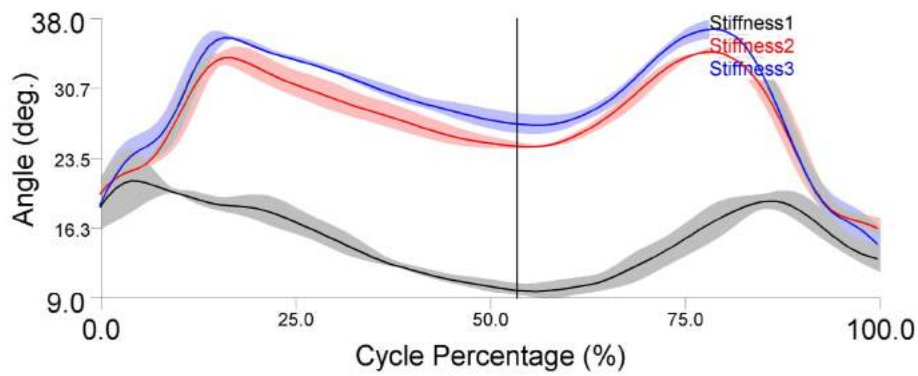

Figure 5.18: RJA (iterated stiffness analysis). Mean and SD of squat exercise.

Figure 5.18 shows differences of the different carbon fiber strips RJA, with values of 10.2, 24.9 and 27.4 degrees for the low, medium and high stiffness elements respectively.

Similar to the iterated based interfaces, RJA increased with increasing stiffness, with similar results for the two higher degrees of stiffness. Stiffness 2 and Stiffness 3 showed 18.5 and 18 degrees respectively, compared to 10.1 degrees for the lowest stiffness condition.

The thigh parallel migration increased as a function of stiffness for both interface geometries. When the stiffer elastic elements were used, the resistance to flexion exerted a force on the interfaces. This led to a variation in results, as seen in Figure 5.19 for the iterated geometry. The difference was of 39 and 45 mm for Stiffness 2 and Stiffness 3 respectively, relative to Stiffness 1.

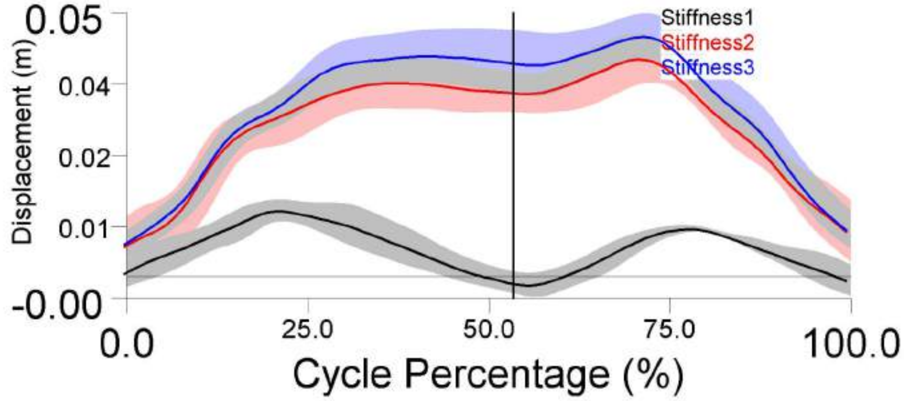

Figure 5.19: Thigh interface parallel migration (iterated stiffness analysis). Mean and SD of squat exercise.

Thigh interface perpendicular migration had comparable results for the different degrees of stiffness, for both interface geometries, indicating that this parameter is independent of the assistance. The results of this parameter may be seen in Table 5.13 and Table 5.14.

The migration of the iterated shank interface was similar for the different testing conditions for both the parallel and perpendicular directions, implying that this migration was independent of the stiffness of the elastic element for this particular geometry.

The 3D scanner based parallel and perpendicular shank interface migration had values of 57, 78 and 70 mm and 9, 22 and 23 mm, respectively and proportionally to the different degrees of stiffness. This indicated that the lower stiffness produced less relative movement of the brace and that the two higher degrees had similar relative movement. Shank interface migration for both geometries can be seen in Figure 5.20

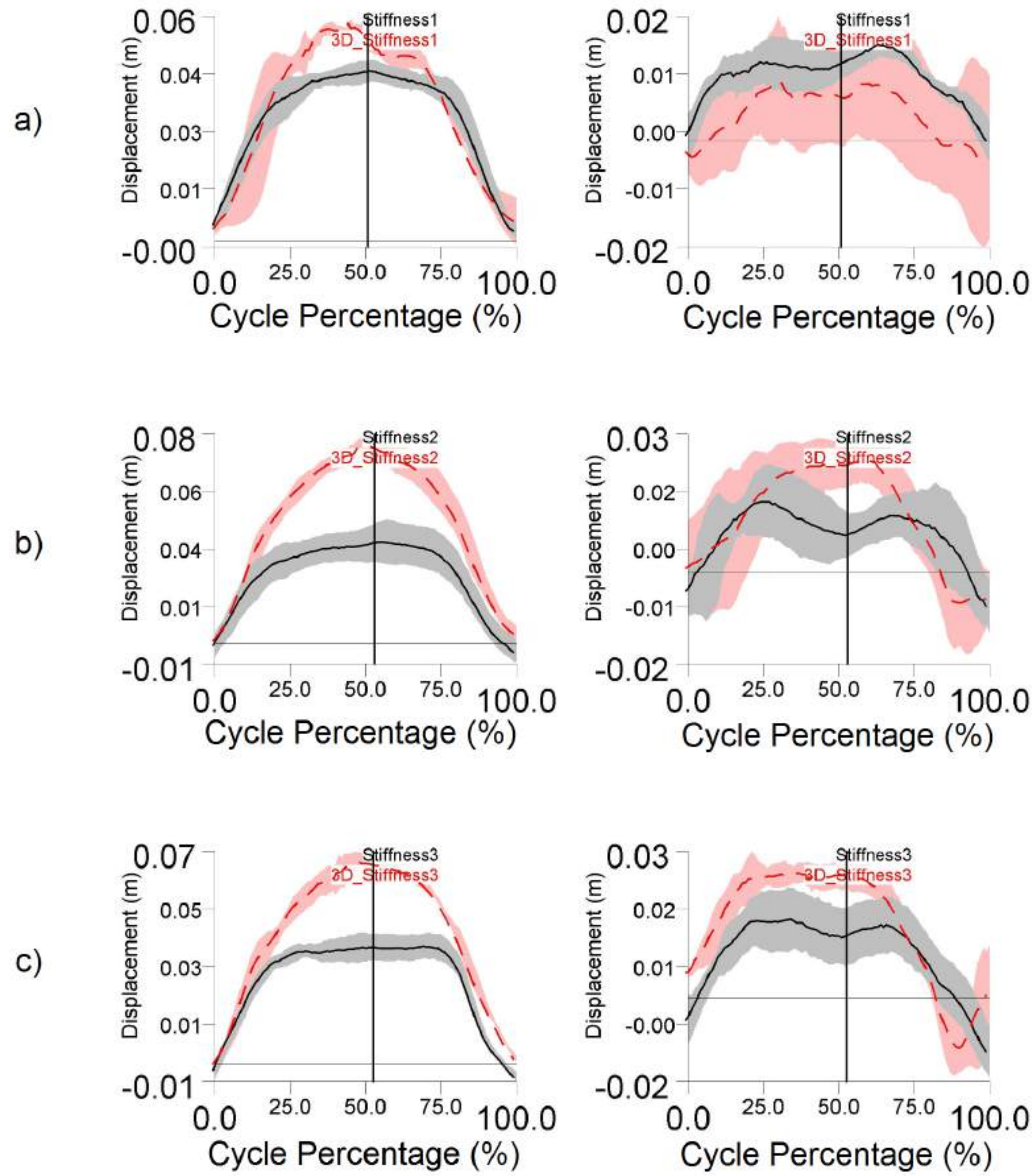

Figure 5.20: Shank interface migration (iterated-3D position analysis). Mean and SD of squat exercise. Left and right columns represent the parallel and perpendicular migrations respectively. a) Stiffness 1, b) Stiffness 2 and c) Stiffness 3.

The anterior-posterior misalignments of the iterated based interface were similar for the two higher degrees of stiffness. The low stiffness element demonstrated less misalignments, with a value of -17 mm, compared to 29 and 30 mm for Stiffness 2 and Stiffness 3 respectively, on average at maximal flexion. The superior-inferior was lower for the Stiffness 1 condition, with a value of -2 mm, compared to 13 and 10 mm for the medium and high degree of stiffness, respectively.

The 3D scanner based interface misalignments in the anterior-posterior direction showed a decrease of 22, 9 and 13 mm in function of stiffness. The superior-inferior misalignment results at maximum flexion showed little difference between the testing conditions. The SI misalignment is contained within a range of 3 mm.

The misalignment of the device (iterated geometry), in both the superior-inferior and anterior-posterior directions, may be seen in Figure 5.21.

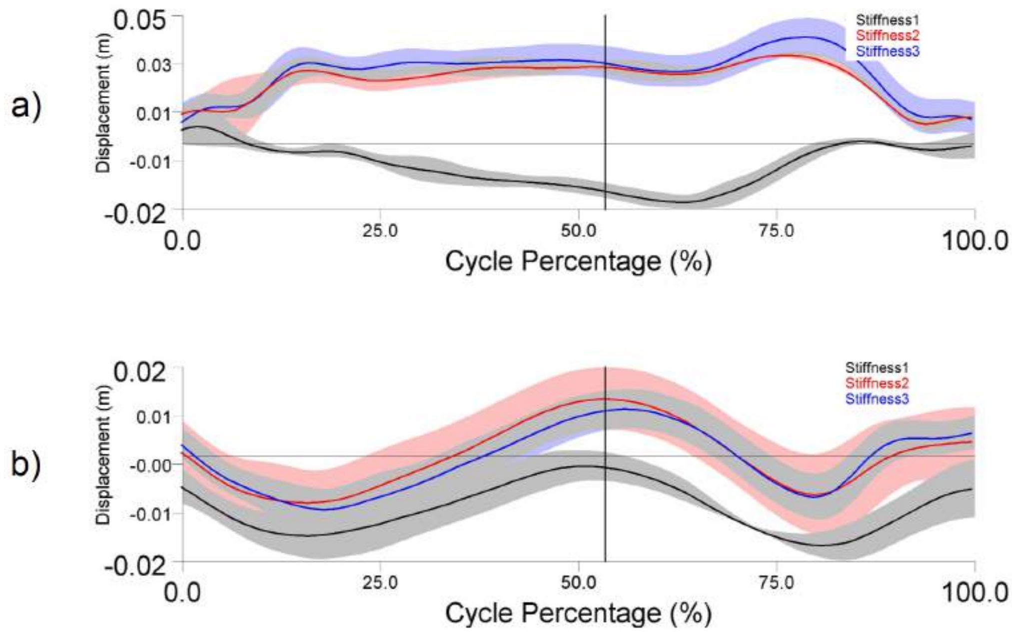

Figure 5.21: Joint misalignment (iterated stiffness analysis). Mean and SD of squat exercise. a) anterior-posterior b) superior-inferior.

In all, stiffer elastic elements had the effect of increasing the relative displacements of the brace relative to the user for both interface geometries. The two stiffer elements had similar results. This can be attributed to their similar mechanical properties, observed during mechanical testing of the brace. A lower stiffness did produce less relative displacement in some instances but did not assist the participant with the motion as much as the two other stiffness conditions.

Higher degrees of stiffness hindered the natural movement of the brace, which was reflected in higher relative movements. These higher degrees of stiffness did produce more force on the limb at maximal flexion, which would have had the effect of producing a greater friction force between the padding surface and the skin of the user. The increase of friction would have resulted in an increased interface adherence or stability.

Table 5.13 and Table 5.14 show that the two higher degrees of stiffness have similar performance and that the lowest elastic element stiffness produced less relative movement but similar misalignments. This suggests that misalignment of the device is mostly affected by the kinematic discrepancies that exist between the two types of joints, the knee joint being polycentric and the brace joint being a hinge joint. All other graphs for the stiffness analysis can be found in Appendix C.

These results show the substantial performance impact when introducing a contributing moment about a joint which is the case for powered assistive devices. Unlike common passive orthotic devices, the added moment by an exoskeleton amplify the deficiency of physical interfaces and non-conforming mechanical joints. Thus, an interface with an increased surface area and improved strapping should be considered to ensure the interface stability of assist devices.

5.2 Kinetics

This section presents the force sensor response for the different interface geometries where the stiffness of the elastic elements is varied while the padding density remained constant, and vice versa. The results shown here are for the squat exercise and the posterior thigh interface at mid position. The results of the different graphs are the average of the maximal recordings of three trials.

The results associated with the iterated geometry can be seen in Figure 5.22, which shows the maximum force recorded by the 12 sensors independently of time for the different testing conditions, which identifies zones of force concentration.

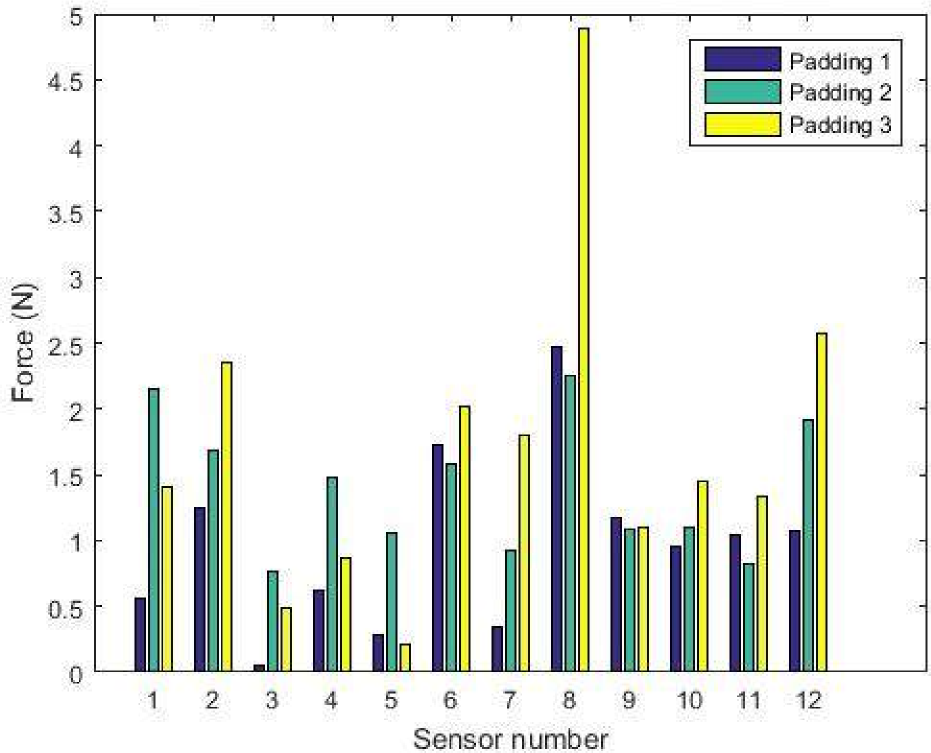

(a) Padding analysis. Mean of maximal recordings of squat exercise.

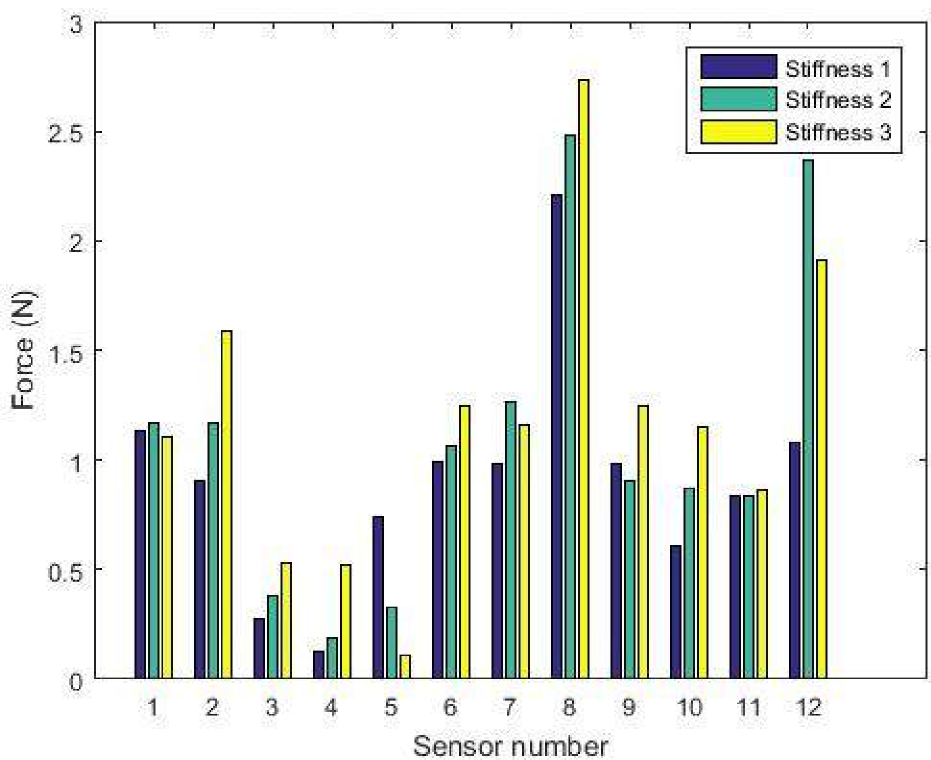

(b) Stiffness analysis. Mean of maximal recordings of squat exercise.

Figure 5.22: Effects of padding and stiffness on the force response of the iterated based interfaces

Figure 5.22a shows that the force response of the iterated based interfaces was not proportional to padding density. For example, sensor 2, 7, 10 and 12 show an increase in the maximal force in function of padding density whereas the other sensors did not have proportional recordings.

The force response of the iterated based interfaces while changing the stiffness of the elastic elements showed in Figure 5.22b demonstrates that the force response was mostly proportional to stiffness of the elastic element. Sensor 2, 3, 4, 6, 8, 10 and 11 do show an increase in force when increasing the stiffness.

Table 5.16 and Table 5.17 show the averaged maximal force values recorded by the sensors and the standard deviations of the associated recordings for the iterated based interface geometry.

Table 5.16: Iterated based interface padding analysis. Average value at instant of maximal force recording with SD in parenthesis for the different testing conditions.

Sensor	1 (N)	2 (N)	3 (N)	4 (N)	5 (N)	6 (N)	7 (N)	8 (N)	9 (N)	10 (N)	11 (N)	12 (N)
Padding 1	0.57 (0.82)	1.24 (0.61)	0.06 (0.10)	0.62 (0.47)	0.28 (0.49)	1.73 (0.69)	0.35 (0.61)	2.47 (1.09)	1.18 (1.17)	0.95 (0.88)	1.04 (1.23)	1.07 (0.30)
Padding 2	2.15 (0.83)	1.68 (0.26)	0.77 (0.40)	1.47 (0.34)	1.06 (0.33)	1.56 (0.14)	0.92 (0.54)	2.26 (0.59)	1.08 (0.34)	1.10 (0.11)	0.83 (0.45)	1.91 (0.68)
Padding 3	1.41 (0.33)	2.36 (0.35)	0.48 (0.25)	0.86 (0.23)	0.21 (0.19)	2.02 (0.29)	1.80 (0.81)	4.90 (0.51)	1.10 (0.20)	1.46 (0.76)	1.34 (0.32)	2.57 (0.59)

Table 5.17: Iterated based interface stiffness analysis. Average value at instant of maximal force recording with SD in parenthesis for the different testing conditions.

Sensor	1 (N)	2 (N)	3 (N)	4 (N)	5 (N)	6 (N)	7 (N)	8 (N)	9 (N)	10 (N)	11 (N)	12 (N)
Stiffness 1	1.13 (0.59)	0.91 (0.15)	0.27 (0.25)	0.13 (0.08)	0.74 (0.06)	0.99 (0.32)	0.99 (0.37)	2.21 (0.25)	0.99 (0.27)	0.61 (0.12)	0.83 (0.51)	1.08 (0.35)
Stiffness 2	1.17 (0.97)	1.17 (0.22)	0.38 (0.16)	0.19 (0.11)	0.33 (0.57)	1.07 (0.24)	1.26 (0.66)	2.48 (0.26)	0.91 (0.34)	0.87 (0.07)	0.84 (0.40)	2.37 (0.75)
Stiffness 3	1.11 (0.74)	1.59 (0.44)	0.52 (0.19)	0.52 (0.06)	0.11 (0.20)	1.25 (0.16)	1.16 (0.21)	2.73 (0.14)	1.25 (0.25)	1.15 (0.56)	0.86 (0.85)	1.91 (0.58)

The following graphs show the force response associated with the 3D scanner based interface geometry.

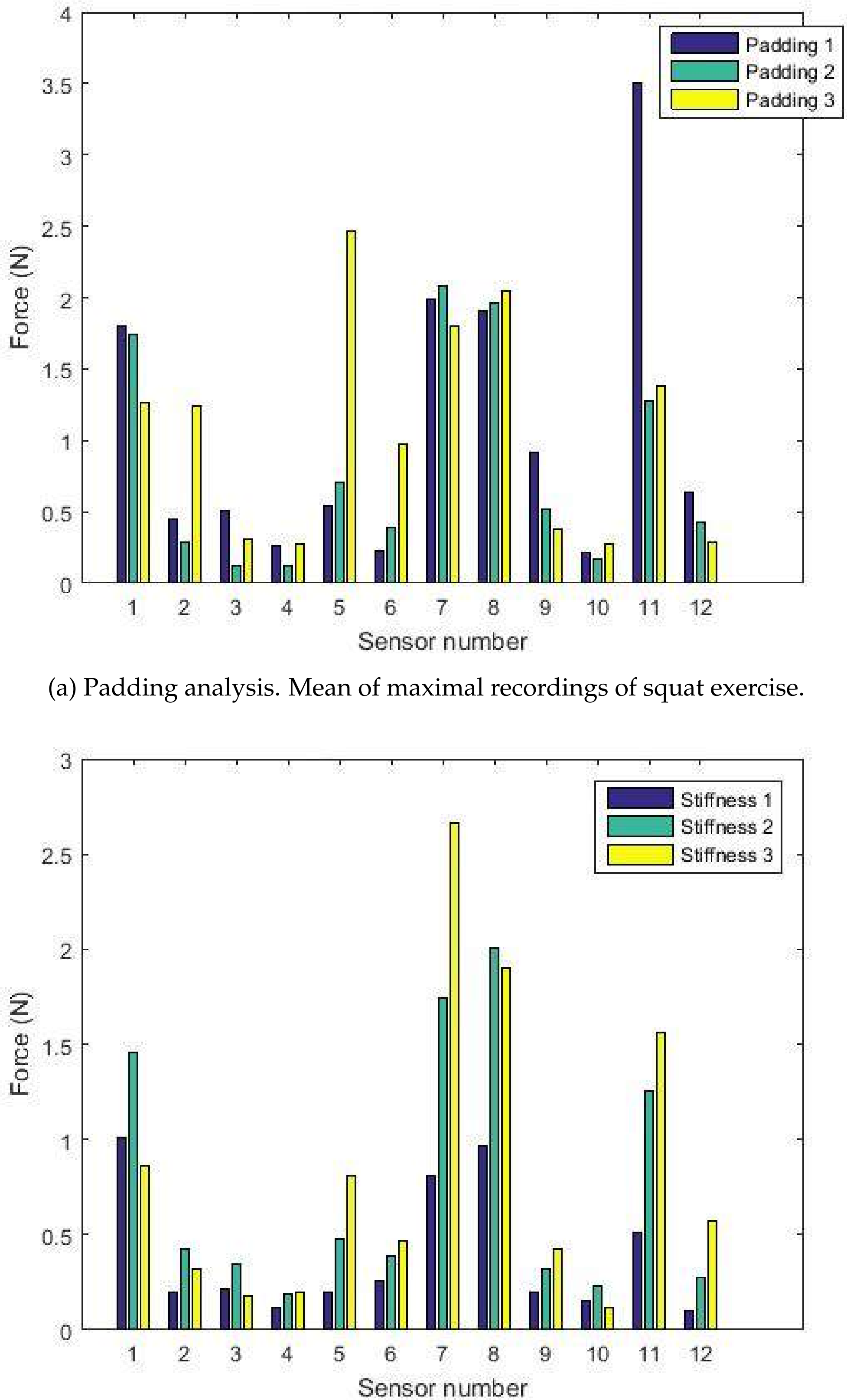

(a) Padding analysis. Mean of maximal recordings of squat exercise.

(b) Stiffness analysis. Mean of maximal recordings of squat exercise.

Figure 5.23: Effects of padding and stiffness on the force response of the 3D scanner based interfaces

Figure 5.23 shows that padding has less of a proportional force response with respect to stiffness for the 3D scanner based interfaces. The padding with the maximal force measurement is random and not proportional to padding density.

The kinetic analysis of the 3D scanner based interfaces while changing the stiffness of the elastic elements showed that the maximal force response was recorded using the medium and high degree of stiffness. In all cases, the maximal force is not recorded by the lower stiffness element, which was expected.

Table 5.18 and Table 5.19 show the averaged maximal force values recorded by the sensors and standard deviations of the associated recordings for the 3D scanner based interface geometry.

Table 5.18: 3D scanner based interface padding analysis. Average value at instant of maximal force recording with SD in parenthesis for the different testing conditions.

Sensor	**1 (N)**	**2 (N)**	**3 (N)**	**4 (N)**	**5 (N)**	**6 (N)**	**7 (N)**	**8 (N)**	**9 (N)**	**10 (N)**	**11 (N)**	**12 (N)**
Padding 1	1.79 (1.45)	0.45 (0.21)	0.5 (0.25)	0.26 (0.45)	0.54 (0.29)	0.23 (0.06)	1.99 (0.57)	1.91 (0.37)	0.91 (1.03)	0.22 (0.33)	3.51 (1.78)	0.64 (0.55)
Padding 2	1.74 (1.98)	0.29 (0.17)	0.12 (0.21)	0.12 (0.15)	0.71 (0.43)	0.4 (0.22)	2.09 (3.33)	1.96 (0.54)	0.52 (0.79)	0.17 (0.15)	1.28 (0.58)	0.43 (0.68)
Padding 3	1.26 (1.35)	1.24 (1.42)	0.3 (0.10)	0.28 (0.18)	2.47 (1.90)	0.97 (1.16)	1.81 (0.76)	2.05 (0.10)	0.38 (0.27)	0.27 (0.44)	1.39 (0.17)	0.29 (0.17)

Table 5.19: 3D scanner based interface stiffness analysis. Average value at instant of maximal force recording with SD in parenthesis for the different testing conditions.

Sensor	**1 (N)**	**2 (N)**	**3 (N)**	**4 (N)**	**5 (N)**	**6 (N)**	**7 (N)**	**8 (N)**	**9 (N)**	**10 (N)**	**11 (N)**	**12 (N)**
Stiffness 1	1.01 (0.74)	0.20 (0.30)	0.22 (0.38)	0.11 (0.18)	0.20 (0.29)	0.26 (0.35)	0.81 (1.33)	0.97 (0.22)	0.20 (0.35)	0.16 (0.23)	0.51 (0.63)	0.10 (0.18)
Stiffness 2	1.46 (1.03)	0.42 (0.08)	0.34 (0.34)	0.19 (0.13)	0.48 (0.57)	0.39 (0.24)	1.74 (1.29)	2.01 (0.31)	0.32 (0.39)	0.23 (0.40)	1.25 (0.26)	0.27 (0.13)
Stiffness 3	0.86 (0.49)	0.32 (0.22)	0.18 (0.31)	0.19 (0.18)	0.81 (0.75)	0.47 (0.23)	2.66 (2.77)	1.90 (0.45)	0.42 (0.42)	0.12 (0.10)	1.56 (1.04)	0.57 (0.46)

The analysis showed that force concentration exist on the medial and lateral edges and in the center of the interface as well. This is indicated by the increased recordings of the sensors 1 and 2, sensors 6, 7 and 8 and sensors 11 and 12, which represent the medial, center and lateral portions of the interfaces respectively. If the whole contact area of the interface was in contact there would be no force concentration. When the interface migrated upwards, the sides of the interface concentrated force against the lateral and medial sides of the leg due to the smaller geometry of the interface section compared to the leg. In the opposite case, where the interface moved downwards, the contact area between the interface and the user was reduced, so that the center of the interface would be primarily in contact, losing contact on the side of the leg since the interface section is larger than the leg. This induced concentrated force recordings in this particular area.

The variability in the results may be attributed to numerous factors. For example, the RJA induces an interface tilt, which reduces the contact area to a single edge of the interface, concentrating the forces on this edge.

The changing limb geometry associated with muscular contractions could have concentrated the force at the area of contracting muscles (hamstring). Furthermore, the stiffness of the limb is increased at this particular area, which would also concentrate, or increase the force recordings.

Softer padding may allow the participant's musculature or the interface edges to compress the padding more easily and exert a concentrated and non-uniform magnitude of force on the sensors. This could explain the higher force recordings by the softer padding even though they were expected to be lower.

5.2.1 Interface geometry comparison

The results in this section are the comparison between the iterated and 3D scanner based interfaces. These measurements were taken for the posterior thigh interface for different padding and stiffness conditions.

Experimental testing showed that the difference in interface contact geometry lowered the overall pressure on the interface. This can be seen in Figure 5.24, where the iterated and 3D scanner based interface are tested under the same conditions. The X axis of the graphs have been divided in the odd and even numbered sensor. The odd numbered sensors correspond to the upper edge of the interface while the even numbered sensors correspond to the lower edge of the interface. This permits an easier evaluation of the force response with respect to the interface edges.

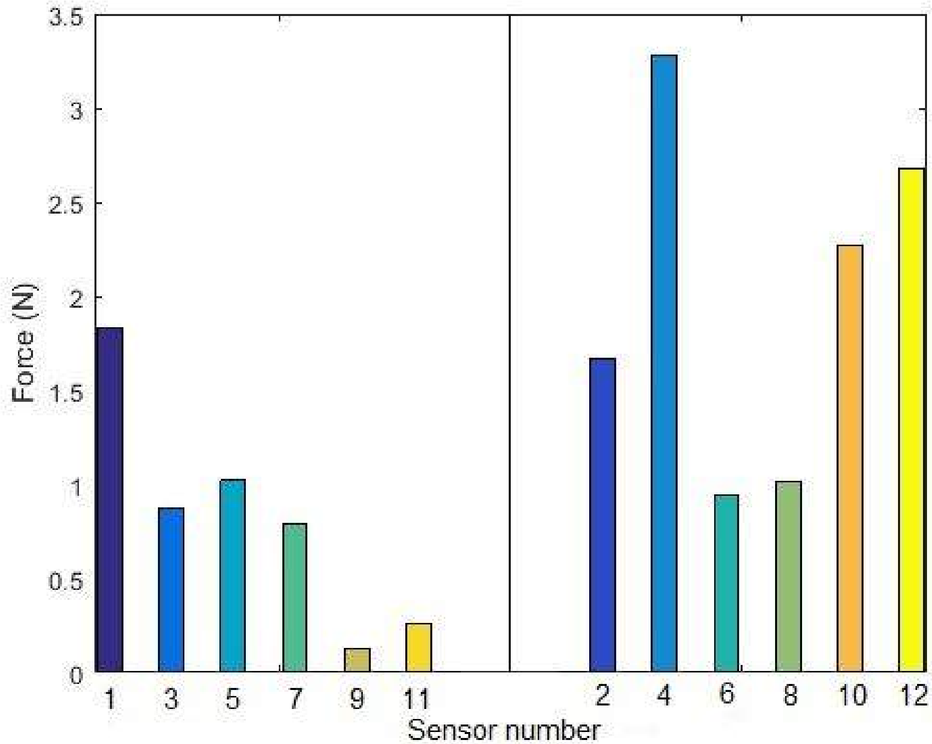

(a)

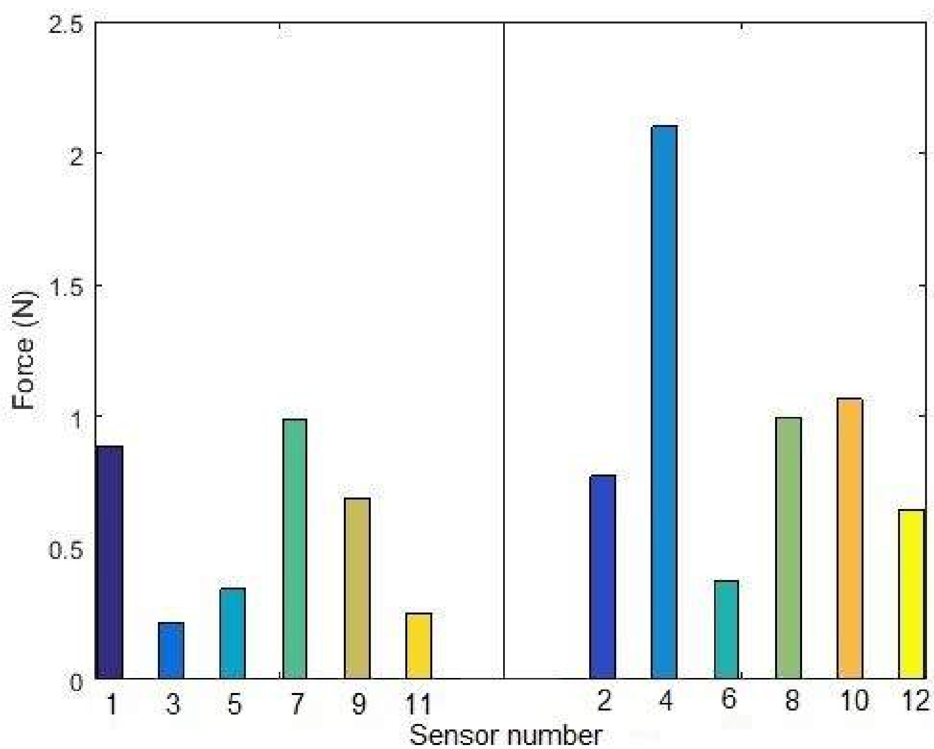

(b)

Figure 5.24: Force response of the two interface geometries. Mean of maximal recordings of squat exercise. a) iterated based interface b) 3D scanner based interface.

Figure 5.24 shows that the average force response is lower for the 3D scanner based interfaces. For the iterated condition, the difference in force relative to the two interface edges is greater in amplitude compared to the 3D scanner based interfaces. This confirms that the tapered geometry of the 3D scanner based interfaces distributed the loads more efficiently and reduced the applied stress at the interface. These interfaces also had less of a tendency to tilt and concentrate the force on a single edge.

The ratio of the recorded force by the 3D scanner based interfaces over the iterated interface can be seen in Table 5.20. In this table, numbers smaller than one indicate a better performance from the 3D scan based interfaces.

Table 5.20: Ratio of of mean value of the sensor maximum force response (interface comparison)

Sensor number (lower edge)	**1**	**3**	**5**	**7**	**9**	**11**
Ratio	0.48	0.24	0.34	1.25	5.31	0.96
Sensor number (upper edge)	**2**	**4**	**6**	**8**	**10**	**12**
Ratio	0.46	0.64	0.40	0.98	0.47	0.24

Table 5.20 shows the reduction of the force amplitude between the two interface geometries, with the exception of sensor 7 and 9, which show an increase. The five-fold increase of sensor 9 is not worrisome since the 3D scanner based interface geometry force recording is of less than 1 Newton. This increase might be due to the fact that the muscle contractions, thus limb stiffness, changed between the two different trials.

5.3 Slider mechanism

Due to the large amount of sliding observed at the shank interface for certain testing conditions, the addition of a sliding degree of freedom along the shank's long axis was investigated. This modification was intended to decrease parallel migration while allowing proper force transfer.

The testing conditions for the sliding interface were set for a specific interface position, combination, and padding. Thus, only the elastic element stiffness was varied.

The chosen exercise to evaluate the modification was the squat. The brace was tested with and without the sliding mechanism, using the 3D scanner based interfaces. The results presented in the following figures and tables are for the medium stiffness. The graphs for the other two degrees of stiffness may be seen in Appendix C. Figure 5.25 demonstrates the effects of an added degree of freedom on the RJA.

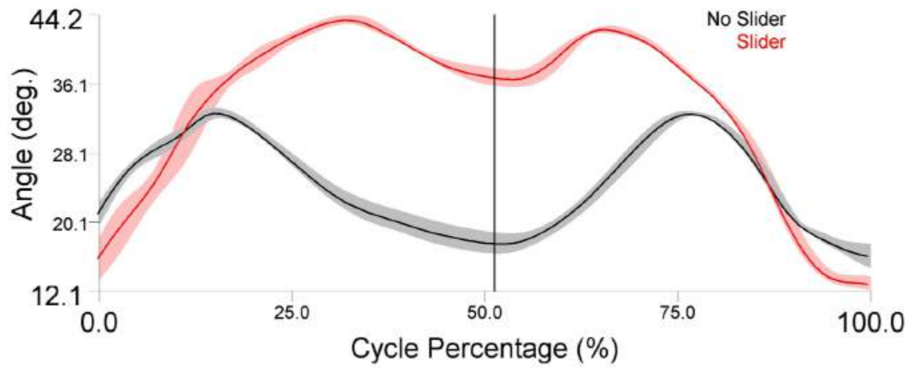

Figure 5.25: RJA (sliding interface, Stiffness 2). Mean and SD of squat exercise.

The RJA increased with the addition of the slider. The slider permitted an easier path for the brace to move downward. This had the effect of decreasing the maximal brace flexion angle. The slider mechanism introduced, on average, 1.9 times more RJA than the static interfaces considering all degrees of stiffness. The thigh interface migration can be seen in Figure 5.26.

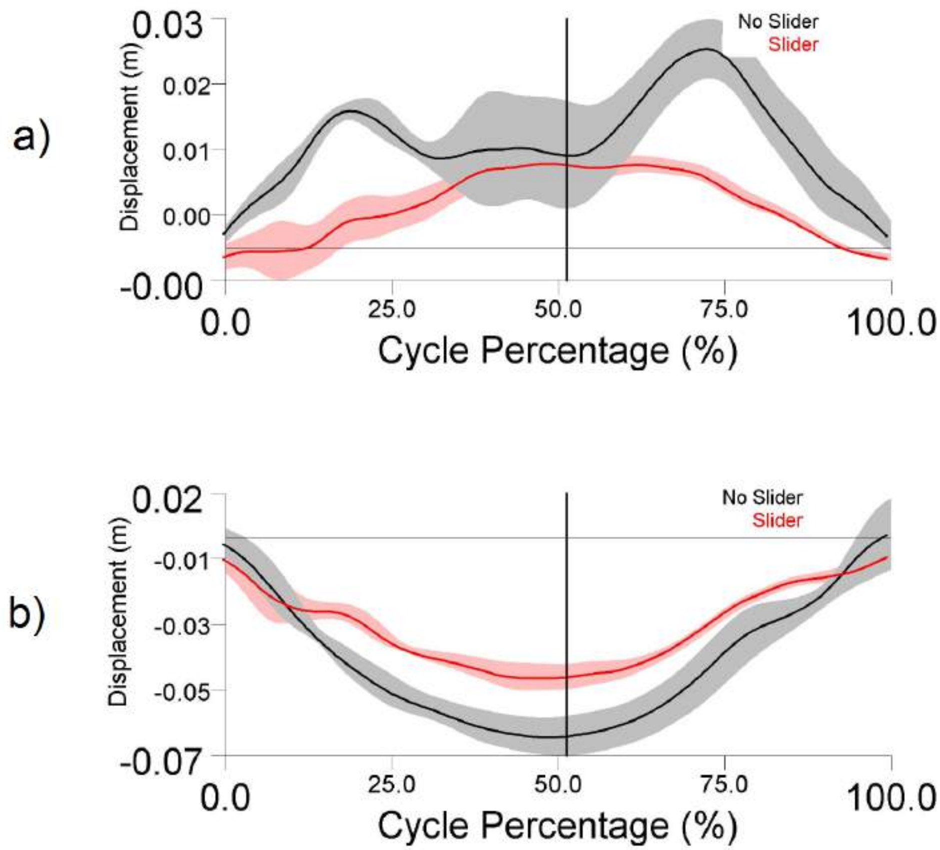

Figure 5.26: Thigh interface migration (sliding interface, Stiffness 2). Mean and SD of squat exercise. a) parallel b) perpendicular

Parallel migration showed better performance with the use of the slider mechanism. Both the parallel and perpendicular migration was decreased, with 1.03 to 6.2 times less migration with the slider mechanism. Figure 5.27 demonstrates the shank interface migration.

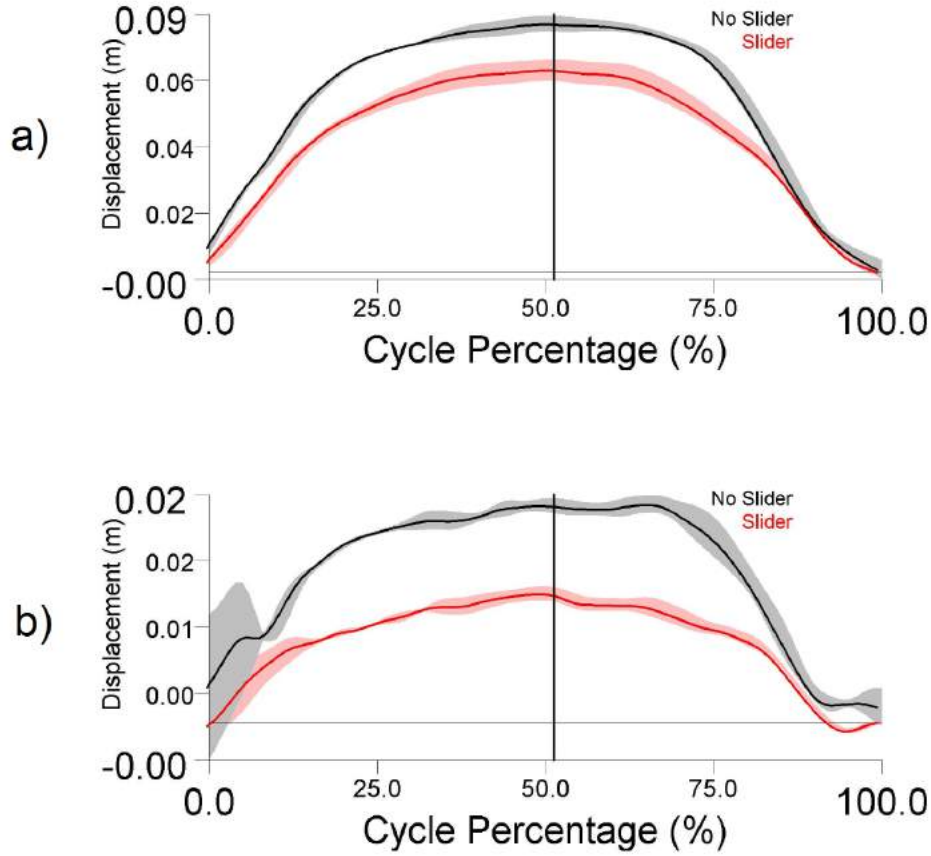

Figure 5.27: Shank interface migration (sliding interface, Stiffness 2). Mean and SD of squat exercise. a) parallel b) perpendicular

Similar to the thigh interface migration, the shank interface migration was improved for all testing conditions, with 1.19 to 1.68 times less migration with the slider mechanism for the parallel and perpendicular directions, respectively. The joint misalignment with and without the slider mechanism can be seen in Figure 5.28.

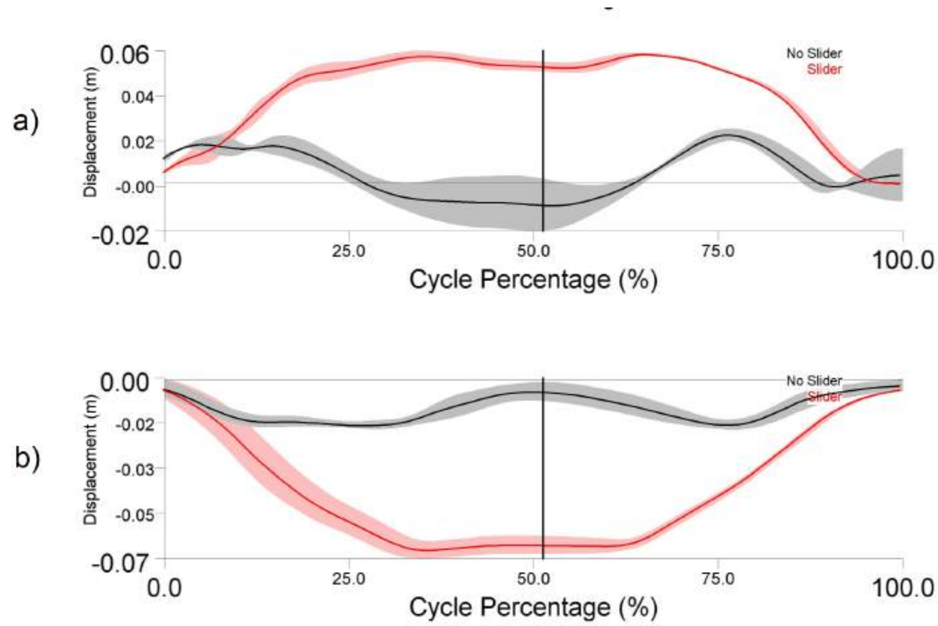

Figure 5.28: Joint misalignment (sliding interface, Stiffness 2). Mean and SD of squat exercise. a) anterior posterior b) superior inferior

Misalignments were generally increased with the addition of a slider. The sliding particularly affected the superior-inferior misalignment since the brace joint center freely moved downwards due to the extra degree of freedom. Although, the introduction of the slider mechanism reduced the anterior-posterior misalignment by about 50% for the Stiffness 1 condition.

Other results for the sliding and non-sliding interfaces at maximum flexion may be seen in Table 5.21, Table 5.22 and Table 5.23. Table 5.23 is the ratio of the no-slider condition over the slider condition. Numbers greater than one indicate a lesser performance from the no-slider condition and vice-versa.

Table 5.21: No-slider condition stiffness analysis (sliding interface). Mean and SD of squat exercise.

Stiffness No slider	**RJA (deg.)**	**TM_Pa (m)**	**TM_Pe (m)**	**SM_Pa (m)**	**SM_Pe (m)**	**M_AP (m)**	**M_SI (m)**
S1	7.3 (0.4)	-0.021 (0.002)	-0.050 (0.003)	0.060 (0.001)	0.008 (0.001)	-0.041 (0.009)	-0.015 (0.001)
S2	17.8 (1.2)	0.014 (0.008)	-0.067 (0.007)	0.082 (0.002)	0.022 (0.001)	-0.010 (0.011)	-0.004 (0.003)
S3	22.3 (2.3)	0.013 (0.007)	-0.055 (0.007)	0.091 (0.008)	0.025 (0.004)	0.000 (0.007)	-0.032 (0.015)

Table 5.22: Slider condition stiffness analysis (sliding interface). Mean and SD of squat exercise.

Stiffness Slider	RJA (deg.)	TM_Pa (m)	TM_Pe (m)	SM_Pa (m)	SM_Pe (m)	M_AP (m)	M_SI (m)
S1	17.9 (0.4)	0.003 (0.006)	-0.045 (0.002)	0.051 (0.003)	0.006 (0.001)	0.020 (0.006)	-0.051 (0.003)
S2	33.8 (4.8)	0.013 (0.002)	-0.047 (0.004)	0.067 (0.004)	0.013 (0.001)	0.052 (0.003)	-0.064 (0.003)
S3	35.8 (0.3)	0.013 (0.000)	-0.048 (0.006)	0.069 (0.001)	0.016 (0.001)	0.040 (0.002)	-0.062 (0.002)

Table 5.23: Slider and no slider comparison stiffness analysis (sliding interface). Ratio of mean value.

Stiffness Comparison	RJA	TM_Pa	TM_Pe	SM_Pa	SM_Pe	M_AP	M_SI
S1	0.41	-6.20	1.10	1.19	1.28	-2.03	0.30
S2	0.53	1.11	1.43	1.23	1.68	-0.19	0.07
S3	0.62	1.03	1.15	1.33	1.56	0.05	0.52

Overall, the sliding interface had some positive and negative effects on brace relative movement. Table 5.23 shows that the slider has a beneficial effect on the migration of both the thigh and shank interface and negative effects on the RJA and misalignment at maximum flexion.

The addition of a slider relived the longitudinal force applied on the interfaces but induced worse RJA and misalignments. It is thus difficult to say if the addition of another degree of freedom would improve the overall device performance.

The addition of the sliding interface mechanism demonstrated the effect of allowing motion along the length of the shank segment. Similarly to Jarrassé and Morel's [43] theory, the misalignment shearing force was eliminated, which had the effect of lowering interface parallel migration. Although, misalignments considerably increased, since the sliding rail was far away from the center of rotation of the knee joint. Polycentric hinges have a rotational and translational component that act together in the same area. This would suggest that this extra degree of freedom would be beneficial if it was moved closer to the knee joint. Despite this, other mechanism with different degrees of freedom might have the ability to reduce both the migration and the misalignment of the brace. All other graphs for the slider mechanism analysis can be found in Appendix C.

5.4 Discussion

5.4.1 Kinematics

The different testing conditions of the APP analysis demonstrated that RJA, the shank migration and SI misalignment was generally greater with the use of 3D scanner based interfaces compared to the iterated based interfaces. Although, it is hard to tell if a specific APP had a best performance, for both interface geometries.

The exercise analysis showed that the RJA, thigh migration and shank perpendicular migration was improved with the use of the 3D scanner based interfaces for most or all exercises. The lunge exercise had the tendency to demonstrate a smaller amplitude of relative movement.

The padding analysis showed improvements or similar performance for the RJA, thigh migration and shank perpendicular migration when using the 3D scanner based interfaces. The firmer padding showed less relative movement.

The LP analysis demonstrated that no single position showed an overall best performance. The extreme positions increased the variability of the results between the two interface geometries so that no clear trends could be observed. The extreme positions placed the interfaces at section of the leg that was either to large or too small for the interface size. This either constrained or allowed greater displacements, which was not a good base for comparison. The climbing of the 3D scanner based interfaces could have also influenced the results.

The stiffness analysis showed that the higher degrees of stiffness produced greater relative movement. Additionally, the 3D scanner based interface had a better performance regarding the RJA, thigh migration and AP misalignment when using the higher degrees of stiffness.

Overall it is difficult to determine if a certain interface geometry has a definitive advantage over the other. In some cases, the iterated interfaces had better performance over the 3D scanner based interfaces and vice versa. The 3D scanner based interface tapered shape offered a surface that has more contact area with the limb and a geometry that offers some resistance to sliding. Generally, the thigh interface had better performance with the 3D scanner based interfaces while the shank interface had better performance with the iterated based interface geometry. This would suggest that the extra constraints (tapered shape) of the 3D scanner based interfaces could cause more kinematic discrepancies. In other words, the shank interface was pushed to greater relative displacement compared to the iterated interface version because the thigh interface was more stable. Since the device joint cannot fully replicate the movements of the biological joint, the relative movement, especially in parallel migration, had to occur mostly at the shank interface. Thus, some relative movement of both interface is perhaps necessary for the best performance of the brace. If the joint type between the brace and knee joint is not the same, a brace with less constraints would have an improved performance, since the allowed movements would compensate for the different joint kinematics. In the opposite case, a brace with identical joint kinematics would have a better performance with a more constrained interface system. Since this particular analysis resembles the former case, a certain degree of interface compliance would be required.

Some of the results from this research did not yield the clear advantage of a testing variables for a particular type of analysis. For example, the APP and LP analysis did not point to a best testing condition. This suggest that the performance of the device is sensitive to the position of the interfaces relative to the limb. These unclear solutions also suggest that there is no unique solution that would fit a large population of test subjects. For example, the participant of this research was in good physical shape, which translates to a limb tissue compliance that is lower than the average population. The limb conditions vary from one individual to another, which make non-uniform limb testing conditions. The interfaces of the device used during this research were of a uniform nature, with static variables. This would suggest that the use of an interface with adaptable variables could improve the performance of the brace.

The variation of the motion capture results was relatively high compared to what could be found in classical knee orthotic studies with no assistance. The majority of the relative movement was probably caused by the fact that the brace is not a custom fitted orthotic. Furthermore, the brace is relatively heavy compared to high performance knee braces, which contributed to the downwards migration of the brace over time. This research focused on assist devices with active actuation. The method of assistance of the knee brace used in this research is much different compared to knee orthotics and had the effect of introducing variability in the results.

5.4.2 Kinetics

The difference between the iterated and 3D scanner based interfaces was noticeable. Results have shown that the 3D scanner based interfaces had about a 40 percent decrease in force amplitude on average, excluding sensor 9. The difference in results is surprising considering the noticeable effects brought on by the addition of a tapered profile.

Furthermore, the 3D scanner based geometry also had the ability to improve force distribution. The difference in force recordings between the two interface edges was lower compared to the iterated interface geometry. For these reasons, active devices that are transferring considerable forces should be designed with interfaces geometries that closely follow the user limb geometry, if not user-specific, as is standard practice in orthotics.

The maximal force produced by the brace divided by the area of the interface falls in the range of ischemic blood level and could impede local blood flow if sustained over time. Although not dangerous, this level of pressure could cause discomfort if the brace were to be used extensively. Powered devices that have assistance in extension should consider pauses in the assistance strategy. A labourer or military personnel carrying a significant payload in a stationary position involving a great amount of knee flexion (e.g. squat or lunge) would be at risk of developing discomfort in a relatively short amount of time, depending on the force transfer of the device.

The summation of the total force of the sensors was not reported here. This parameter could have indicated if the force response was constant between the two types of geometries. Under the same brace assistance, the total sensor force response would have been similar between the two interface geometries. The sensor forces would have been lower in the case of a greater interface force distribution compared to the case where the interface would not have had as much force distribution. This is assuming uniform force distribution. This parameter, the total force response, was not incorporated in the analysis because the large tissue deformations would have influenced the force flow, with an unknown portion passing through the material adjacent to the sensors.

The posterior position showed better force transfer compared to the anterior position since the interface rigid portion would push on the limb instead of transferring forces with the strap portion. The force response of a particular sensor of the anterior thigh interface may be seen in Figure 5.29.

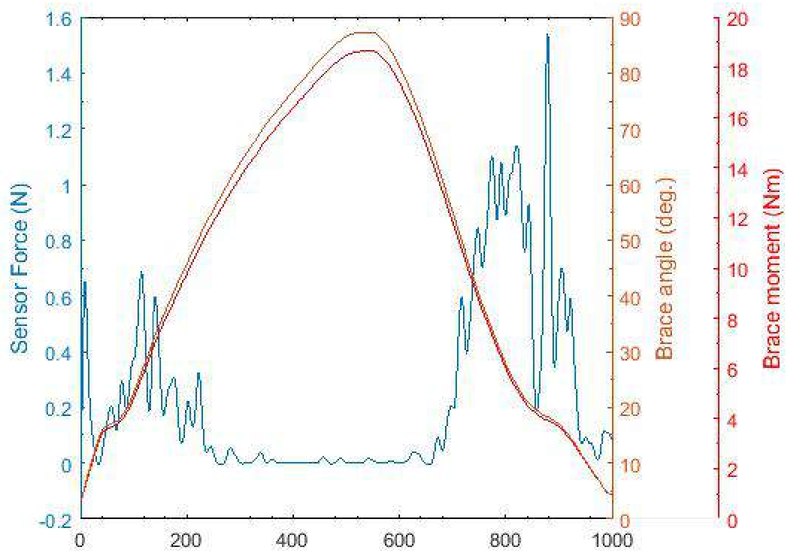

Figure 5.29: Contact loss of the anterior interface

Figure 5.29 shows that at first, the force tends to increase, then drops to zero at about 40 degrees of flexion then increases again at about 50 degrees of flexion after the maximum brace angle has been reached. The loss of contact is represented by the force being zero in between these two brace angles. In some instances, the anterior interface would completely loose contact with the limb, this was usually seen in the extreme positions of the interface. All of the sensors would then have a zero force reading. This could be seen visually, as per Figure 5.30.

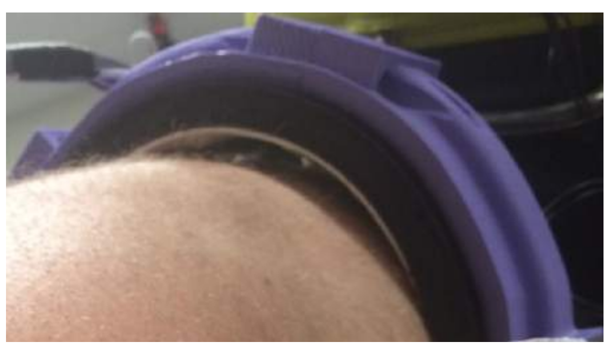

Figure 5.30: Loss of interface contact could visually be seen

Since this contact loss does not properly represent the true force distribution on the interface, only the posterior interface force analysis was presented in the results section.

5.4.3 Design recommendations

Design recommendations that could be applied to the design of assist devices have emerged from the analysis and are as follow:

- Rigid portions of the interfaces should be positioned on the brace in function of assistance. This configuration is more stable.
- The padding analysis suggested the use of firmer interface padding. The highest padding density used in this research lowered relative movement.
- The LP analysis confirmed that the shank interface should be designed to be positioned on the upper or mid portion of the shank segment. The thigh interface should be positioned on the mid or low portion of the thigh segment.
- Introduce tilting interfaces in the sagittal plane to reduce interface tilt, which would improve contact as the brace angle increases.
- Some free longitudinal motion is suggested to reduce interface migration, especially if the user and brace joints are not the same.
- Design interface geometry with user-specific parameters to improve interface force distribution.

5.5 Limitations and sources of error

5.5.1 Brace testing

While testing the prototype knee brace with the universal linear testing machine, the 100 kN load cell was used since there were no compatible attachments. This carries a certain error. The fluctuations in the 100 kN load cell are about 3N which could correspond to about 4 percent error at maximal flexion.

The size and weight of the prototype knee brace was not designed for dynamic exercises such as walking. The brace frame and elastic elements made the brace too wide to be comfortably used for walking and would affect the users gait in the event of experimental testing. This limited the design to activities where the participant remained stationary. The brace frame was not designed to be form fitting, compared to high performance custom fitted knee braces, which would further decrease the walking ability. If the experimental knee brace was to be used for other physical activities such as walking or stair climb, the current design should be revised so the passive actuation and the device frame would be more compact.

5.5.2 Force sensors

The sensors used in this study are not well suited for compliant materials such as skin and soft tissues. The large deformations, or the tissue depressions had the effect of bending the sensors while recording data, which had an effect on the force recordings. Since these sensors were against compliant material, the large deformations of the skin would cover all the sensors and a portion of the force flow was directed in the adjacent material. A polymeric sheet acting as a backing material was added to mitigate this effect. These sensors wee chosen since they have been used in other engineering applications as, for example, car seat studies and instrumented shoe insole to measure pressure distribution. These sensor were also chosen since they specifications with above average performance at an affordable cost.

While calibrating the sensors, the force applicator tip as well as the base material had a great effect on the sensor's response. Therefore, the calibration performed does not perfectly recreate the actual testing environment; however, these conditions would be very difficult to achieve. Since properties such as geometry and stiffness of the lower limb differ from person to person, the calibration should ideally be performed on the test participant. The limb stiffness also changes at every instance of the experimental exercises, depending on muscle activity and local blood flow. In addition, the linear testing machine is limited to relatively low speeds of force application, which are much slower than real-world experiments.

Force recordings obtained with the sensors would not reflect the true value of the force over the interface. The differences that exist between the calibration and the actual contact surface make it hard to have a reliable sensor. These differences make it virtually impossible to determine the amount of error. The force measurements were used as relative measurements between sensors. This identifies the zones where high relative forces are transmitted to the limb. Furthermore, some variables changed during testing (i.e. padding density) which would have affected the force response. In particular, the stiffness of the limb played a considerable role. Further testing was performed in order to see the effects of the changing lower limb stiffness. A static known weight was applied directly on the center of the thigh interface when the participant was sitting. Two testing conditions were recorded, when the participant was in a relaxed state and when the participant was flexing his quadriceps muscles. Data were gathered over a period of 10 seconds and then averaged. The force readings were 25 to 40 % higher for the flexed condition. This is just to show the effect of muscle contraction, or limb stiffness on the instrumentation under controlled conditions

5.5.3 Human testing

The computation of migration and misalignment analysis was only performed in the sagittal plane. Thus, the motion of the markers was not entirely described. A 3D analysis where the relative movements would have been defined in function of the orientation of the leg instead of a reference plane would have enabled the participant to perform the exercises in whatever orientation relative to the reference coordinate axis. This would have also enabled the recording of the motion of the markers in all planes.

Only one participant was chosen since the interfaces were manufactured to the dimensions of the participant's limb. Having multiple participants would have taken greater amount of time and resources, which was not deemed feasible for this research. Since the human testing was only performed with one participant, the results of this work can not be extrapolated for a larger population.

When the testing was conducted, the participant did produce some perspiration which increased skin humidity and has effects on skin properties. The microclimate at the surface of the skin was altered. Skin humidity increases the coefficient of friction, which improve interface adhesion. This change of friction over time could have affected the amount of relative movement of the brace during testing.

The migration results do not represent the amount of interface rubbing against the skin. Skin has the ability to stretch, so that the relative movement between the skin and interface could have been of a zero-value even if interface migration exists. A marker was placed on the interface and was moved without any dynamic friction occurring. The test showed that there was approximately 37 and 28 mm of parallel and perpendicular migration respectively at the thigh interface location, and 14 and 16 mm of parallel and perpendicular migration at the shank interface position. Even if the position of the reference markers was chosen so skin stretching would be minimal, the reference markers could have moved by a certain amount during motion, which would have affected the amplitude of the migration.

The initial fitting of the device could also have played a role in the amplitude of variation of the results. The brace was fitted in the same manner between the different testing conditions. The position of the brace relative to the limb was verified by measuring the distance between a marker on the brace frame and the participant's body. Despite these attempts, a small difference in fit could have influenced the migration and misalignment results.

Furthermore, it is currently impossible to say if the participant's muscle contractions were constant during the whole testing period. The participant could have well compensated with his other leg while performing the exercises, introducing variability in limb stiffness over the different trials.

Chapter 6: Conclusion and future work

6.1 Conclusion

An experimental extension assist knee brace was developed using orthotic uprights, machined aluminium parts, 3D printed components and carbon fiber strips. Testing of the brace using motion capture and a force mapping apparatus was used to analyse and compare the device performance. The difference in performance between the different testing variables for a given analysis were measured to determine the variables that had the greatest effect on performance.

Motion capture demonstrated how the RJA, migration and misalignment varied with the different testing conditions. No single testing parameter had an overall best performance. Nevertheless, some results seemed to be recurrent. For example, the 3D printed interfaces migration was lower than the iterated interfaces at the thigh interface location. Furthermore, the addition of a sliding interface demonstrated lesser parallel migration but a higher misalignment.

Force mapping demonstrated that force concentrations exist. The forces were higher on a particular edge of the interface and at particular areas, suggesting that the interfaces were not in proper contact on the limb at all times. This supports the notion that the tilt of the interfaces was due to the kinematic mismatch between the device and the user's joint. Padding had less of an effect on force transmission than stiffness of the elastic element. 3D scanned interfaces showed better force distribution over the iterated interfaces.

On a final note, comfort and safety are very important aspects that must be accounted for during the development of medical devices, including mobility assist devices. Any device with interfaces that are not comfortable, easy to use or properly designed for specific operating conditions will simply be discarded. The uniqueness of every individual does not offer a point of attachment with uniform properties. More research efforts in the particular field of assist device interactions are required to further understand the relationships that exist between user and machine, whether biological, kinematic or kinetic to introduce an attachment system that has the capability to adapt to the user's changing conditions. This would also permit the emergence of strong design considerations and guidelines that should be applied and enforced for the standardisation of design of these relatively new devices.

6.2 Future work

The elastic elements responsible for creating the brace moment were very susceptible to misalignments of the device frame upper and lower portions. In addition, the failure of the carbon fiber strips occurred multiples times. A design that is independent of misalignments and that does not rely on large deformation would improve the prototype. For example, a linear spring and cam system could be implemented on the upper portion of the brace and would be linked to the lower portion with a cable. The flexion of the brace would make the cam rotate and thus pull on the cable, which in turn would pull on the spring, exerting a joint reaction moment. This mechanism can be seen in Figure 6.1

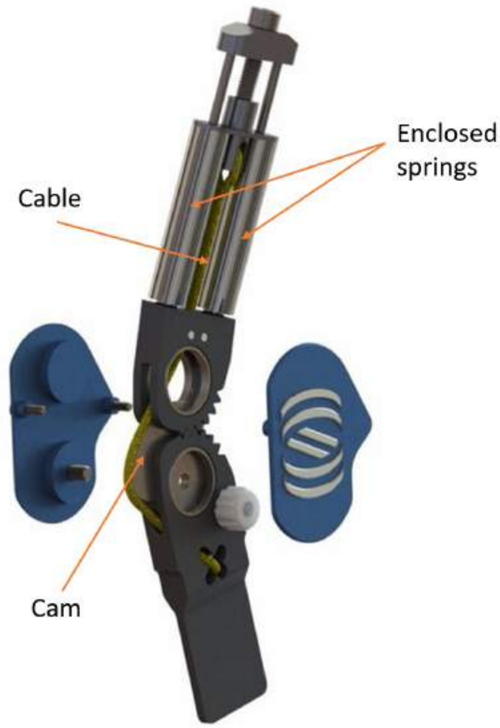

Figure 6.1: Spring and cam mechanism of the Leviation knee brace by Spring Loaded Technology LLC [53].

The addition of the sliding interface demonstrated some advantages. The testing of a polycentric brace joint would very well validate the addition of this extra degree of freedom. The evaluation of the performance of this particular joint could be compared to the results of this study using the same methodology. Furthermore, the testing of a self aligning joint would be of interest. An example of such self aligning joint maybe seen in an article by Cempini et al. [6].

Extreme interface positions increased the relative tilt of the interfaces with respect to the limb. This was shown in both the motion capture results, as well as communicated by the participant. Designing an interface with an added tilting degree of freedom at the junction of the interface supports and the brace frame could help ensure a flat contact, and thus a better pressure distribution.

The development of an interface padding with an adaptable density or variable stiffness could further improve the brace performance. This would allow to examine if a custom fitted padding element along side with the 3D printed interfaces would lower interface migration and contact forces. The padding would be designed from measurements taken on the limb of the participant to determine the change in stiffness along the medial-lateral axis, to construct a custom padding. The review of the current assist devices available on the market or in research found no interface solutions that offers a variable stiffness or padding material that matches the compliance of the lower limbs.

The measurement of blood flow would also improve the research. A photoplethysmogram (PPG) sensor could have been implemented in a particular area near the brace interface and the force sensors. These two simultaneous measurements could have shown the variation in blood flow in function of the force applied on the limb.

While calibrating the force sensors, the force applicator tip as well as the base material had a great effect on sensor response. The force sensing instrumentation would be improved with the development of a force sensor that would be more suited for this application. Alternatively, perhaps placing the sensors in between a rigid interface structure (housing) with a sliding element would isolate the sensors from the soft tissues but would still permit them to record data. Furthermore, the development of an improved calibration interface would produce a calibration with more representative measures of the force applied to the limb. In the future, the research would benefit from the development of novel material with properties similar to the leg's soft tissues. As an alternative, cadaver limbs could also be used for calibration but was not included in the scope of this study. The sensors used in this study only permitted the recording of normal force acting on the interface. Shear forces would have also been present since the interfaces moved longitudinally. Shear forces have a great effect on skin comfort. A new type of sensor will be developed to enhance this research. In other words, a sensor which is not affected by large tissue deformations and that would be able to record shear forces.

References

[1] A.B. Zoss, H. Kazerooni, and A. Chu. Biomechanical design of the Berkeley lower extremity exoskeleton (BLEEX). *IEEE/ASME Transactions on Mechatronics*, 11(2):128–138, April 2006.

[2] K. A. Strausser and H. Kazerooni. The development and testing of a human machine interface for a mobile medical exoskeleton. In *2011 IEEE/RSJ International Conference on Intelligent Robots and Systems*, pages 4911–4916, September 2011.

[3] L. Levesque, S. Pardoel, Z. Lovrenovic, and M. Doumit. Experimental comfort assessment of an active exoskeleton interface. *IEEE International Symposium on Robotics and Intelligent Sensors (IRIS)*, 2017.

[4] A. M. Dollar and H. Herr. Design of a quasi-passive knee exoskeleton to assist running. In *2008 IEEE/RSJ International Conference on Intelligent Robots and Systems*, pages 747–754, September 2008.

[5] Ken Yasuhara, Kei Shimada, Taiji Koyama, Tetsuya Ido, Keishiro Kikuchi, and Yosuke Endo. Walking assist device with stride management system. *Honda R&D Tech. Rev. 21 (2)*, 2009.

[6] Francesco Giovacchini, Federica Vannetti, Matteo Fantozzi, Marco Cempini, Mario Cortese, Andrea Parri, Tingfang Yan, Dirk Lefeber, and Nicola Vitiello. A light-weight active orthosis for hip movement assistance. *Robotics and Autonomous Systems*, 73:123–134, November 2015.

[7] Kamran Shamaei, Paul C. Napolitano, and Aaron M. Dollar. A quasi-passive compliant stance control knee-ankle-foot orthosis. In *Rehabilitation Robotics (ICORR), 2013 IEEE International Conference on*, pages 1–6. IEEE, 2013.

[8] Daniel K. Ramsey and Venkat N. Krovi. Smart Knee Brace Design With Parallel Coupled Compliant Plate Mechanism and Pennate Elastic Band Spring. *J. Mechanisms Robotics 7(4), 041024*, 2015.

[9] Wilian M. dos Santos, Glauco A.P. Caurin, and Adriano A.G. Siqueira. Design and control of an active knee orthosis driven by a rotary Series Elastic Actuator. *Control Engineering Practice*, 58:307–318, January 2017.

[10] Gregory S Sawicki and Daniel P Ferris. A pneumatically powered knee-ankle-foot orthosis (KAFO) with myoelectric activation and inhibition. *Journal of NeuroEngineering and Rehabilitation*, 6(1):23, 2009.

[11] André Schiele. *Fundamentals of ergonomic exoskeleton robots.* PhD thesis, Delft University of Technology, Mekelweg 2, 2628 CD Delft, Netherlands, 2008.

[12] José L. Pons, editor. *Wearable robots: biomechatronic exoskeletons*. Wiley, Hoboken, N.J, 2008.

[13] Nathanaël Jarrasse and Guillaume Morel. Connecting a Human Limb to an Exoskeleton. *IEEE Transactions on Robotics*, 28(3):697–709, June 2012.

[14] Jesús Tamez-Duque, Rebeca Cobian-Ugalde, Atilla Kilicarslan, Anusha Venkatakrishnan, Rogelio Soto, and Jose Contreras-Vidal. Real-Time Strap Pressure Sensor System for Powered Exoskeletons. *Sensors*, 15(2):4550–4563, February 2015.

[15] Ashish Rathore, Matthew Wilcox, Dafne Zuleima Morgado Ramirez, Rui Loureiro, and Tom Carlson. Quantifying the human-robot interaction forces between a lower limb exoskeleton and healthy users. In *Engineering in Medicine and Biology Society (EMBC), IEEE 38th Annual International Conference of the*, pages 586–589. IEEE, 2016.

[16] ”FlexiForce A301 Sensor” [online], Available: https://www.tekscan.com/products-solutions/force-sensors/a301, [Accessed: August 11th 2016].

[17] ”Levitation knee brace” [online], Available: https://springloadedtechnology.com/, [Accessed: March 8th 2018].

[18] ”The frontal plane” [online], Available: http://www.gustrength.com/kinesiology:whatis-the-frontal-plane, [Accessed: March 14th 2016].

[19] ”Anatomical references” [online], Available: https://www.pinterest.com/pin/737042295236536294/, [Accessed: April 28th 2016].

[20] J. Gordon Betts, OpenStax College, and Rice University. *Anatomy & physiology.* 2013. OCLC: 900895954.

[21] S. Derler and L.-C. Gerhardt. Tribology of Skin: Review and Analysis of Experimental Results for the Friction Coefficient of Human Skin. *Tribology Letters*, 45(1):1–27, January 2012.

[22] Robert L. Williams, Wei Ji, John N. Howell, and Robert R. Conatser. Device for measurement of human tissue properties in vivo. *Journal of Medical Devices*, 1(3):197–205, 2007.

[23] Guohao Dai, J. P. Gertler, and R. D. Kamm. The effects of external compression on venous blood flow and tissue deformation in the lower leg. *Journal of biomechanical engineering*, 121(6):557–564, 1999.

[24] "Kinect for Windows: Sensor Components and Specifications" [online], Available: https://msdn.microsoft.com/en-us/library/jj131033.aspx, [Accessed: August 5th 2017].

[25] Merja Rantakokko, Erja Portegijs, Anne Viljanen, Susanne Iwarsson, Markku Kauppinen, and Taina Rantanen. Changes in life-space mobility and quality of life among community-dwelling older people: a 2-year follow-up study. *Quality of Life Research*, 25(5):1189–1197, May 2016.

[26] Jason Shafrin, Jeff Sullivan, Dana P. Goldman, and Thomas M. Gill. The association between observed mobility and quality of life in the near elderly. *PloS one*, 12(8):e0182920, 2017.

[27] Daniel P. Ferris, Gregory S. Sawicki, and Monica A. Daley. A Physiologist's perspective on robotic exoskeleton for human locomotion. *International journal of HR : humanoid robotics*, 4(3):507–528, September 2007.

[28] Hugh Herr. Exoskeletons and orthoses: classification, design challenges and future directions. *Journal of NeuroEngineering and Rehabilitation*, 6(1):21, 2009.

[29] Marco Cempini, Stefano Marco Maria De Rossi, Tommaso Lenzi, Nicola Vitiello, and Maria Chiara Carrozza. Self-Alignment Mechanisms for Assistive Wearable Robots: A Kinetostatic Compatibility Method. *IEEE Transactions on Robotics*, 29(1):236–250, February 2013.

[30] Xiaobo Zhou, Daniel K. Ramsey, and Venkat N. Krovi. Smart Knee Brace Design with Parallel Coupled Compliant Plate (PCCP) Mechanism and Pennate Elastic Band (PEB) Spring. *JMR*, 14:1184, 2015.

[31] Paula C. Silva, Miguel T. Silva, and Jorge M. Martins. Evaluation of the contact forces developed in the lower limb/orthosis interface for comfort design. *Multibody System Dynamics*, 24(3):367–388, October 2010.

[32] Mohammad Esmaeili, Kumudu Gamage, Eugene Tan, and Domenico Campolo. Ergonomic considerations for anthropomorphic wrist exoskeletons: A simulation study on the effects of joint misalignment. In *Intelligent Robots and Systems (IROS), 2011 IEEE/RSJ International Conference on*, pages 4905–4910. IEEE, 2011.

[33] Yasuhiro Akiyama, Shogo Okamoto, Yoji Yamada, and Kenji Ishiguro. Measurement of Contact Behavior Including Slippage of Cuff When Using Wearable Physical Assistant Robot. *IEEE Transactions on Neural Systems and Rehabilitation Engineering*, 24(7):784–793, July 2016.

[34] Yasuhiro Akiyama, Yoji Yamada, Koji Ito, Shiro Oda, Shogo Okamoto, and Susumu Hara. Test method for contact safety assessment of a wearable robot-analysis of load caused by a misalignment of the knee joint. In *RO-MAN, 2012 IEEE*, pages 539–544. IEEE, 2012.

[35] Andrew Chu, Hami Kazerooni, and Adam Zoss. On the biomimetic design of the berkeley lower extremity exoskeleton (BLEEX). In *Robotics and Automation, 2005. ICRA 2005. Proceedings of the 2005 IEEE International Conference on*, pages 4345–4352. IEEE, 2005.

[36] Harrison P. Crowell III, Angela C. Boynton, and Michael Mungiole. Exoskeleton power and torque requirements based on human biomechanics. Technical report, Army Research Lab Aberdeen Proving Ground, 2002.

[37] Hyo-gon Kim, Jong-won Lee, Jaeho Jang, Changsoo Han, and Sangdeok Park. Mechanical design of an exoskeleton for load-carrying augmentation. In *Robotics (ISR), 2013 44th International Symposium on*, pages 1–5. IEEE, 2013.

[38] Kan Kanjanapas and Masayoshi Tomizuka. 7 Degrees of Freedom Passive Exoskeleton for Human Gait Analysis: Human Joint Motion Sensing and Torque Estimation during Walking. *IFAC Proceedings Volumes*, 46(5):285–292, 2013.

[39] R. J. Farris, H. A. Quintero, and M. Goldfarb. Performance evaluation of a lower limb exoskeleton for stair ascent and descent with Paraplegia. pages 1908–1911. IEEE, August 2012.

[40] Zhiqiang Li, Hanxing Xie, Weilin Li, and Zheng Yao. Proceeding of human exoskeleton technology and discussions on future research. *Chinese Journal of Me-*

chanical Engineering, 27(3):437–447, May 2014.

[41] A.H.A. Stienen, E.E.G. Hekman, F.C.T. van der Helm, and H. van der Kooij. Self-Aligning Exoskeleton Axes Through Decoupling of Joint Rotations and Translations. *IEEE Transactions on Robotics*, 25(3):628–633, June 2009.

[42] M. A. Regalbuto, J. S. Rovick, and P. S. Walker. The forces in a knee brace as a function of hinge design and placement. *The American journal of sports medicine*, 17(4):535–543, 1989.

[43] Damiano Zanotto, Yasuhiro Akiyama, Paul Stegall, and Sunil K. Agrawal. Knee Joint Misalignment in Exoskeletons for the Lower Extremities: Effects on User's Gait. *IEEE Transactions on Robotics*, 31(4):978–987, August 2015.

[44] Baptiste Pierrat, Carine Millot, Jérôme Molimard, Laurent Navarro, Paul Calmels, Pascal Edouard, and Stéphane Avril. Characterisation of Knee Brace Migration and Associated Skin Deformation During Flexion by Full-Field Measurements. *Experimental Mechanics*, 55(2):349–360, February 2015.

[45] Jonathan C. Singer and Mario Lamontagne. The effect of functional knee brace design and hinge misalignment on lower limb joint mechanics. *Clinical Biomechanics*, 23(1):52–59, January 2008.

[46] Saeedeh Seyed Mohseni, Farzam Moss, Hossein Karimi, and Mohammad Kamali. Arthrometric evaluation of stabilizing effect of knee functional bracing at different flexion angles. *Journal of sports science & medicine*, 8(2):247, 2009.

[47] Mario Lamontagne. Pressure Measurement Between A Functional Knee Brace And The Leg. In *ISBS-Conference Proceedings Archive*, volume 1, 2002.

[48] Dan Ramsey, Per Wretenberg, Mario Lamontagne, and Gunnar Németh. Electromyographic and biomechanic analysis of anterior cruciate ligament deficiency and functional knee bracing, 2002.

[49] Bruce Brownstein. Migration and design characteristics of functional knee braces. *Journal of Sport Rehabilitation*, 7:33–43, 1998.

[50] Jorma Styf. The influence of external compression on muscle blood flow during exercise. *The American journal of sports medicine*, 18(1):92–95, 1990.

[51] Jorma R. Styf, Manoutch Nakhostine, and David H. Gershuni. Functional knee braces increase intramuscular pressures in the anterior compartment of the leg. *The American journal of sports medicine*, 20(1):46–49, 1992.

[52] Jorma R. Styf, Olof Lundin, and David H. Gershuni. Effects of a functional knee brace on leg muscle function. *The American journal of sports medicine*, 22(6):830–834, 1994.

[53] Olof Lundin and Jorma R. Styf. Intramuscular Pressure in the Leg and Thigh Related to Tensile Strap Force During Knee Brace Wear An Experimental Study in Man. *The American journal of sports medicine*, 26(4):567–570, 1998.

[54] Heather Ashton. Effect of inflatable plastic splints on blood flow. *British medical journal*, 2(5527):1427, 1966.

[55] "Types of transducers" [online], Available: http://www.npl.co.uk/reference /faqs/how-many-different-types-of-force-transducer-are-there-(faq-force), [Accessed: November 5th 2017].

[56] Hon Keung Yuen and Donna Garrett. Comparison of three wheelchair cushions for effectiveness of pressure relief. *American Journal of Occupational Therapy*, 55(4):470–475, 2001.

[57] Fernando Vidal-Verdú, Maria Jose Barquero, Julián Castellanos-Ramos, Rafael Navas-González, Jose Antonio Sánchez, Javier Serón, and Alfonso García-Cerezo. A Large Area Tactile Sensor Patch Based on Commercial Force Sensors. *Sensors*, 11(12):5489–5507, May 2011.

[58] "What is motion capture?" [online], Available: https://www.vicon.com/what-is-motion-capture, [Accessed: November 5th 2017].

[59] ICRC-Manufacturing gidelines, Available: https://www.icrc.org/eng/assets/ files/other/eng-kafo.pdf, [Accessed: November 5th 2017].

[60] William D. Callister and David G. Rethwisch. *Materials science and engineering: an introduction*. John Wiley & Sons, Hoboken, NJ, 8th ed edition, 2010. OCLC: ocn401168960.

[61] Nathan J. Givoni, Tuan Pham, Trevor J. Allen, and Uwe Proske. The effect of quadriceps muscle fatigue on position matching at the knee: Position matching at the knee after exercise. *The Journal of Physiology*, 584(1):111–119, October 2007.

[62] Billy Sperlich, Dennis-Peter Born, Kimmo Kaskinoro, Kari K. Kalliokoski, and Marko S. Laaksonen. Squeezing the Muscle: Compression Clothing and Muscle Metabolism during Recovery from High Intensity Exercise. *PLoS ONE*, 8(4):e60923, April 2013.

[63] Hikaru Hisaeda, Minoru Shinohara, Motoki Kouzaki, and Testuo Fukunaga. Effect of local blood circulation and absolute torque on muscle endurance at two different knee-joint angles in humans. *European journal of applied physiology*, 86(1):17–23, 2001.

[64] Derek Field and Jane S. Owen Hutchinson. *Field's anatomy, palpation, and surface markings*. Elsevier Health Sciences, 2006.

[65] Robert M. Szabo and Richard H. Gelberman. Peripheral Nerve Compression-Etiology, Critical Pressure Threshold, and Clinical Assessment.pdf, 1984.

[66] G.-M. Rotaru, D. Pille, F.K. Lehmeier, R. Stämpfli, A. Scheel-Sailer, R.M. Rossi, and S. Derler. Friction between human skin and medical textiles for decubitus prevention. *Tribology International*, 65:91–96, September 2013.

[67] B. N. J. Persson, A. Kovalev, and S. N. Gorb. Contact Mechanics and Friction on Dry and Wet Human Skin. *Tribology Letters*, 50(1):17–30, April 2013.

[68] C. Pailler-Mattei, S. Bec, and H. Zahouani. In vivo measurements of the elastic mechanical properties of human skin by indentation tests. *Medical Engineering & Physics*, 30(5):599–606, June 2008.

[69] Aisling Ní Annaidh, Karine Bruyère, Michel Destrade, Michael D. Gilchrist, and Mélanie Otténio. Characterization of the anisotropic mechanical properties of excised human skin. *Journal of the Mechanical Behavior of Biomedical Materials*, 5(1):139–148, January 2012.

[70] HAKAN Oflaz and ONDER Baran. A new medical device to measure a stiffness of soft materials. *Acta of Bioengineering and Biomechanics*, 16(1), 2014.

[71] International review. Pressure ulcer prevention: pressure, shear, friction and microclimate in context. A consensus document. london: Wounds international, 2010.

[72] Mohsen Makhsous, Dohyung Lim, Ronald Hendrix, James Bankard, William Z. Rymer, and Fang Lin. Finite element analysis for evaluation of pressure ulcer on the buttock: development and validation. *Neural Systems and Rehabilitation Engineering, IEEE Transactions on*, 15(4):517–525, 2007.

[73] W. Li, X.D. Liu, Z.B. Cai, J. Zheng, and Z.R. Zhou. Effect of prosthetic socks on the frictional properties of residual limb skin. *Wear*, 271(11-12):2804–2811, September 2011.

[74] Massimo Cenciarini and Aaron M. Dollar. Biomechanical considerations in the design of lower limb exoskeletons. In *Rehabilitation Robotics (ICORR), 2011 IEEE International Conference on*, pages 1–6. IEEE, 2011.

Appendix A

Human anatomy and physiology

This section of the document will focus on general information regarding human anatomy and physiology.

A.1 Terminology

The study of human movements requires some general terminology in order to fully understand the directions and references used to describe the motion of the human body. First, anatomical planes are used to describe motion with reference to a particular view of the human body. For example, gait is usually studied in the sagittal plane since most of the motion occurs in this plane. Figure A.1 illustrates the different anatomical planes.

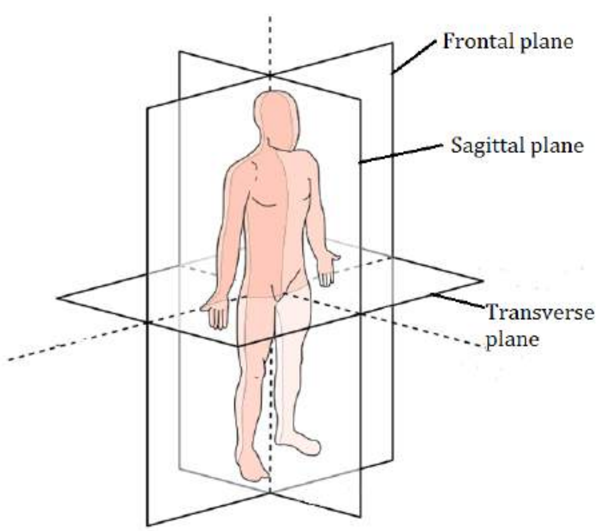

Figure A.1: The different anatomical planes [54]

Limb movements in these particular planes are usually referred as flexion, extension and rotation of a particular joint. This research focuses on the knee joint. Hence, the flexion and extension of this joint is important. Flexion of the knee joint describes the motion of bending the lower leg towards the upper leg and the extension describes the straitening of the leg. Figure A.2 illustrates the main movements performed by the knee joint.

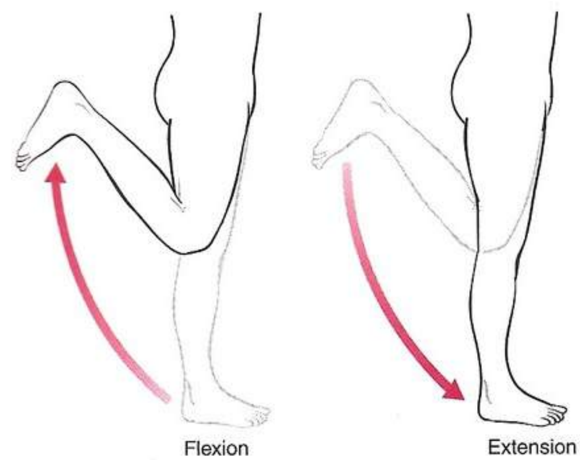

Figure A.2: Flexion and extension of the knee joint [ThingLink.com]

When referring to different positions on the leg, the medial, lateral, anterior, posterior, superior and inferior terms are used. This is to identify locations irrespective of the orientation of the subject. Figure A.3 illustrates the terminology.

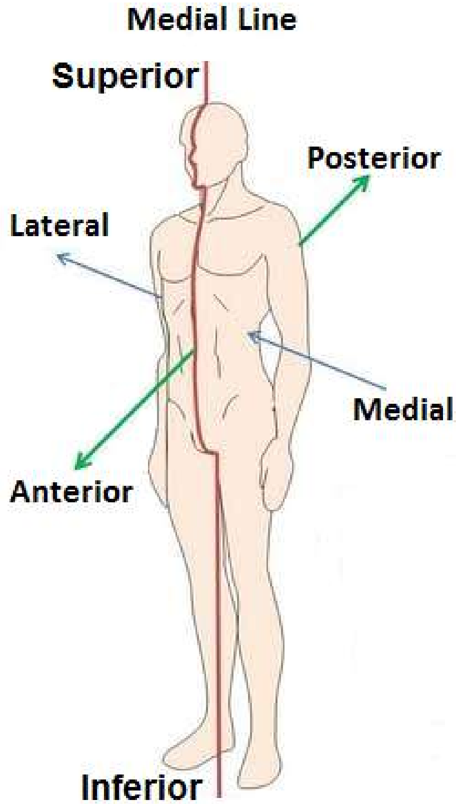

Figure A.3: The different sides of the leg. Modified from [55].

Specifically, the anterior term refers to the front of leg, the posterior term refers to the back of the leg, the medial term refers to the inside of the leg and the lateral term refers to the outside of the leg. The superior term is used to refer to a point that is above a point of reference while inferior refers to something that is underneath. This terminology as been adopted for the identification of the interfaces.

A.2 The knee joint

The legs are the limbs responsible for supporting the body. The bones of the leg include the pelvic bones, the femur, tibia, fibula and the bones of the foot. The three main joints of the leg are the hip, knee and ankle which connect the pelvis to the upper leg, the upper leg to the lower leg and the lower leg to the foot respectively. The anatomy of the lower limb may be seen in Figure A.4.

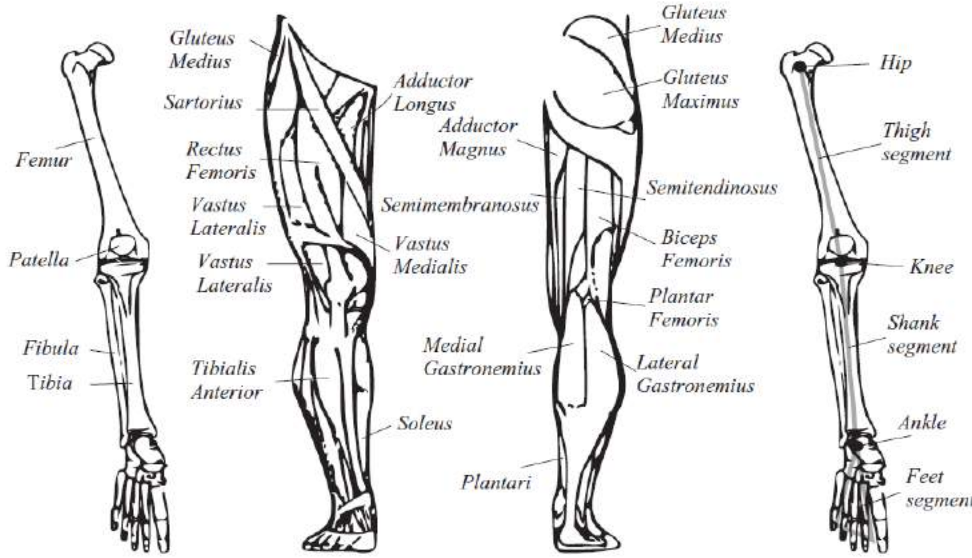

Figure A.4: Anatomy of the lower leg [42]

In our particular case, the knee joint is of special importance since the actuation of many exoskeleton devices rely greatly on this joint to provide assistance during walking or during particular exercises. This is due to the fact that this joint links the upper and lower segments of the leg. Actuation at the knee permits the artificial flexion and extension of the leg, which is one of the most important action in the gait cycle. Unlike a hinge, the knee has a polycentric action, meaning that the center of rotation of the knee is not fixed and varies with flexion. This allows the leg to shorten and to clear the ground when in the swing phase of the gait cycle. The importance of this polycentric design will become apparent when examining misalignments between the device and the native knee joint centres. The knee joint has no muscles surrounding it, making it a location where tissues are superficial, especially blood vessels and nerves.

A.3 Muscles

In general, the strength and other properties of muscle vary greatly between individuals. These organs have visco-elastic properties, which include: creep, hysteresis and non-linear behaviours. In the case of this study, muscle compliance is of interest. Individuals that have a more developed musculature tend to have muscles that are less compliant, or stiffer. This has the effect of changing the interface contact conditions, thus influencing the pressure felt at the interface.

Generally speaking, muscles are very efficient actuators. They have a short response time and can contract up to 40 percent of their original length [42]. The main muscles involved in the flexion of the leg are the biceps femoris, sartorius, gracilis and gastrocnemius. The muscles involved in extension are the rectus femoris and the vastii (medialis, lateralis and intermedius). These muscles may be seen in Figure A.4.

A contractile muscle unit may be separated into three distinct segments. The muscle itself, the attachment points and the tendons extending between the attachment points and the muscle. When a muscle contracts, the change in muscle volume occurs mainly at the muscle belly. The attachments points dictate the orientation of the generated force. Applying an external force on any of these segments, could alter their function. Limiting the expansion of the muscle by applying a lateral force on the muscle belly, or changing the orientation of the muscle force by pressing on the tendons and attachment points could both lead to premature fatigue and joint injury since this would introduce abnormal forces. Furthermore, muscles are located under the different skin layers and are susceptible to a cut in blood supply form an external force from a motorised assist device. The user could experience premature muscle fatigue if device interface pushes against the limb with a force capable of collapsing the supplying blood vessels.

A.3.1 Consequences of muscle fatigue

Muscle fatigue can also impede the accuracy of movement of the joint. Givoni et al. [56] hypothesise that when the motor command is increased to compensate for the effects of fatigue, the comparison between predicted and actual feedback from quadriceps leads to the impression that the muscle is longer than it actually is. Moreover, muscle fatigue would be associated to effects regarding proprioception and may have implications for sports injuries and for the evaluation of the factors leading to falls in the elderly. Their study was focused on the position matching at the knee before and after eccentric-biased or concentric-biased exercise of the quadriceps. It demonstrated that the blindfolded subjects had more difficulty matching the position of one leg relative to the other after exercise, or when having muscle fatigue. When wearing an active exoskeleton providing a high level of assistance, the proprioception accuracy of the user at the knee would decrease, meaning involuntary range of motion and movement, making the user more dependant on the device to support him. This could become a reoccurring pattern where the user is increasingly dependant on the device in order to perform the required movements efficiently.

Sperlich et al. [57] have demonstrated that wearing compression shorts with about

37 mmHg of external pressure reduces blood flow both in the deep and superficial regions of muscle tissue during recovery from high intensity exercise.

The application of an orthotic brace, or of an exoskeleton, on the human body requires a certain amount of tension in its fastening method, usually straps. This induces a pressure on the limb which may cause discomfort and affect the endurance of the muscles due to decreased blood circulation. If the tension is important, the local perfusion might be altered and if this amount is too low, the device may not be solidly attached to the user, causing unwanted migration and relative movements between the device and the user. There is then an optimal point where the tension in the straps should be adjusted.

A study conducted by Hisaeda et al. [58] demonstrated that altered circulation with the use of a pneumatic cuff lowered muscle endurance and oxygenation. Another study showed the same tendency. Lundin and Styf [40] demonstrated that a knee brace with a certain amount of force in the straps decreases local blood perfusion pressure. In the case of their experiment during which the subjects were laying supine, the pressure decreased by 16 to 42 percent in the compressed muscles.

This shows that any strap tension on the limb will have the effect of reducing the blood flow. This indicates that adequate strap tension should be an issue in the fitting of active exoskeleton.

A.4 Blood vessels

When systemic arterial blood pressure is measured, it is recorded as a ratio of two numbers (e.g., 120/80 is a normal adult blood pressure), expressed as systolic pressure over diastolic pressure. The systolic pressure is the higher value and reflects the arterial pressure resulting from the ejection of blood during ventricular contraction, or systole. The diastolic pressure is the lower value and represents the arterial pressure of blood during ventricular relaxation, or diastole. A pressure exerted by an external force over a blood vessel should definitively not be above the value of the systolic pressure since it would be cutting off blood supply.

The main blood vessels that are found in the thigh and lower leg are the femoral artery, the femoral vein, the popliteal artery and the posterior tibial artery. A more extensive representation of the numerous arteries and veins may be seen in Figure A.5 and Figure A.6.

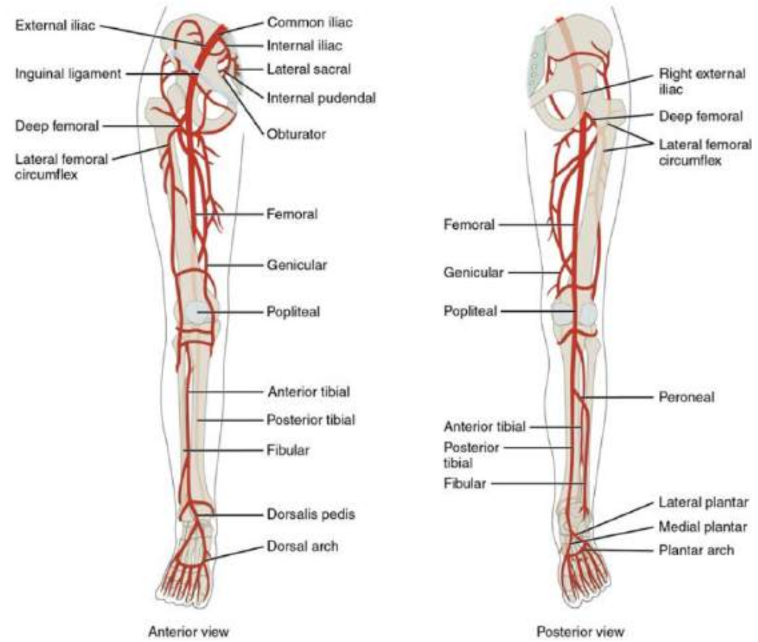

Figure A.5: Main arteries of the lower leg shown in anterior and posterior views [59]

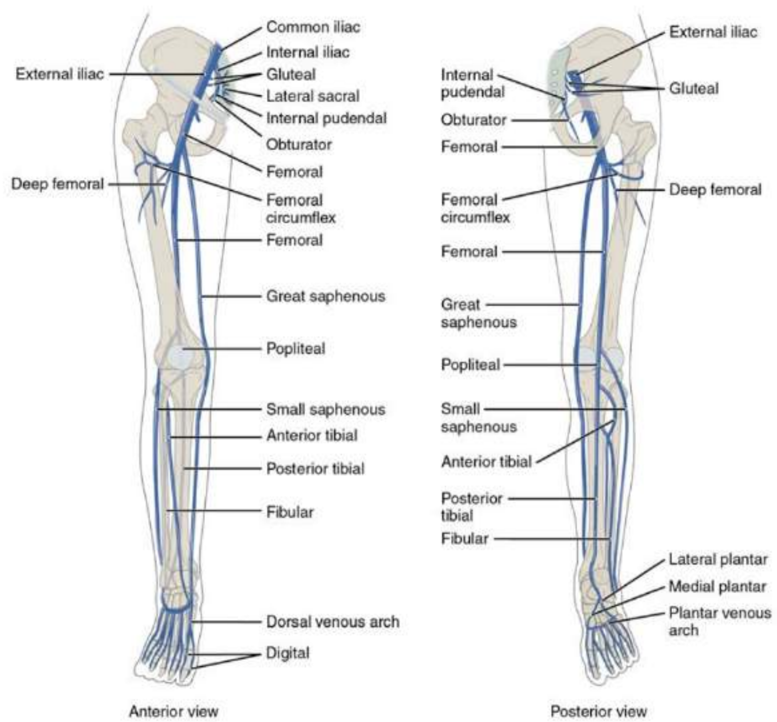

Figure A.6: Main veins of the lower leg shown in anterior and posterior views [59]

A.4.1 External pressure

These vessels have the ability to sustain a certain amount of externally applied pressure. Some studies [38] suggest that this value is about 30 to 50 mmHg. Superficial vessels are the ones most affected when an external force is applied on the limb. These palpable vessels, which could be affected by the external force from the interfaces, are the posterior and anterior tibial arteries. These arteries are located on the tibia, and become more superficial as they get closer to the foot. In the case of veins, it seems that none of them are palpable except on the foot [60]. One must bear in mind that even if these vessels are not palpable at the mid-portion of the upper and lower limb, they may become prominent at the knee joint since there are fewer muscles and little space for soft tissue to connect both ends of the joint.

A.5 Nerves

Nerves are organs responsible for the transmission of action potentials. These nerve impulses carry the signal that will trigger an action or a reaction in an organism. Superficial nerves, similarly to superficial blood vessels will be the most affected by an external force. The nerves that are of interest are found in the lower leg and mostly run down the lateral side of the lower leg. Nerves can be damaged, whether being stretched or compressed, usually resulting from an external compression. Nerve injury might be an issue when wearing an active orthosis which has the capability of exerting important forces on the limb.

Szabo and Gelberman [61] utilized a specialized compression device for producing median nerve compression in the carpal tunnel. This model proved to be useful for studying the effects of compression on human nerves because the median nerve is superficial in the wrist and very accessible to controlled localized pressure. When the device applied a compression pressure greater than 50 mmHg in subjects with normal blood pressure, sensory response disappeared 10 to 60 minutes after application of pressure. When 40 mmHg pressure was applied to the nerve, significant neurophysiological changes did not occur in any subject for a period of up to four hours. In each case, a small decline in the amplitude of the sensory and motor action potentials were the earliest findings.

This suggests that there is a very defined pressure value at which the nerve ceases to function properly. An active device should evidently not apply a pressure that is over these pressure values. Since the force application is cyclical, the nerves are probably not exposed to forces long enough to cause injury.

A.6 Skin properties and injury mechanism

A.6.1 Anatomy of the skin

The skin is the largest human organ and it acts as the barrier between the interior and exterior of the body. It covers between 1.6 and 2 square meters of surface area on the human body in adults, and it accounts for approximately 16 percent of a person's weight. Composed of three functional layers, it may be considered as a composite material. The layers are made up of an upper avascular cellular layer (epidermis), directly connected to the dermis and an underlying fatty layer, the subcutis. These different layers may be seen in Figure A.7:

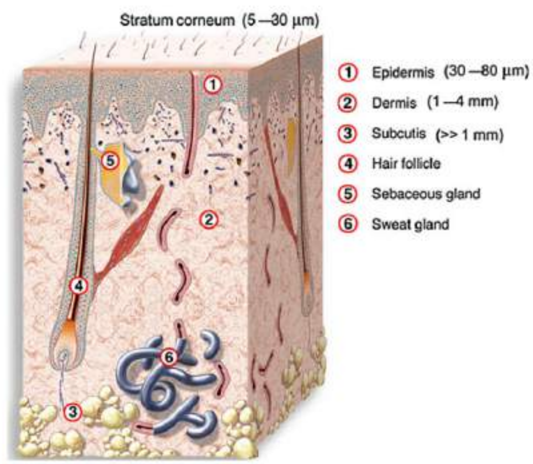

Figure A.7: The skin layers [62]

A.6.2 Proprieties of the skin

In the last decade, research efforts concerning mechanical properties of the skin have been performed with a focus on the effects of skin care products. However, little work has been accomplished regarding friction caused by wearing clothes, orthotics or an exoskeleton [62]. This is important because a better understanding of the skin's reaction to various materials may lead to the design of assist devices that are more biocompatible and ergonomic.

The friction at the skin will be greatly dependant of the material it will be in contact with. A study conducted by Rotaru et al.[63] demonstrated that proper choice of textile may have a significant impact on the friction coefficient against skin. They underlined the fact that textiles should be designed to repel or evacuate moisture as much as possible. For example, their study showed that conventional cotton hospital sheets were not the best suited in terms of diminishing friction. Skin and garments have a constant dynamic interaction. Although they are used to provide comfort and protection, there are still common dermatological injuries due to fabric actions. Yet, there is still no general numerical method or standard for measuring or evaluating skin-garment contact interactions, especially, during intense sports or the wearing of active orthotic devices.

The determination of the mechanical properties of the skin is a very complex topic. This is due to the layered nature of skin, to its viscoelasticity, and to its great sensitivity to humidity. In terms or a load versus displacement curve, soft tissue first shows a large deformation over a small amount of force, then stiffens until the point of failure. Visco-elastic materials such as skin also exhibit hysteresis. This means that skin will not return to its initial state or deformation instantaneously after load removal. Repetitive loading could elongate skin periodically, increasing its stiffness that could cause skin wear and injury.

The effective elastic modulus of the skin's top-layer is very dependant upon the ambient humidity. In fact, it may change by a factor of 100 to 1000 as the humidity increases from zero to 100%. At low humidity skin has an elastic modulus similar to rubber in the glassy region (with a Young's modulus E of between 1 and 3 GPa), while in the wet state it behaves as rubber in the rubbery region with the Young's modulus in the order of 5 to 10 MPa [64]. The mechanical properties of the skin may be calculated with the use of indentation, suction or extension methods. In vitro testing is a common way to asses the human skin properties.

In vivo measurements of the skin mechanical properties are usually conducted using the indentation method. This type of test is relatively easy to implement however, the recorded properties of the skin are affected by the underlying layers of tissues such has muscles and fat. Therefore, the skin's mechanical properties alone may be difficult to obtain. In any case, it is better to include the effects of the sub-layers to have a more representative value of the skin's mechanical properties in the case of exoskeleton interface design. This mechanical property is expressed in terms of the apparent Young's modulus. The apparent Young's modulus increases in function of penetration depth. Pallier-Mattei et al [65], reported average values between 4.5 and

8 kPa for the skin's apparent modulus in vivo tests on the inner forearm of 10 middle-aged male subjects. One difficulty often encountered with the testing of biological tissue is the large variation in experimental results across samples[66].

The inverse of skin stiffness, or the compliance, may be calculated experimentally, also using indentation methods. This compliance can be measured using simple hand-held instruments or programmed robot arm with a haptic probe. Oflaz and Baran [67] developed a compact hand-held device for the measurement of skin compliance. The application probe is composed of a small rod with a semi sphere tip which will deform under a certain force applied on the skin. The probe is linked to the data acquisition component where the force transducer is located.

A more precise way of measuring skin properties is to use a haptic interface to apply known step changes in force while recording the corresponding displacement. Williams et al. [68] used a commercial haptic interface (PHANToM 3.0s) to apply forces and measure displacements. This solution is a computer controlled robotic arm with a probe which can be positioned on the desired interface following predetermined landmarks in order to create a compliance map. Such apparatus may be seen in Figure A.8.

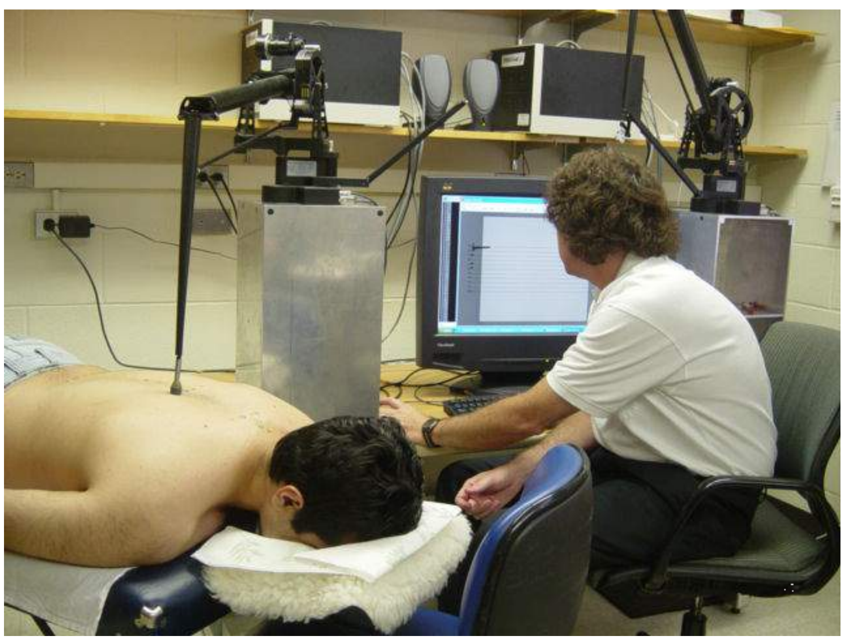

Figure A.8: Haptic interface [68]

After applying a force and recording the compliance over a certain area, the authors generated a compliance map of the back of the subject, as can be seen in Figure A.9.

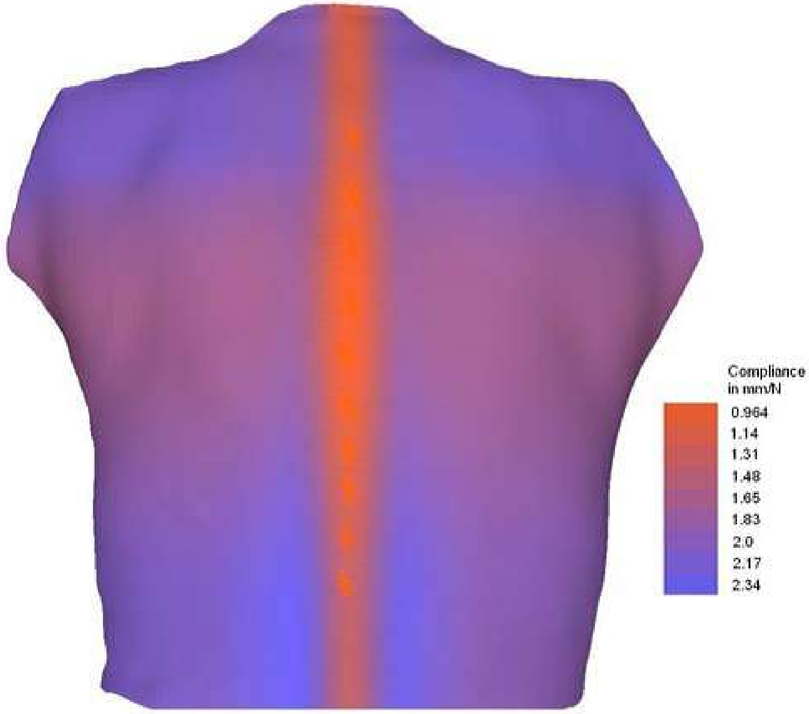

Figure A.9: Haptic compliance map [68]

This technique could be used to create a compliance map of the thigh and shin of the user in order to construct a custom-built interface with a variable stiffness.

A.6.3 Skin injury

Pressure injury is a localised injury of the skin usually over a bony prominence. Pressure, shear, friction, or a combination of these factors causes the interruption of blood flow to the tissue. A pressure injury can develop in as short as 30 minutes if there is high pressure in a small area [69]. Increased pressure, over short periods of time and light pressure for long periods of time, have been shown to cause equal damage.

Injuries created by moisture are caused by the prolonged exposure of skin to body fluids, such as perspiration. Such injuries are characterized by inflammation of the skin. For example, if active device interfaces are not properly designed to evacuate moisture, the skin could be damaged after prolonged use. The accumulation of moisture creates a microclimate between fabric and skin. When a device is placed on the skin, the climate conditions are altered in the same way as with clothing. These climate conditions are especially important when the device is designed to transmit loads to the body. In conditions of high temperature and humidity, skin may soften and the user would sense discomfort more quickly from the microclimate conditions. This feeling of discomfort is in many cases the first warning of adverse conditions that can ultimately lead to injury.

A.6.4 Deep tissue pressure

The amplitude of an externally applied force will not be carried throughout the thickness of the limb and its different constituents. Therefore, the experienced pressure is lesser in deeper tissues than in superficial tissues. Finite element analysis can be used in order to approximate the compression of the venous blood flow or tissue deformations under the skin. Dai et al. [70] constructed a finite element (FE) model of the lower limb in order to investigate the behaviour of a vein under compression from an inflatable cuff. The model only had one vein embedded in muscle, fascia and skin. The properties of the different biological tissues were approximated with a simple experiment. The elastic modulus was determined by calculating the displacement of the tissues under a known force and then iterating the simulation with different values for the Young's modulus until there was agreement with the displacement. They demonstrated that the wall of the vein would collapse between a pressure of 40 and 50 mmHg that was applied externally by the cuffs. Figure A.10 shows the finite element model.

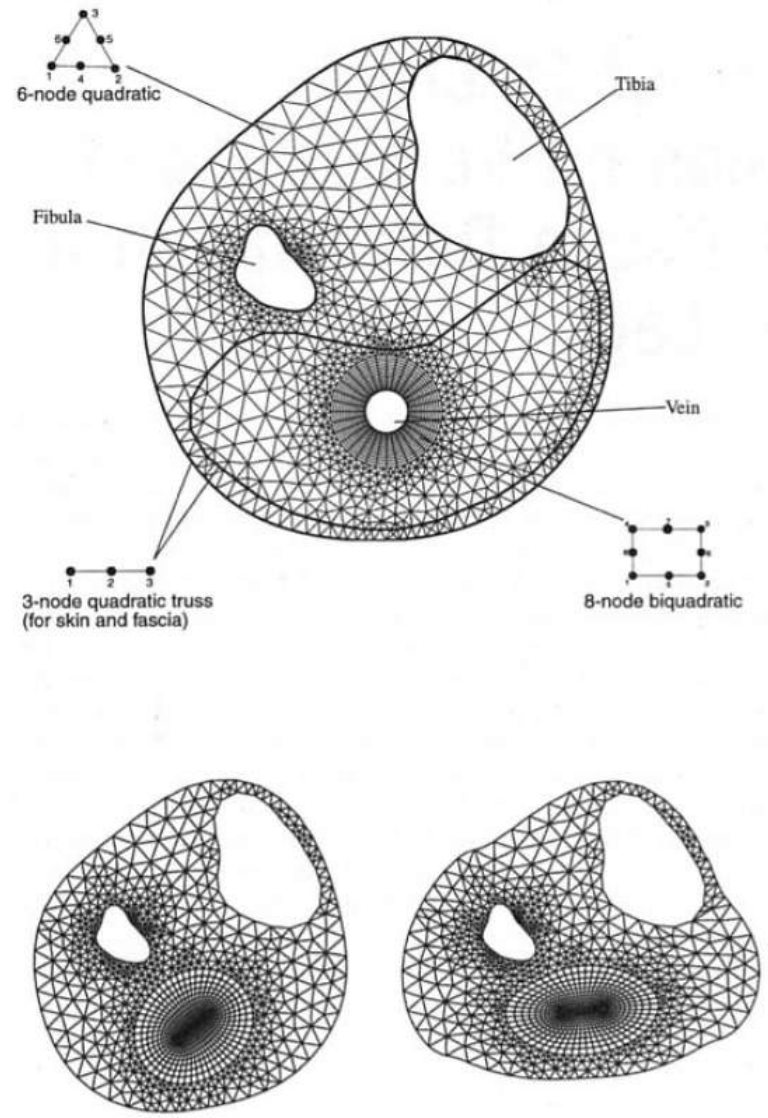

Figure A.10: FE model of the lower leg [70]

A more representative way of conducting such a FE simulation is acquiring the dimensions of the muscles, bone and skin tissue thickness with the aid of MRI. Makhsous et al. [71] constructed one such 3D model from MRI images of the buttock-thigh area in order to simulate a sitting posture. This enabled the study of the mechanical responses in the deep tissue when subjected to sitting pressure over a long period of time with realistic anatomical and environmental conditions. The highest pressures were located over bony prominences, which the authors considered the most important etiologic factor in pressure ulcer formation.

Finite element simulations such as the one mentioned previously could help conceptualise a new and improved interface. The pressures could be estimated using this type of modelling.

A.7 Design parameter impacting comfort

Textiles are often used to increase interface comfort, whether in a simple brace or a fully active exoskeleton. However not all types of fabric are well suited for this application. For example, Li et al. [72] have demonstrated that silk and cotton were well suited for prosthetic socks used in sockets of individuals with an amputation. They used a reciprocating test lasting about 10 minutes. The different fabrics, silk, cotton, nylon and wool, were placed on a small spherical probe then mechanically rubbed on the surface of the residual stump with parameters recreating normal walking. In addition, they assessed microscopic skin trauma with the use of a laser scanning microscope. When comparing materials like these for the design of prosthetic socks, one must consider pain, drag and heat sensations. Cotton and silk showed the best results regarding these sensations. Knitting weave patterns play a major role in the performance of those fabrics. A coarse knitting pattern (or surface), will likely cause more friction and therefore more heat and discomfort.

Other design considerations include whether or not the device structure is anthropometric, the weight and inertia of the device, and how it will be interfaced with the user. The device is considered anthropometric when it is designed following anthropometric data so it may fit a wide range of users. The weight of the device also greatly influences its performance [73]. Generally, if the exoskeleton is not weight-bearing, a lighter device will translate in better performance.

Appendix B

Brace fabrication and instrumentation

B.1 Conceptual design

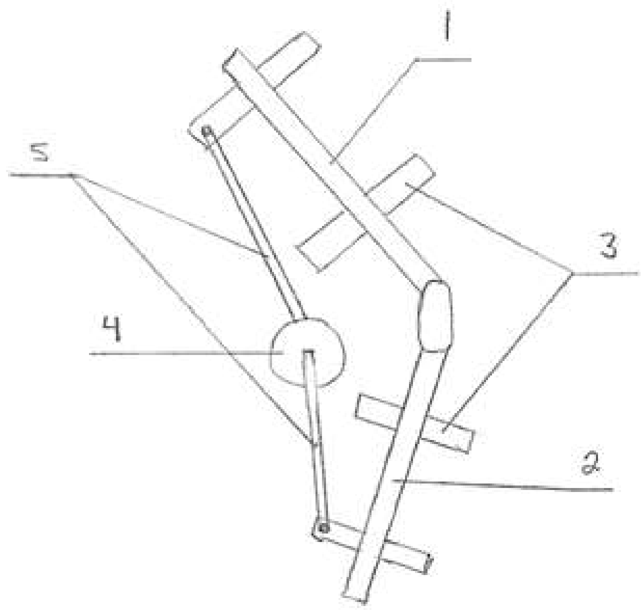

Figure B.1: Conceptual design 1. Side view. Knee brace where the assistance is provided by a mechanism located behind the brace. 1: superior upright, 2: inferior upright, 3: interfaces, 4: rotary spring mechanism and 5: force transmitting links.

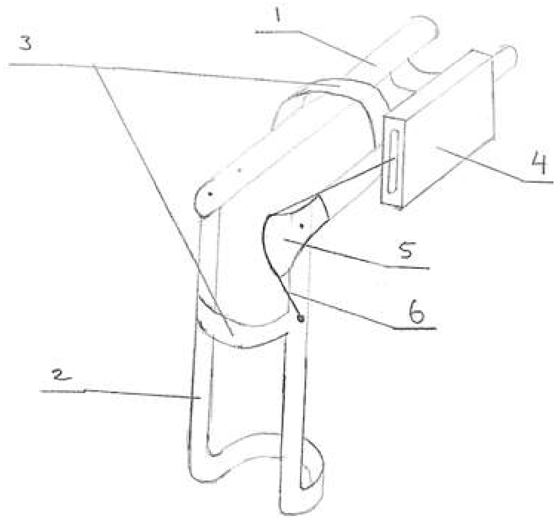

(a) 1: superior upright, 2: inferior upright, 3: interfaces, 4: linear spring mechanism, 5: cam and 6: cable.

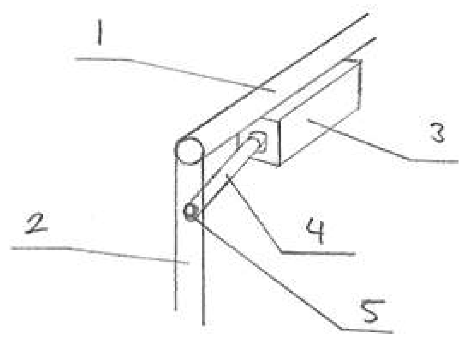

(b) 1: superior upright, 2: inferior upright, 3: linear spring mechanism, 4: push link and 5: pivot joint.

Figure B.2: Conceptual design 2. Isometric view. Knee brace where the assistance is provided by linear spring and cam mechanism located to the side the brace. Figure B.2b shows a different version of the assist mechanism.

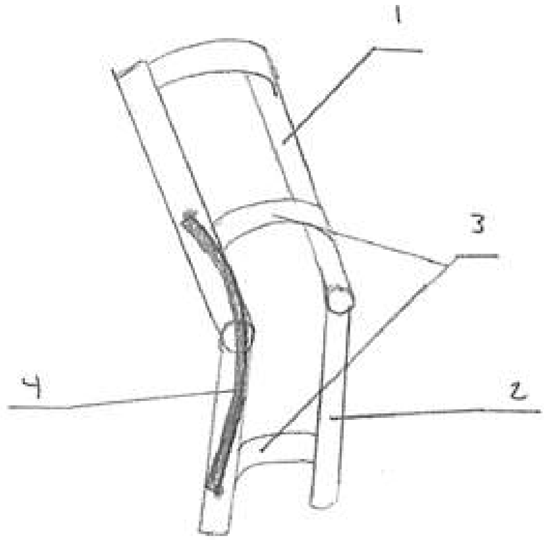

Figure B.3: Conceptual design 3. Isometric view. Knee brace where the assistance is provided by leaf springs attached to the sides of the brace. 1: superior upright, 2: inferior upright, 3: interfaces and 4: leaf spring.

B.2 3D scanning

The scanning process started with a software used to reconstruct the images taken with the scanner to a 3D image (Skanect, Occipital Inc.). The motion sensor, or scanner, was moved around the static subject in order to create a 3D image in Skanect. The scan performed included more than 100 000 polygons, which is the number of 2D mesh elements used to make a workable file (.STL). There were two scans taken: one in a relaxed standing position, and one in a 90 degree squatting position.

The scanner used was a XBOX Kinect device, a line of motion sensing input devices by Microsoft (Microsoft Inc.). The specifications of the 3D scanner can be seen in Table B.1.

Table B.1: Microsoft Kinect motion sensor specifications. These specifications were taken from the manufacturer's website [74]

Kinect	**Array specifications**
Viewing angle	43° vertical by 57° horizontal field of view
Vertical tilt range	± 27 °
Frame rate (depth and color stream)	30 frames per second (FPS)
Audio format	16-kHz, 24-bit mono pulse code modulation (PCM)
Audio input characteristics	A four-microphone array with 24-bit analog-to-digital converter (ADC),and Kinect-resident signal processing including acoustic echo, cancellation and noise suppression
Accelerometer characteristics	A 2G/4G/8G accelerometer configured for the 2G range, with a 1° accuracy upper limit.

The 3D image was processed in other software (Meshmixer, Autodesk Inc.). This mesh editing software was used to screen unwanted part of the scan and make sure the mesh had no defects such as holes or irrelevant geometry. While doing this, only the right leg was kept from the waist down. After screening and simplifications, the standing scan had 2828 vertices and 5672 triangular mesh elements. The scan containing the squat image contained 4198 vertices and 8392 triangular mesh elements. The generated mesh in Skanect is from the default settings. The software enables an infinite number of mesh elements which can increase the accuracy of the model. Despite this, the low number of mesh elements currently achieved was enough to recreate an accurate model of the leg. Additionally, the number of elements used permitted good computational performance. The resulting file was saved with an .STL or .OBJ extension. The mesh of the leg may be seen in Figure B.4.

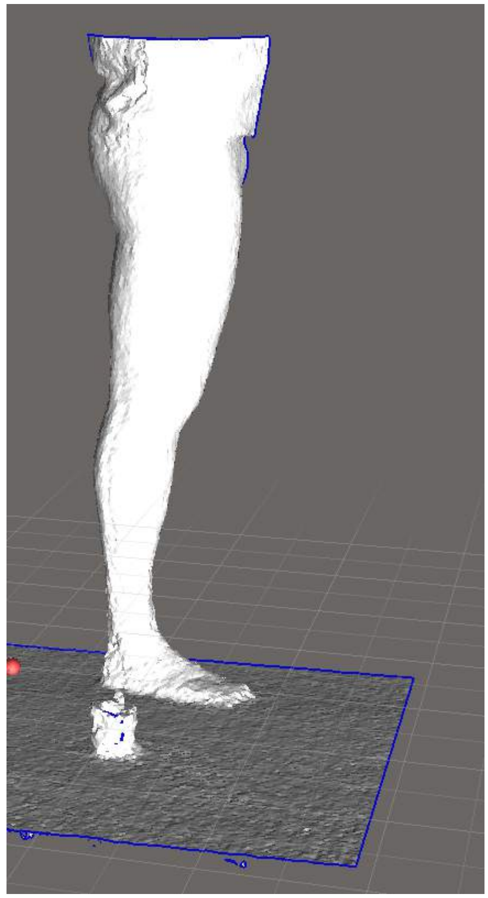

Figure B.4: Mesh of the lower leg

In order to use the 3D model geometry and create the custom interface, the cleaned mesh was opened as a mesh file in Solidworks through the Scanto3D add-in. The Curve Wizard function was used to enable the placement of multiple planes in the mesh and creates a contour of the mesh on these particular planes. To maintain good accuracy, the planes were positioned closely to one another. More specifically, the planes for the standing position were spaced at an interval of 10 mm, and 8 mm for the squat position. This had the effect of slicing the mesh at about 90 evenly spaced points in the vertical direction. Then, the loft function was used to extrude the contours between every plane. Since the contours are smooth and the elements are triangular, there exist a difference in dimensions between the mesh and the solid object. This difference is small and does not significantly affect the solid model accuracy and is suitable for our application. This solid model was then shelled, cut and modified so that it could be installed on the knee brace frame while keeping the user's leg contour. The file was then saved as an .STL and 3D printed. The standing position was used for the development of the interfaces since there was no noticeable differences between the two positions after the post-processing.

B.3 3D printer specifications

The material used for 3D printing was polylactide (PLA). This is a common type of filament and is relatively inexpensive. The models were created using an Ultimaker 2+ (Ultimaker Inc.) and an Idea Builder 3D20 (Dremel Inc.) 3D printers. The prints had an internal honeycomb structure to reduce the weight and printing time of the parts. However, a 30 percent infill was applied to the internal material structure. Compared to conventional printing of non-functional models this percent of infill is about three times as important, making relatively strong parts. The layer height was set to 0.2 mm, which is relatively high and tends to give a rough finish, but significantly reduced the printing time.

3D printing was selected as the manufacturing technique for several reasons. First, due to the number of different prototypes being made, this was a cost-effective option. Second, the printer is able to make complex shapes and contours that otherwise would have taken time and skill to manufacture. Lastly because of the time frame and the uncertainty of the success of the prototypes, more elaborative and expensive methods such as working with fibre glass or carbon fibre composite materials would have not been possible.

B.4 Sensor circuitry

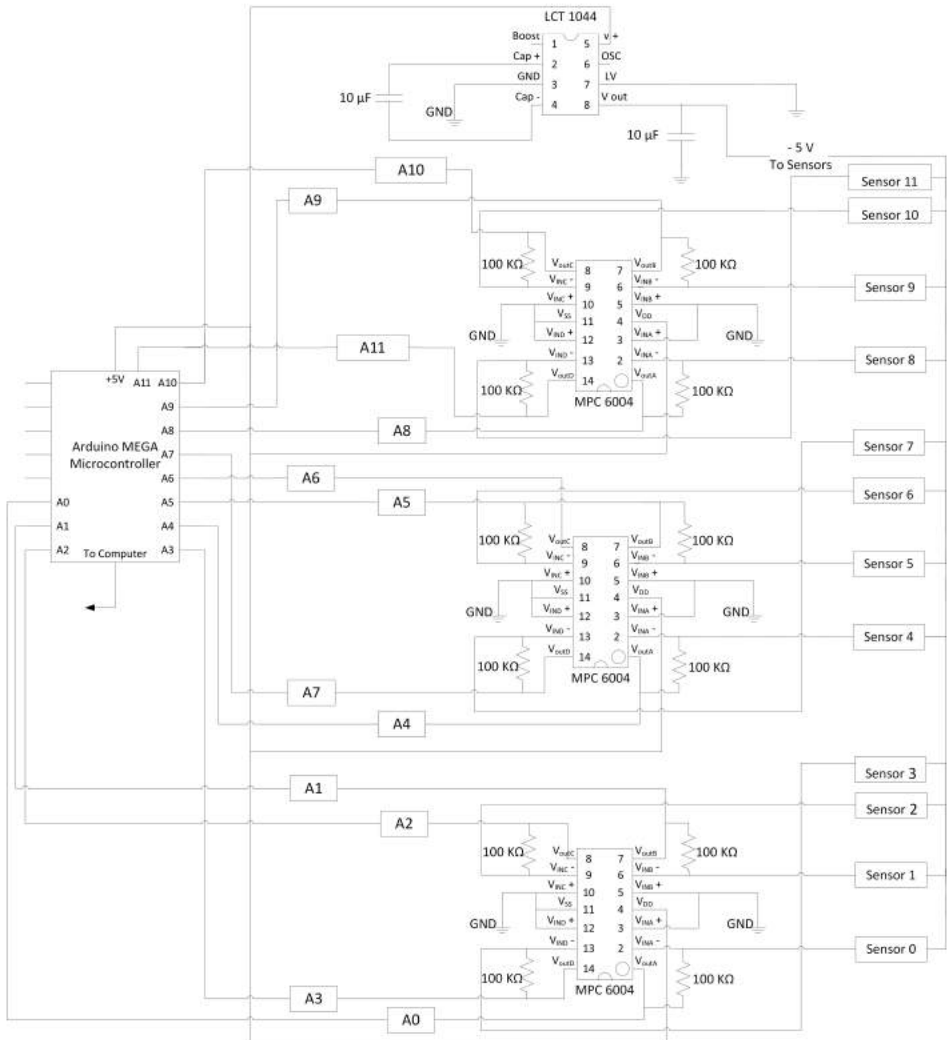

Figure B.5: Conditioning circuit of the Flexiforce A301 sensors. Note that the boxes containing capital A simply indicate the analog input port of the micro controller.

B.5 Force sensor calibration curves

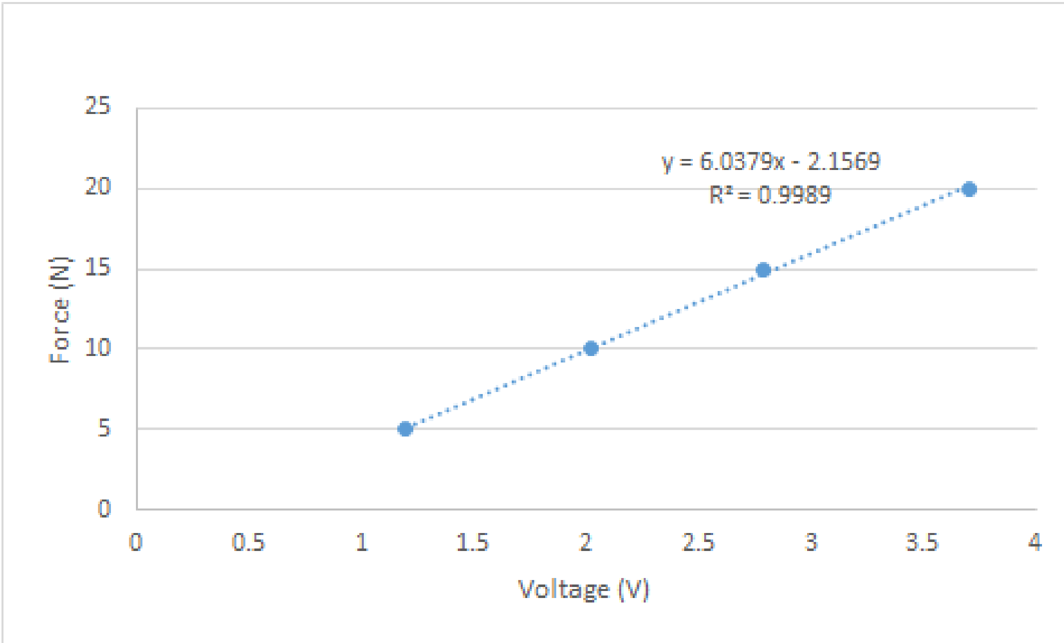

Figure B.6: Calibration curve of Sensor 1

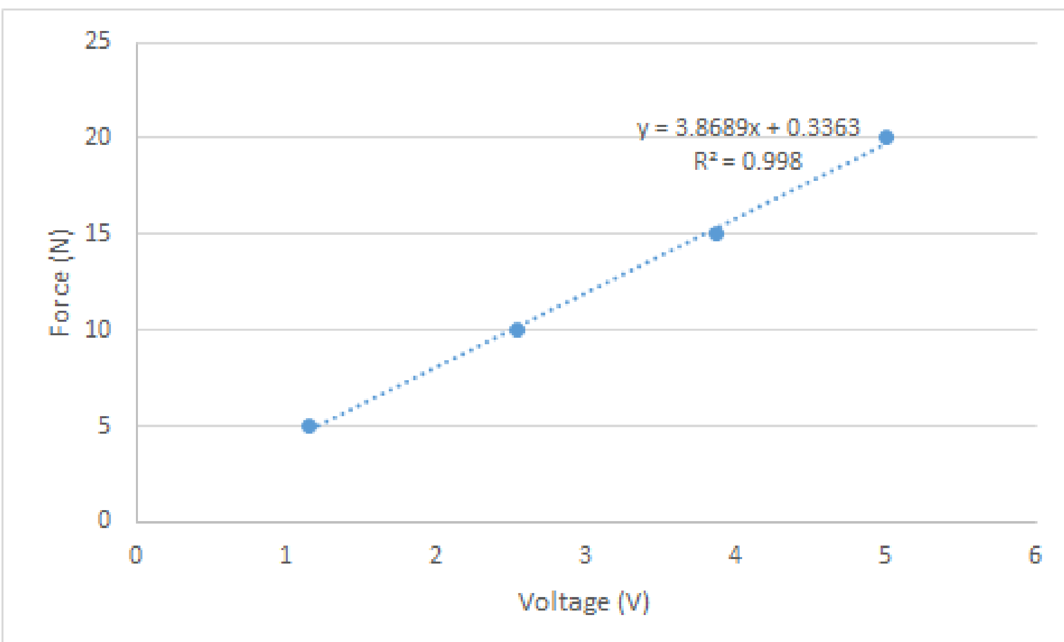

Figure B.7: Calibration curve of Sensor 2

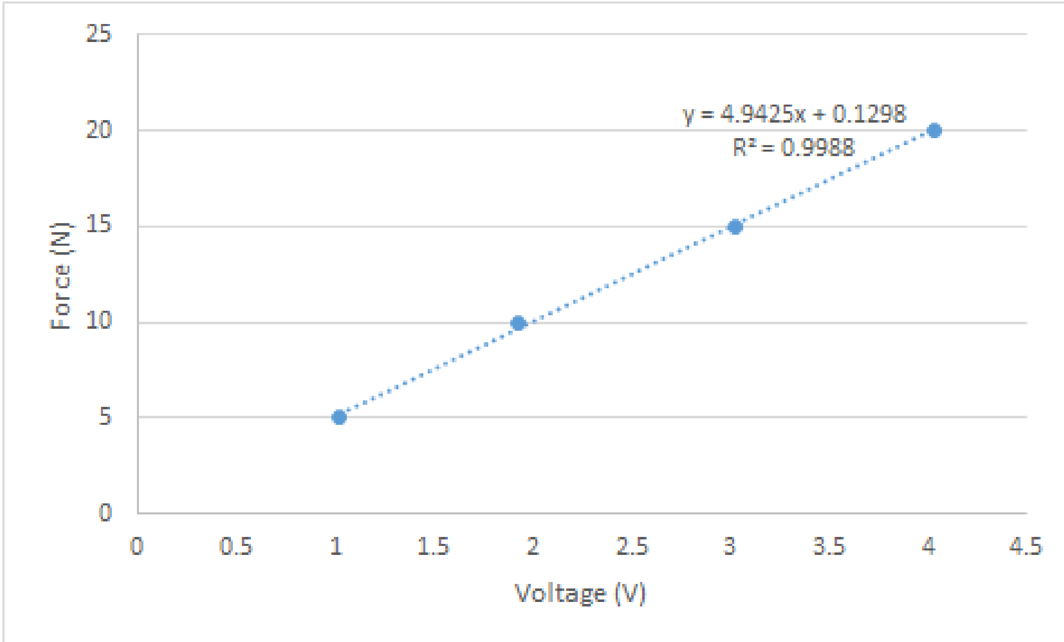

Figure B.8: Calibration curve of Sensor 3

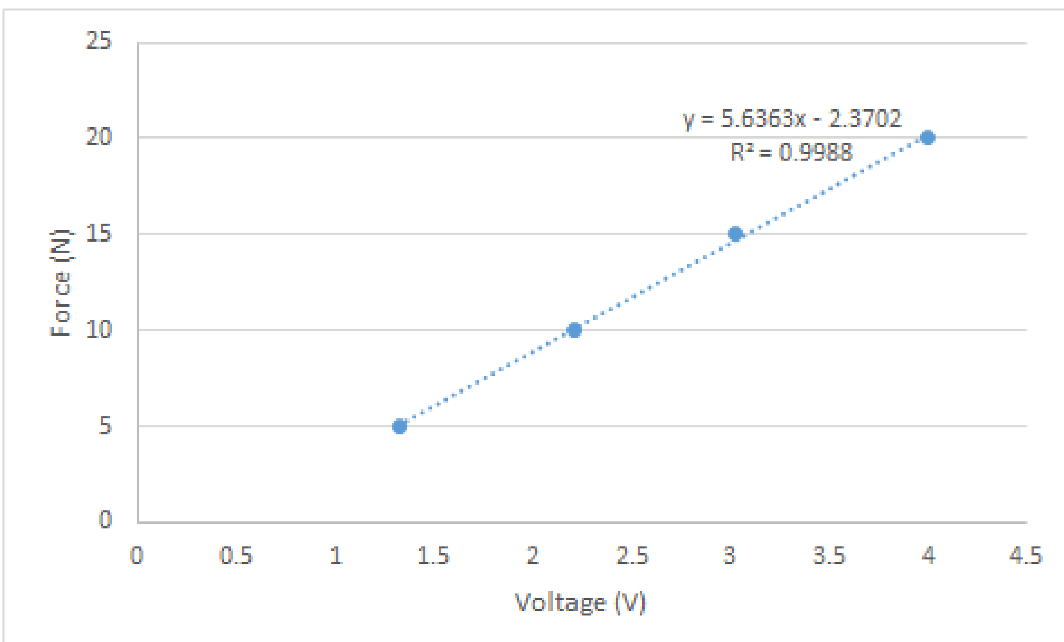

Figure B.9: Calibration curve of Sensor 4

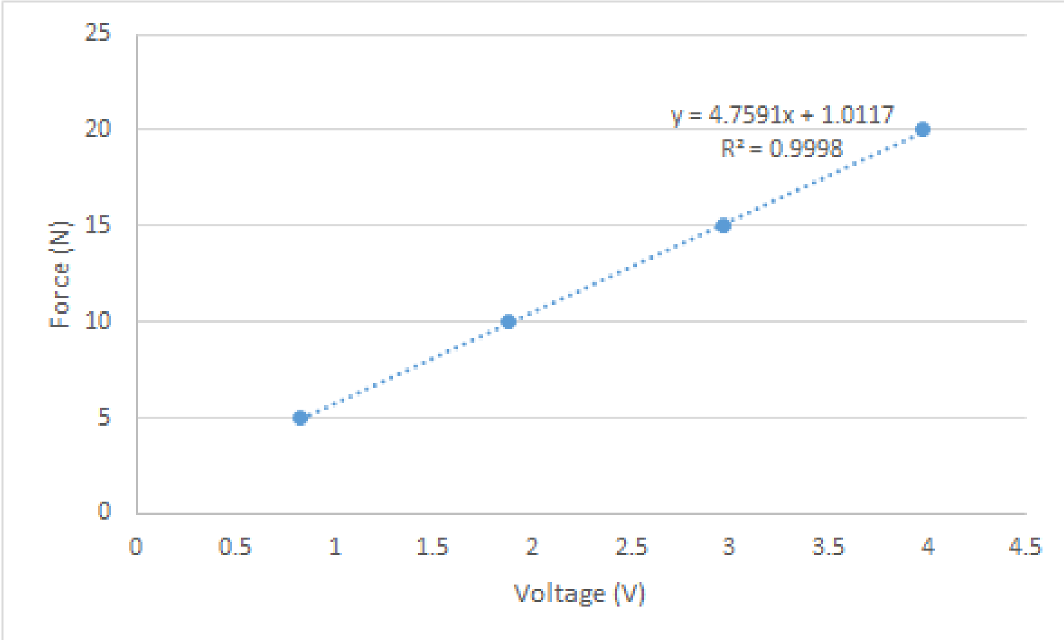

Figure B.10: Calibration curve of Sensor 5

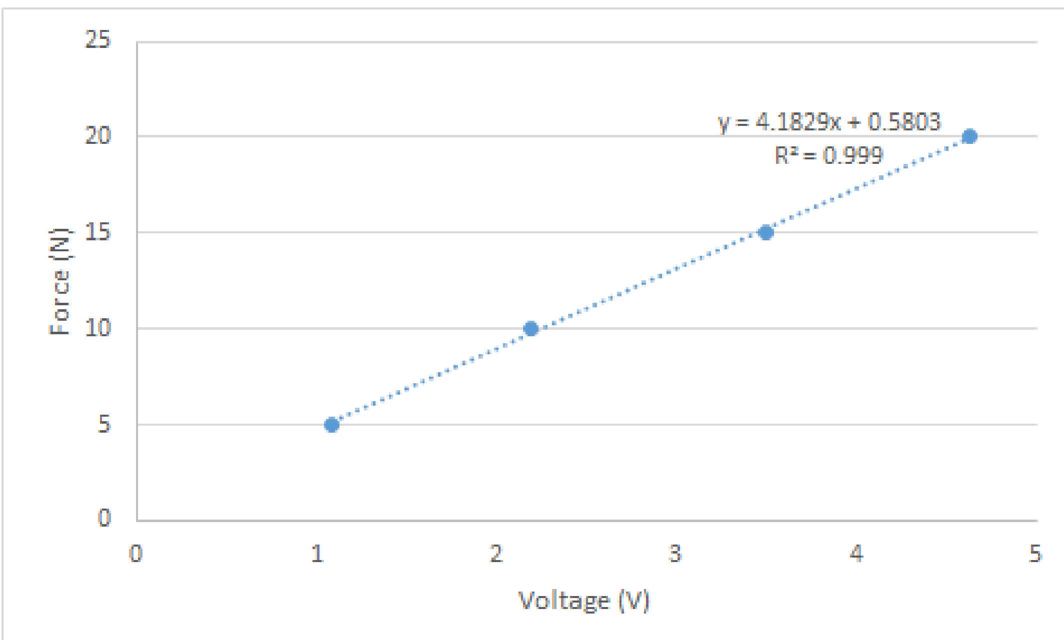

Figure B.11: Calibration curve of Sensor 6

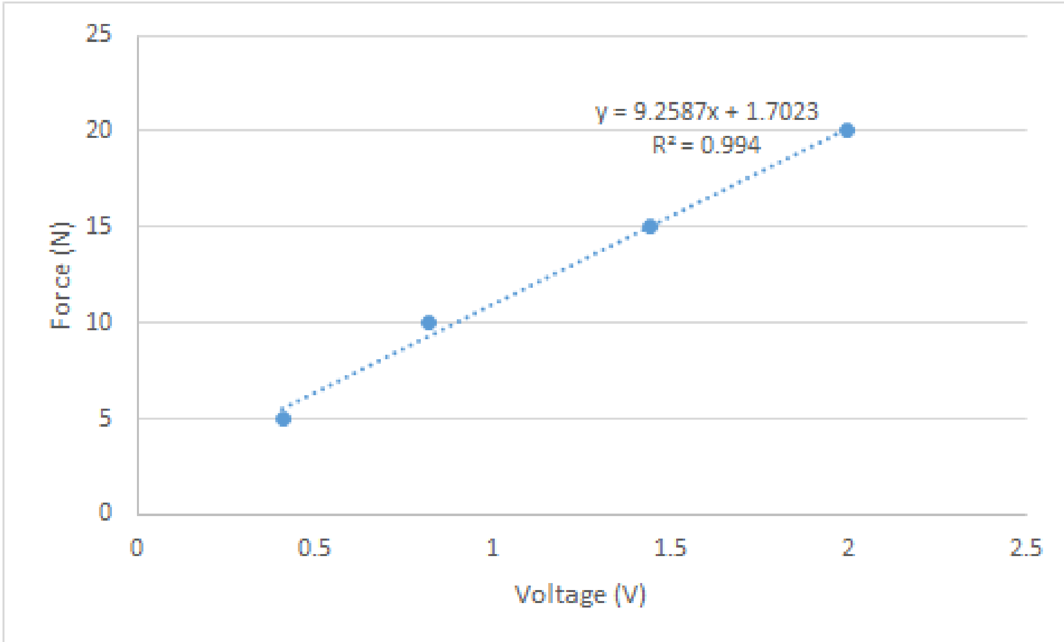

Figure B.12: Calibration curve of Sensor 7

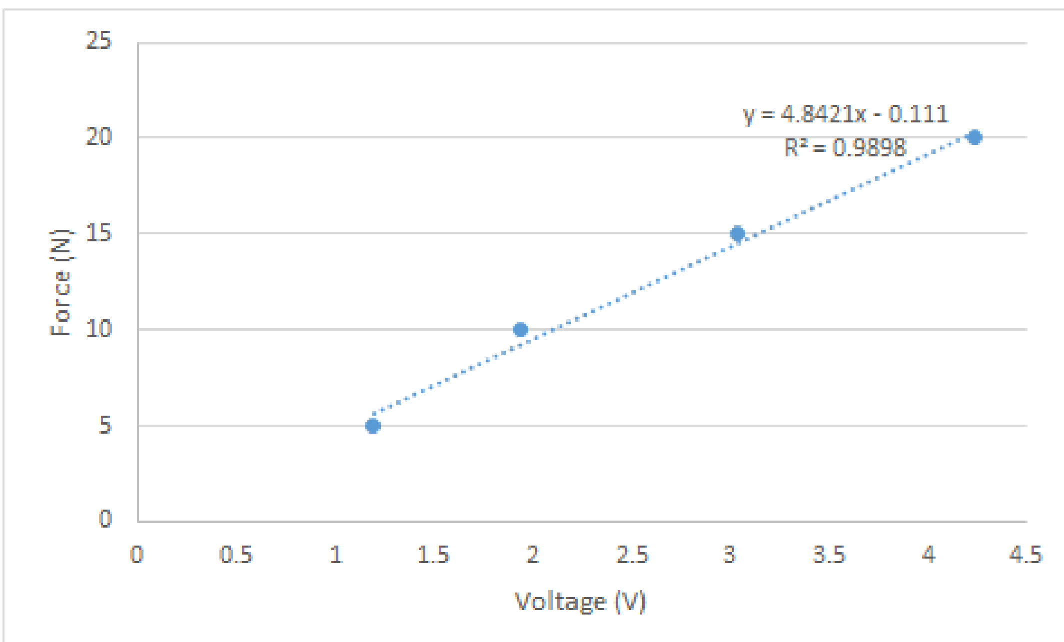

Figure B.13: Calibration curve of Sensor 8

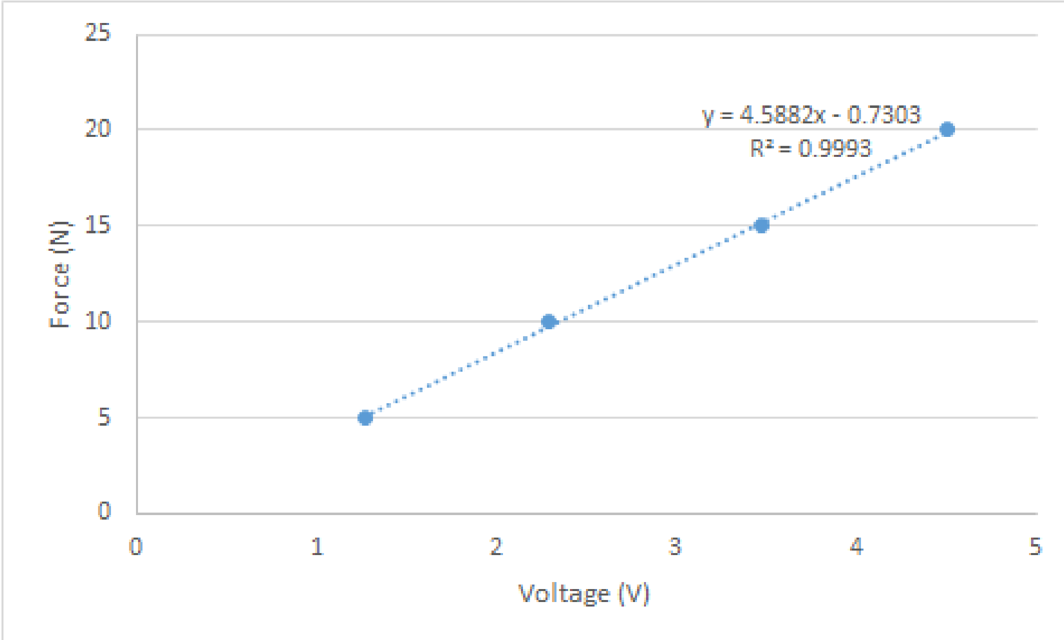

Figure B.14: Calibration curve of Sensor 9

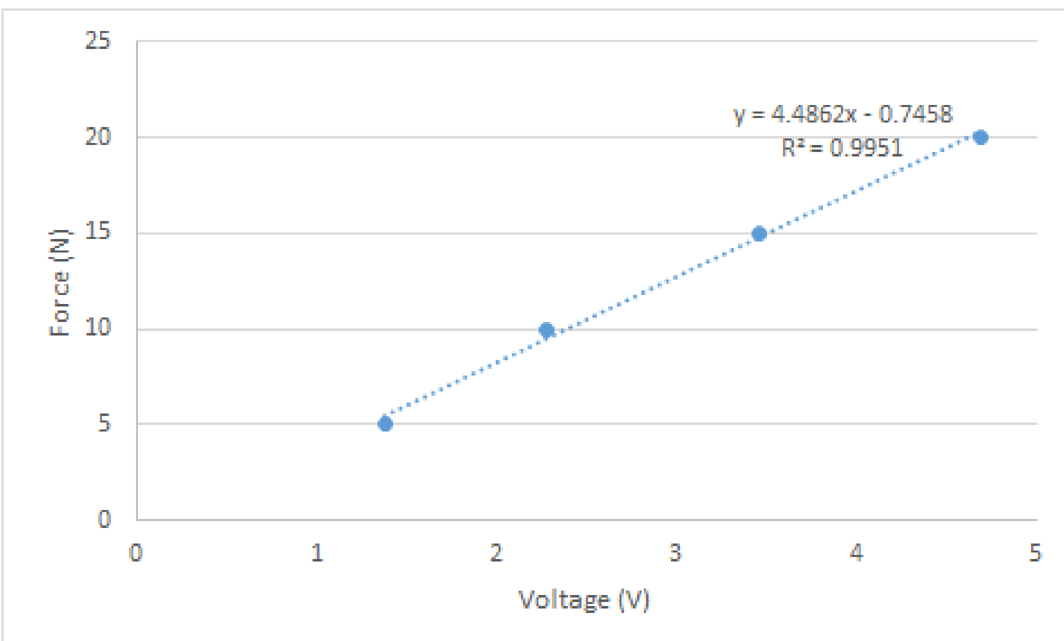

Figure B.15: Calibration curve of Sensor 10

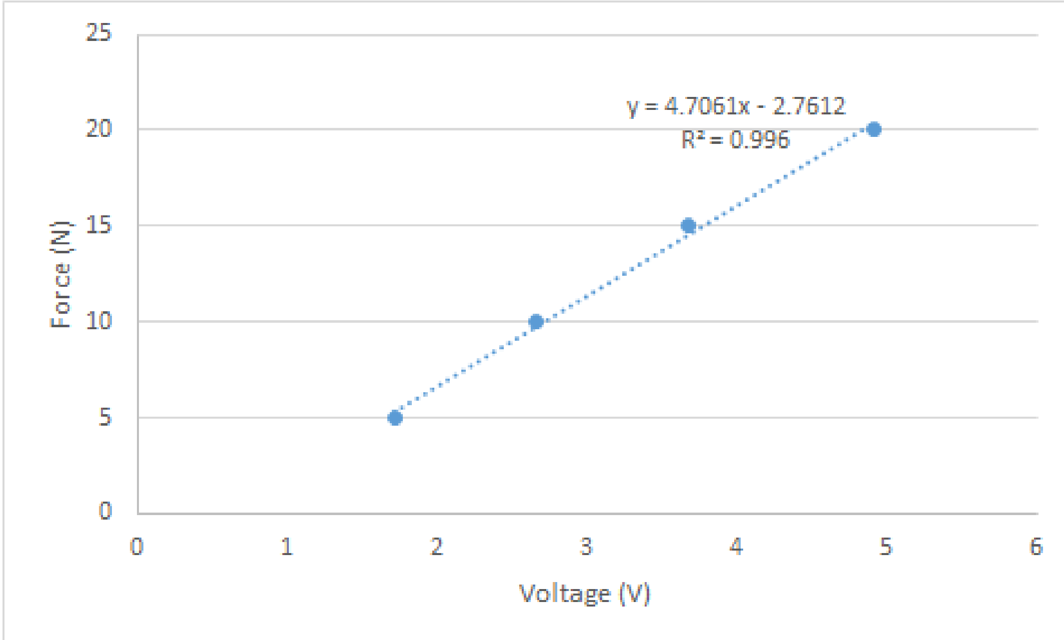

Figure B.16: Calibration curve of Sensor 11

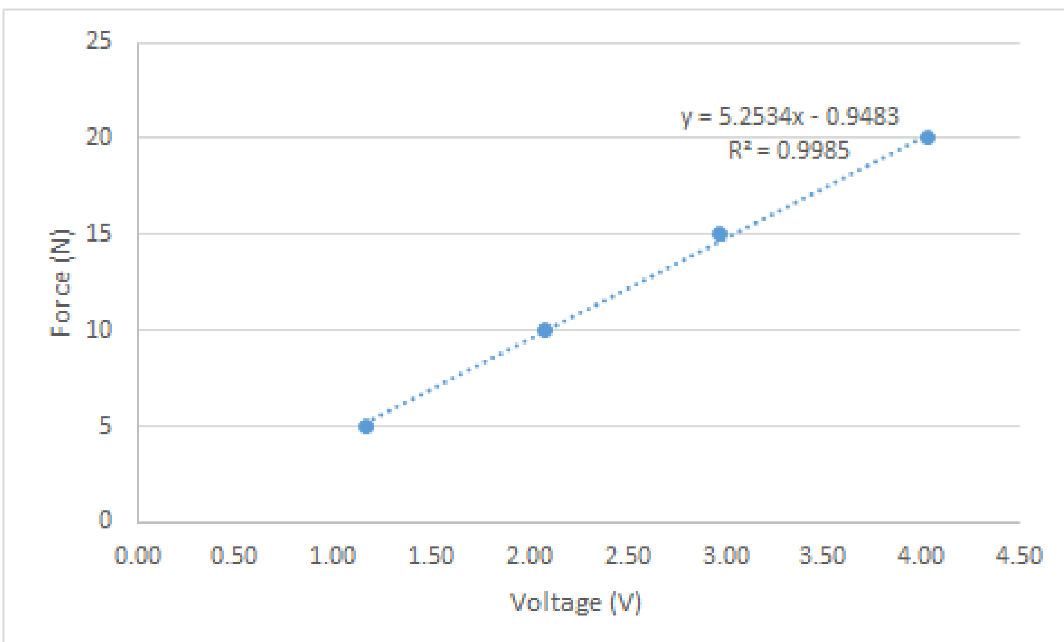

Figure B.17: Calibration curve of Sensor 12

B.6 Brace mechanical characterization

Figure B.18 and Figure B.19 illustrate the brace moment in function of the brace angle for the other two stiffness's, namely the low and high stiffness.

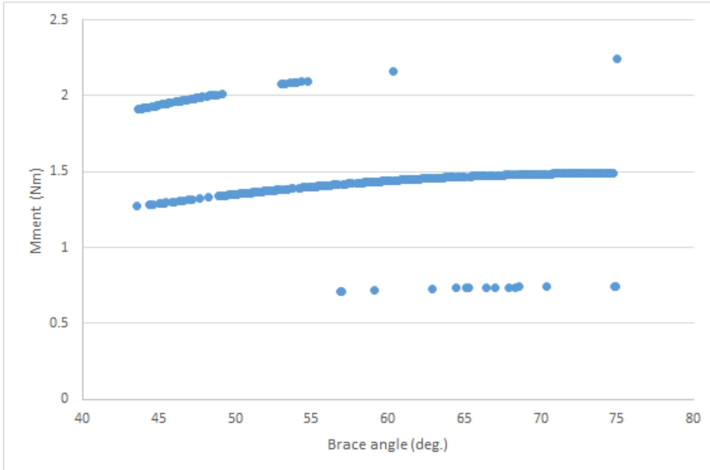

Figure B.18: Brace moment in function of brace angle for stiffness 1

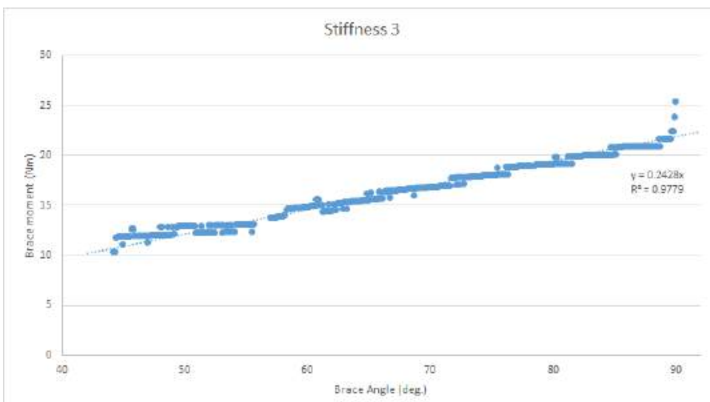

Figure B.19: Brace moment in function of brace angle for stiffness 3

Figure B.18 shows that Stiffness1 has a different response than the other two stiffness's. The thickness of this particular carbon fiber strip was not able to produce a force that was high enough to be reliably recorded by the 100kN load cell. The sensitivity of the load cell is too low to record data for this stiffness reliably. Plus, the friction occurring at the testing interface, or between the brace and load cell attachment, was not as consistent as the other two stiffness's. The brace would slide intermittently and not constantly, which had the effect of transferring the force to the load cell intermittently as well.

B.7 Motion capture

B.7.1 Software

When using motive, a conventional marker set had to be selected for automatic marker labelling. For this study, Helen Hayes marker set was chosen. Any conventional marker set, including the Helen Hayes, enables the modelling of body segments, identifies the joints between these segments and recognises many other segment relationships simply with markers placed on anatomical landmarks. Since the Helen Hayes model is dedicated for a lower limbs study, the pelvis, thigh, shank and foot were generated as seen in Figure B.20.

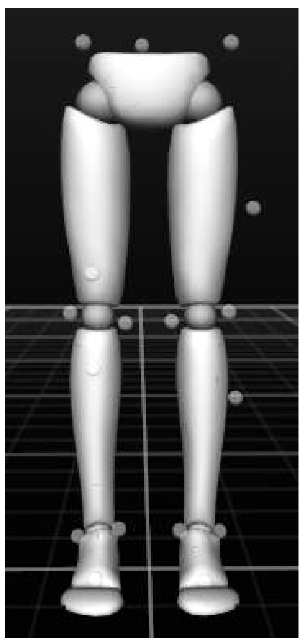

(a) Front view

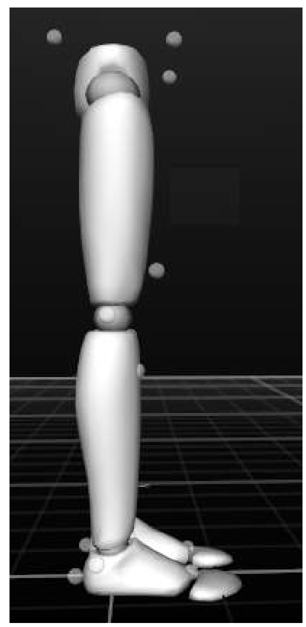

(b) Side view

Figure B.20: Frontal and side view of the modified Helen Hayes marker set

After the creation of the lower limb segments and installing the brace on the participant, all the trials could be performed and recorded. The data then was exported as a .c3d file into Visual3D.

Visual3D is a biomechanics analysis software designed to bridge the gap between raw data and presented results. The model was created after importing all data and defining the body segments. Landmarks and segments defining the brace were then added. The model can be seen in Figure B.21.

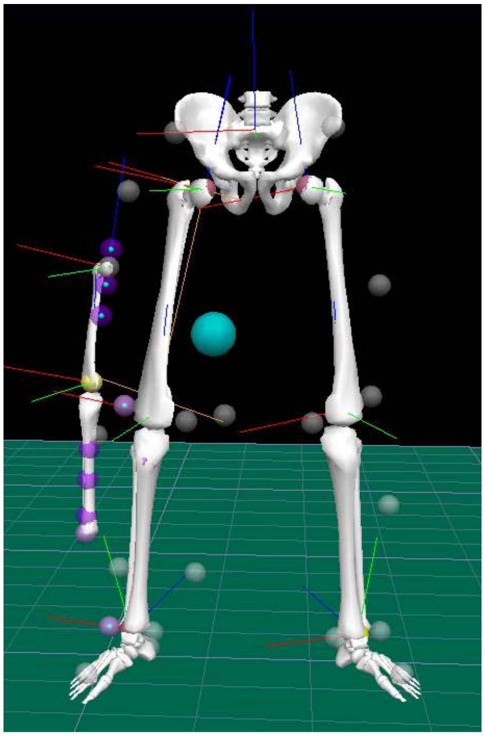

(a) Front view

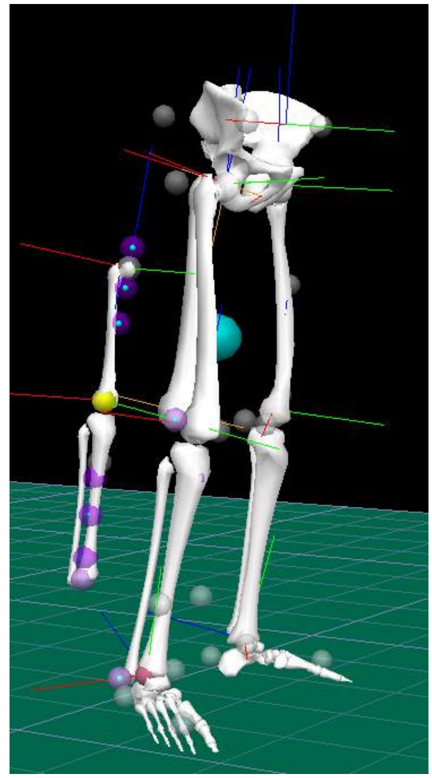

(b) Side view

Figure B.21: Frontal and side view of the model used for data processing

The created model was then applied to motion files, which correspond to the trials of the various testing conditions, in order to compute relevant parameters. This was achieved with the reporting tool in Visual3D, choosing the segments of interest and plotting the results in a 2D graph.

Visual3D also offers a pipeline tool that uses command language to automate the process of reporting results. The Pipeline processor provides access to the core of Visual3D functionality through commands. For the purpose of the experimental testing, a custom pipeline was created and can be found in Appendix E. The pipeline was used to open the relevant files, assign tags to files and create kinematic events used for the normalisation and processing of the data.

B.7.2 Marker set

Table B.2: Marker identification for motion capture trials, knee brace and Helen Hayes model. ASIS: anterior superior iliac spine. UpperBrace rigid body marker positions are relative to hip joint. LowerBrace rigid body marker positions are relative to knee joint.

	Marker label	**Position**
Helen Hayes	WaistRFront	Right ASIS
	WaistLFront	Left ASIS
	WaistBack	Sacrum
	RThigh3	Distal anterior thigh marker
	RKneeOut	Femur lateral epicondyle
	RKneeIn	Femur medial epicondyle
	RShin3	Proximal anterior shank marker
	RAnkleOut	Fibula apex of lateral malleolus
	RAnkleIn	Tibia apex of medial malleolus
	RHeel	Posterior surface of calcaneus
	RToeIn	Head of second metatarsus
	LThigh	Thigh lateral mid-position
	LKneeOut	Femur lateral epicondyle
	LKneeIn	Femur medial epicondyle
	LShin	Shank lateral mid position
	LAnkleOut	Fibula Apex of lateral malleolus
	LAnkleIn	Tibia apex of medial malleolus
	LHeel	Posterior surface of calcaneus
	LToeIn	Head of second metatarsus
Brace	UpperBrace_Marker1	Medial, proximal
	UpperBrace_Marker2	Medial, joint axis
	UpperBrace_Marker3	Lateral, joint axis
	UpperBrace_Marker4	Lateral, proximal
	LowerBrace_Marker1	Medial, distal
	LowerBrace_Marker2	Lateral, distal
	LowerBrace_Marker3	Lateral proximal
	LowerBrace_Marker4	Medial, proximal

B.7.3 Visual3D pipeline

The pipeline used in Visual3D was constructed so that the user choose a calibration file, motion files, assign tags to motion files and then choose a report template. The application of a filter and interpolation of the data was performed in the pipeline. Computation of the migration and misalignment vectors was performed with the equation used to find the distance between two points and a pipeline function to find an angle between three markers. experimental events dictating the start and end of the various testing exercises was implemented in the pipeline. Figure B.22 shows the first few commands of the pipeline.

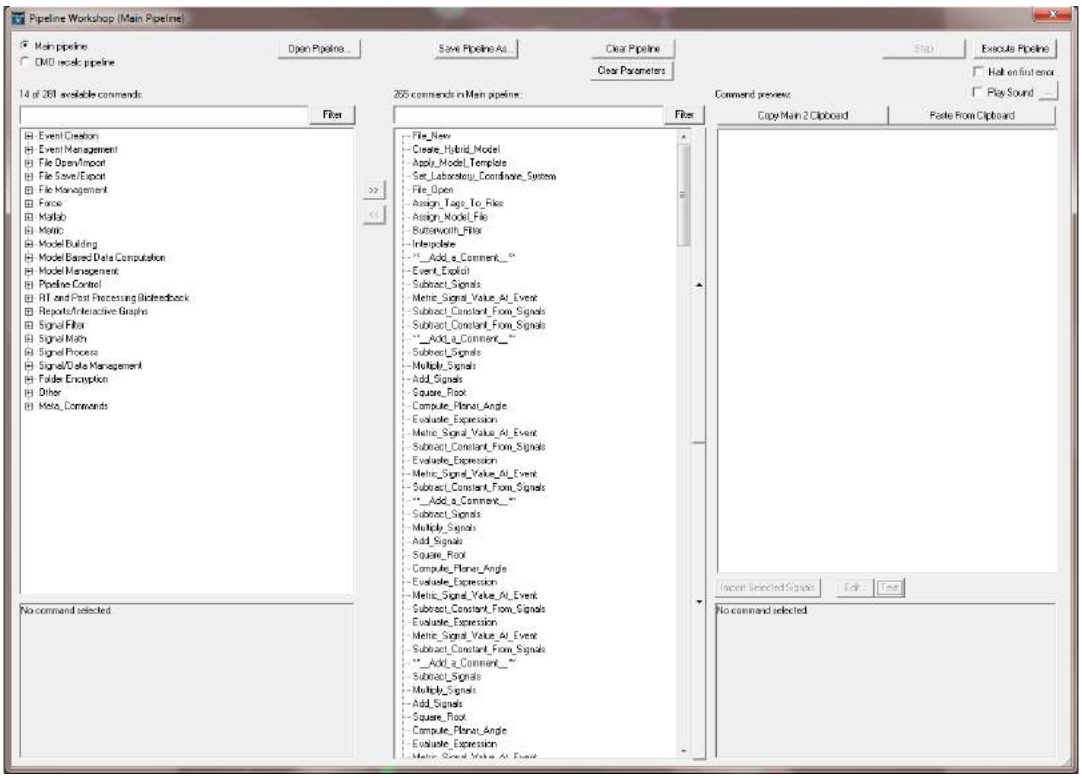

Figure B.22: Example of pipeline commands

B.7.4 Camera specifications

Table B.3: Specifications of the V100:R2 Motion Capture Camera. These specifications were taken from the manufacturer's website (http://optitrack.com/)

Specification	**Value**
Resolution	0.3 MP (640×480)
Shutter Speed	Default 1 ms (Minimum 20us)
Frame Rate	100 Hz
Latency	10 ms
Operating range	15 cm – 6m (depending on marker size)
Input / Output	USB 2.0 Hi-speed
Accuracy	2D sub millimeter (depending on marker size)

Appendix C

Motion capture and force mapping results

C.1 Kinematics

C.1.1 Combination analysis

Iterated based interfaces

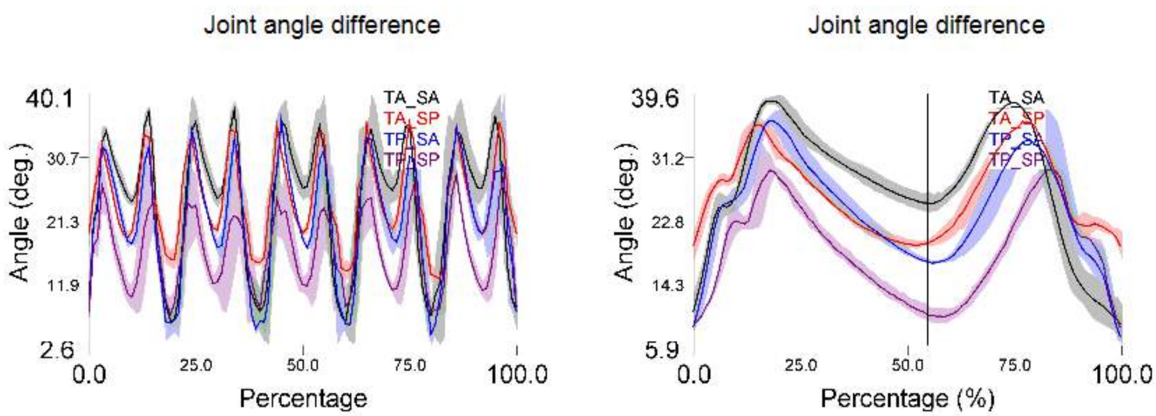

Figure C.1: Relative joint angle

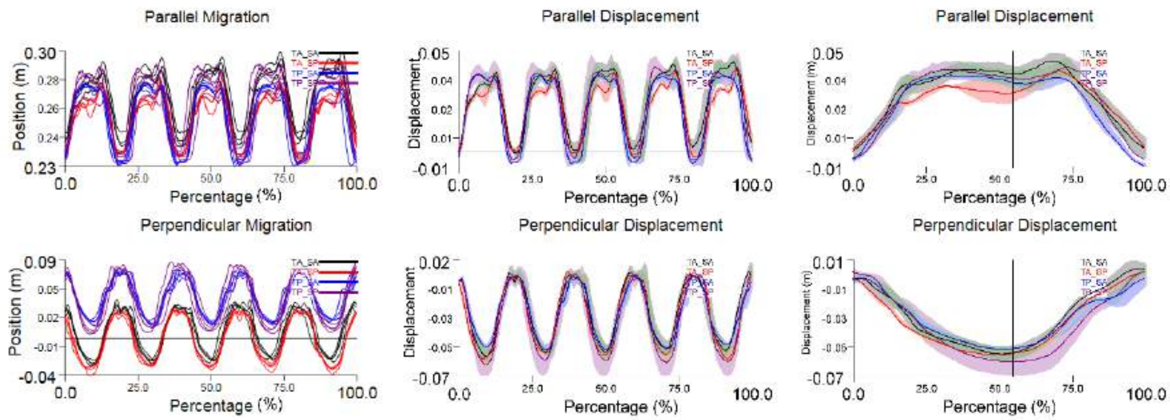

Figure C.2: Thigh interface migration

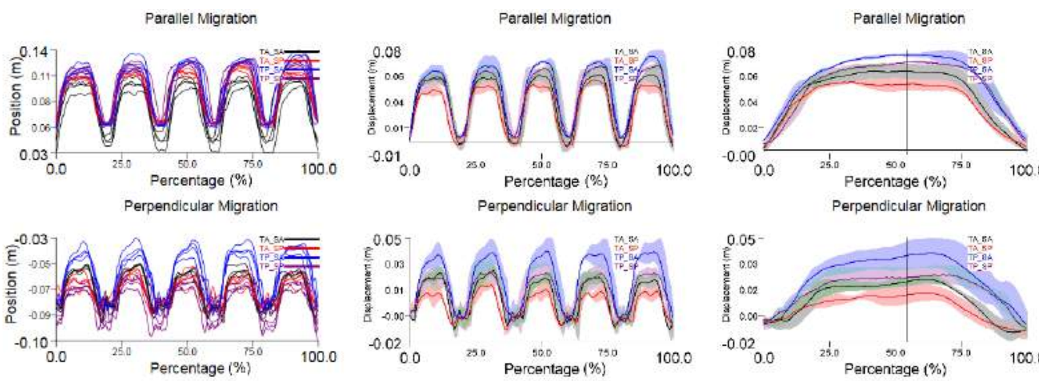

Figure C.3: Shank interface migration

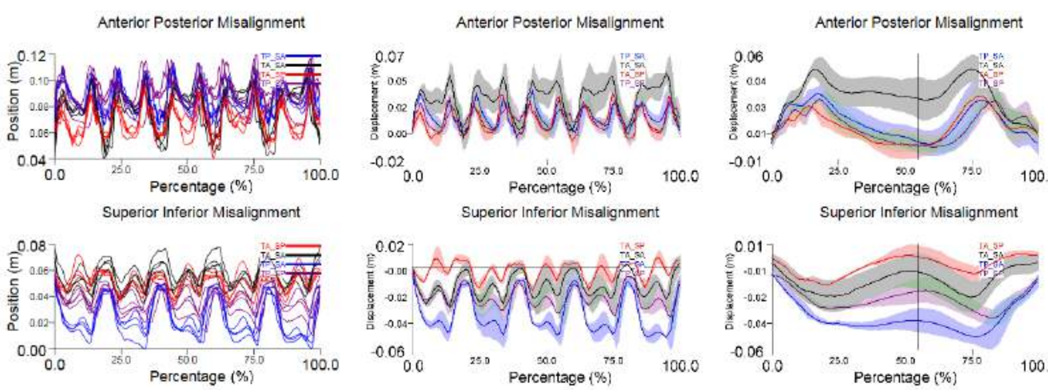

Figure C.4: Joint misalignment

3D scanner based interfaces

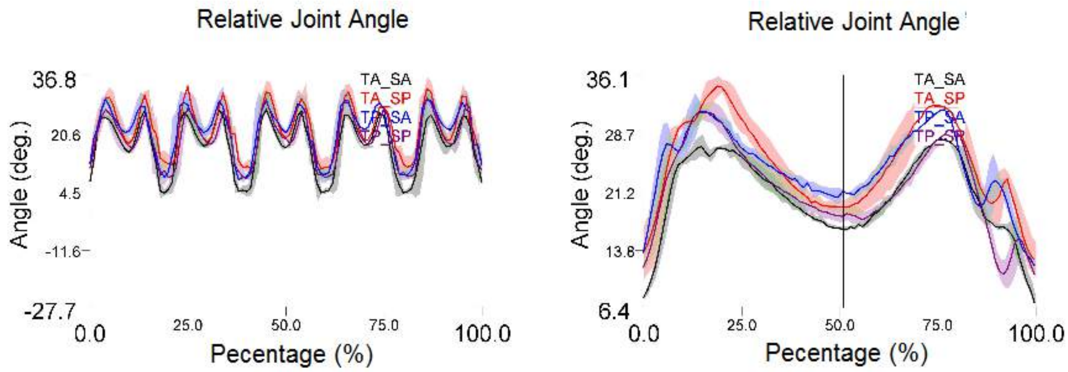

Figure C.5: Relative joint angle

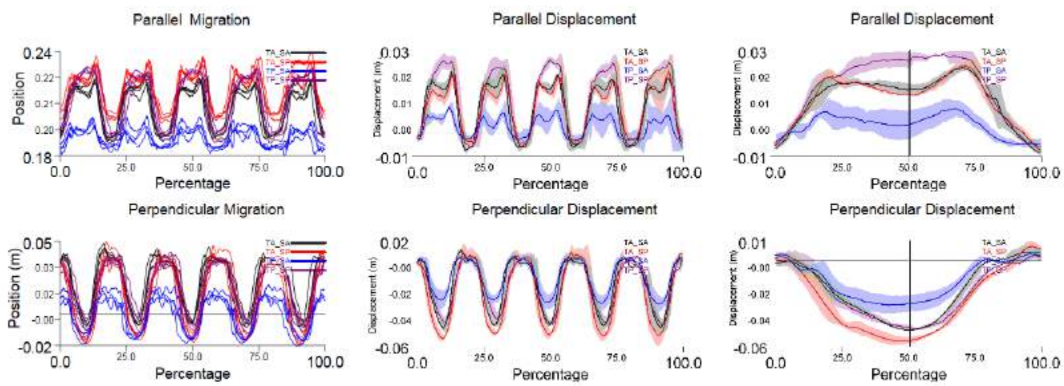

Figure C.6: Thigh interface migration

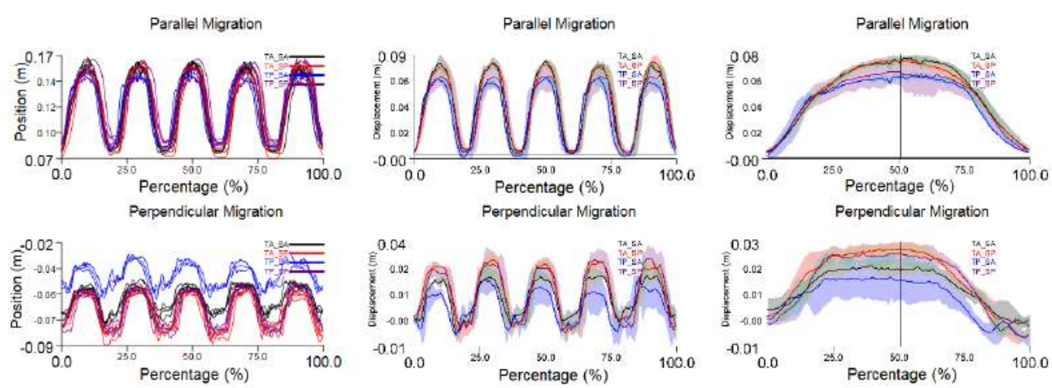

Figure C.7: Shank interface migration

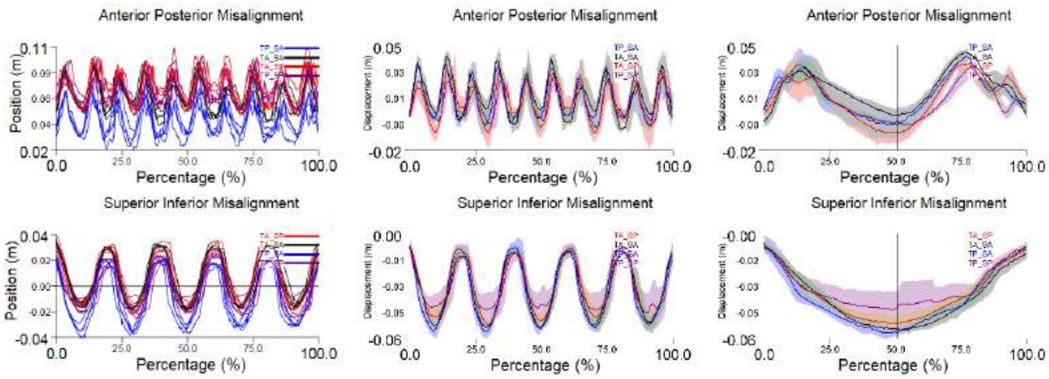

Figure C.8: Joint misalignment

C.1.2 Exercise analysis

Iterated based interfaces

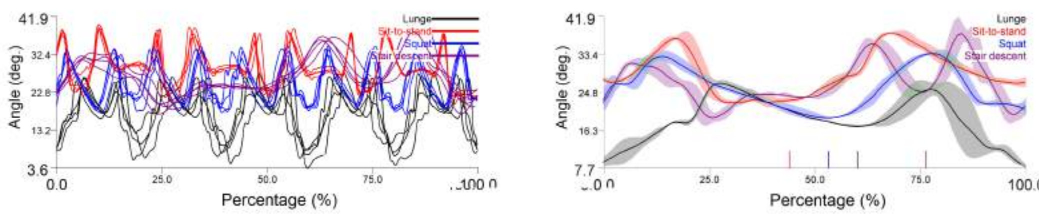

Figure C.9: Relative joint angle

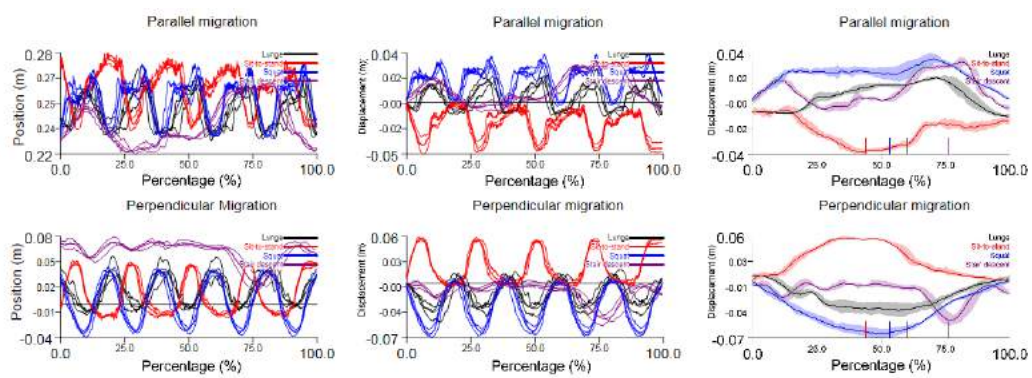

Figure C.10: Thigh interface migration

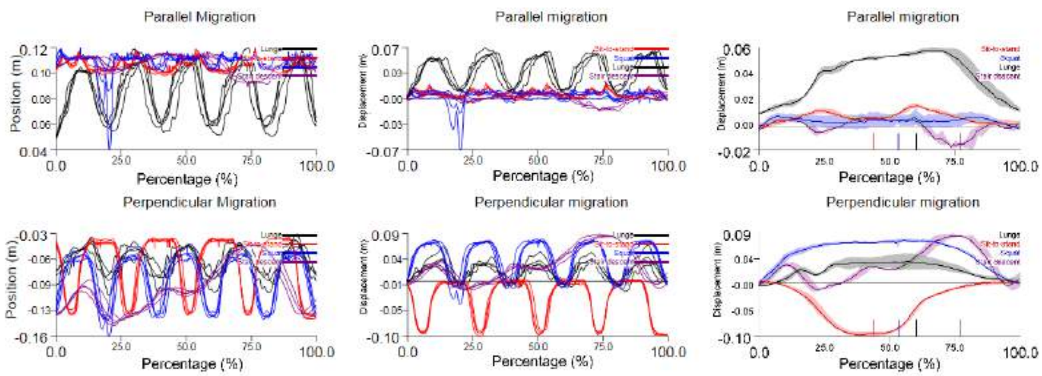

Figure C.11: Shank interface migration

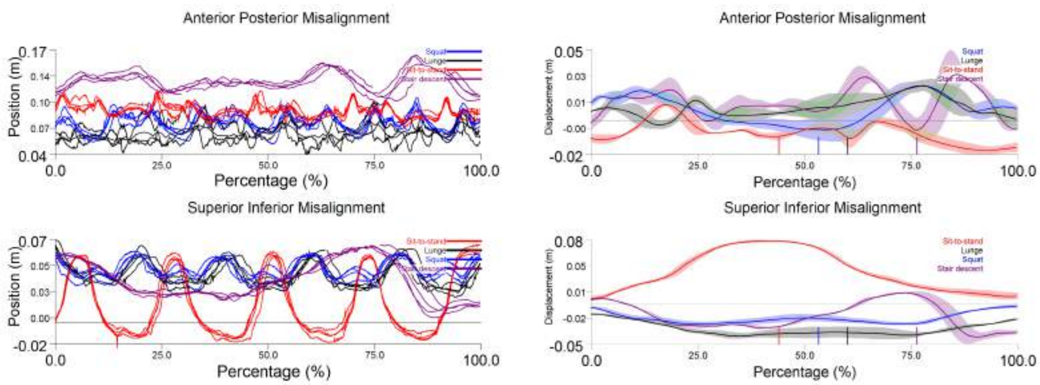

Figure C.12: Joint misalignment

3D scanner based interfaces

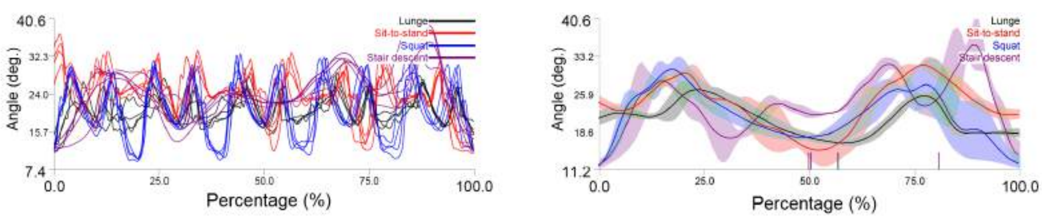

Figure C.13: Relative joint angle

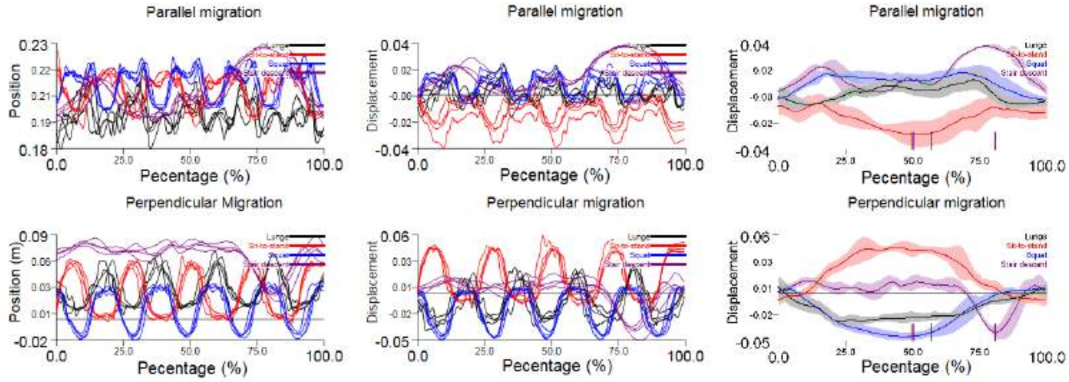

Figure C.14: Thigh interface migration

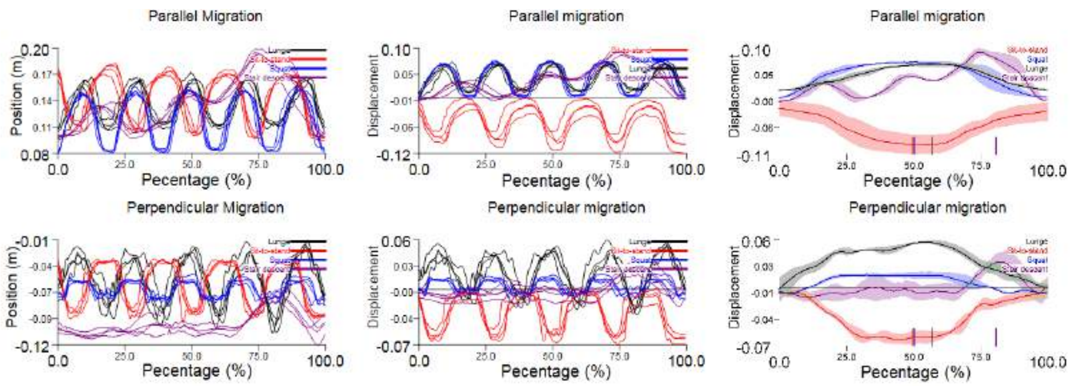

Figure C.15: Shank interface migration

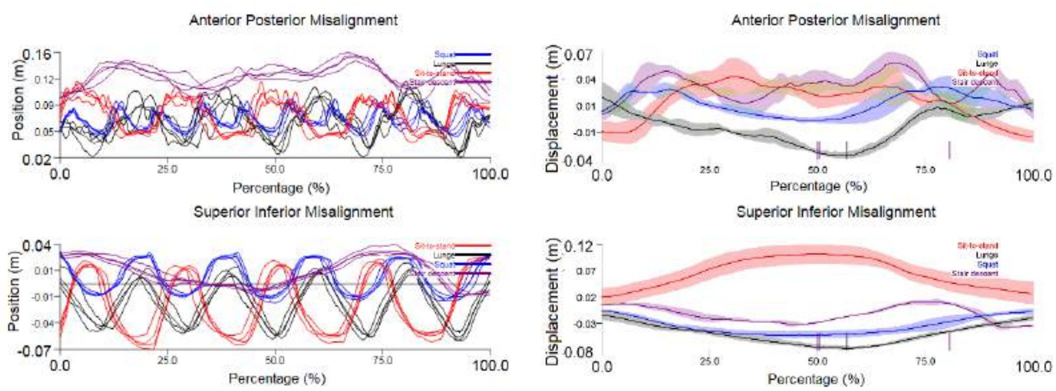

Figure C.16: Joint misalignment

C.1.3 Padding analysis

Iterated based interfaces

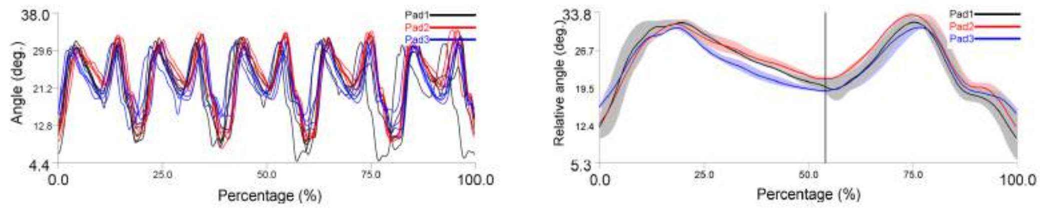

Figure C.17: Relative joint angle

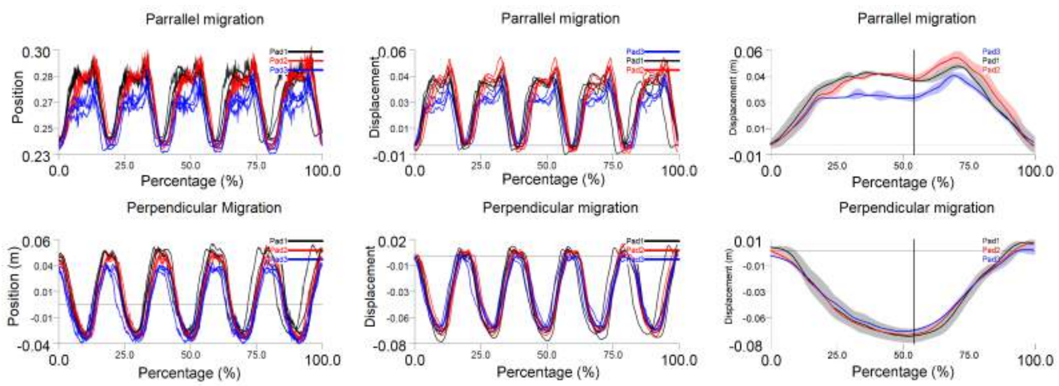

Figure C.18: Thigh interface migration

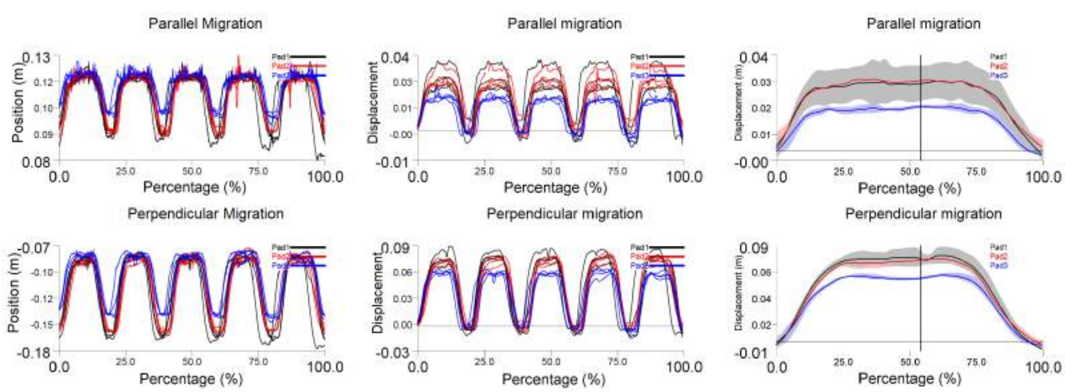

Figure C.19: Shank interface migration

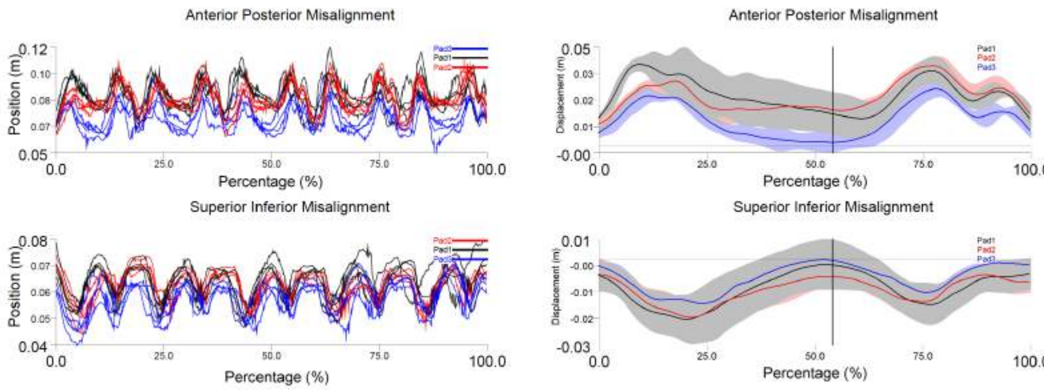

Figure C.20: Joint misalignment

3D scanner based interfaces

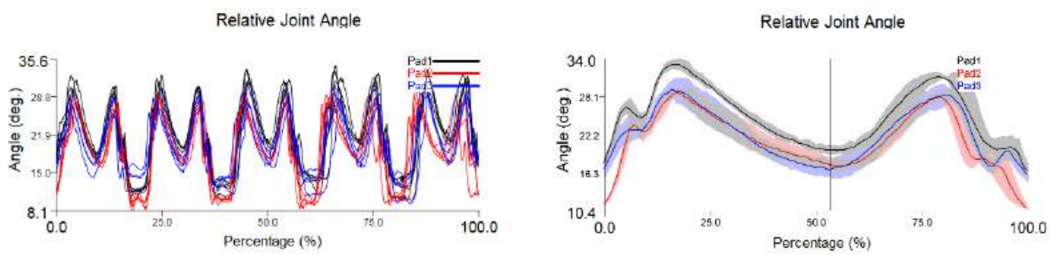

Figure C.21: Relative joint angle

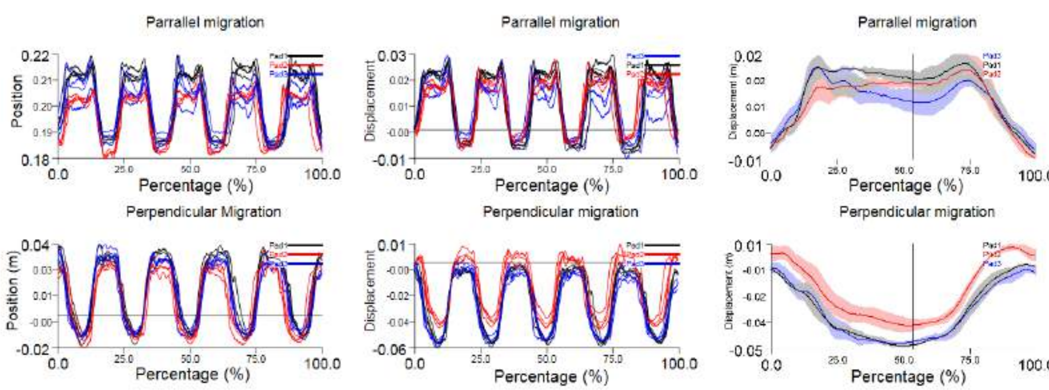

Figure C.22: Thigh interface migration

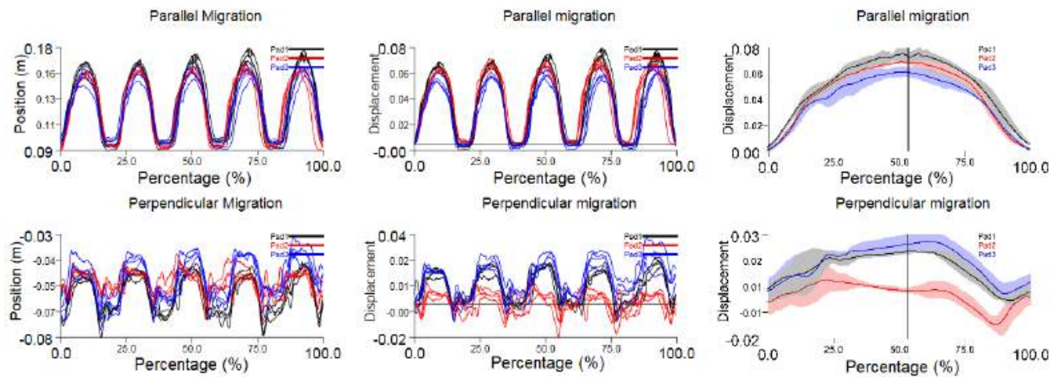

Figure C.23: Shank interface migration

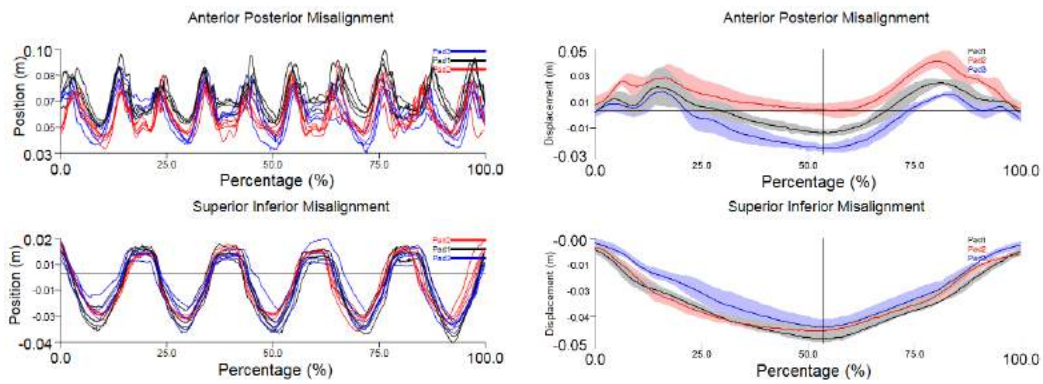

Figure C.24: Joint misalignment

C.1.4 Position analysis

Iterated based interfaces

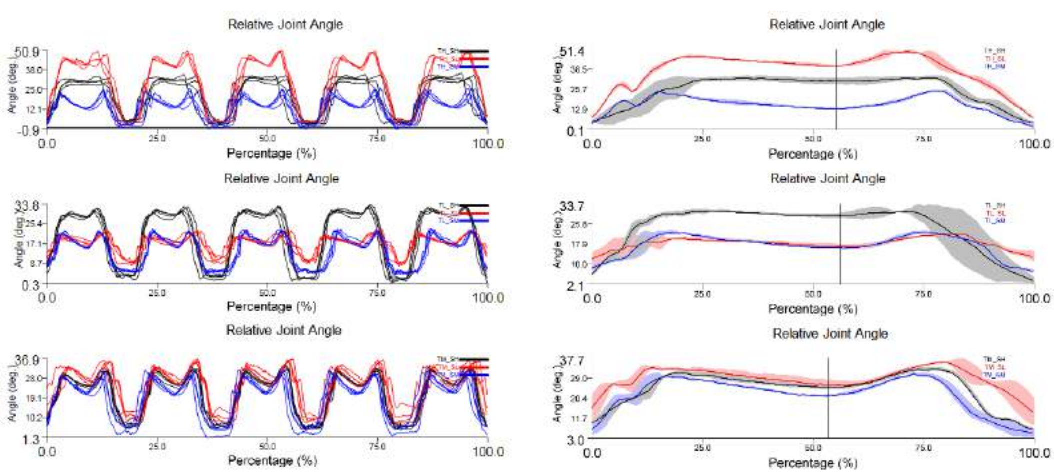

Figure C.25: Relative joint angle

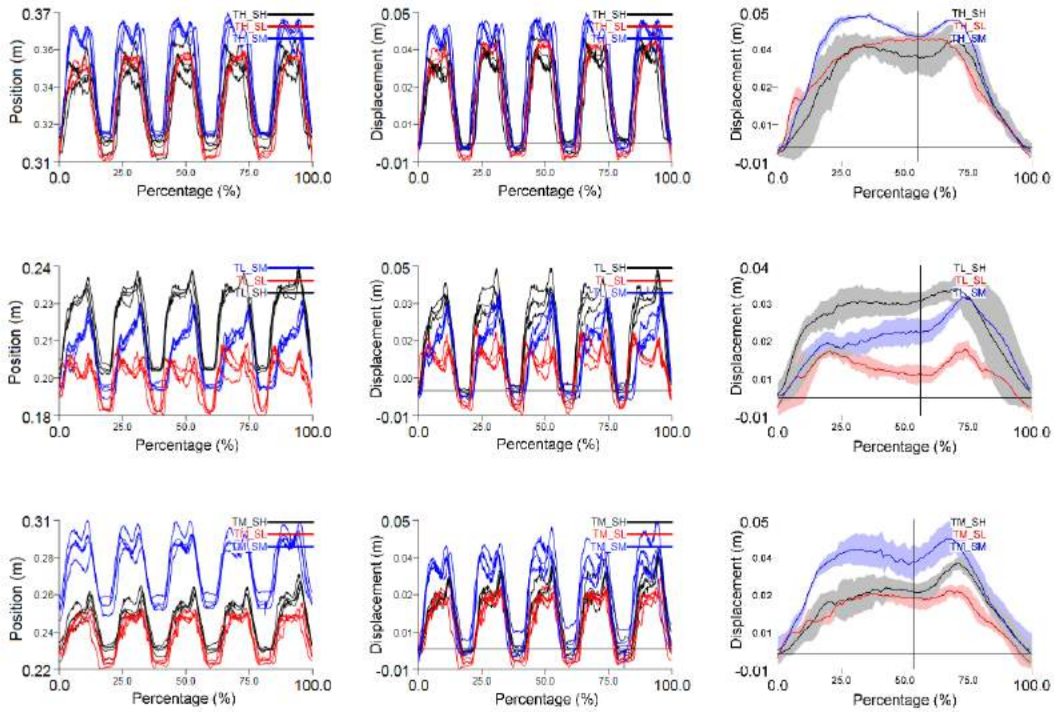

Figure C.26: Thigh interface migration (parallel)

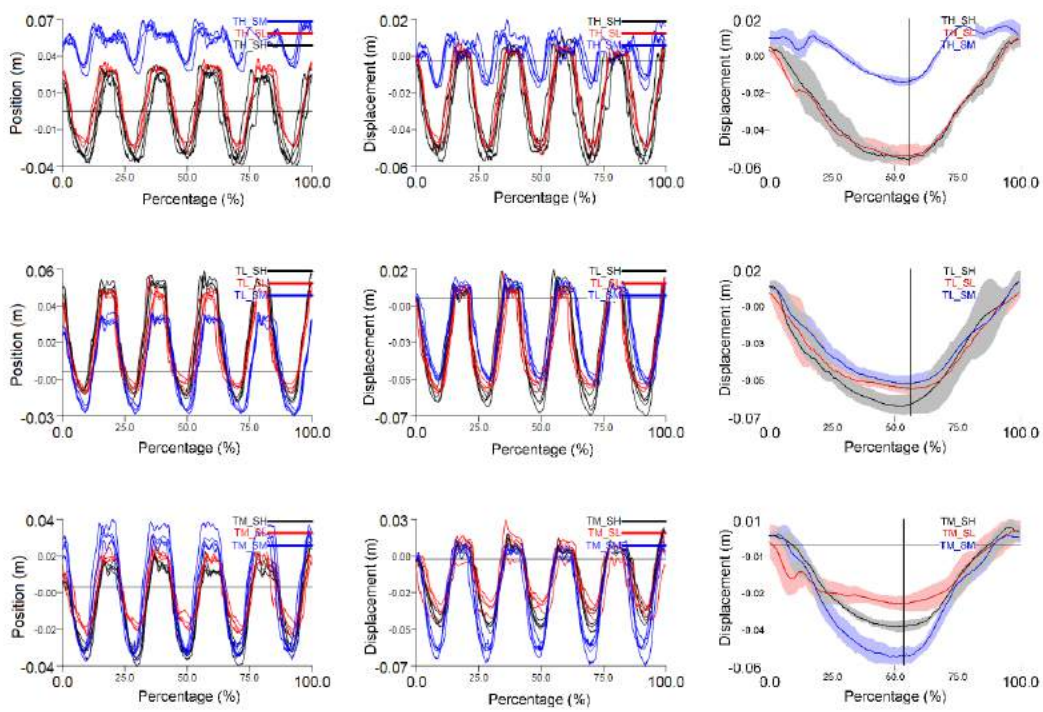

Figure C.27: Thigh interface migration (perpendicular

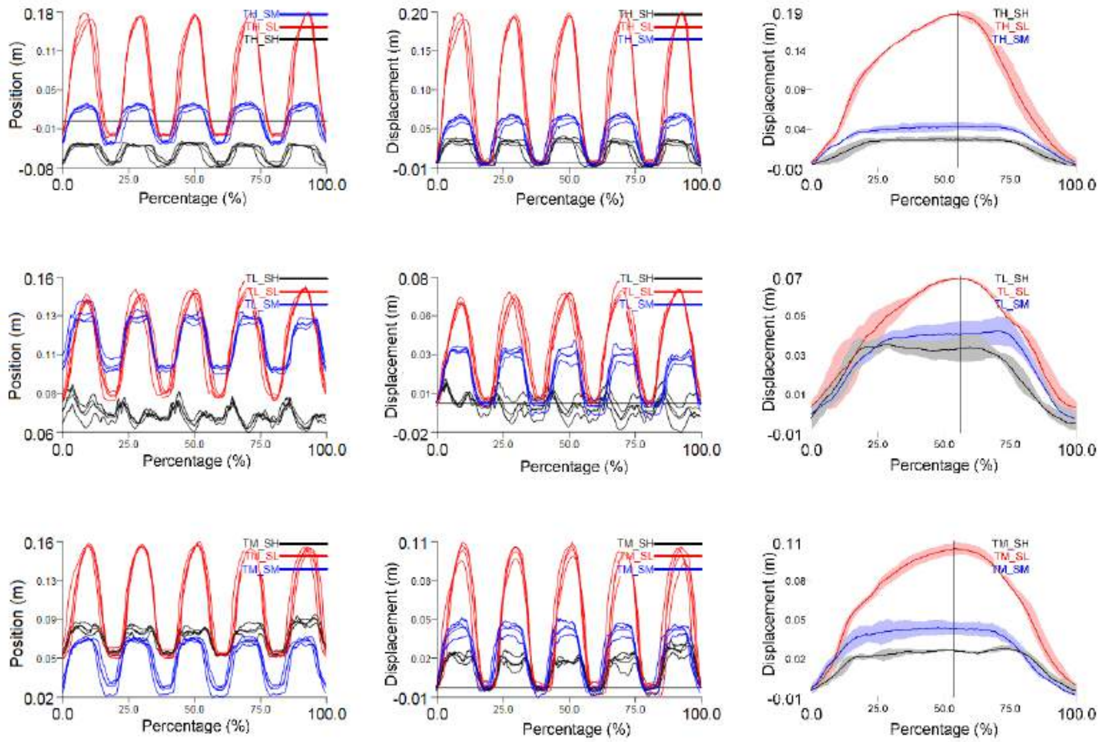

Figure C.28: Shank interface migration (parallel)

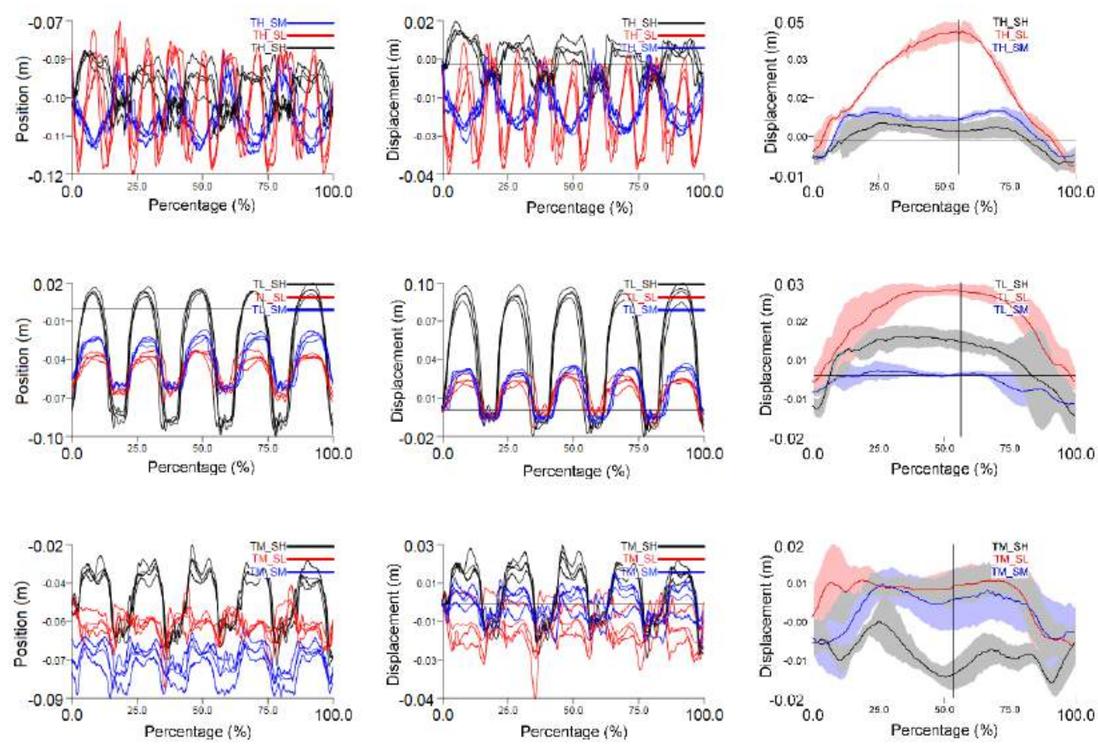

Figure C.29: Shank interface migration (perpendicular)

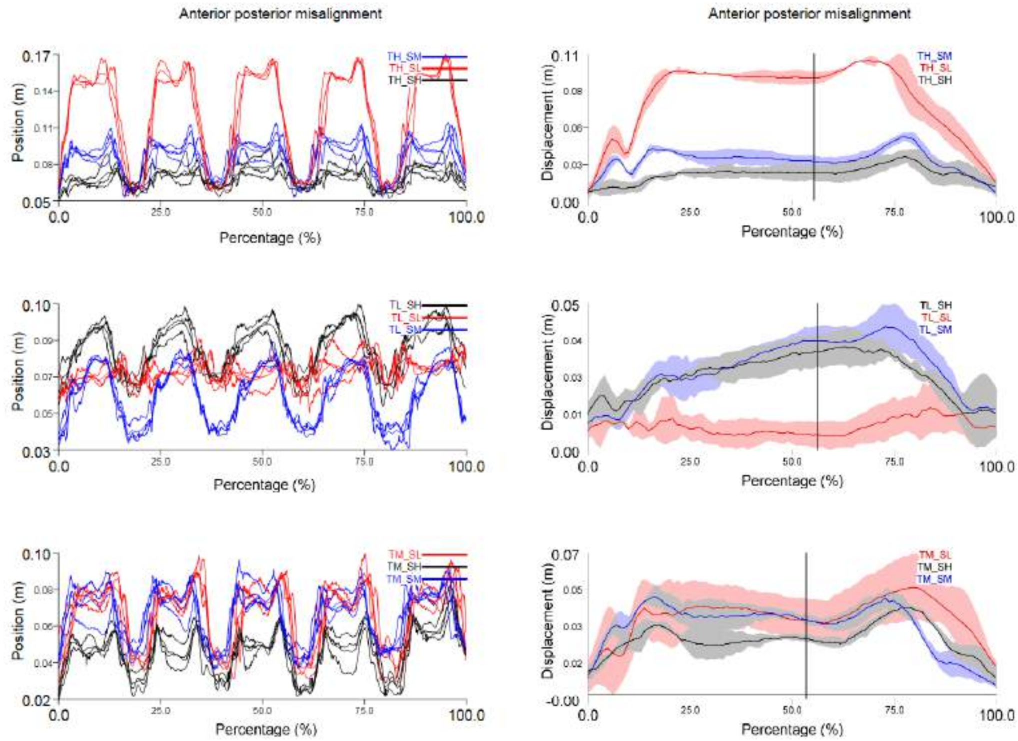

Figure C.30: Joint misalignment (anterior-posterior)

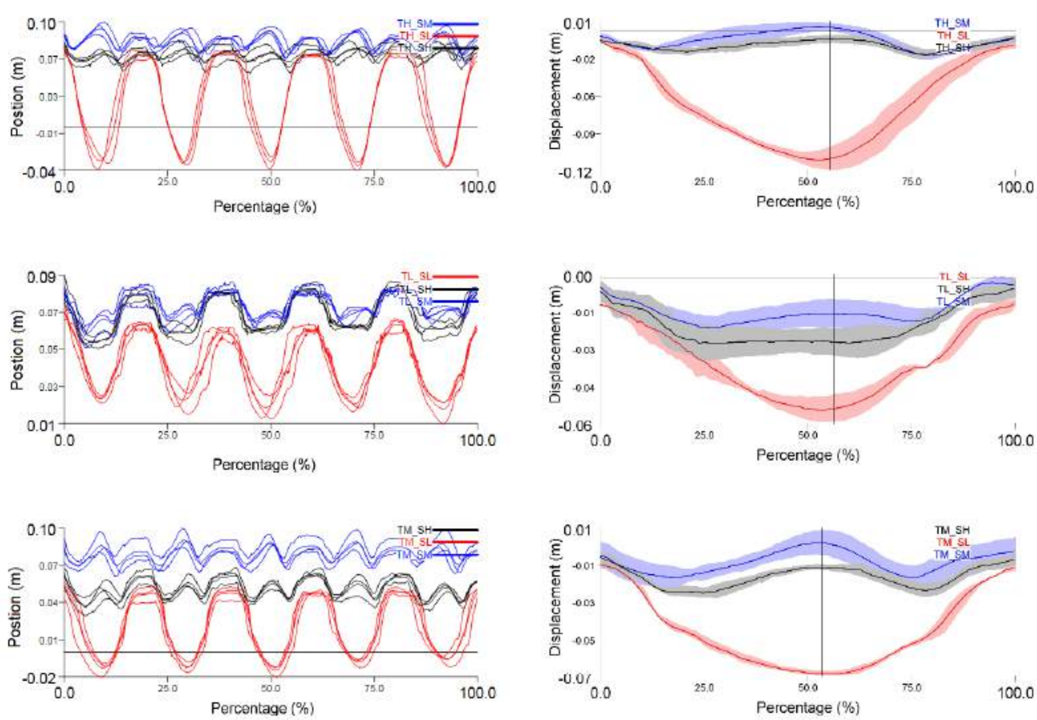

Figure C.31: Joint misalignment (superior-inferior)

3D scanner based interfaces

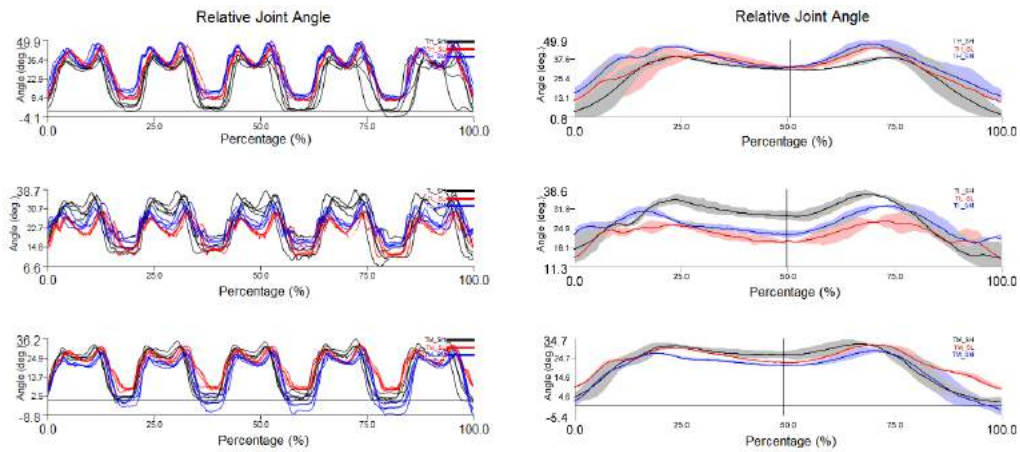

Figure C.32: Relative joint angle

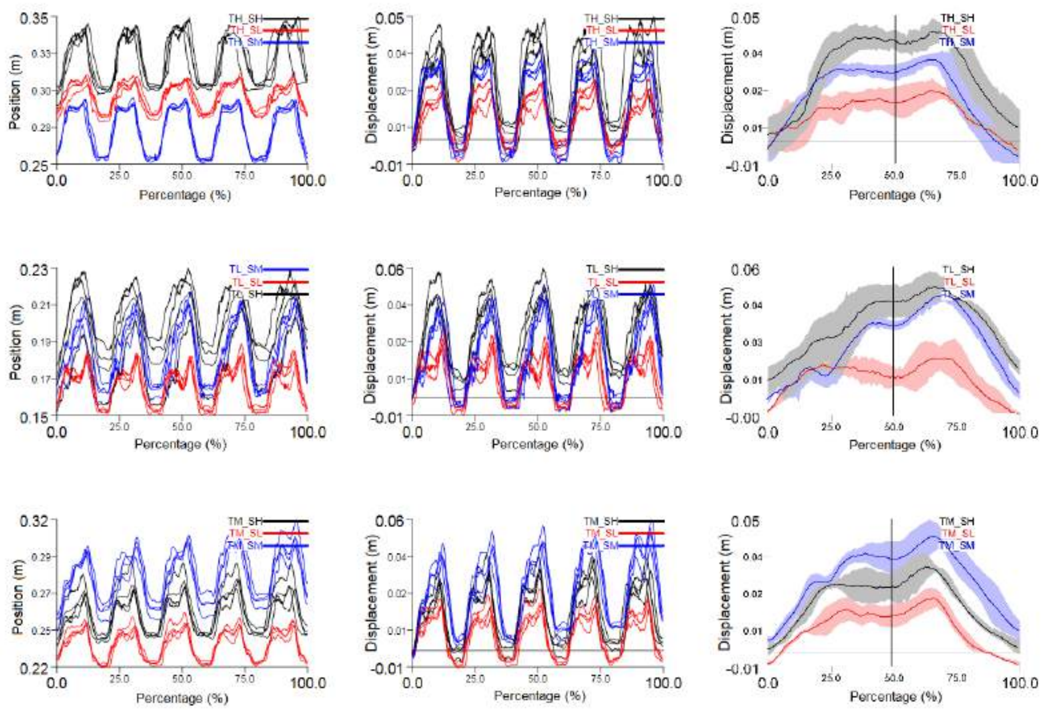

Figure C.33: Thigh interface migration (parallel)

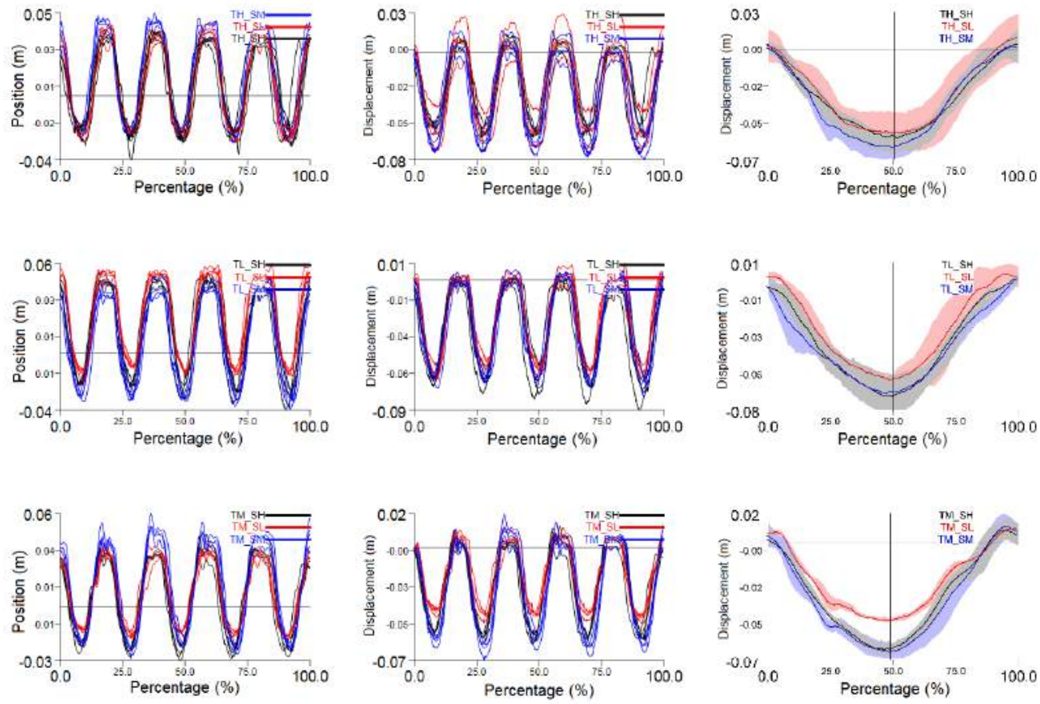

Figure C.34: Thigh interface migration (perpendicular

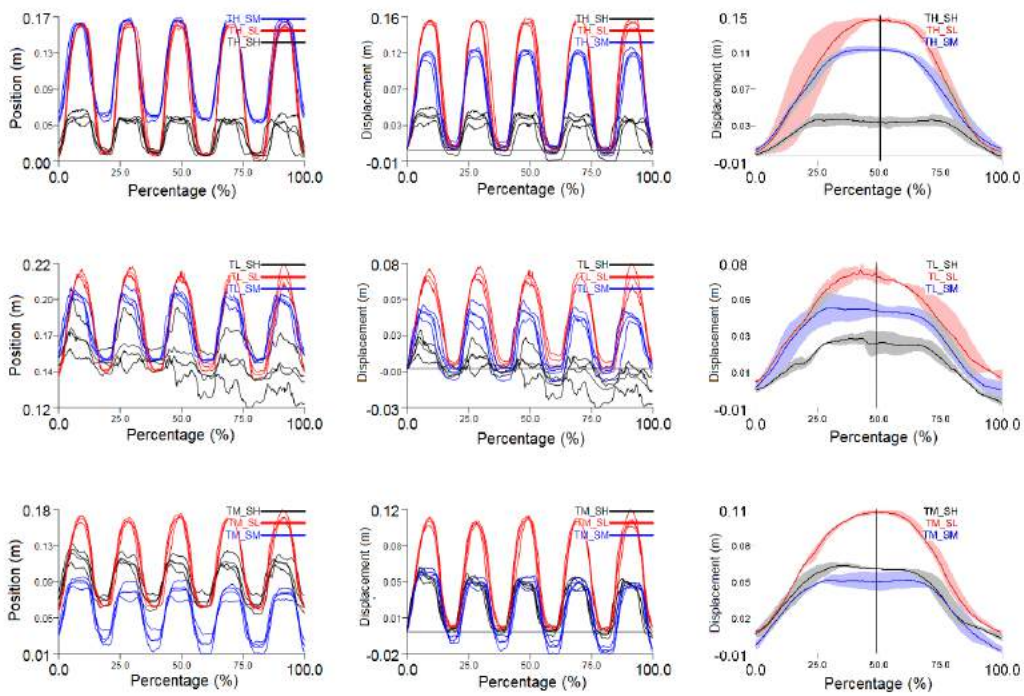

Figure C.35: Shank interface migration (parallel)

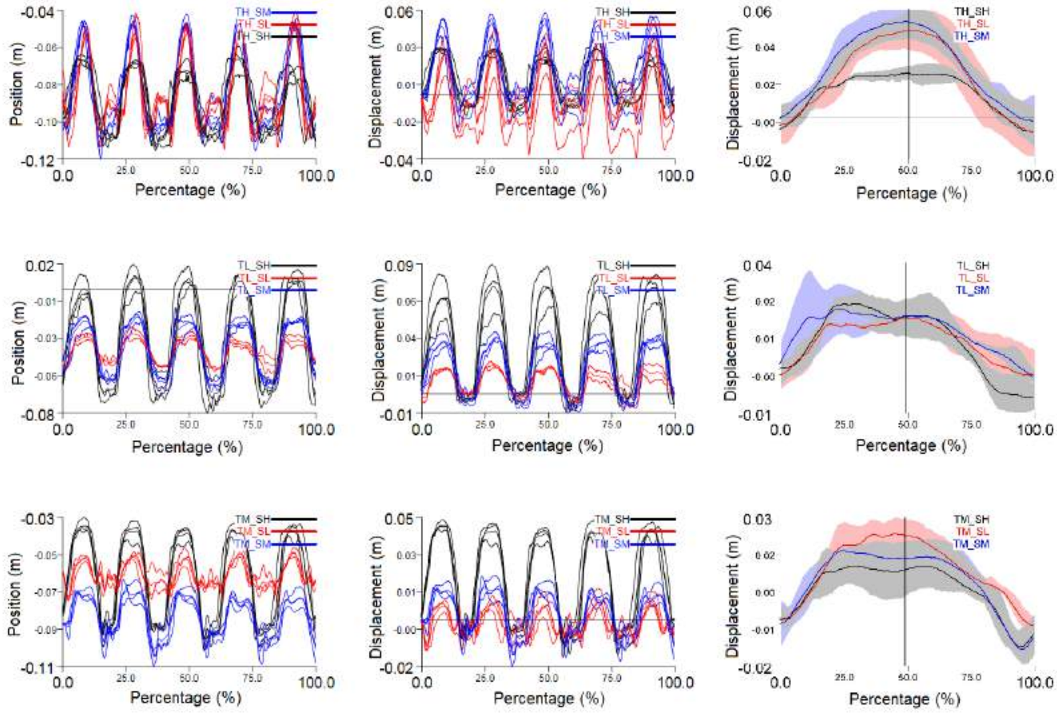

Figure C.36: Shank interface migration (perpendicular)

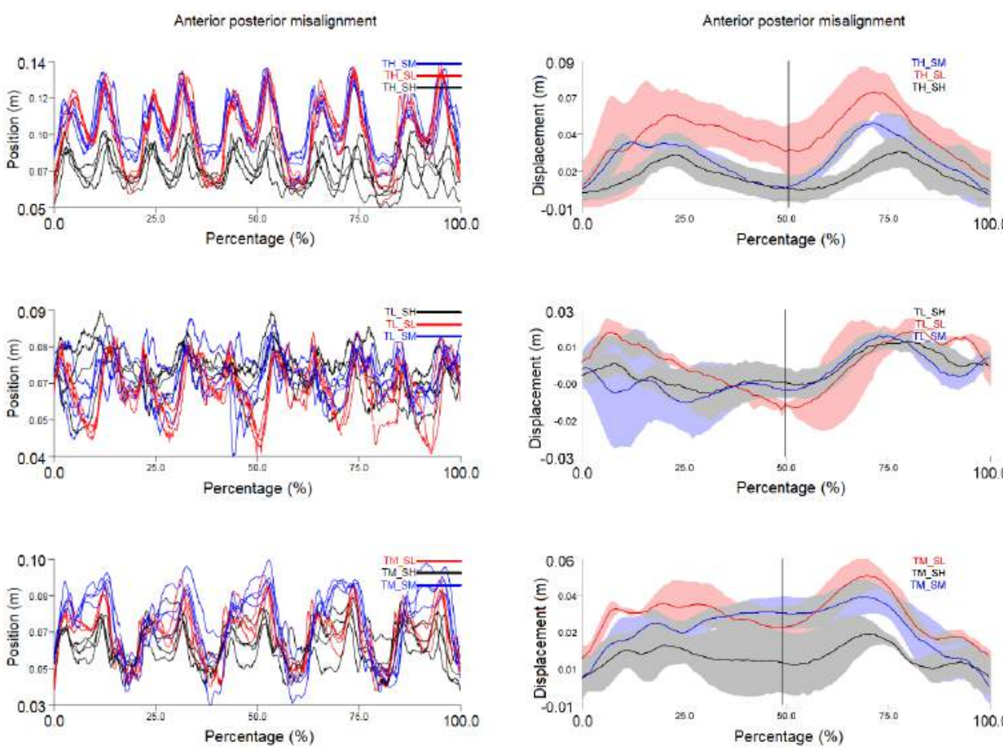

Figure C.37: Joint misalignment (anterior-posterior)

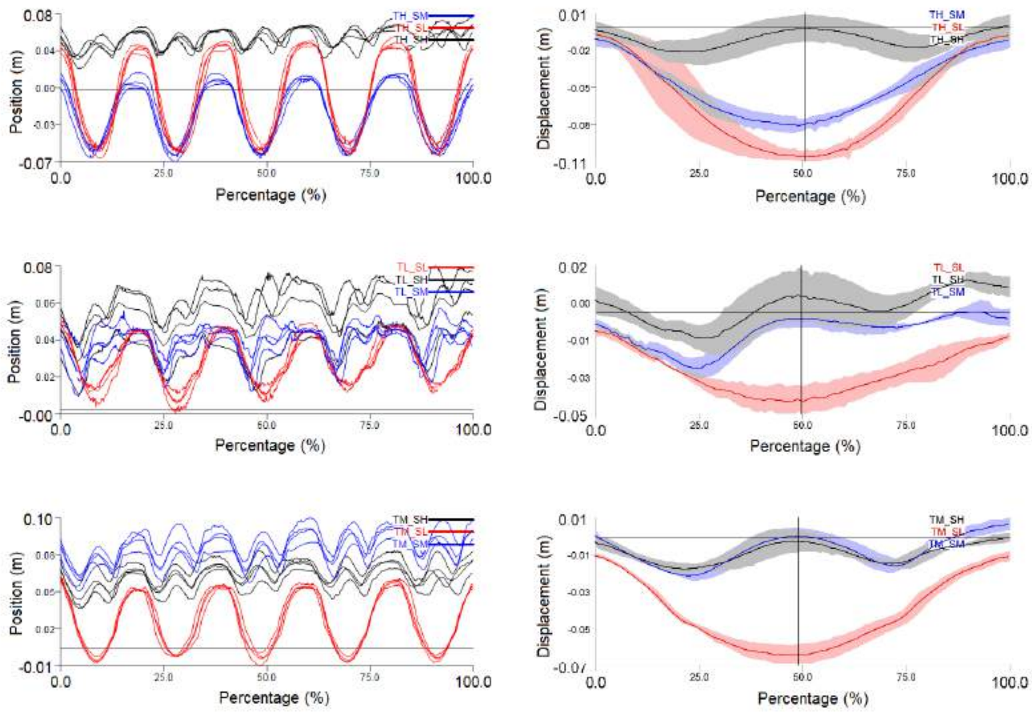

Figure C.38: Joint misalignment (superior-inferior)

C.1.5 Stiffness analysis

Iterated based interfaces

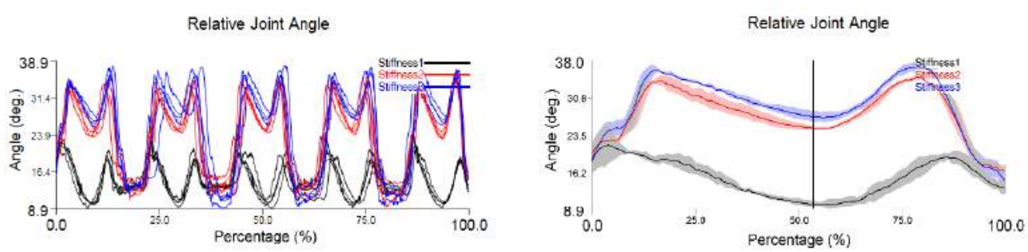

Figure C.39: Relative joint angle

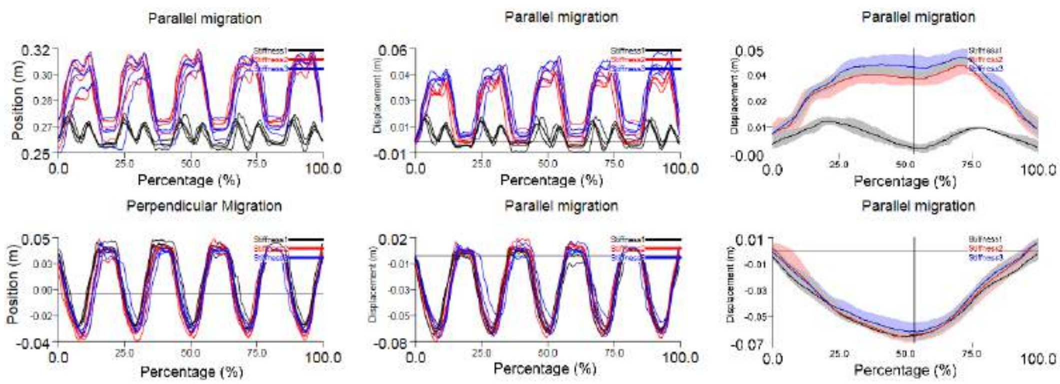

Figure C.40: Thigh interface migration

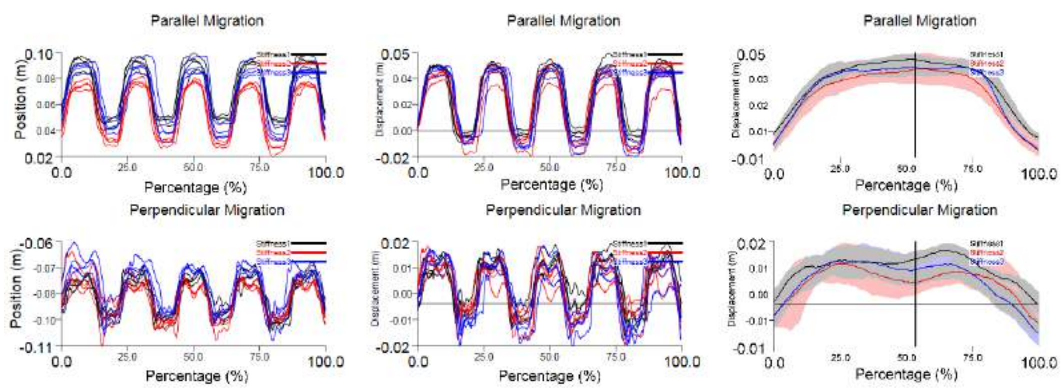

Figure C.41: Shank interface migration

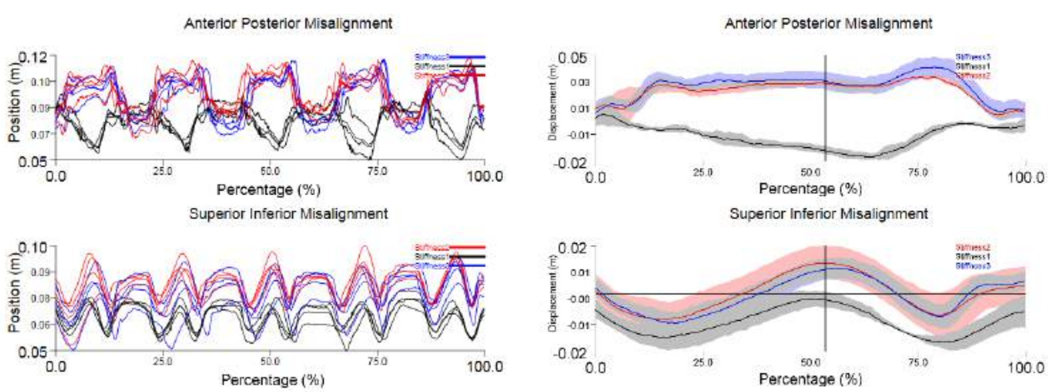

Figure C.42: Joint misalignment

3D scanner based interfaces

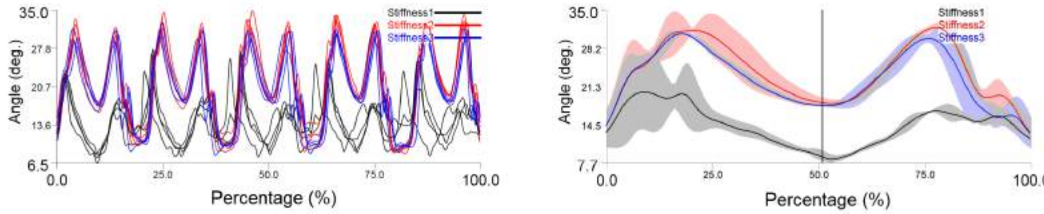

Figure C.43: Relative joint angle

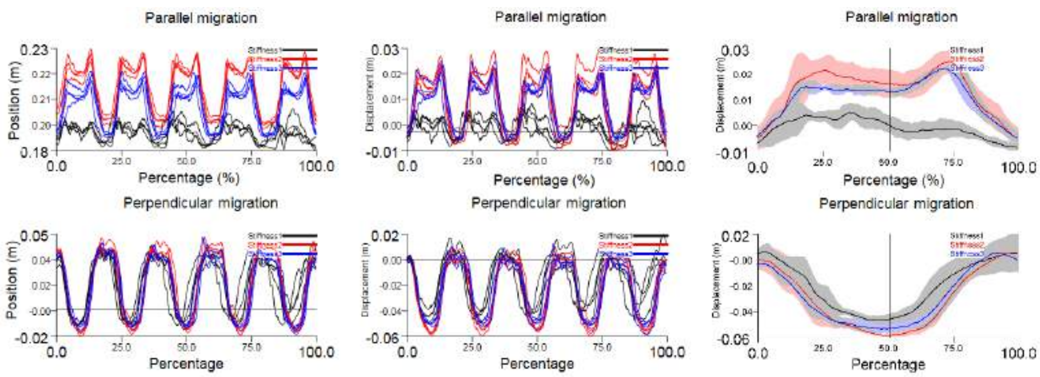

Figure C.44: Thigh interface migration

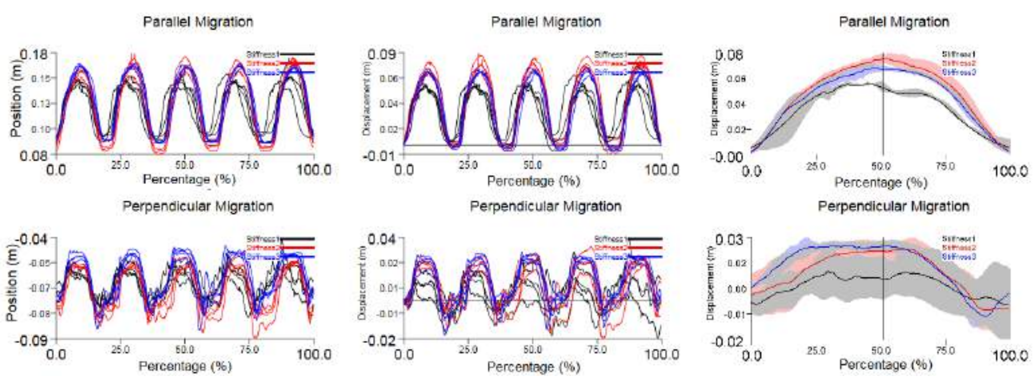

Figure C.45: Shank interface migration

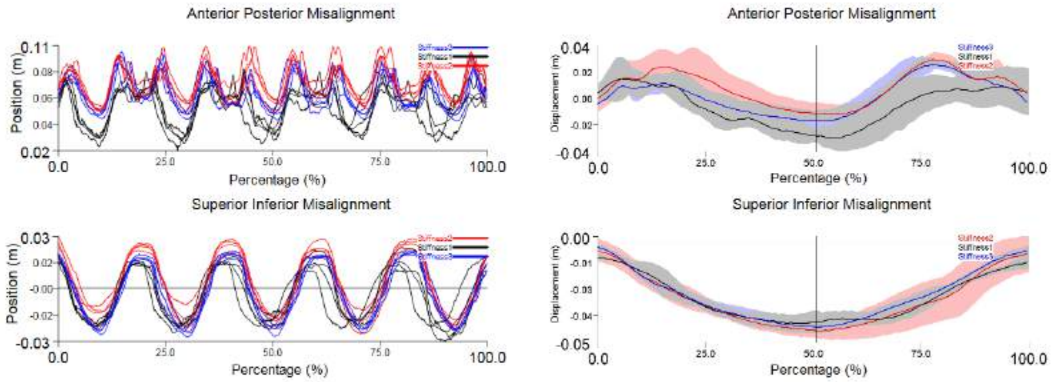

Figure C.46: Joint misalignment

C.1.6 3D scanner-Iterated interface comparison

Combination analysis

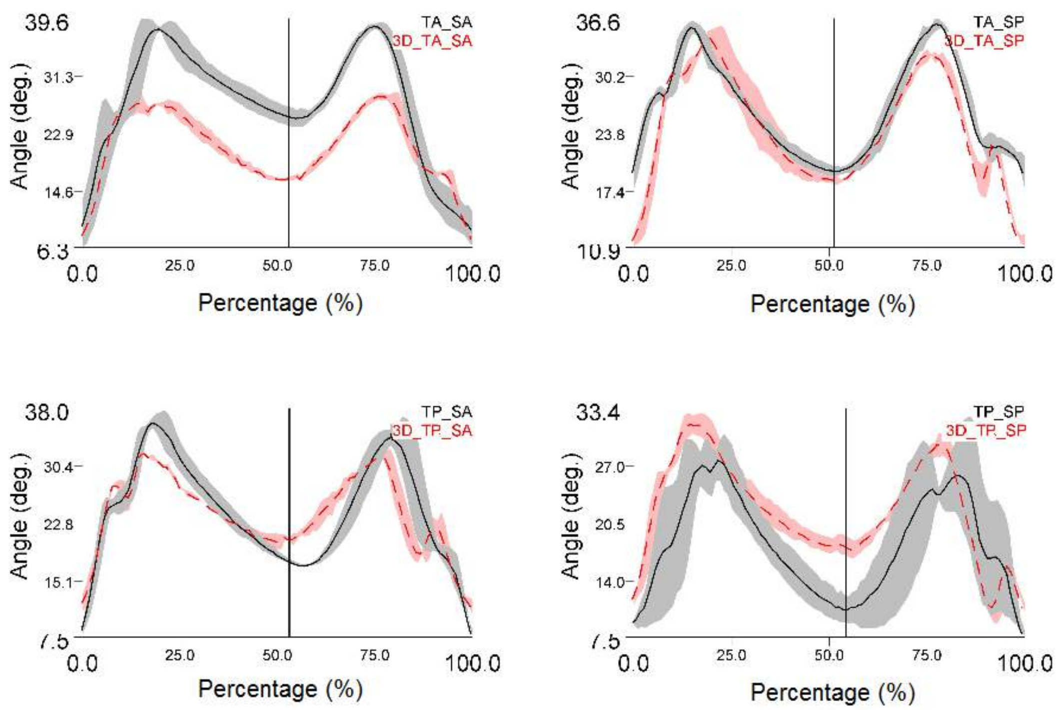

Figure C.47: Relative joint angle

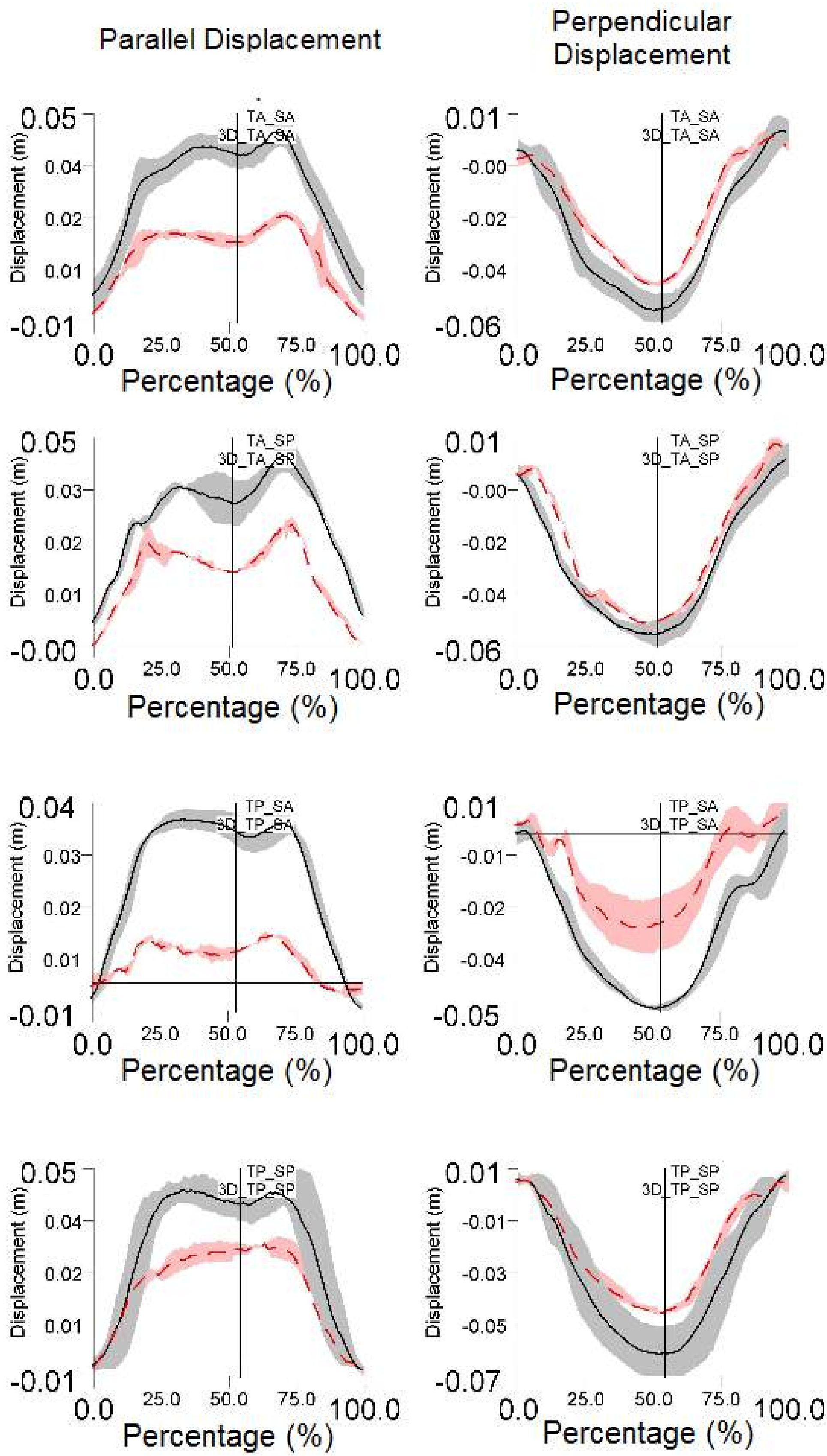

Figure C.48: Thigh interface migration

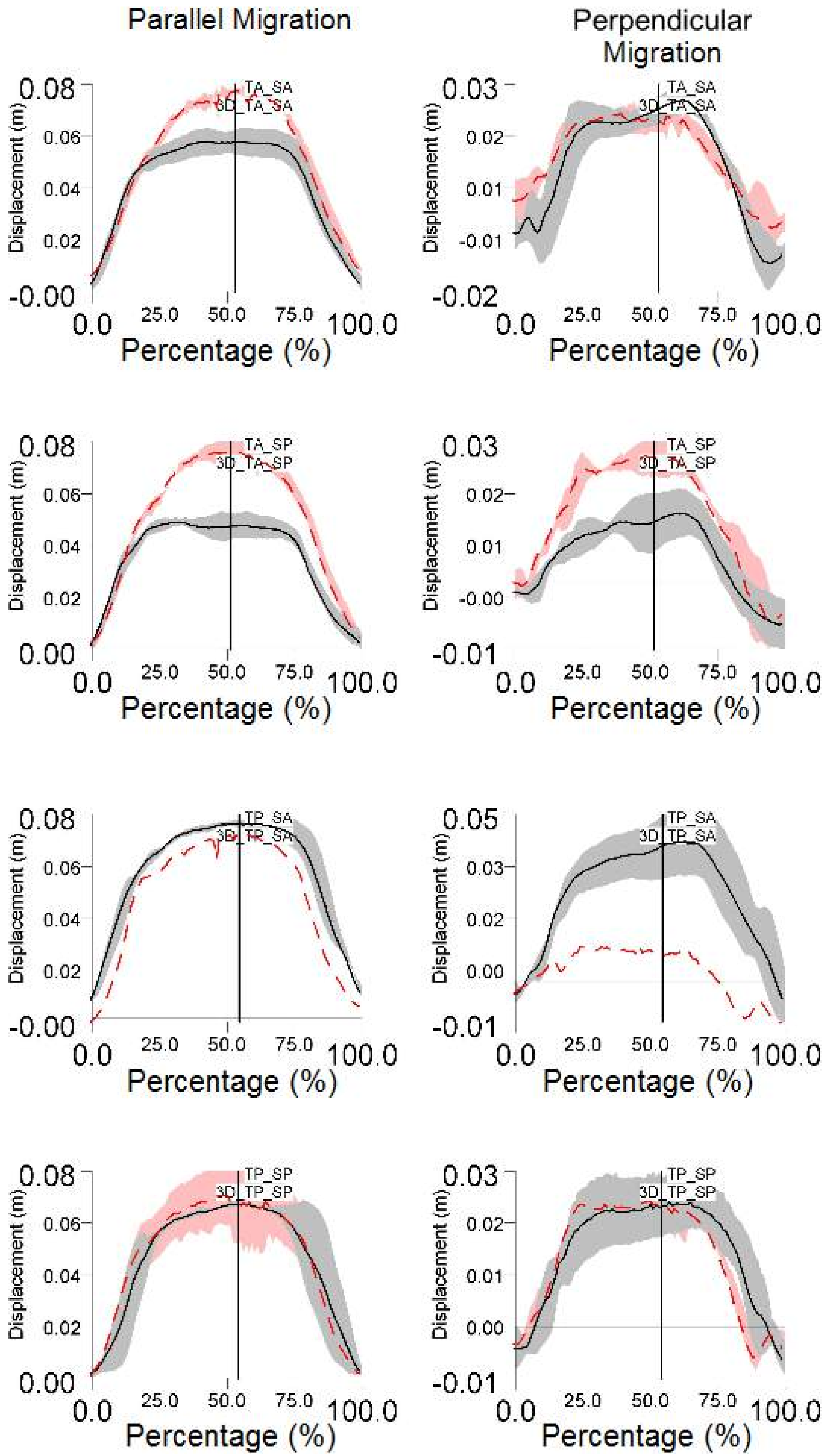

Figure C.49: Shank interface migration

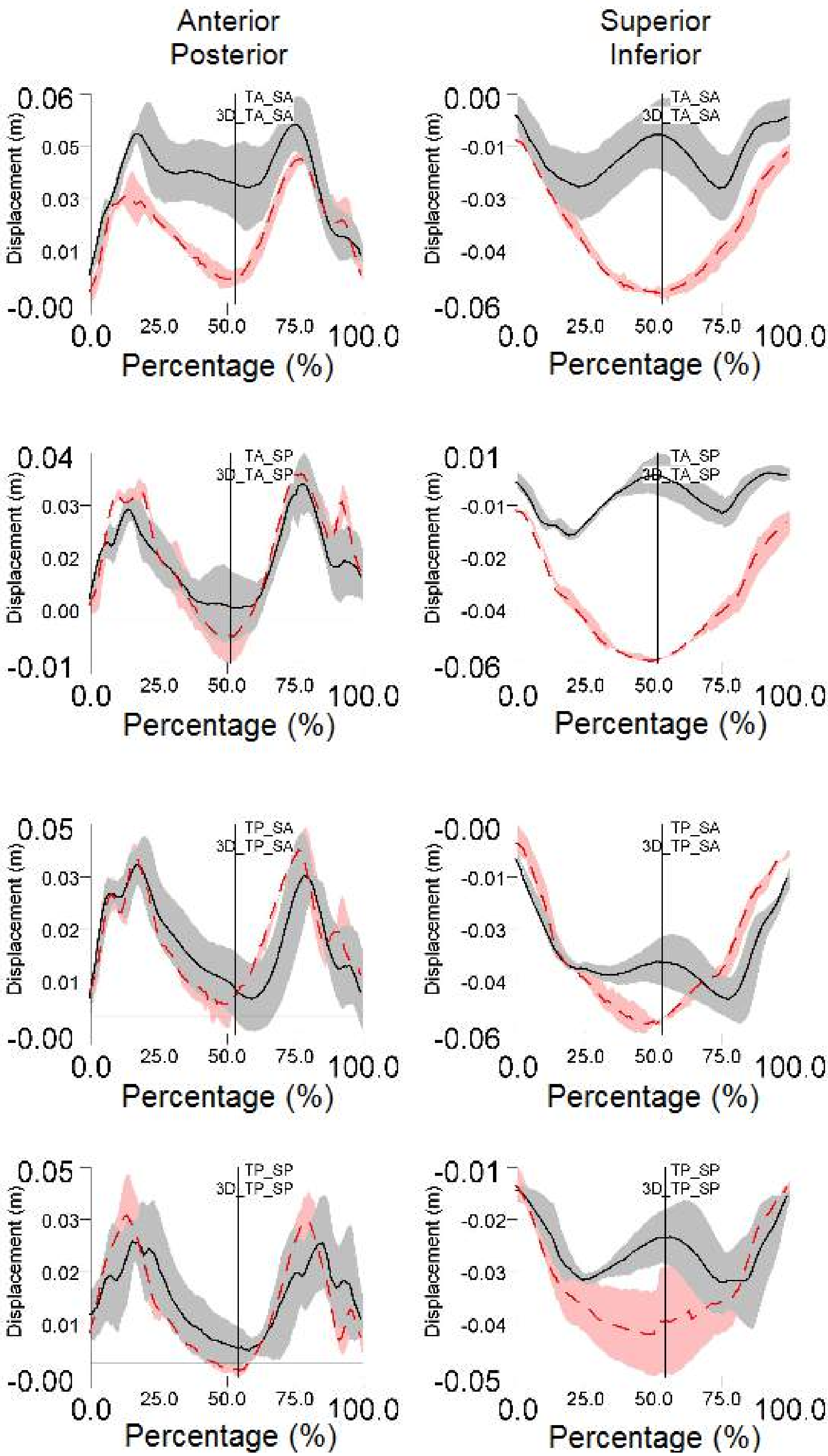

Figure C.50: Joint misalignment

Exercise analysis

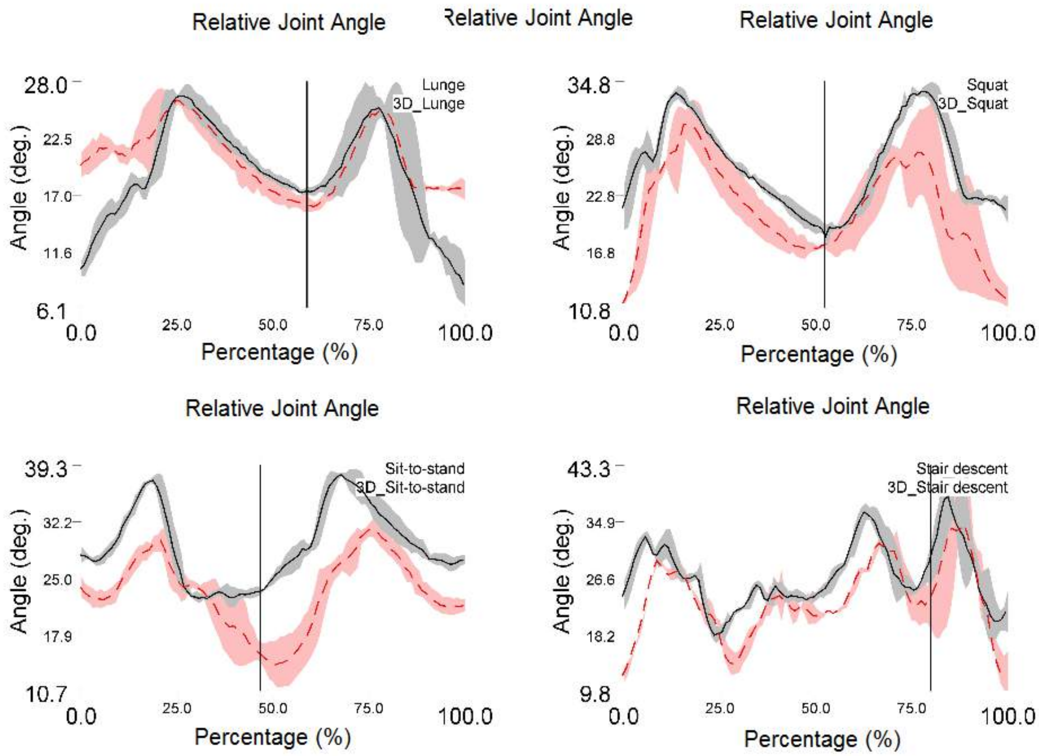

Figure C.51: Relative joint angle

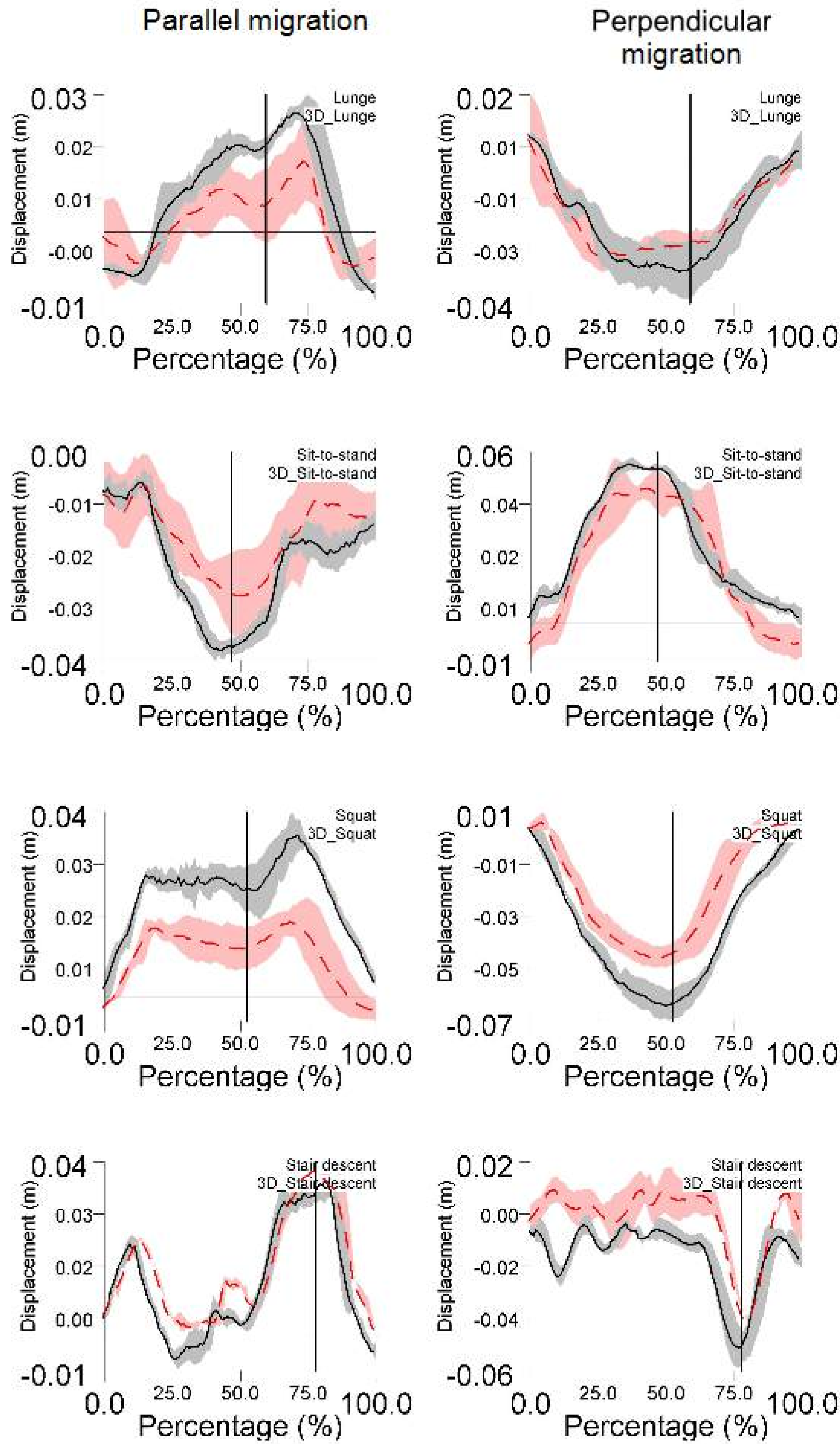

Figure C.52: Thigh interface migration

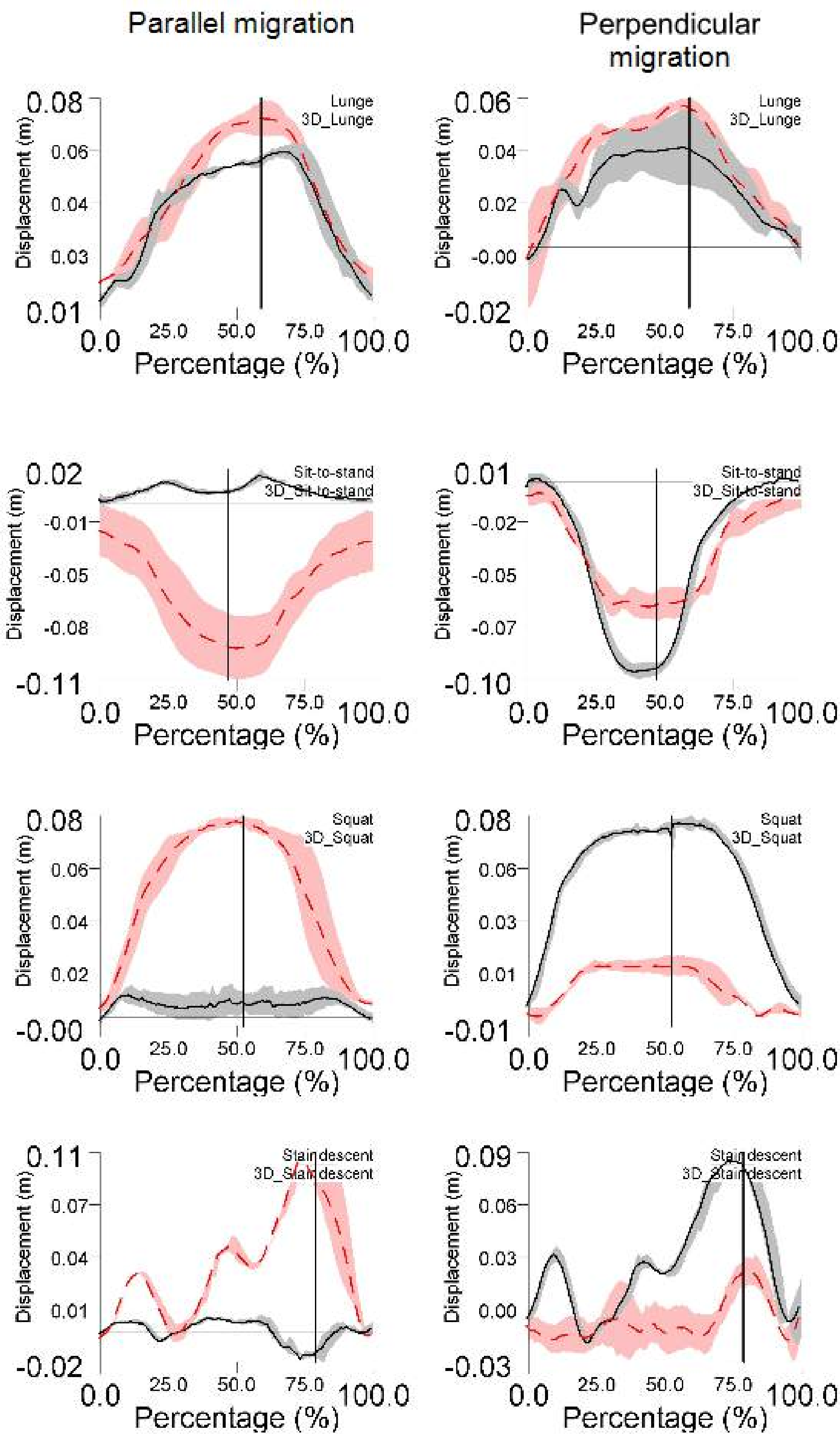

Figure C.53: Shank interface migration

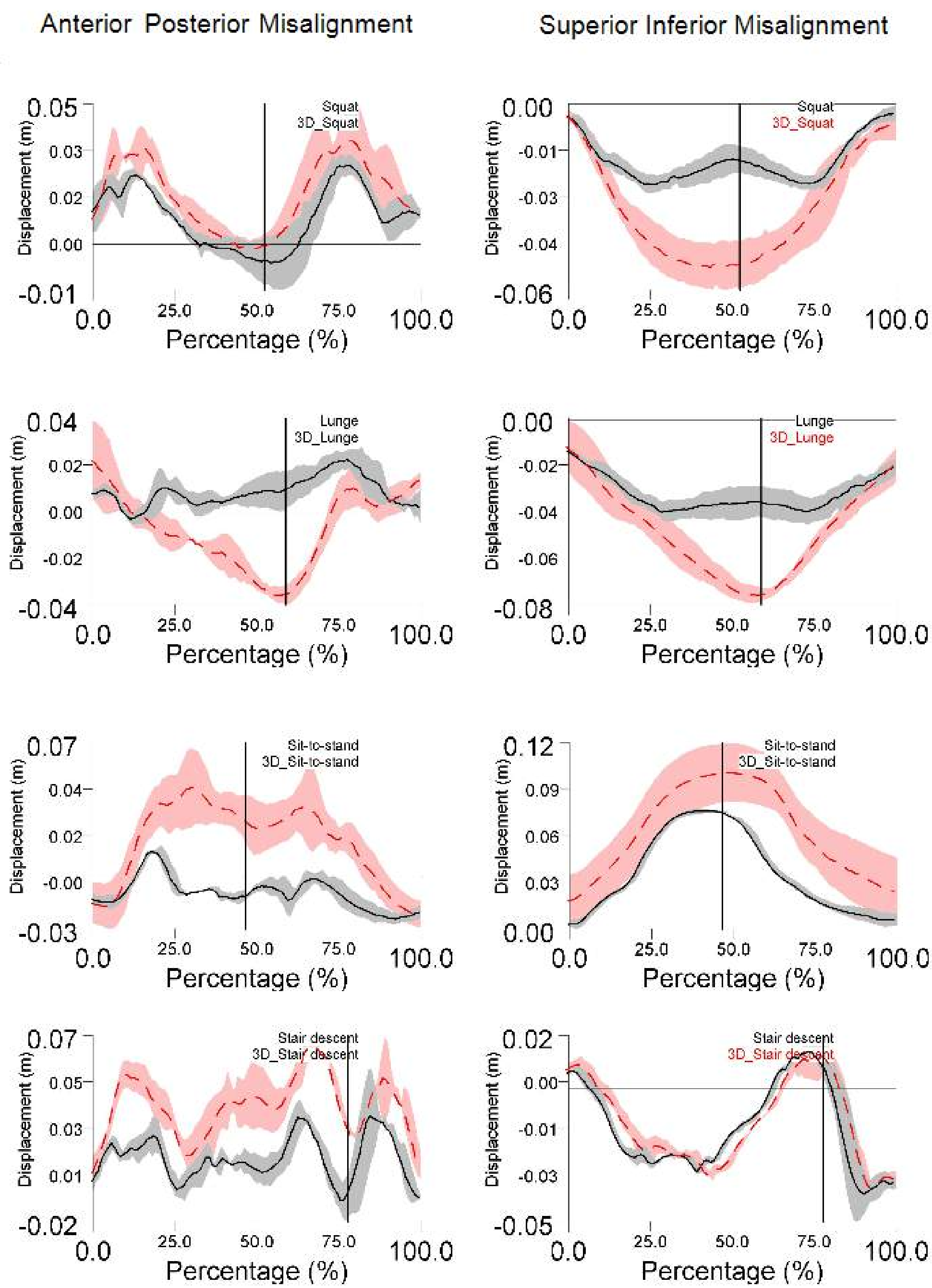

Figure C.54: Joint misalignment

Padding analysis

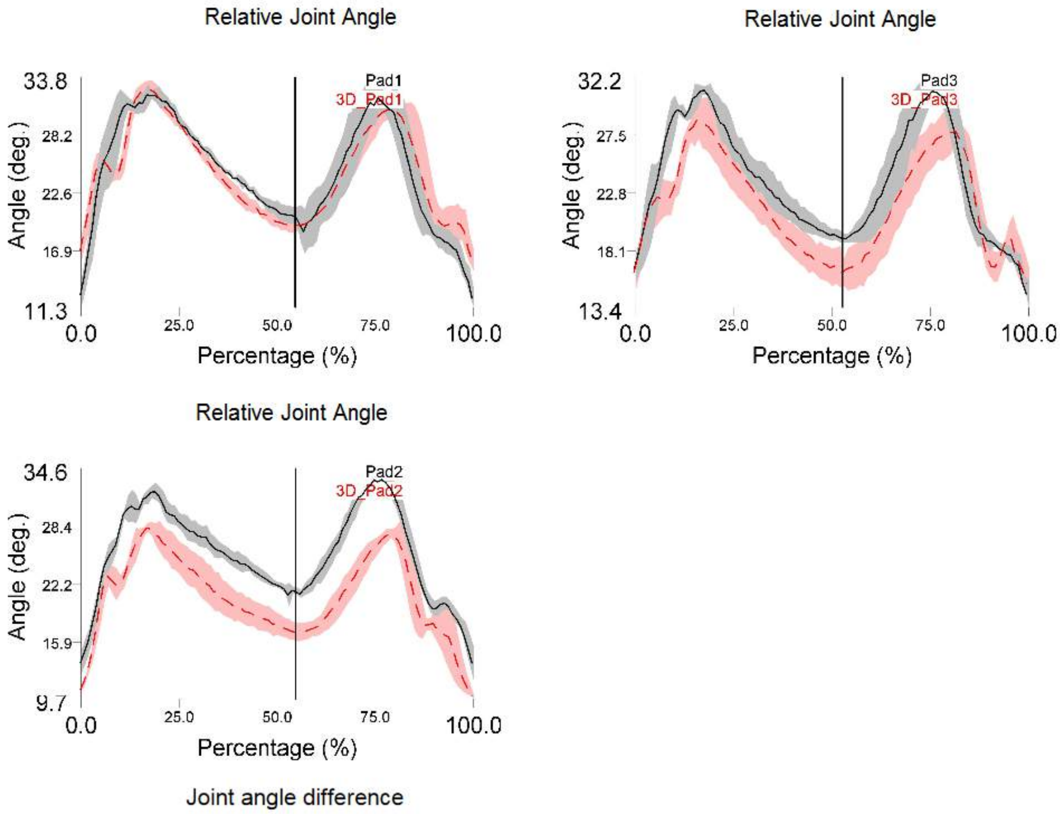

Figure C.55: Relative joint angle

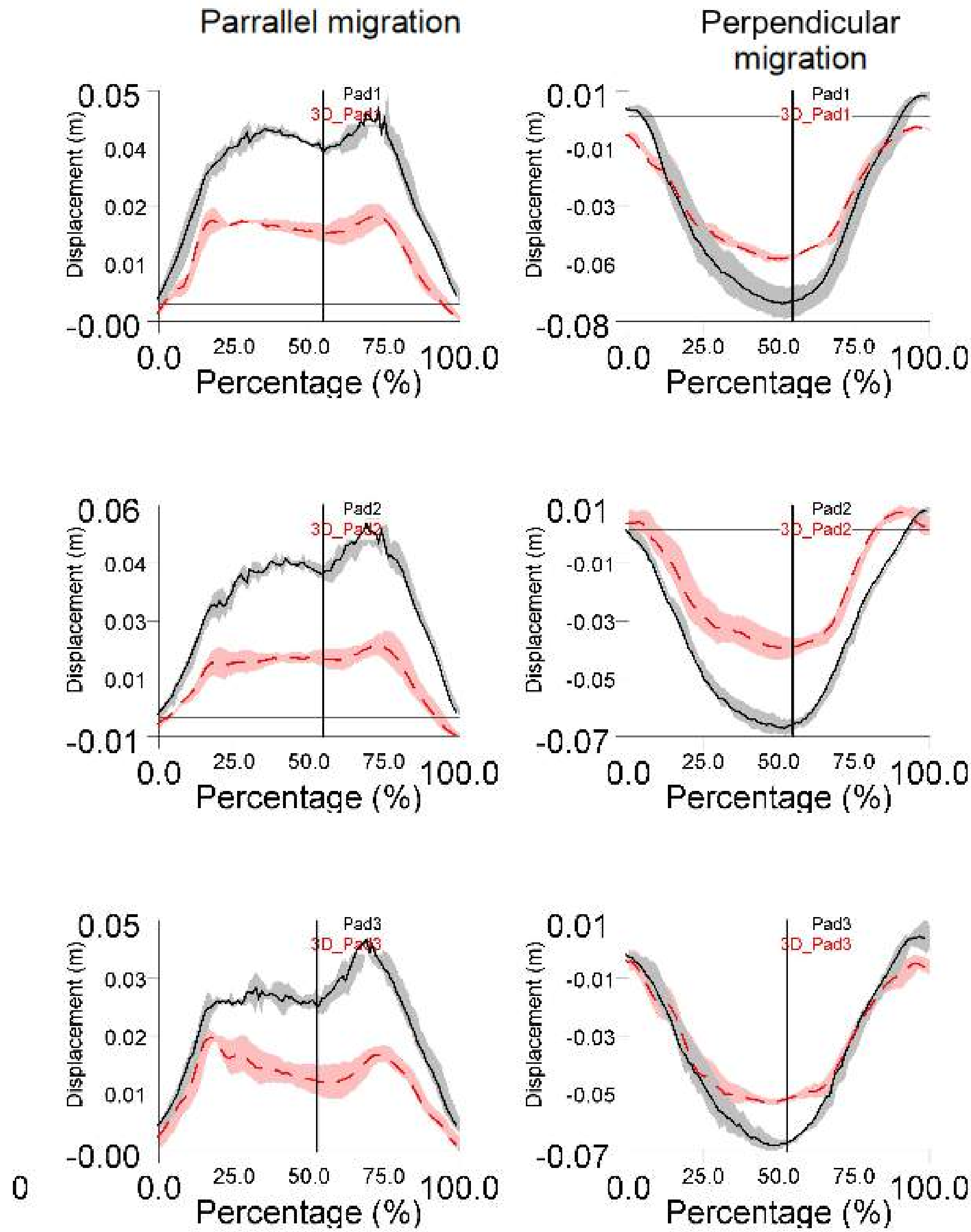

Figure C.56: Thigh interface migration

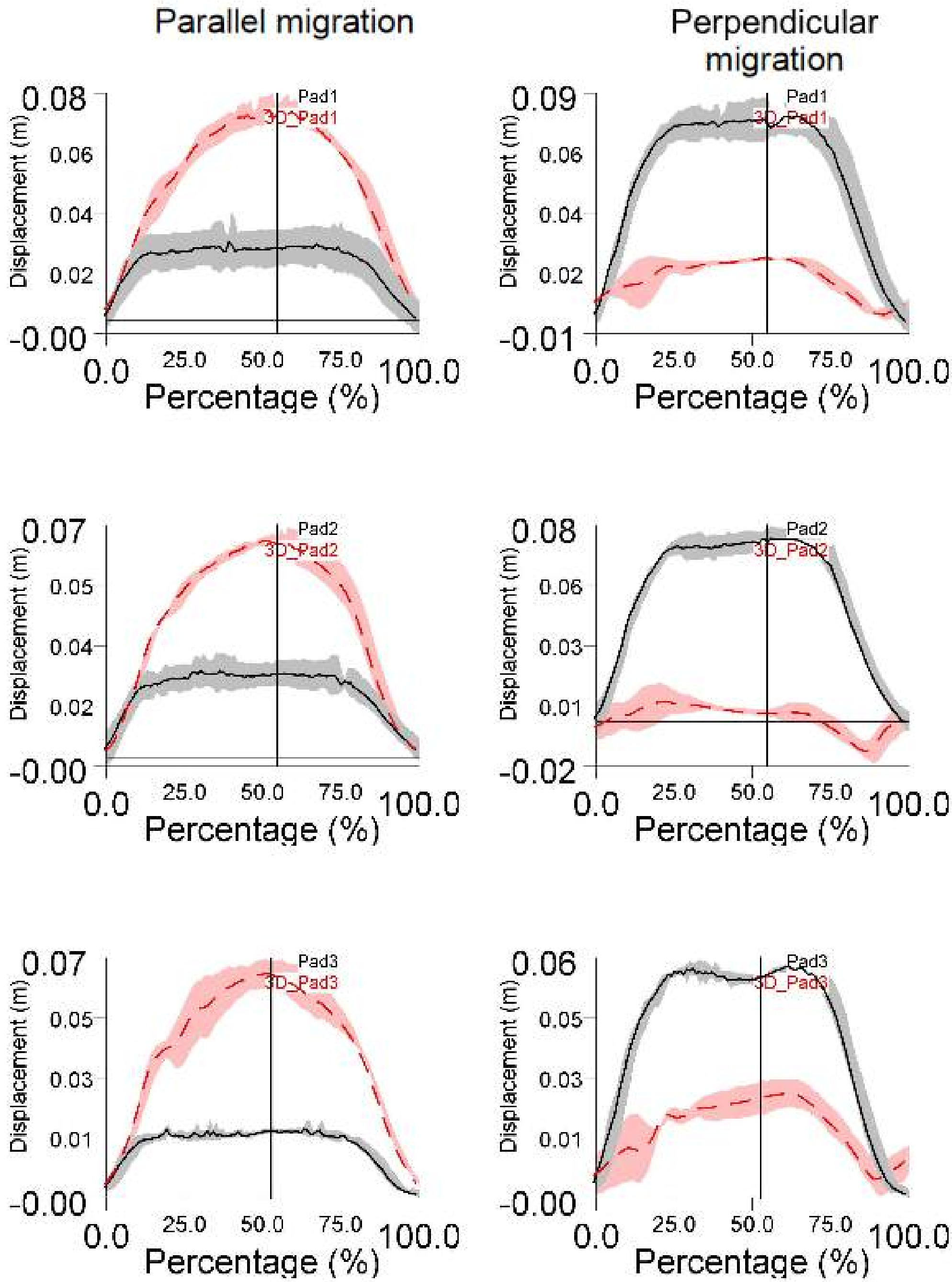

Figure C.57: Shank interface migration

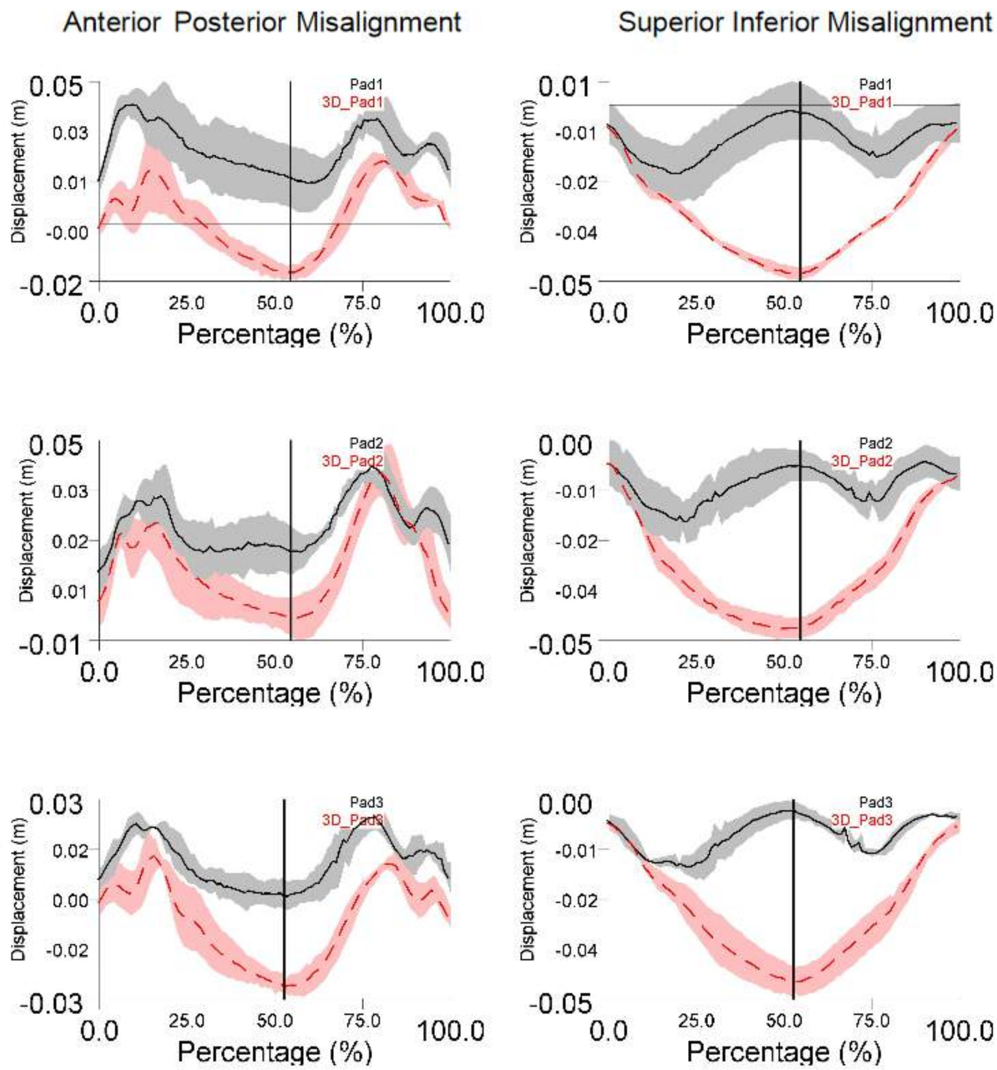

Figure C.58: Joint misalignment

Position analysis

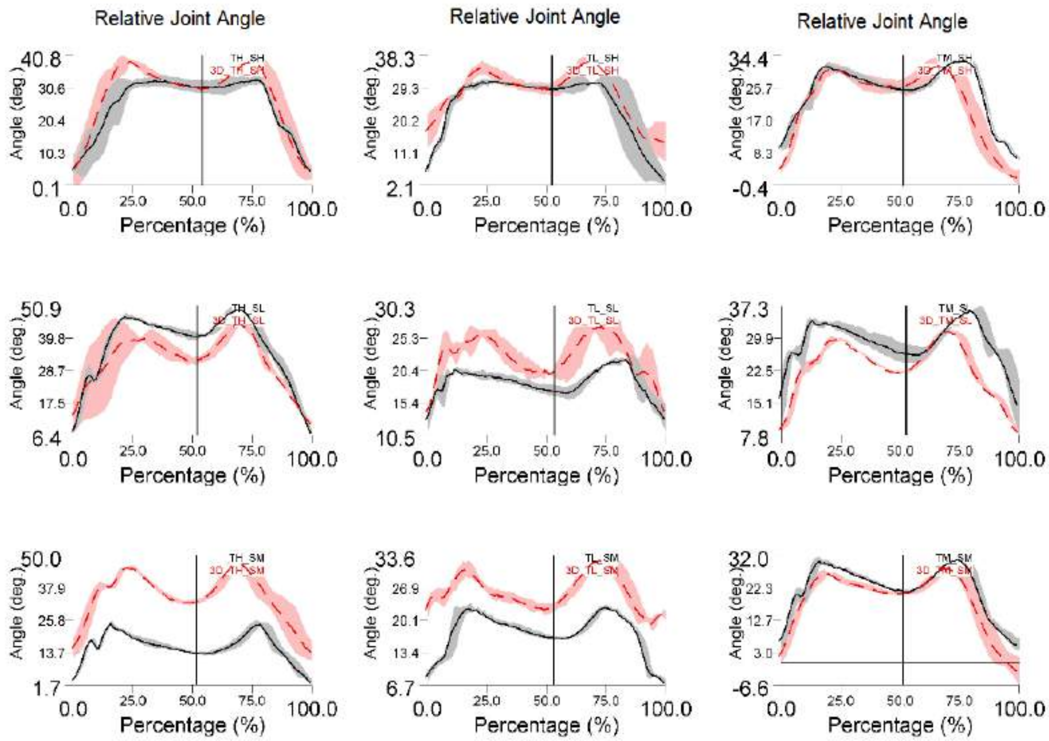

Figure C.59: Relative joint angle

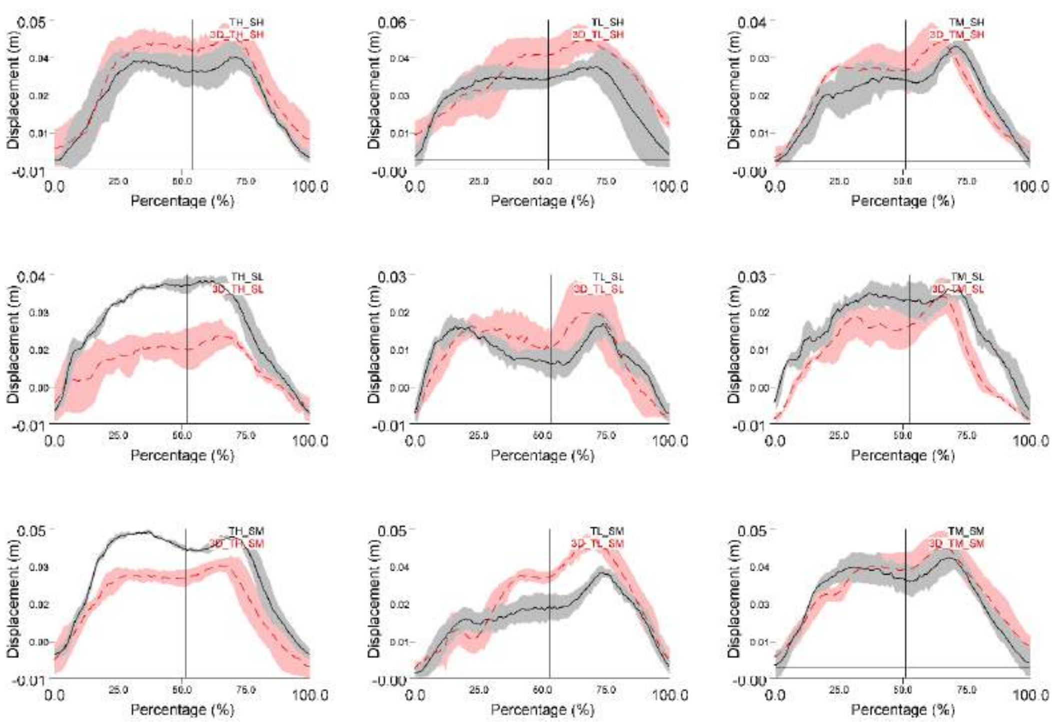

Figure C.60: Thigh interface migration (parallel)

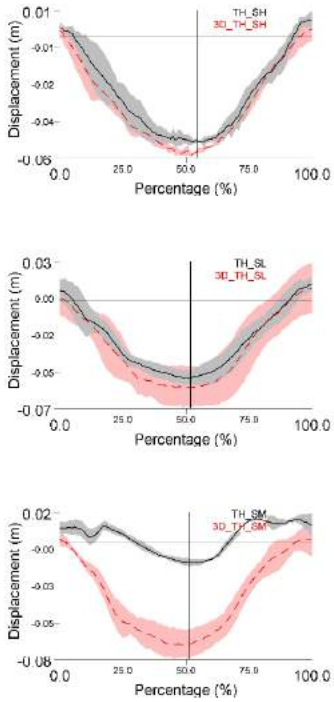

Figure C.61: Thigh interface migration (perpendicular)

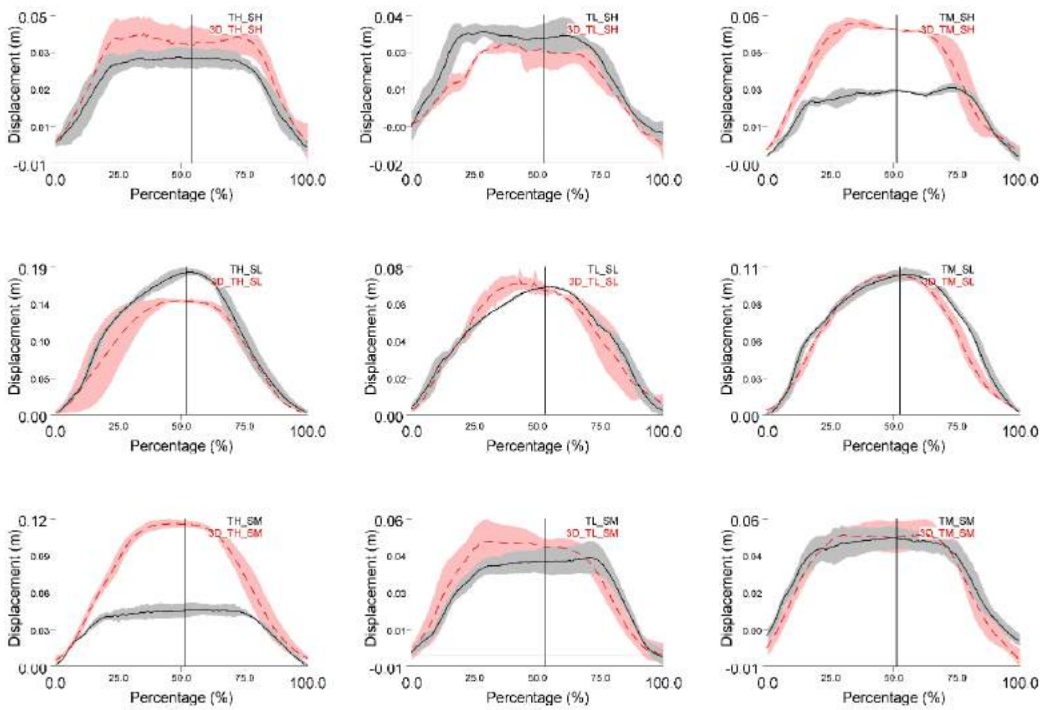

Figure C.62: Shank interface migration (parallel)

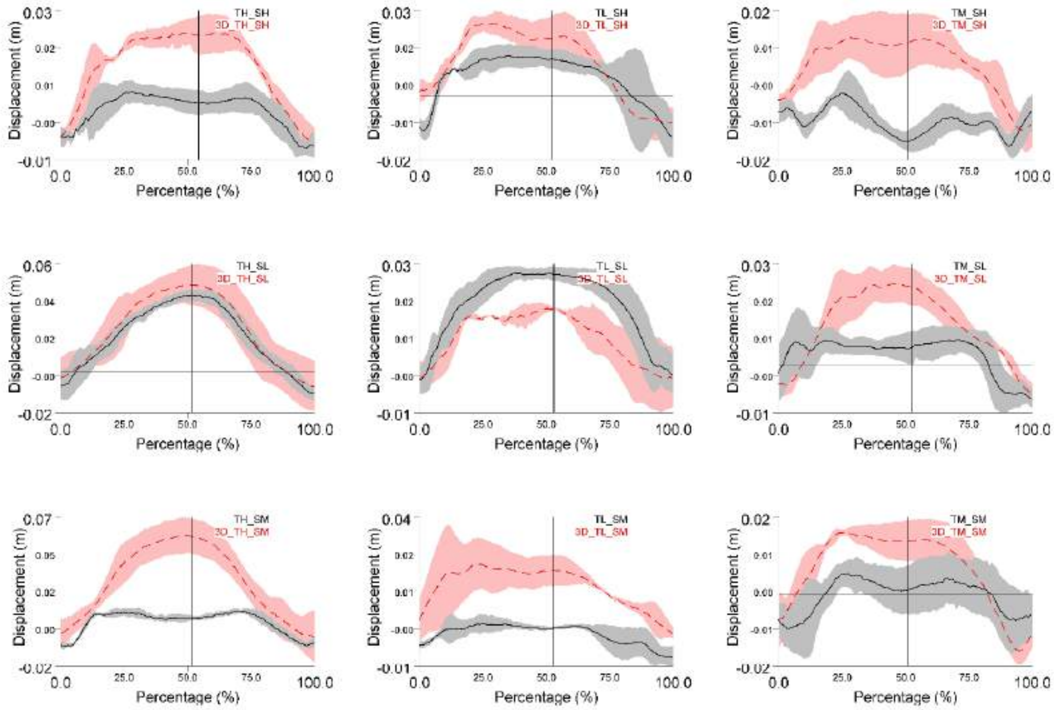

Figure C.63: Shank interface migration (perpendicular)

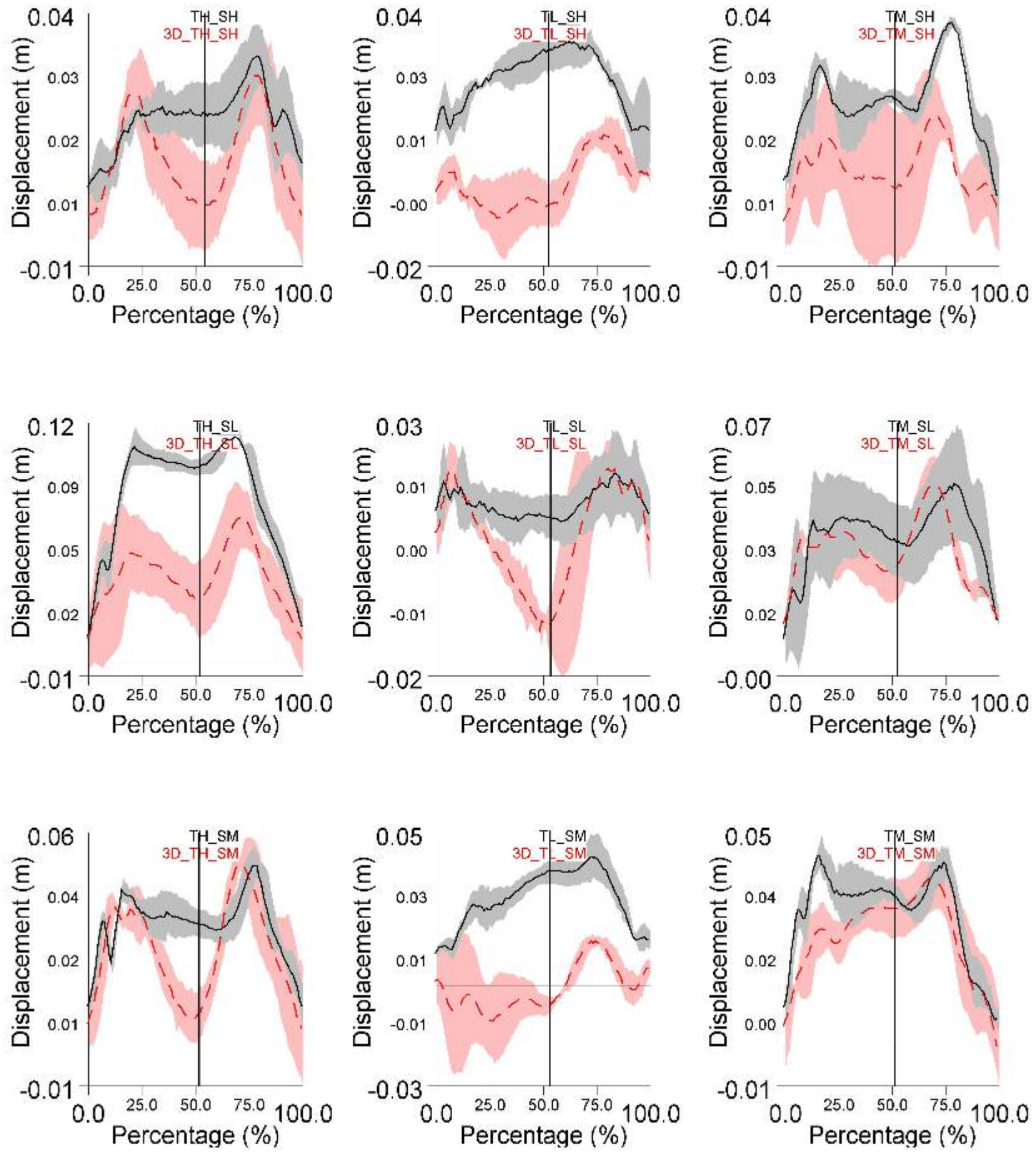

Figure C.64: Joint misalignment (anterior-posterior)

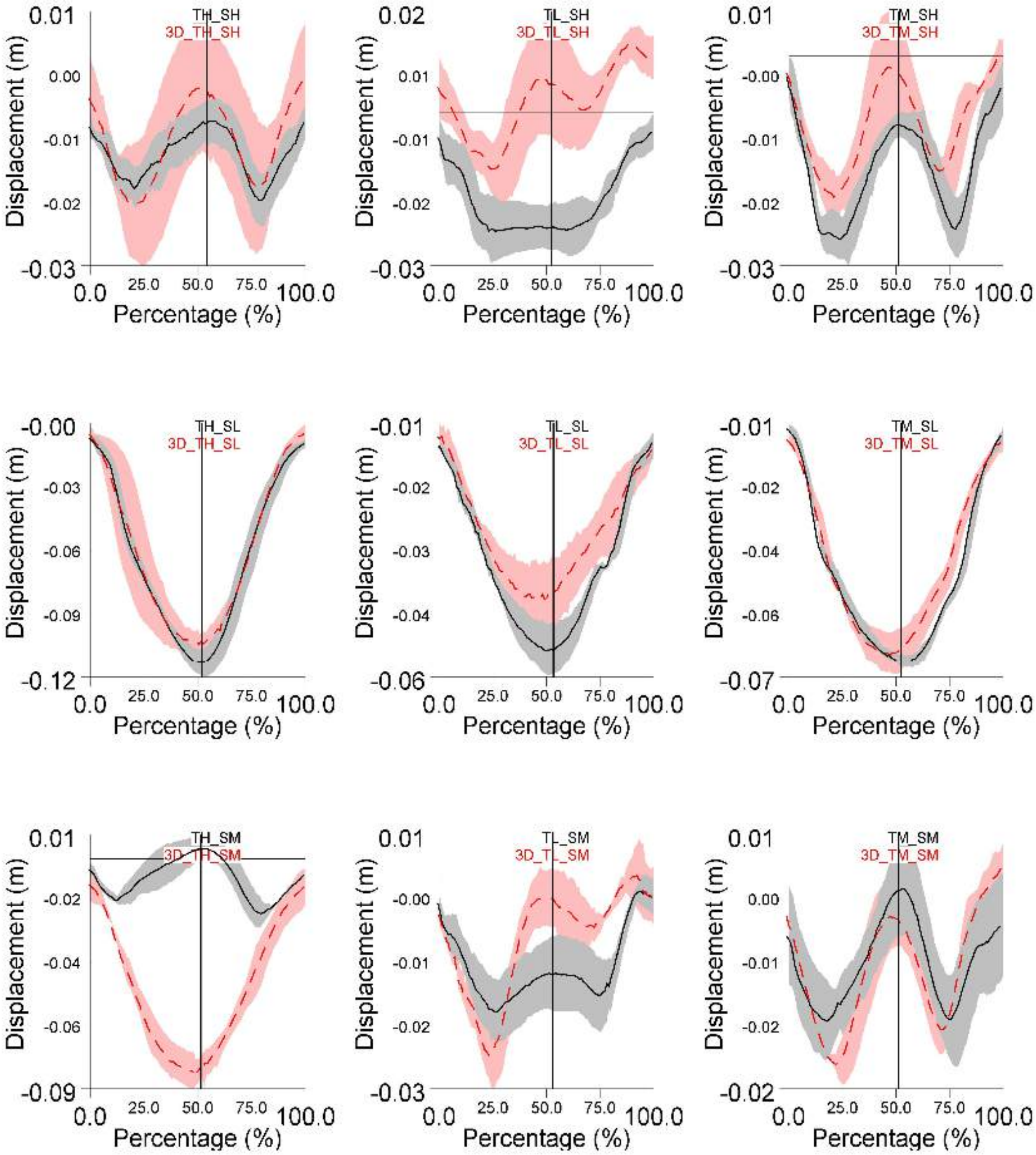

Figure C.65: Joint misalignment (superior-inferior)

Stiffness analysis

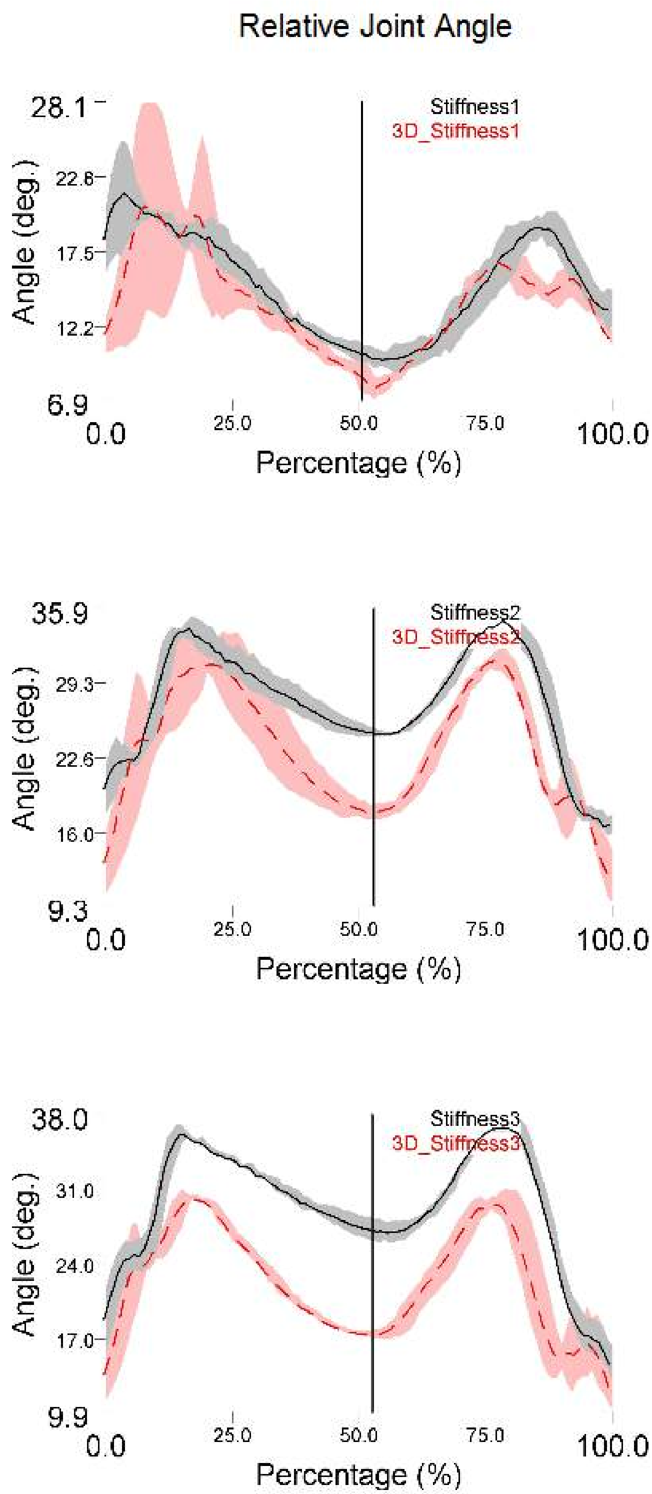

Figure C.66: Relative joint angle

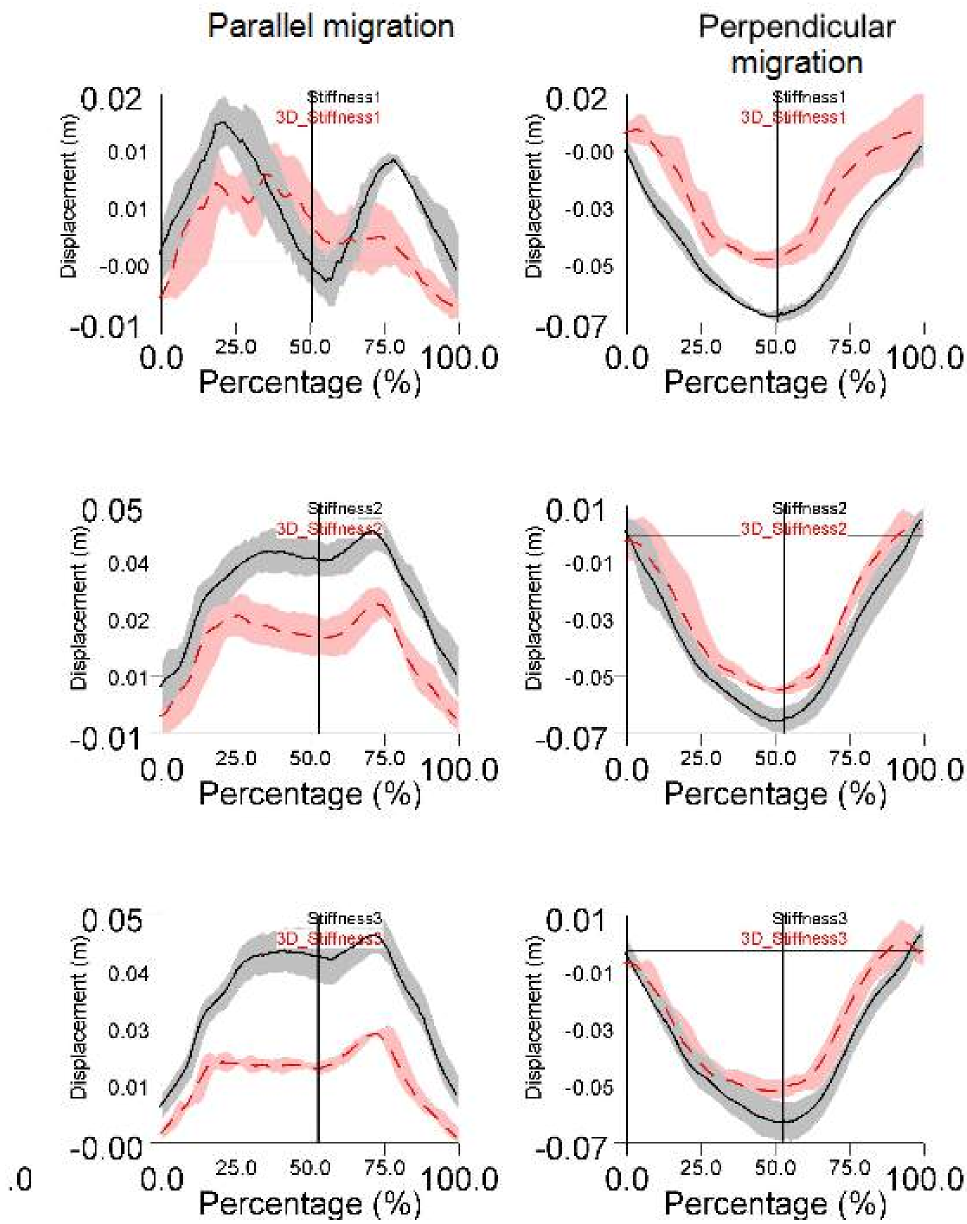

Figure C.67: Thigh interface migration

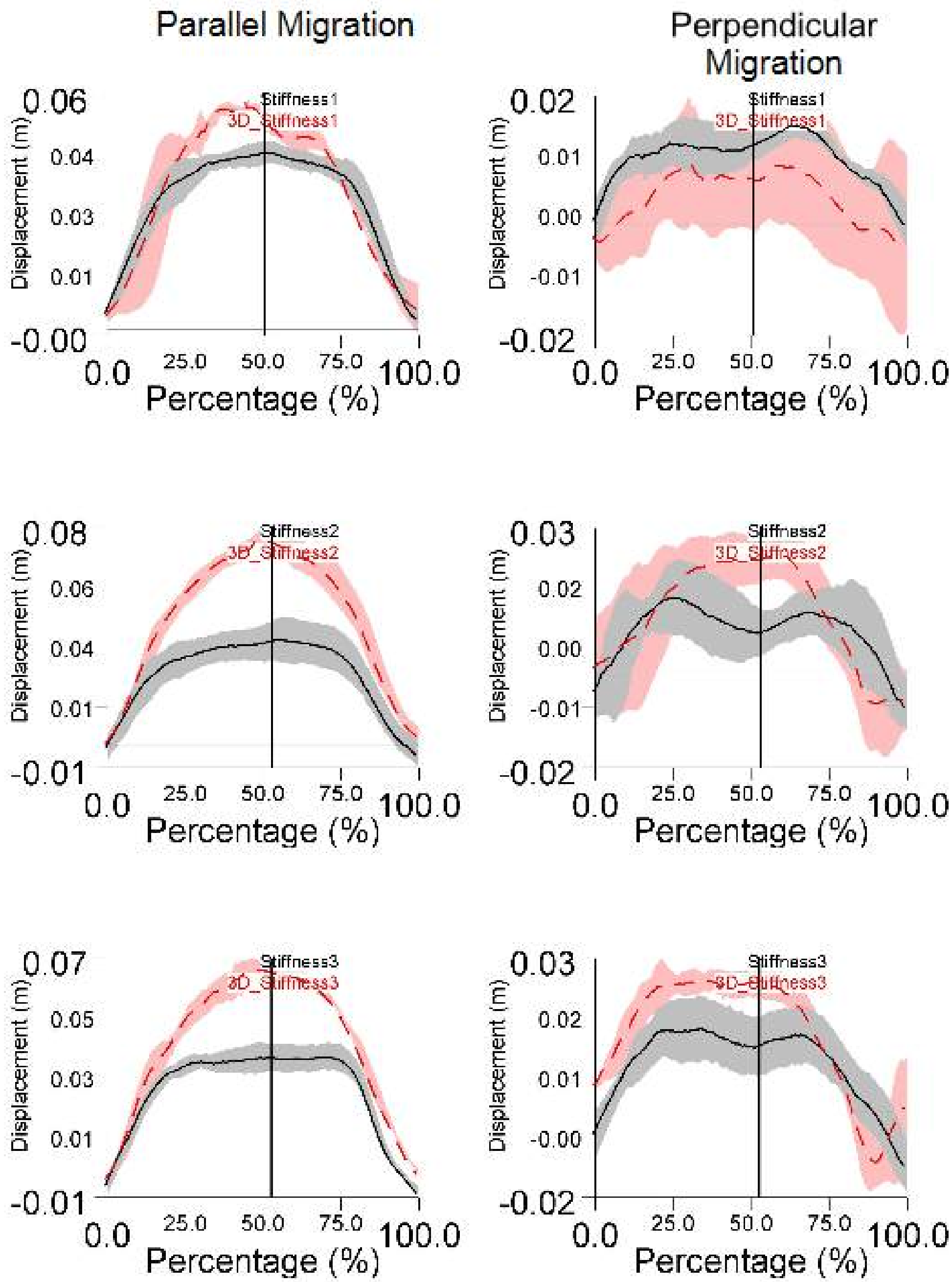

Figure C.68: Shank interface migration

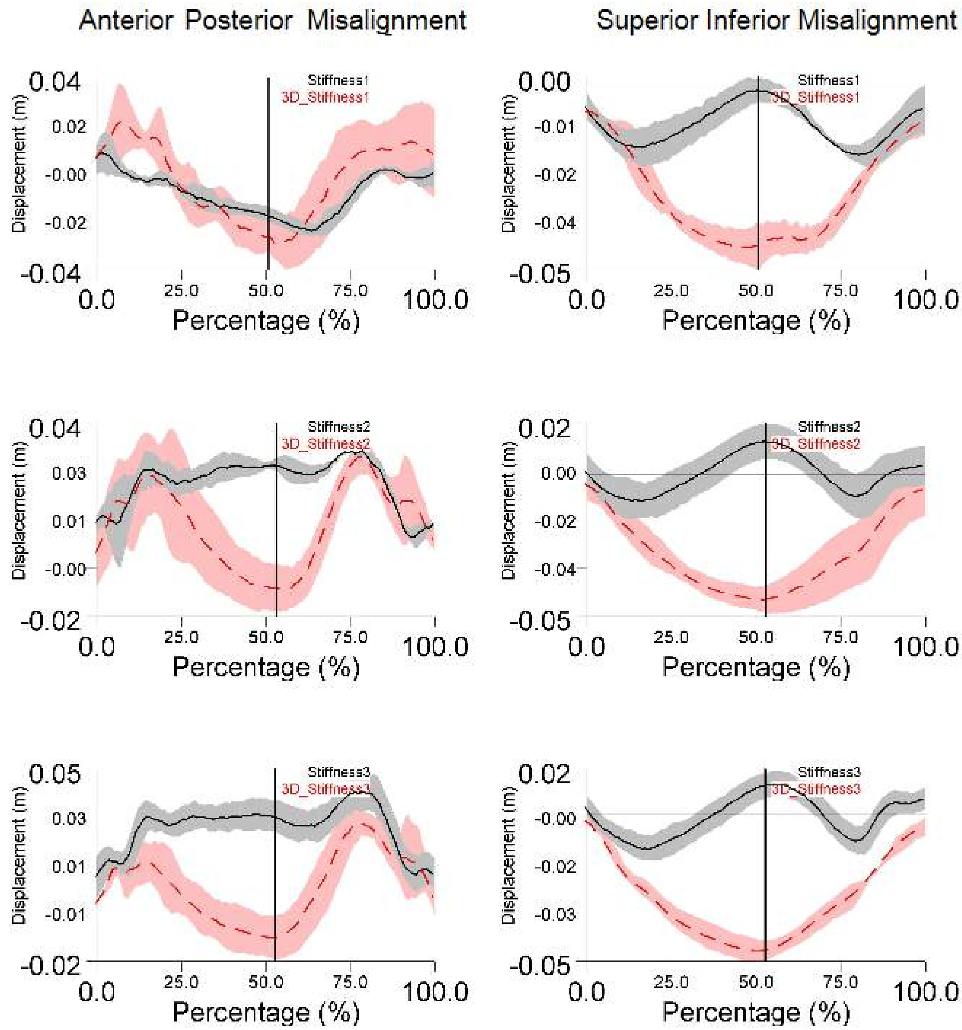

Figure C.69: Joint misalignment

C.1.7 Sliding mechanism

Stiffness 1

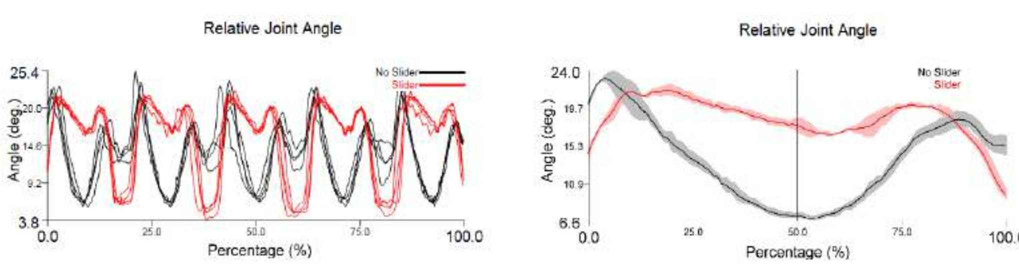

Figure C.70: Relative joint angle

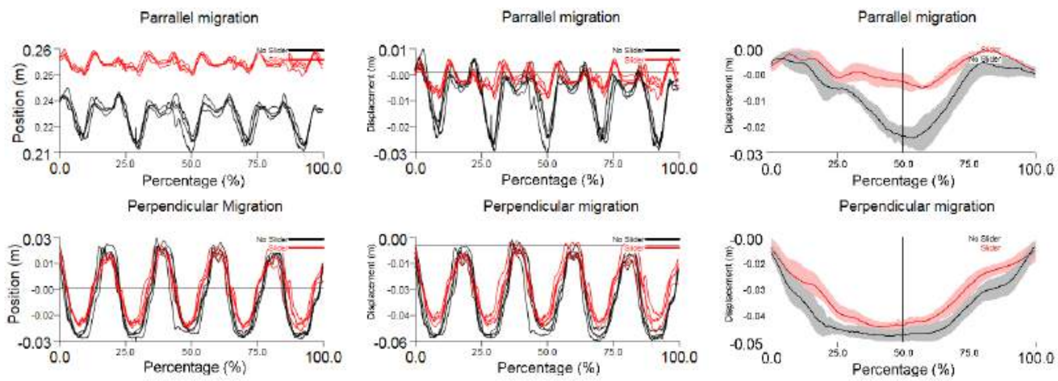

Figure C.71: Thigh interface migration

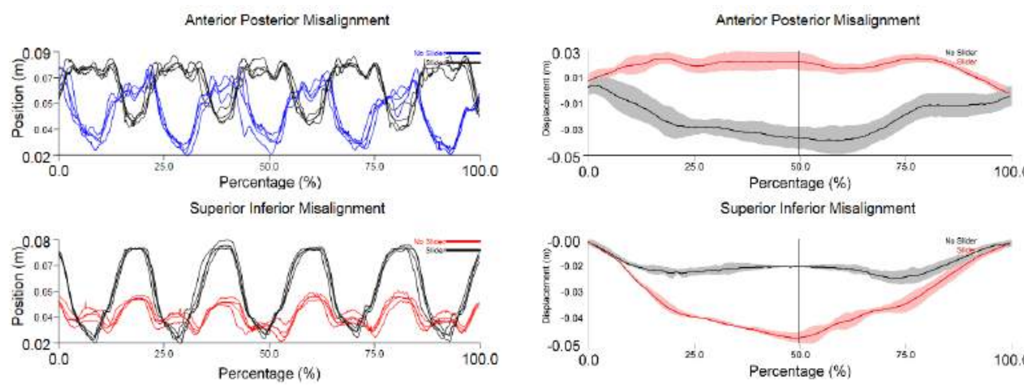

Figure C.72: Joint misalignment

Stiffness 2

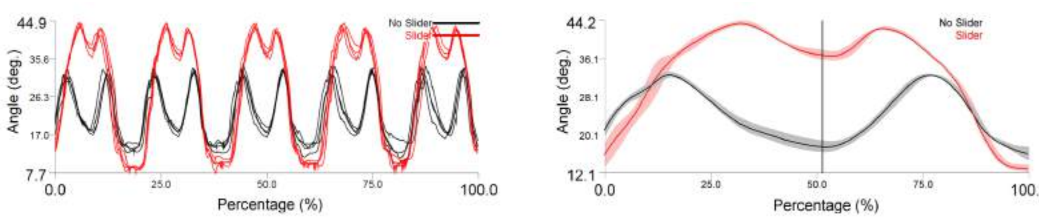

Figure C.73: Relative joint angle

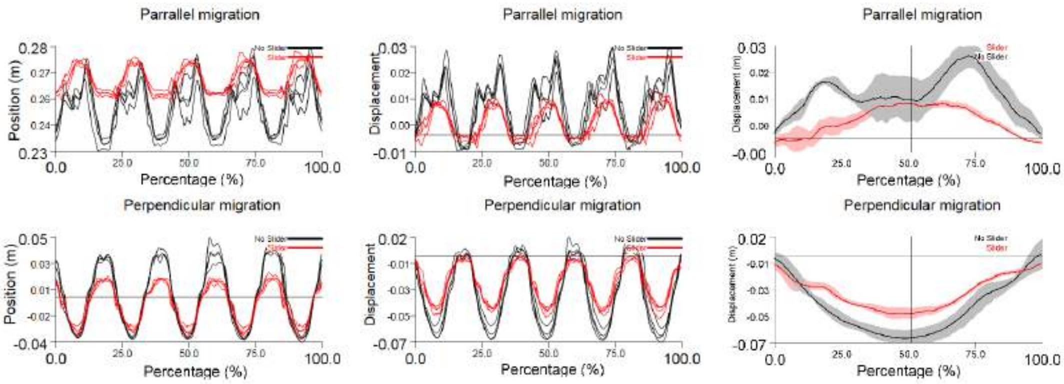

Figure C.74: Thigh interface migration

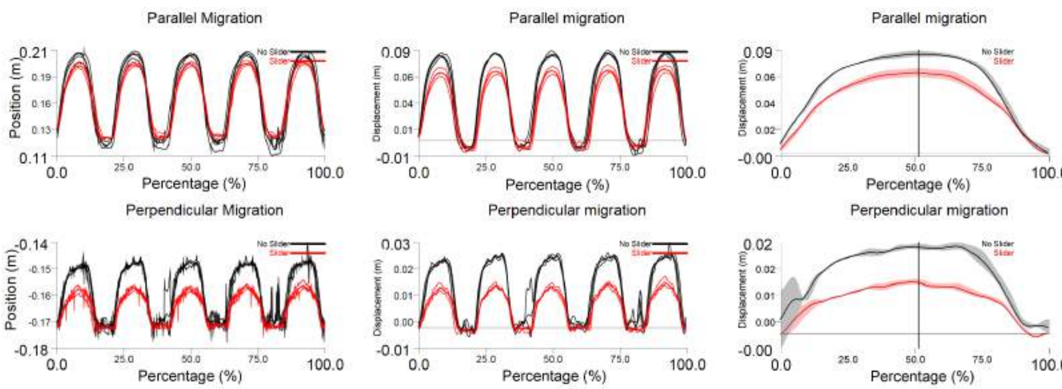

Figure C.75: Shank interface migration

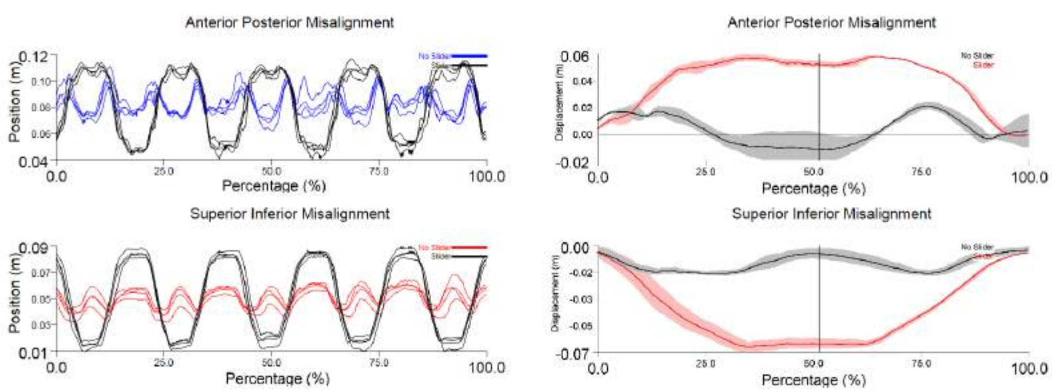

Figure C.76: Joint misalignment

Stiffness 3

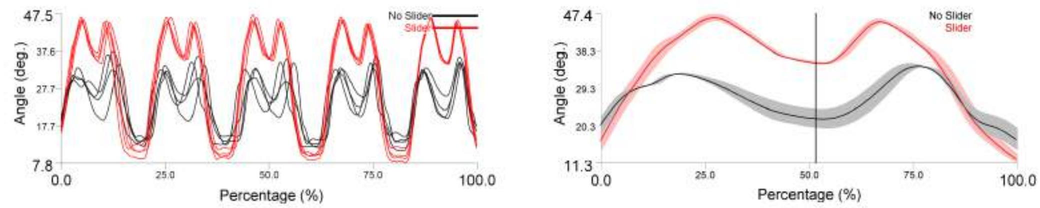

Figure C.77: Relative joint angle

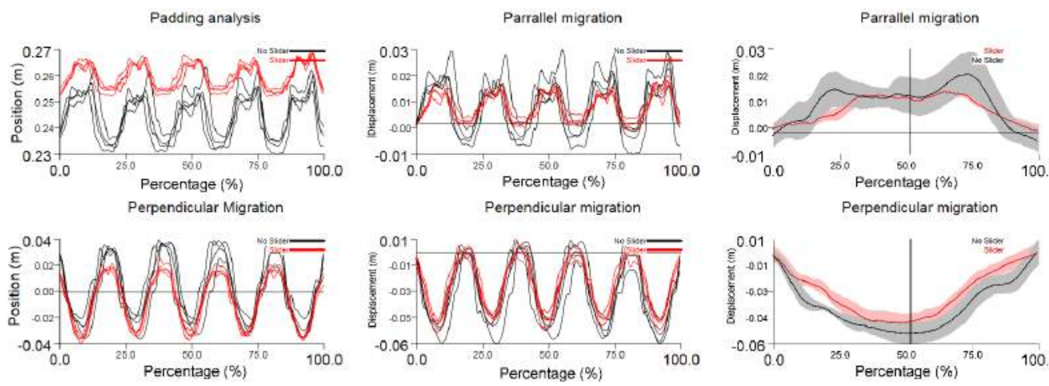

Figure C.78: Thigh interface migration

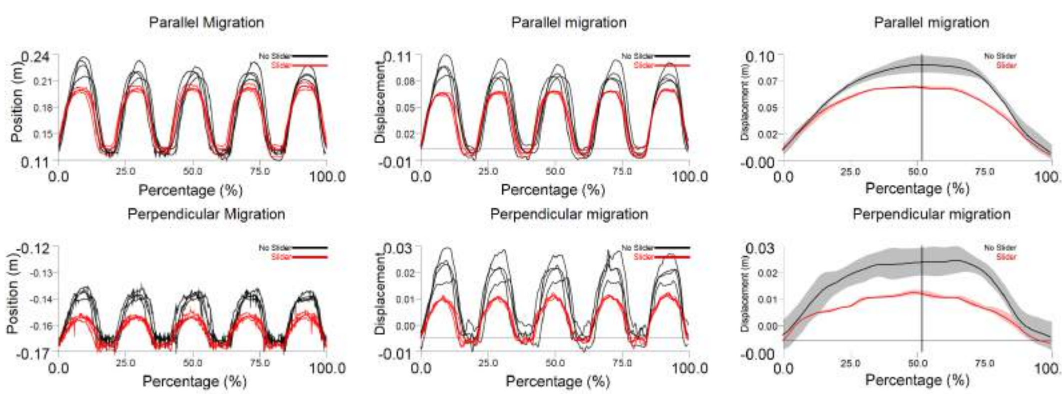

Figure C.79: Shank interface migration

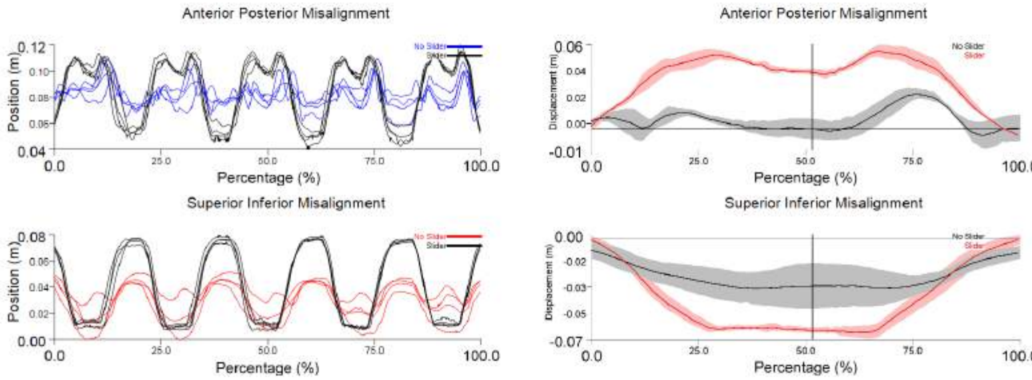

Figure C.80: Joint misalignment

Appendix D

Ethics certificate

Université d'Ottawa University of Ottawa

Bureau d'éthique et d'intégrité de la recherche Office of Research Ethics and Integrity

Ethics Approval Notice

Health Sciences and Science REB

Principal Investigator / Supervisor / Co-investigator(s) / Student(s)

First Name	Last Name	Affiliation	Role
Marc	Doumit	Engineering / Mecanical Engineering	Supervisor
Laurent	Levesque	Engineering / Mecanical Engineering	Student Researcher

File Number: H02-17-03

Type of Project: Master's Thesis

Title: Experimental evaluation of interface contact pressure developed with a spring loaded knee brace

Approval Date (mm/dd/yyyy)	Expiry Date (mm/dd/yyyy)	Approval Type
03/06/2017	03/05/2018	Approval

Special Conditions / Comments:
N/A.

550, rue Cumberland, pièce 154 550 Cumberland Street, room 154
Ottawa, Ontario K1N 6N5 Canada Ottawa (Ontario) K1N 6N5 Canada
Téléc./Fax (613) 562-5338 • (613) 562-5387
www.recherche.uottawa.ca/deontologie/ www.research.uottawa.ca/ethics/

File Number: H02-17-03

Date (mm/dd/yyyy): 03/06/2017

Université d'Ottawa   University of Ottawa

Bureau d'éthique et d'intégrité de la recherche   Office of Research Ethics and Integrity

This is to confirm that the University of Ottawa Research Ethics Board identified above, which operates in accordance with the Tri-Council Policy Statement (2010) and other applicable laws and regulations in Ontario, has examined and approved the ethics application for the above named research project. Ethics approval is valid for the period indicated above and subject to the conditions listed in the section entitled "Special Conditions / Comments".

During the course of the project, the protocol may not be modified without prior written approval from the REB except when necessary to remove participants from immediate endangerment or when the modification(s) pertain to only administrative or logistical components of the project (e.g., change of telephone number). Investigators must also promptly alert the REB of any changes which increase the risk to participant(s), any changes which considerably affect the conduct of the project, all unanticipated and harmful events that occur, and new information that may negatively affect the conduct of the project and safety of the participant(s). Modifications to the project, including consent and recruitment documentation, should be submitted to the Ethics Office for approval using the "Modification to research project" form available at: https://research.uottawa.ca/ethics/forms.

Please submit an annual report to the Ethics Office four weeks before the above-referenced expiry date to request a renewal of this ethics approval. To close the file, a final report must be submitted. These documents can be found at: https://research.uottawa.ca/ethics/forms.

If you have any questions, please do not hesitate to contact the Ethics Office at extension 5387 or by e-mail at: ethics@uOttawa.ca.

Gabriel Petitti
Protocol Officer for Ethics in Research
For Daniel Lagarec, Chair of the Health Sciences and Sciences REB

550, rue Cumberland, pièce 154   550 Cumberland Street, room 154
Ottawa, Ontario K1N 6N5 Canada   Ottawa (Ontario) K1N 6N5 Canada
Téléc./Fax (613) 562-5338 • (613) 562-5387
www.recherche.uottawa.ca/deontologie/ www.research.uottawa.ca/ethics/

Appendix E

Coding

E.1 Matlab and Arduino code

This appendix contains the Matlab and Arduino code used for calibration and data acquisition of the force sensing apparatus. In general, the Arduino code reads the voltages from the different analog pins, applies the calibration factors and output the results visually. The Matlab code was used to output graphs of the data.

E.1.1 Matlab

This is the Matlab code.

```


function Flexiforcegraphing ()


clc
close all
clear all
multiselectstate='on';
[filename, path] = uigetfile('*.txt','Pick a file','multiselect',multiselectstate);
[q NumFiles]= size(filename); % number of files

numberofsensors = 14; %Including Rot. Pot.
```

```
Pot_row = 13;

%3Dmatrice(x,y,z) - Rows,Cols,Pages
Data=zeros(10000,numberofsensors,NumFiles);

%initialise Data Matrix

for i=1:NumFiles

fullname = fullfile(path, filename(1,i))
fullname=char(fullname);
fid=fopen(fullname,'r');
formatSpec='%f';
sizeA=[numberofsensors Inf];
A=fscanf(fid,formatSpec,sizeA);
A=A'; % Matrix A of the file i is extracted and transposed

[row col]=size(A);
Rmax=row;

    [R C P]=size(Data); %Row, column, page
    if R>row
        Rmax=R;

    end

    % 3D matrices needs to have the same dimensions between pages. Here we compared the size of the different file matrices to determine the ''longest'' file to increase the size of smaller ones.

data=zeros(Rmax,col,NumFiles); % New matrix that is erased at each loop
% but carry the data of the files.


for k=1:i
```

```
    if k==i %If only one file
        for L=1:row % row is for A
             data(L,:,k)=A(L,:);
        end
    else


     for L=1:row %R (row) is for Data matrix
          data(L,:,k)=A(L,:);
     end

     % The file data i was transfered to the data matrix

    end
end
for z=1:row
          Data(z,:,i)=data(z,:,i); % data is transfered to Data
             and then used again for the file data transfer
end
end

%At this point the files are loaded into a 3D matrix called
   Data. each page of the matrix is a seperate file.

% The code below trims the data, using 4 degrees of flexion as
    the strating and ending point of the data.

[Rows Cols Pages]=size(Data);

%Find the cell number that contains the first 4 degree value

BeginPoint=zeros(1,Pages);
EndPoint=zeros(1,Pages);

for p=1:Pages

for i=1:Rows
```

```
    number=Data(i,Pot_row,p);
    if number >= 4
        break
    end
end
BeginPoint2(1,p)=i;

%Find the cell number that contains the second 2 degree value

for k=i:Rows
    number=Data(k,Pot_row,p);
    if number <= 4
        break
    end
end
EndPoint2(1,p)=k;


% Find second set


for l=k:Rows
    number=Data(l,Pot_row,p);
    if number >= 4
        break
    end
end
BeginPoint3(1,p)=l;


for m=l:Rows
    number=Data(m,Pot_row,p);
    if number <= 4
        break
    end
end
EndPoint3(1,p)=m;
```

```
% The third squat will be used for the representation of the
    results.

for q=m:Rows
    number=Data(q,Pot_row,p);
    if number >= 4
        break
    end
end
BeginPoint(1,p)=q;


for v=q:Rows
    number=Data(v,Pot_row,p);
    if number <= 4
        break
    end
end
EndPoint(1,p)=v;

end


%fit and decide the number of points so that all trials have
    the same number of points.

NumberofPoints=1000;

NewData=zeros(NumberofPoints,numberofsensors,Pages);    %
    Initialise new data matrix


for i=1:Pages

    NewData(:,:,i)=Normalize(Data(:,:,i),BeginPoint(i),
        EndPoint(i),NumberofPoints);
```

```
end

function [Matrix] =  Normalize(data,begin,ending,points)

    %normalise before curve fitting
    [~, column]=size(data);
    length=ending-begin;
    trimmed=zeros(length,column);
    time=zeros(length,1);
    for j=1:length
        trimmed(j,:)=data(begin-1+j,:);
        time(j,1)=(j/length)*100;
    end
    %Divide the normalise into the 1000 points
 Matrix=zeros(points,column);
    for n=1:column
        F=fit(time(:,1),trimmed(:,n),'smoothingspline');
        for s=1:points
            t=(s/points)*100;
            Matrix(s,n)=F(t);
        end
    end

end

% At this point the matrices included in NewData contain 1000
    data points for each sensors for each pages.

% We want the average of the different trials (pages). We will
     then add the different sensor signals individually and
    divided by the number of trials (pages). First we apply a
    filter.

figure
for i=1:Pages

```

```
    plot(NewData(:,13,i))
    hold on
end

AddData1=zeros(NumberofPoints,numberofsensors);
AddData2=zeros(NumberofPoints,numberofsensors);
AddData3=zeros(NumberofPoints,numberofsensors);

AvgData1=zeros(NumberofPoints,numberofsensors);
AvgData2=zeros(NumberofPoints,numberofsensors);
AvgData3=zeros(NumberofPoints,numberofsensors);


for i=1:Pages

Sensor1(i,:)=NewData(:,1,i);
Sensor2(i,:)=NewData(:,2,i);
Sensor3(i,:)=NewData(:,3,i);
Sensor4(i,:)=NewData(:,4,i);
Sensor5(i,:)=NewData(:,5,i);
Sensor6(i,:)=NewData(:,6,i);
Sensor7(i,:)=NewData(:,7,i);
Sensor8(i,:)=NewData(:,8,i);
Sensor9(i,:)=NewData(:,9,i);
Sensor10(i,:)=NewData(:,10,i);
Sensor11(i,:)=NewData(:,11,i);
Sensor12(i,:)=NewData(:,12,i);

end


% using Butterworth filter function

FiltData_butter = zeros(NumberofPoints,numberofsensors,9);

%N=2; %order of the filter
N=2
```

```
%Low pass Filter
    samplingfrequency = 20;
    Wn = 1/(samplingfrequency/2);   % Normalized cutoff frequency
    [B,A] = butter(N,Wn,'low');     % Creates the filter coefficients for Low Pass Filter

for i = 1:9,
    FiltData_butter(:,:,i) =  filter(B,A,NewData(:,:,i));
end

% -----------------------------------------------------------------------


for i=1:3
    AddData1(:,:)=AddData1(:,:)+FiltData_butter(:,:,i);
    AddData2(:,:)=AddData2(:,:)+FiltData_butter(:,:,i+3);
    AddData3(:,:)=AddData3(:,:)+FiltData_butter(:,:,i+6);
end

AvgData1(:,:)=AddData1(:,:)/3;
AvgData2(:,:)=AddData2(:,:)/3;
AvgData3(:,:)=AddData3(:,:)/3;


a=AvgData1(:,4);
b=AvgData2(:,4);
c=AvgData3(:,4);

figure
plot(a);
hold on
plot(b);
hold on
plot(c);
```

```
Sensor_MAX1=zeros(1,numberofsensors);
Sensor_MAX2=zeros(1,numberofsensors);
Sensor_MAX3=zeros(1,numberofsensors);


for i=1:numberofsensors
Sensor_MAX1(1,i)=max(AvgData1(:,i));
Sensor_MAX2(1,i)=max(AvgData2(:,i));
Sensor_MAX3(1,i)=max(AvgData3(:,i));
end


Z1 = [Sensor_MAX1(1,1) NaN Sensor_MAX1(1,2) NaN Sensor_MAX1(1,3) NaN Sensor_MAX1(1,4) NaN Sensor_MAX1(1,5) NaN Sensor_MAX1(1,6) NaN;
        NaN Sensor_MAX1(1,7) NaN Sensor_MAX1(1,8) NaN Sensor_MAX1(1,9) NaN Sensor_MAX1(1,10) NaN Sensor_MAX1(1,11) NaN Sensor_MAX1(1,12)
      ]

Z2 = [Sensor_MAX2(1,1) NaN Sensor_MAX2(1,2) NaN Sensor_MAX2(1,3) NaN Sensor_MAX2(1,4) NaN Sensor_MAX2(1,5) NaN Sensor_MAX2(1,6) NaN;
        NaN Sensor_MAX2(1,7) NaN Sensor_MAX2(1,8) NaN Sensor_MAX2(1,9) NaN Sensor_MAX2(1,10) NaN Sensor_MAX2(1,11) NaN Sensor_MAX2(1,12)
      ]

Z3 = [Sensor_MAX3(1,1) NaN Sensor_MAX3(1,2) NaN Sensor_MAX3(1,3) NaN Sensor_MAX3(1,4) NaN Sensor_MAX3(1,5) NaN Sensor_MAX3(1,6) NaN;
```

```
        NaN Sensor_MAX3(1,7) NaN Sensor_MAX3(1,8) NaN Sensor_MAX3(1,9) NaN Sensor_MAX3(1,10) NaN Sensor_MAX3(1,11) NaN Sensor_MAX3(1,12)
        ]

Z=[Z1(1,1) Z2(1,1) Z3(1,1); Z1(1,3) Z2(1,3) Z3(1,3); Z1(1,5) Z2(1,5) Z3(1,5); Z1(1,7) Z2(1,7) Z3(1,7); Z1(1,9) Z2(1,9) Z3(1,9); Z1(1,11) Z2(1,11) Z3(1,11);
      Z1(2,2) Z2(2,2) Z3(2,2); Z1(2,4) Z2(2,4) Z3(2,4); Z1(2,6) Z2(2,6) Z3(2,6); Z1(2,8) Z2(2,8) Z3(2,8); Z1(2,10) Z2(2,10) Z3(2,10); Z1(2,12) Z2(2,12) Z3(2,12);
      ]

figure
bar(Z)
title('Force response in function of padding')
xlabel('Sensor number')
ylabel('Force (N)')
legend('Padding 1','Padding 2','Padding 3')



x=1:1:1000;

figure

% Create some data for the two curves to be plotted

y1 = AvgData1(:,7);
y2 = AvgData1(:,13);
y3 = 0.2137*y2;
 % Brace moment: find polynominal of brace moment

% Create a plot with 2 y axes using the plotyy function
fig = figure;
[ax, h1, h2] = plotyy(x, y1, x, y2, 'plot');

```

```
% Add title and x axis label
xlabel('Data points');
title('Force vs angle response');

% Use the axis handles to set the labels of the y axes
set(get(ax(1), 'Ylabel'), 'String', 'Sensor force (N)');
set(get(ax(2), 'Ylabel'), 'String', 'Brace angle (deg)');

title('Sensor 0')
%end

%_________________________________________


ylabels{1}='Sensor Force (N)';
ylabels{2}='Brace angle (deg.)';
ylabels{3}='Brace moment (Nm)';

[ax,hlines] = plotyyy(x,y1,x,y2,x,y3,ylabels);
%legend(hlines, 'y = x','y = x^2','y = x^3',2)

function [ax,hlines] = plotyyy(x1,y1,x2,y2,x3,y3,ylabels)

if nargin==6
   %Use empty strings for the ylabels
   ylabels{1}=' '; ylabels{2}=' '; ylabels{3}=' ';
elseif nargin > 7
   error('Too many input arguments')
elseif nargin < 6
   error('Not enough input arguments')
end

% figure('Name','Second squat, Sensor 7','units','normalized',...
%        'DefaultAxesXMinorTick','on','DefaultAxesYminorTick','on');

```

```
%Plot the first two lines with plotyy
[ax,hlines(1),hlines(2)] = plotyy(x1,y1,x2,y2);
cfig = get(gcf,'color');
pos = [0.1  0.1  0.7  0.8];
offset = pos(3)/5.5;

%Reduce width of the two axes generated by plotyy
pos(3) = pos(3) - offset/2;
set(ax,'position',pos);

%Determine the position of the third axes
pos3=[pos(1) pos(2) pos(3)+offset pos(4)];

%Determine the proper x-limits for the third axes
limx1=get(ax(1),'xlim');
limx3=[limx1(1)   limx1(1) + 1.2*(limx1(2)-limx1(1))];
%Bug fix 14 Nov-2001: the 1.2 scale factor in the line above
%was contributed by Mariano Garcia (BorgWarner Morse TEC Inc)

ax(3)=axes('Position',pos3,'box','off',...
    'Color','none','XColor','k','YColor','r',...
    'xtick',[],'xlim',limx3,'yaxislocation','right');

hlines(3) = line(x3,y3,'Color','r','Parent',ax(3));
limy3=get(ax(3),'YLim');
limy3=[0,25];

%Hide unwanted portion of the x-axis line that lies
%between the end of the second and third axes
line([limx1(2) limx3(2)],[limy3(1) limy3(1)],...
    'Color',cfig,'Parent',ax(3),'Clipping','off');
axes(ax(2))

%Label all three y-axes
set(get(ax(1),'ylabel'),'string',ylabels{1})
set(get(ax(2),'ylabel'),'string',ylabels{2})
set(get(ax(3),'ylabel'),'string',ylabels{3})
```

```
hold on
end
% ------------------------------------------------------------------


figure
for i=1:4
plot(AvgData1(:,i),'color','k','LineWidth',2)
hold on
%title('Sensor 0')
end

figure
for i=5:8
plot(AvgData1(:,i),'color','k','LineWidth',2)
hold on
%title('Sensor 0')
end

figure
for i=9:12
plot(AvgData1(:,i),'color','k','LineWidth',2)
hold on
%title('Sensor 0')
end
```

E.1.2 Arduino

This is the Arduino Code.

```
/*
//This code is used to read and output data from force and angle sensors

//Define generals

```

```
#define BAUD_RATE                    115200
#define NUM_SENSORS                   12
#define NUM_READINGS                  2

//Force sensors
#define P0  A0
#define P1  A1
#define P2  A2
#define P3  A3
#define P4  A4
#define P5  A5
#define P6  A6
#define P7  A7
#define P8  A8
#define P9  A9
#define P10  A10
#define P11  A11

//rotational potentiometer
#define P12  A12



void setup() {


  Serial.begin(BAUD_RATE);
  pinMode(P0, INPUT);
  pinMode(P1, INPUT);
  pinMode(P2, INPUT);
  pinMode(P3, INPUT);
  pinMode(P4, INPUT);
  pinMode(P5, INPUT);
  pinMode(P6, INPUT);
  pinMode(P7, INPUT);
  pinMode(P8, INPUT);
  pinMode(P9, INPUT);
  pinMode(P10, INPUT);
  pinMode(P11, INPUT);
  pinMode(P12, INPUT);
}

void loop() {
```

```
//Force sensor calibration
  float  m0 = 6.04;    float   b0 = 0.000;
  float  m1 = 3.87;    float   b1 = 0.000;
  float  m2 = 4.94;    float   b2 = 0.000;
  float  m3 = 5.64;    float   b3 = 0.000;
  float  m4 = 4.76;    float   b4 = 0.000;
  float  m5 = 4.18;    float   b5 = 0.000;
  float  m6 = 9.26;    float   b6 = 0.000;
  float  m7 = 4.84;    float   b7 = 0.000;
  float  m8 = 4.59;    float   b8 = 0.000;
  float  m9 = 4.49;    float   b9 = 0.000;
  float  m10 = 4.71;   float   b10 = 0.000;
  float  m11 = 5.25;   float   b11 = 0.000;
}

for (int i=0; i < NUM_READINGS; i ++)
{

    double raw_reading = analogRead(P0);                        //Read
   Seonsor 0
    raw_reading=0.0049* raw_reading*(m0)+b0;
    //raw_reading=0.0049* raw_reading;
    //printFixed(raw_reading);
    Serial.print(raw_reading,2);
    Serial.print("    ");

    raw_reading = analogRead(P1);                               //Read
   Seonsor 1
    raw_reading= 0.0049*raw_reading*(m1)+b1;
   // raw_reading= 0.0049*raw_reading;
    Serial.print(raw_reading,2);
    Serial.print("    ");

    raw_reading = analogRead(P2);                          //Read Seonsor 2
    raw_reading=0.0049* raw_reading*(m2)+b2;
    //raw_reading=0.0049* raw_reading;
    Serial.print(raw_reading,2);
    Serial.print("    ");

    raw_reading = analogRead(P3);                               //Read
   Seonsor 3
    raw_reading= 0.0049*raw_reading*(m3)+b3;
   // raw_reading= 0.0049*raw_reading;
```

```
    Serial.print(raw_reading,2);
    Serial.print("    ");

    raw_reading = analogRead(P4);                          //Read Seonsor 4
    raw_reading=0.0049* raw_reading*(m4)+b4;
    //raw_reading=0.0049* raw_reading;
    Serial.print(raw_reading,2);
    Serial.print("    ");

    raw_reading = analogRead(P5);                                  //Read
   Seonsor 5
    raw_reading= 0.0049*raw_reading*(m5)+b5;
   // raw_reading= 0.0049*raw_reading;
    Serial.print(raw_reading,2);
    Serial.print("    ");

    raw_reading = analogRead(P6);                          //Read Seonsor 6
    raw_reading=0.0049* raw_reading*(m6)+b6;
    //raw_reading=0.0049* raw_reading;
    Serial.print(raw_reading,2);
    Serial.print("    ");

    raw_reading = analogRead(P7);                                  //Read
   Seonsor 7
    raw_reading= 0.0049* raw_reading*(m7)+b7;
   // raw_reading= 0.0049*raw_reading;
    Serial.print(raw_reading,2);
    Serial.print("    ");

    raw_reading = analogRead(P8);                          //Read Seonsor 8
    raw_reading=0.0049* raw_reading*(m8)+b8;
    //raw_reading=0.0049* raw_reading;
    Serial.print(raw_reading,2);
    Serial.print("    ");

    raw_reading = analogRead(P9);                                  //Read
   Seonsor 9
    raw_reading= 0.0049*raw_reading*(m9)+b9;
   // raw_reading= 0.0049*raw_reading;
    Serial.print(raw_reading,2);
    Serial.print("    ");

    raw_reading = analogRead(P10);                         //Read Seonsor 10
    raw_reading=0.0049* raw_reading*(m10)+b10;
```

```
    //raw_reading=0.0049* raw_reading;
    Serial.print(raw_reading,2);
    Serial.print("    ");

    raw_reading = analogRead(P11);                              //Read Seonsor 11
    raw_reading=0.0049* raw_reading*(m11)+b11;
    //raw_reading=0.0049* raw_reading;
    Serial.print(raw_reading,2);
    Serial.print("    ");

    //————————

    raw_reading12 = analogRead(P12);                              //Read
   Rotational potentiometer
    raw_reading12=0.0049*raw_reading12;
    raw_reading=((1.3824*raw_reading12*raw_reading12*raw_reading12)
   -(12.136*raw_reading12*raw_reading12)-(4.3373*raw_reading12)+102.94);
    //raw_reading=0.0049* raw_reading;
    Serial.print(raw_reading,2);
    Serial.print("    ");

    Serial.println(" ");

}

void printFixed(byte value)
{
  if(value < 10)
  {
    Serial.print("   ");
  }
  else if(value < 100)
  {
    Serial.print(" ");
  }
  Serial.print(value);
}
}
```